

**Advanced Closed-Loop Reservoir Management for
Computationally Efficient Data Assimilation and Real-Time
Production Optimization of SAGD Reservoirs**

by

Rajan Patel

A thesis submitted in partial fulfillment of the requirements for the degree of

Doctor of Philosophy

in

Petroleum Engineering

Department of Civil and Environmental Engineering
University of Alberta

© Rajan Patel, 2018

Abstract

Steam-assisted gravity drainage (SAGD), an in-situ thermal oil recovery method is successfully utilized to extract bitumen from the Canadian oil sands. To improve the reservoir performance, an idea of closed-loop reservoir management (CLRM) was proposed that comprises near-continuous data assimilation to estimate unknown parameters and model-based optimization at distinct decision-making levels. Commercialization of CLRM is vital, however, it poses a significant challenge given the intensive computational requirements of data assimilation techniques, highly nonlinear nature of SAGD process and rare field-scale testing of the concept. In this research, limitations of the fundamental elements of CLRM i.e., data assimilation and short-term production optimization are addressed by developing computationally efficient dynamic modeling workflows and advanced control frameworks.

Data assimilation using contemporary techniques at reservoir scale requires high fidelity simulation of many stochastic realizations, resulting in an impractical computational cost. Two solutions proposed in this work are initial sampling method and metamodel. To select few realizations from the ensemble in proposed “scenario reduction” method, Kantorovich distance that quantifies disparity between ensembles

using static measures is minimized by solving a mixed-integer linear programming (MILP) problem. In another approach, computationally expensive reservoir simulator is replaced by an integrated Karhunen-Loeve (KL) parameterization and polynomial chaos expansion (PCE) metamodel in Ensemble Kalman Filter (EnKF) and Markov chain Monte Carlo (MCMC).

Short-term (or real-time) production optimization using model predictive control (MPC) requires adequate representation of a complex, spatially distributed, nonlinear SAGD process. Variants of MPC that integrate real-time production and temperature data along with well and surface constraints are implemented in this research to achieve steam conformance and an optimum subcool. Adaptive MPC involves continuous re-estimation of model coefficients at each control interval, reflecting the current reservoir dynamics while gain-scheduled MPC decomposes the control problem in a parallel manner with a separate controller for each operating region. Also, nonlinear MPC (NMPC) is employed using Hammerstein-Wiener model, which is either linearized or nonlinear optimization problem is solved using interior point method.

Proposed workflows/frameworks are tested using a field-scale model of a SAGD reservoir located in northern Alberta, Canada. Both "scenario reduction" sampling method and PCE metamodel significantly reduce the computational cost while obtaining reasonable posterior distribution and production forecast. In addition, all four MPC variants successfully control the subcool in real-time, leading to lower cumulative steam-oil-ratio (cSOR) and more than 20% increment in the net present value (NPV).

Practical implications of the proposed research will be consequential in designing accurate and energy efficient CLRM workflows while satisfying the constraints offered by the SAGD surface facilities, reducing carbon footprints, and improving economics.

Preface

The research presented in this dissertation was accomplished under the supervision of Dr. Japan Trivedi. In chapters *Chapter 3*, *Chapter 4*, *Chapter 5*, and *Chapter 6*, he contributed to the concept formulation, reviewed and edited the initial draft composed by me.

A version of *Chapter 3* has been published as Patel R.G., Trivedi J., Rahim S., Li Z., 2015 "Initial sampling of ensemble for steam-assisted-gravity-drainage-reservoir history matching", *Journal of Canadian Petroleum Technology*, volume 54, issue 6, 424-441. Also, a full-length paper based on this chapter has been published in the proceedings of the *World Heavy Oil Congress 2015*. I prepared codes for various sampling methods and assisted history matching, developed the reservoir model for the case study, and analyzed the results obtained after sampling and history matching. Mr. Shahed Rahim formulated and solved an MILP problem. Dr. Zukui Li reviewed and contributed to manuscript edits.

A version of *Chapter 4* is submitted as Patel R.G., Jain T., Trivedi J., 2017 "Performance of ensemble Kalman filter and Markov chain Monte Carlo under uncertainty in forecast model", *Journal of Petroleum Science and Engineering*. Also, a full-length paper based on this chapter has been published in the proceedings of the *SPE Europec featured at 79th EAGE Conference and Exhibition*. I was responsible for the coding of conventional iterative EnKF and MCMC, running the simulations using CMG STARS, and qualitative and quantitative analysis of the history matching results. Mr. Tarang Jain developed the KL-PCE metamodel and incorporated in EnKF with my assistance.

A version of *Chapter 5* is submitted as Patel R.G., Prasad V., Trivedi J., 2017 "SAGD real-time production optimization using adaptive and gain-scheduled model-predictive-control: a field case study", *SPE Production & Operations*. Also, a full-length paper based on this chapter has been published in the proceedings of the *SPE Western Regional Meeting*. I developed routines and subroutines to construct the advanced control frameworks using adaptive and gain-scheduled MPC, performed the case study, and evaluated various aspects of the performance of the different control methods. Dr. Vinay Prasad was involved in manuscript composition.

A version of *Chapter 6* is in progress for submission as Patel R.G., Trivedi, J., 2017 "Nonlinear model predictive control of SAGD well operations for real-time production optimization" to *Journal of Process Control*. Also, a part of this chapter was presented at the *66th Canadian Chemical Engineering Conference*. I designed and coded the workflows to implement two NMPC approaches, applied nonlinear system identification techniques, and investigated the results qualitatively and using statistical measures.

To

Supreme Lord Swaminarayan

“ભારી મરજી વિના રે, કોઈથી તરણું નવ તોડાય”

(Without my wish, not a blade of grass can be broken)

and

My Fabulous Family

(Bapuji, Ba, Papa, Mummy, Vadil, Bhabhi, and Vyom)

Acknowledgements

First and foremost, many thanks to almighty supreme Lord Swaminarayan who created these petroleum reservoirs millions of years ago, providing me an opportunity to pursue my Ph.D. and pen down this thesis.

I would like to thank my supervisor, Dr. Japan Trivedi for being an ideal “sarathi” (charioteer) in this journey of doctoral studies. Being a source of immense knowledge, guidance, and motivation, he has provided an excellent research environment to enhance my research experience and learning. I appreciate the flexibility he has granted to explore and execute new ideas despite the various research challenges. From research to writing and badminton to board games, his advice has always been a piece of gem.

I express my sincere gratitude to Dr. Zukui Li for helping me with mixed-integer linear programming techniques and supervisory committee members Dr. Vinay Prasad for his guidance on process control through meaningful discussions and valuable suggestions and Dr. Juliana Leung for providing the feedback on my research.

I wish to thank my parents, Mr. Ghanshyambhai Patel and Mrs. Shardaben Patel, my backbones, who taught me to dream big and imparted the virtues to achieve them. Without their motivation and selfless sacrifices, this degree would not have been possible. I also thank my elder brother Maulik Patel and sister-in-law Apexa Patel for their never-ending love and moral support through all the highs and lows of this journey. How can I forget Vyom, our little champ who never missed to check on me saying, “Uncle! Make sure you study hard.”

While many other friends and families have provided wonderful support outside the university, I would like to extend my sincere appreciation to the families of Gaurangbhai, Mukundbhai, and Japanbhai who provided both cuisines and compassion ever since I have been in Edmonton. Their support has created a long-lasting memory in my life that I will cherish forever. In a nutshell, thank you for providing a home, away from home!

Kudos to my colleagues at NREF L2 office who are now an inevitable part of the lifelong memories. I wish to thank them for all the fun moments, summer trips, LAN and badminton games after work, and eternal (and sometimes meaningless) discussions on subjects spanning from research ideas to religions and politics to petroleum. I would also like to mention my friends back home for their unwavering motivation, the perpetual pleasure they create, and memorable holiday excursions.

I gratefully acknowledge the financial support from Natural Sciences and Energy Research Council of Canada (NSERC) and the University of Alberta for this research. Also, scholarships from ConocoPhillips Canada Limited and Faculty of Graduate Studies and Research (FGSR) in addition to the software support by Computer Modelling Group (CMG) and Schlumberger are greatly appreciated.

Table of Contents

<i>Chapter 1 – Introduction</i>	1
1.1 Background.....	2
1.1.1 Overview of Assisted History Matching.....	3
1.1.2 Real-Time Production Optimization of SAGD Reservoirs	7
1.2 Problem Statement	11
1.3 Key Objectives of Research	13
1.4 Thesis Outline.....	15
 <i>Chapter 2 – Literature Review</i>	 18
2.1 Screening/Ranking/Sampling Methods.....	19
2.2 Proxy Models Used in Assisted History Matching.....	21
2.3 Strategies Used for Real-Time Production Optimization	24
 <i>Chapter 3 – Initial Sampling of Ensemble for SAGD Reservoir History Matching</i>	 29
3.1 Introduction	30
3.2 Contemporary Sampling Techniques.....	30
3.2.1 Orthogonal Ensemble Members	31
3.2.2 Importance Sampling	32
3.2.3 K-Means Clustering	33

3.3 Proposed Scenario Reduction Method	34
3.3.1 Static Measures and Quantification of Dissimilarity in Realizations.....	34
3.3.2 Kantorovich Distance and its Minimization.....	37
3.4 Ensemble Kalman Filter	40
3.5 Application to a SAGD Reservoir	43
3.5.1 Description of the Reservoir Model	43
3.5.2 Application of Orthogonal Ensemble Members Method	44
3.5.3 Application of Importance Sampling	45
3.5.4 Application of K-Means Clustering	46
3.5.5 Application of Scenario Reduction Method	47
3.5.6 Application of EnKF	48
3.6 Results and Discussions	48
3.6.1 Screening for reduced initial ensemble	49
3.6.2 Effect of initial screening/sampling on EnKF	59
3.7 Summary.....	65
<i>Chapter 4 – Polynomial-Chaos-Expansion Based Integrated Dynamic Modeling</i> <i>Workflow for Computationally Efficient Reservoir Characterization</i>	<i>66</i>
4.1 Introduction	67
4.2 Markov Chain Monte Carlo (MCMC)	70
4.3 EnKF Algorithm.....	71
4.4 PCE Metamodel.....	74
4.4.1 Karhunen-Loeve Parameterization.....	74
4.4.2 Polynomial Chaos Expansion (PCE)	77
4.4.3 Probabilistic Collocation Method (PCM)	82
4.4.4 Integration of PCE Metamodel in EnKF Framework	85
4.5 SAGD Field Case Study	87

4.5.1 SAGD Reservoir Model.....	87
4.5.2 PCE Forward Model	88
4.5.3 Numerical Experiments.....	92
4.6 Results and Discussion	95
4.6.1 Distribution of QoI	96
4.6.2 Sensitivity of QoI to Forecast Model Uncertainty	106
4.6.3 Characterization of Posterior Distribution	109
4.7 Summary.....	113
<i>Chapter 5 – SAGD Real-Time Production Optimization Using Adaptive and Gain-Scheduled Model Predictive Control</i>	<i>114</i>
5.1 Introduction	115
5.2 Identification of Dynamic Systems	115
5.3 Model Predictive Control	121
5.3.1 Adaptive MPC	125
5.3.2 Gain-Scheduled MPC	126
5.3.3 Control Framework for Real-Time Production Optimization Using MPC ..	128
5.4 Application to the SAGD Field: A Case Study	130
5.4.1 Details of History-Matched Reservoir Model.....	130
5.4.2 Application of System Identification Techniques.....	132
5.4.3 Application of Linear MPC.....	136
5.4.4 Application of Adaptive MPC	138
5.4.5 Application of Gain-Scheduled MPC	138
5.5 Results and Discussion	140
5.5.1 Performance in Real-Time Subcool Control.....	140
5.5.2 Impact on Input (Manipulated) Variables	142
5.5.3 Effect on Production Parameters	144

5.5.4 Quantitative Analysis Using Statistical Performance Measures	146
5.6 Summary	148
<i>Chapter 6 – Nonlinear Model Predictive Control of SAGD Well Operations for Real-Time Production Optimization</i>	<i>149</i>
6.1 Introduction	150
6.2 Nonlinear Dynamic Models	150
6.3 Nonlinear Model Predictive Control	154
6.3.1 Linearization	157
6.3.2 Interior Point Algorithm	159
6.3.3 Advanced Control Workflows for SAGD Well Operations Using NMPC	162
6.4 SAGD Field Application	164
6.4.1 Identification of Nonlinear Dynamic Model.....	164
6.4.2 Application of NMPC Using Linearization.....	169
6.4.3 Application of NMPC Using Nonlinear Optimization	169
6.5 Results and Discussion	170
6.5.1 Subcool Control with NMPC	170
6.5.2 Behavior of Manipulated Variables.....	172
6.5.3 Impact on Production Performance.....	174
6.5.4 Statistical Analysis of NMPC Performance.....	176
6.6 Summary.....	178
<i>Chapter 7 – Concluding Remarks and Recommendations</i>	<i>179</i>
7.1 Concluding Remarks.....	180
7.2 Recommendations for Future Research	182
<i>Bibliography</i>	<i>184</i>

List of Tables

Table 3.1 – Quantitative analysis of production data at 1200 days after sampling... 50	50
Table 3.2 – Quantitative analysis of production data at 1200 days after update 60	60
Table 4.1 – Reservoir model parameters for the case study 88	88
Table 4.2 – Quantitative assessment of QoI approximated using 2 nd and 3 rd order PCE model at $t = 1200$ days 91	91
Table 4.3 – Quantitative analysis of QoI at $t = 1200$ days in numerical exp 1 107	107
Table 4.4 – Quantitative analysis of QoI at $t = 1200$ days in numerical exp 2 108	108
Table 4.5 – Quantitative analysis of QoI at $t = 1200$ days in numerical exp 3 109	109
Table 4.6 – Final estimates and pdf variance of model parameters estimated in experiments 2 and 3 111	111
Table 4.7 – Computational cost of different numerical experiments 112	112
Table 5.1 – Various linear model structures in System Identification 118	118
Table 5.2 – Specifics of system identification models identified for each subcool .. 134	134
Table 5.3 – Design of MPC controller for real-time production optimization 137	137
Table 5.4 – Quantitative analysis of various control algorithms used for real-time production optimization 147	147
Table 6.1 – Design parameters for input signals in nonlinear system identification 166	166
Table 6.2 – Specifics of Hammerstein-Wiener models identified for each subcool.. 166	166
Table 6.3 – Statistical analysis of nonlinear control algorithms used for real-time production optimization 176	176

List of Figures

Figure 1.1 – Workflow of closed-loop reservoir management.	3
Figure 1.2 – Overview of assisted history matching techniques.	4
Figure 1.3 – Workflow of assisted history matching using EnKF.	7
Figure 1.4 – Different types of optimization carried out at various decision-making levels in field development.	8
Figure 1.5 – Non-uniform steam chamber growth along the wellbore in SAGD.	10
Figure 1.6 – Workflow for real-time production optimization of SAGD reservoirs.	11
Figure 3.1 – Permeability values (in i-direction) of grid blocks containing core holes that were used as conditional data in Sequential Gaussian Simulation.	44
Figure 3.2 - Proportionality between $\ln(k_A^v)$ and normalized oil rate at 1200 days. .	45
Figure 3.3 – Realizations in multidimensional space where square box shows realizations selected by K-Means clustering.	46
Figure 3.4 – Normalized oil rate of reduced ensembles (blue lines) obtained using different sampling methods, superimposed on normalized oil rate of the initial ensemble (green lines). Red line shows history from field data. SC = surface conditions.	51
Figure 3.5 – Histogram of normalized oil rate at 1200 days for realizations obtained using different sampling methods and the original ensemble. SC = surface conditions.	52
Figure 3.6 – Histogram of normalized cumulative oil production at 1200 days for realizations obtained using different sampling methods and initial ensemble. .	53

Figure 3.7 – Normalized cumulative oil production of reduced ensembles (blue lines) obtained using different sampling methods, superimposed on normalized cumulative oil production of the initial ensemble (green lines). Red line shows history from field data.....	54
Figure 3.8 – Histogram of normalized steam oil ratio at 1200 days for realizations obtained using different sampling methods and the initial ensemble.	55
Figure 3.9 – Normalized steam oil ratio of reduced ensembles (blue lines) obtained using different sampling methods, superimposed on normalized steam oil ratio of the initial ensemble (green lines). Red line shows history from field data. ..	56
Figure 3.10 – Box and whisker plots representing distributions of different normalized production parameters at 1200 days obtained using simulations of all realizations of the original ensemble as well as reduced ensembles obtained using different sampling methods. Red line shows the median of each distribution.....	58
Figure 3.11 – Normalized oil rate of reduced ensembles (grey lines) obtained after EnKF update. Red line shows history from field data.	59
Figure 3.12 – Normalized water rate of reduced ensembles (grey lines) obtained after EnKF update. Red line shows history from field data.	61
Figure 3.13 – Normalized cumulative oil production of reduced ensembles (grey lines) obtained after EnKF update. Red line shows history from field data.	62
Figure 3.14 – Normalized steam oil ratio of reduced ensembles (grey lines) obtained after EnKF update. Red line shows history from field data.....	63
Figure 3.15 – Box and whisker plots representing distributions of different production parameters at 1200 days, obtained using simulations of all realizations of reduced ensembles obtained after EnKF update	64
Figure 4.1 – Proposed idea of comprising PCE metamodel in the EnKF framework. .	70
Figure 4.2 – Monotonic reduction in eigen values of covariance matrix obtained using singular value decomposition.	76
Figure 4.3 – Number of total terms (P) for different orders and dimensions of random variables in PCE.	80
Figure 4.4 – Representation of Gaussian quadrature technique where roots of the 2 nd order polynomial span high probability region of $P(X)$ and gives good linear approximation of output $Y(X)$	83
Figure 4.5 – Reservoir characterization workflow using PCE metamodel with EnKF.	86

Figure 4.6 – 3D view of the field-scale reservoir model (left) and trajectories of all wells (right).....	87
Figure 4.7 – First 100 normalized eigen values of the covariance matrix (left) and energy associated with each of them (right).	89
Figure 4.8 – Blind test results of 2 nd order PCE metamodel using 100 random vectors (left) and convergence of PCE coefficients for each QoI (right).....	90
Figure 4.9 – QoIs for initial ensemble (grey lines) in traditional EnKF demonstrating sufficient solution space mapped by the prior distribution. The red curve shows the history obtained from the field.....	92
Figure 4.10 – Experimentation for scaling of proposal variance in MCMC. Top left: high acceptance rate. Top right: low acceptance rate. Bottom: optimal acceptance rate.	94
Figure 4.11 – First 1000 proposals displaying smaller burn-in period for model parameters in Markov chain with 10 million samples.....	95
Figure 4.12 – Normalized oil rate after each data assimilation step in numerical experiment 1 (benchmark case). Red curve represents the field history and grey-shaded area corresponds to the ensemble predictions.....	96
Figure 4.13 – Normalized cumulative oil production after each data assimilation step in numerical experiment 1 (benchmark case). Legends in this figure can be described similarly as Figure 4.12.....	97
Figure 4.14 – Normalized cumulative water production after each data assimilation step in numerical experiment 1 (benchmark case). Legends in this figure can be described similarly as Figure 4.12.....	98
Figure 4.15 – Normalized steam oil ratio after each data assimilation step in numerical experiment 1 (benchmark case). Legends in this figure can be described similarly as Figure 4.12.....	99
Figure 4.16 – Normalized oil rate after each data assimilation step in numerical experiment 2 (EnKF under PCE uncertainty). Legends in this figure can be described similarly as Figure 4.12.....	100
Figure 4.17 – Normalized cumulative oil production after each data assimilation step in numerical experiment 2 (EnKF under PCE uncertainty). Legends in this figure can be described similarly as Figure 4.12.	101

Figure 4.18 – Normalized cumulative water production after each data assimilation step in numerical experiment 2 (EnKF under PCE uncertainty). Legends in this figure can be described similarly as Figure 4.12.	102
Figure 4.19 – Normalized steam oil ratio after each data assimilation step in numerical experiment 2 (EnKF under PCE uncertainty). Legends in this figure can be described similarly as Figure 4.12.....	103
Figure 4.20 – Normalized QoI for every 1000 th sample of Markov chain in numerical experiment 3 (MCMC under PCE uncertainty). Legends in this figure can be described similarly as Figure 4.12.....	104
Figure 4.21 – Box plots comparing the distribution of QoI at 1200 days for all numerical experiments. Red line and blue dots show median and mean of each distribution respectively while continuous green line depicts true value of the QoI. The top and bottom of every box correspond to percentiles P25 and P75 and end points of the whisker represent the minimum and maximum values.	105
Figure 4.22 – Every 1000 th sample of well-mixed Markov chain in numerical experiment 3 (MCMC under PCE uncertainty).....	105
Figure 4.23 – Posterior characterization of model parameters after each assimilation step in numerical experiment 2 (EnKF under PCE uncertainty).	110
Figure 4.24 – Posterior density estimate of stochastic variables obtained in numerical experiments 2 and 3. The prior is $\mathcal{N}(0,1)$ for all model parameters.	111
Figure 5.1 – Structure of Prediction Error (PE) model in System Identification.	116
Figure 5.2 – Workflow for linear model order selection in System Identification....	121
Figure 5.3 – Control framework of Model Predictive Control.	124
Figure 5.4 – Schematic representation of Adaptive MPC.	126
Figure 5.5 – Schematic representation of Gain-Scheduled MPC.	127
Figure 5.6 – Control framework for real-time subcool control using (a) Linear MPC (b) Adaptive MPC and (c) Gain-Scheduled MPC.....	129
Figure 5.7 – 3D view (left) and IK view for plane 26 along j-direction with well pair divided in five sections (right) of history-matched reservoir model.	130
Figure 5.8 – History matching results of reservoir model selected for real-time production optimization.....	131
Figure 5.9 – Results of autocorrelation and cross-correlation tests for Subcool 2. Yellow rectangle box shows 99% confidence interval.	133

Figure 5.10 – Results of cross-validation for all subcools. Blue line represents predicted output from the model while grey line depicts validation data.	135
Figure 5.11 – Segmentation of operating range of subcool in real-time production optimization using gain-scheduled MPC.	139
Figure 5.12 – Subcool of all segments of the well pair obtained using different control methods in real-time production optimization.	141
Figure 5.13 – Minimum subcool of the well pair obtained using different control methods in real-time production optimization.	142
Figure 5.14 – Performance of steam injection rate (short tubing) in adaptive MPC (left) and gain-scheduled MPC (right) as compared to base case and linear MPC. .	143
Figure 5.15 – Performance of steam injection rate (long tubing) in adaptive MPC (left) and gain-scheduled MPC (right) as compared to base case and linear MPC. .	144
Figure 5.16 – Performance of liquid production rate in adaptive MPC (left) and gain-scheduled MPC (right) when compared with base case and linear MPC.	144
Figure 5.17 – Effect of adaptive MPC (left) and gain-scheduled MPC (right) on oil production rate. SC = surface conditions.	145
Figure 5.18 – Effect of adaptive MPC (left) and gain-scheduled MPC (right) on cumulative oil production.	145
Figure 5.19 – Effect of adaptive MPC (left) and gain-scheduled MPC (right) on cumulative steam oil ratio.	146
Figure 6.1 – Hammerstein-Wiener model in nonlinear model identification.	152
Figure 6.2 – Linearization of a nonlinear model for a given input signal (left) and in the neighbourhood of an operating point (right).	157
Figure 6.3 – Control framework for real-time SAGD well operations using NMPC with (a) Linearization and (b) Interior Point algorithm.....	163
Figure 6.4 – RBS signals generated for nonlinear system identification in NMPC. ..	165
Figure 6.5 – Results of cross-validation for Hammerstein-Wiener models identified in nonlinear system identification. Blue line represents predicted output from the model while grey line depicts validation data.	167
Figure 6.6 – Results of residual tests for Hammerstein-Wiener model of Subcool 2. Yellow rectangle box shows 99% confidence interval.	168
Figure 6.7 – Subcool of all segments of the well pair obtained using different linear/nonlinear control methods in real-time production optimization.....	171

Figure 6.8 – Minimum subcool of the well pair obtained using different linear/nonlinear control methods in real-time production optimization.....	172
Figure 6.9 – Performance of steam injection rate (short tubing) in NMPC using linearization (left) and interior point algorithm (right) when compared with base case and linear MPC.....	173
Figure 6.10 – Performance of steam injection rate (long tubing) in NMPC using linearization (left) and interior point algorithm (right) when compared with base case and linear MPC.....	173
Figure 6.11 – Performance of liquid production rate in NMPC using linearization (left) and interior point algorithm (right) when compared with base case and linear MPC.....	174
Figure 6.12 – Effect of NMPC using linearization (left) and interior point algorithm (right) on oil production rate. SC = surface conditions.	175
Figure 6.13 – Effect of NMPC using linearization (left) and interior point algorithm (right) on cumulative oil production.	175
Figure 6.14 – Effect of NMPC using linearization (left) and interior point algorithm (right) on cumulative steam oil ratio.....	176

Chapter 1

Introduction

1.1 Background

Alberta's oil sands are the third largest proven crude oil reserves in the world, which is 70% of Alberta's and 25% of Canada's total oil reserves. Only 10% of the oil sands are located near the surface for which surface mining can be economical. As a result, a thermal in-situ recovery process is used to extract bitumen, widely known as Steam Assisted Gravity Drainage (SAGD). The primary mechanism of this process is viscosity reduction by heating the bitumen to increase its mobility. In this process, steam is injected through horizontal well at the top of the reservoir and bitumen is produced through gravity drainage from the horizontal well at the bottom. SAGD was devised in 1978 and it has been implemented successfully in oil sands. However, the research and field experience indicate the substantial chances of improvement and optimization of the process. In order to optimize various process parameters, it is necessary to enhance and update our knowledge about reservoir parameters because reservoir dynamics play a larger role in production performance and often drives the decision related to oil/gas fields. Though uncertainty in geological properties cannot be removed, it can certainly be reduced up to a level that firm decisions can be made related to the reservoir. The process of reducing uncertainty in reservoir parameters by integrating the abundant different types of data available from the field is widely known as history matching. Once the history matched model is obtained, it can be further used for production optimization at various decision-making levels.

Recently, Closed-Loop Reservoir Management (CLRM) – a combination of near-continuous data assimilation and model-based optimization – has been proposed by several authors. While the data-assimilation reduces uncertainty in the unknown reservoir properties, optimization provides the best operating strategy. The aim of CLRM is to improve the reservoir performance in terms of oil recovery and hence the economics of the process. Jansen et al. (2009) provide a detailed explanation of the CLRM concept. Foss and Jensen (2011) further develops the concept of CLRM and provides new insights. *Figure 1.1* outlines the different elements of the CLRM. The improvement of two of the elements i.e., assisted history matching and short-term (or real-time) production optimization is focused in this thesis. In the next two sub-sections *1.1.1* and *1.1.2*, an overview of assisted history matching methods and real-time production optimization of SAGD reservoirs are explained respectively.

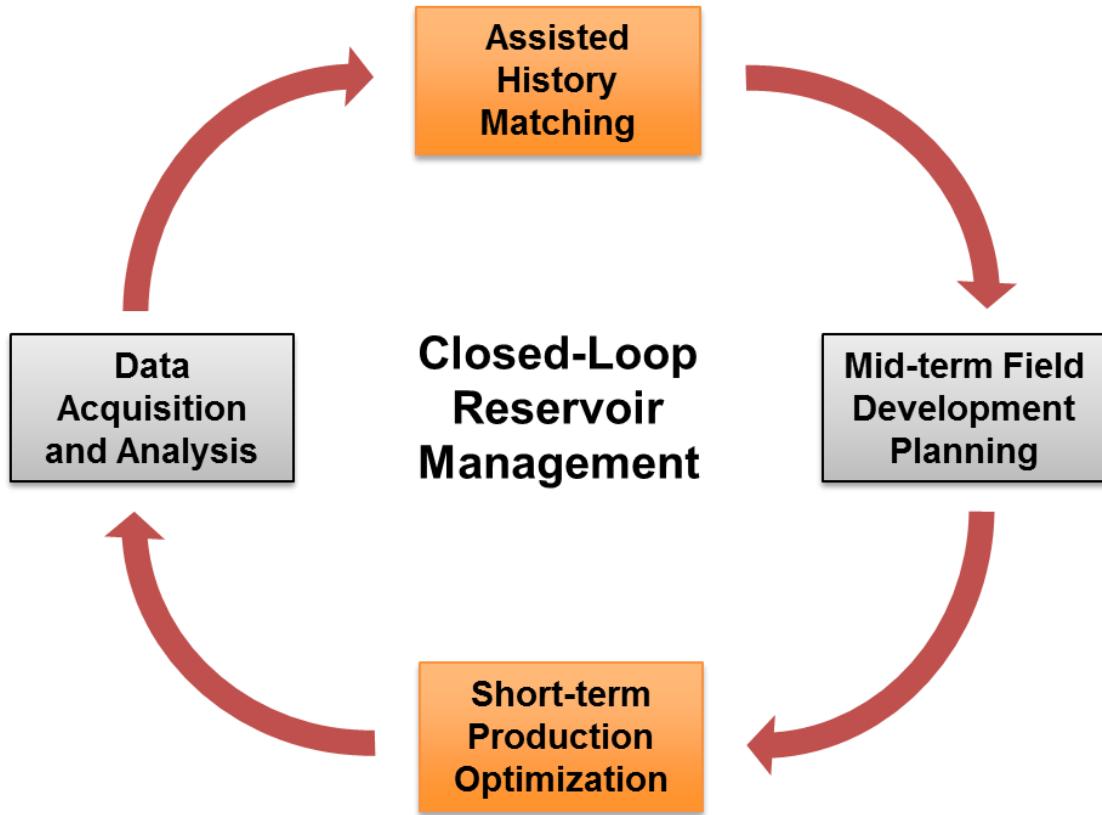


Figure 1.1 – *Workflow of closed-loop reservoir management.*

1.1.1 Overview of Assisted History Matching

History matching is an inverse problem in which observations are used to calculate the unknown model parameters. Like other inverse problems, history matching is also challenging to solve due to its non-uniqueness. To try various possible combinations of unknown parameters manually is a tedious and inefficient task. Agarwal et al. (2000) noted that it took them almost 12 months of intensive work to obtain history match manually, which is not a desirable approach, especially in the era of real-time history matching. Therefore, various statistical and mathematical methods have been applied in history matching (see *Figure 1.2*) with the help of easily available computing resources. It is widely known as assisted/automatic history matching. The process is systematic, computationally efficient, and capable of providing fruitful results. Therefore, many applications of the assisted history matching techniques can be found in the literature.

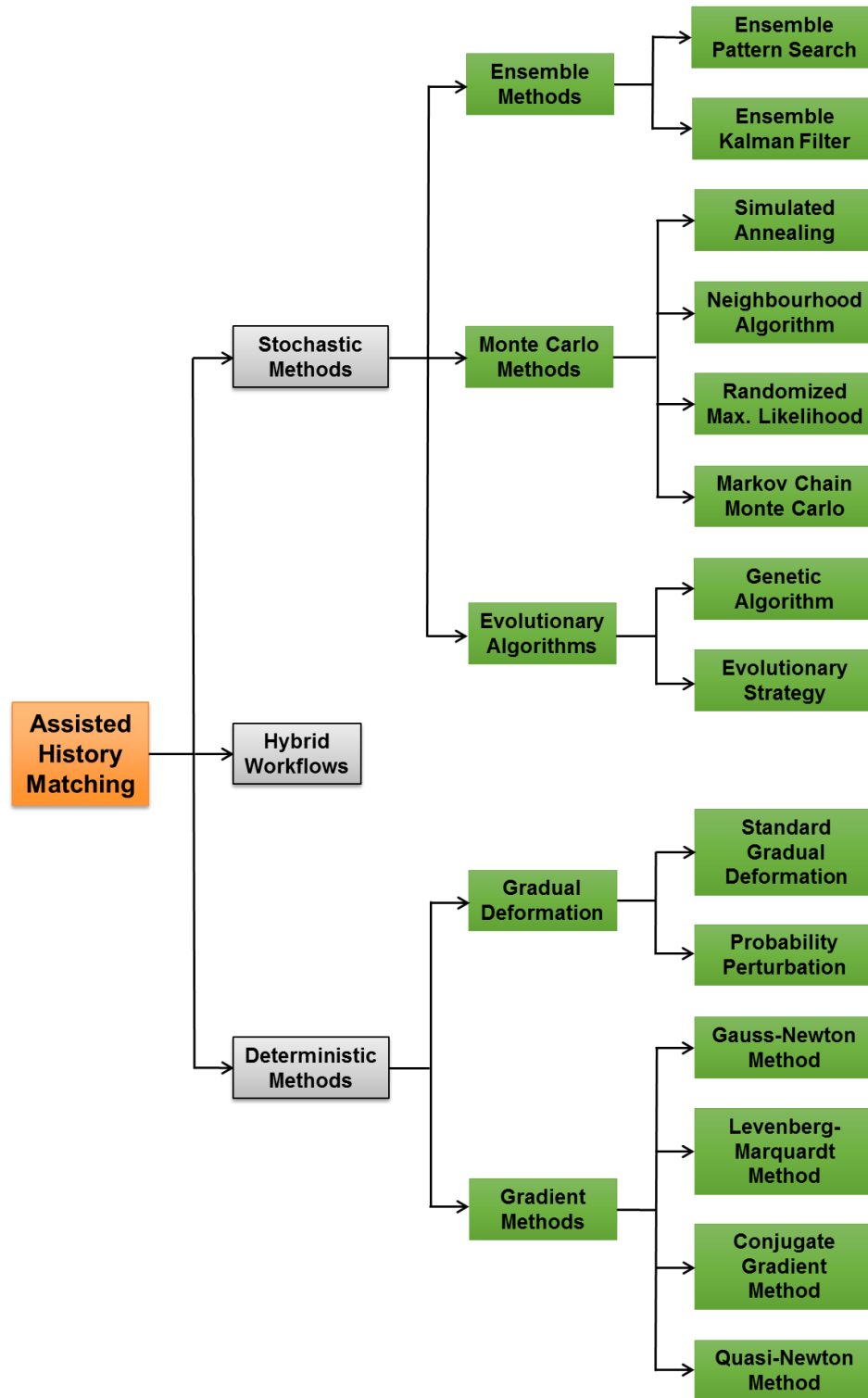


Figure 1.2 – Overview of assisted history matching techniques.

Multiple history-matched models are required to quantify risk and uncertainty associated with the reservoir management. Randomized Maximum Likelihood (RML) comprises joint sampling of model parameters (m) and observation data from the Gaussian prior and then conditional realization m_{rml} is obtained by solving the following equation:

$$m_{rml} = \underset{m}{\operatorname{argmax}} \left[\exp\left(-\frac{1}{2}(m - m^*)^T C_M^{-1}(m - m^*) - \frac{1}{2}(g(m) - d_{obs}^*)^T C_D^{-1}(g(m) - d_{obs}^*)\right)\right] \quad (1.1)$$

where m^* and d_{obs}^* are the unconditional realizations of model variables and observation data respectively, $g(m)$ is the functional relationship between model parameters and data while C_M^{-1} and C_D^{-1} are covariance of model parameters and error variance respectively. The only difficulty in RML is minimizing Eq. (1.1). Markov chain Monte Carlo (MCMC) method is another technique capable of producing several reservoir models from posterior distribution such that its probability depends on the prior distribution. The process includes two steps i.e. proposal step and acceptance step. Initially, a model is proposed from the prior distribution and at each step in the chain, new model is proposed. Based on acceptance probability defined by Hastings, the model is tested and it is decided whether to accept the new model or retain the old model. However, this technique requires large number of iterations to converge to a stationary posterior and ultimately results into impractical computational cost, especially when number of model parameters are large.

Ensemble Kalman Filter (EnKF) has emerged as an efficacious tool of history matching, mainly because of its ability to adapt large-scale nonlinear systems and simplicity. EnKF, unlike other assisted history matching methods, can provide sequential updating of multiple reservoir models simultaneously, assimilate different types of data, and manage a large number of model parameters. Also, it offers the uncertainty quantification as an outgrowth. EnKF was used initially for estimation of approximately known parameters in the dynamic two-phase model by Lorentzen et al. (2001). Application of EnKF in history matching was first proposed by Naevdal et al. (2003) indicating promising results.

As demonstrated in *Figure 1.3*, the workflow of history matching using EnKF primarily includes two steps: Forecast Step and Analysis Step. In forecast step, all the realizations in the ensemble are forwarded using numerical simulation from current timestep to next timestep. Equation that represents forecast step can be shown as,

$$\begin{bmatrix} u_k^j \\ d_k^j \end{bmatrix} = f \begin{bmatrix} m_{k-1}^j \\ u_{k-1}^j \end{bmatrix} \quad \forall j \in [1, N_e] \quad (1.2)$$

where u_k^j denotes state variables of j^{th} realization at timestep k , d_k^j denotes production data for the forecast realization j at timestep k , m_{k-1}^j is the model parameters of j^{th} realization at timestep $k - 1$ that can be either initial timestep or previously updated timestep, and N_e shows total number of realizations in ensemble. Then, state vectors are used to calculate covariance of predicted model states using equation,

$$C_{Y_k}^p = \frac{1}{N_e - 1} (Y_k^p - \overline{y_k^p})(Y_k^p - \overline{y_k^p})^T \quad (1.3)$$

where subscript p symbolizes predicted state (before update), $C_{Y_k}^p$ denotes covariance matrix calculated for all state vectors Y_k while $\overline{y_k^p}$ shows mean of state variables calculated across the ensemble before update. Then, Kalman gain denoted as K_{gain} is computed using equation,

$$K_{gain} = C_{Y_k}^p H^T (H C_{Y_k}^p H^T + R)^{-1} \quad (1.4)$$

where H and R are measurement operator and measurement error covariance matrix respectively.

Next, in the analysis step, each realization of the ensemble is updated using the Kalman gain where the value of update is different for each realization, which is proportional to the error between predicted output and noisy measurements (d_k^{obs}), equation for which can be written as,

$$y_k^{j,a} = y_k^{j,p} + K_{gain} (d_k^{j,obs} - H y_k^{j,p}) \quad \forall j \in [1, N_e] \quad (1.5)$$

where subscript a represents analyzed (updated) state vector. As the history matching using EnKF only depends on the predicted ensemble (or ensemble from the previous analysis step) and measurements from the field, it has an upper hand for continuous or real-time updating of reservoir model as compare to other methods.

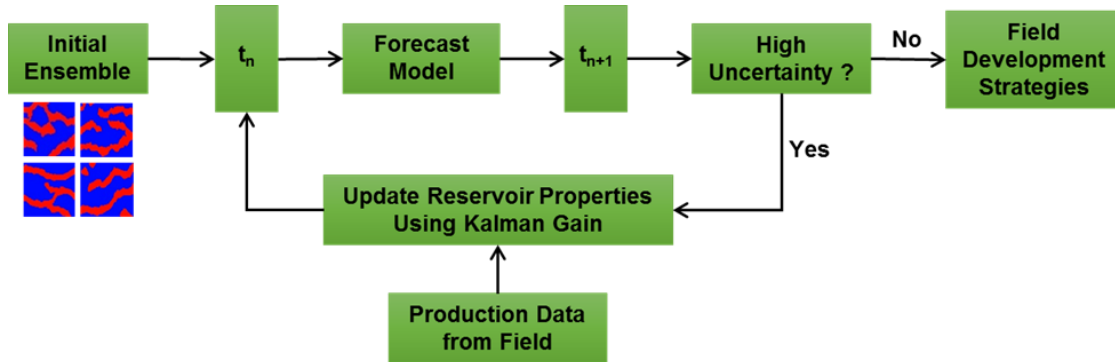


Figure 1.3 – Workflow of assisted history matching using EnKF.

Non-iterative nature of EnKF makes it computationally efficient in analysis step; however, forward simulation of each ensemble member in forecast step is generally performed by a numerical simulator. Iterative solution of highly nonlinear pressure and saturation equations in the simulator results into impractical computing cost, especially in case of SAGD reservoirs. Therefore, it has been a major challenge against the application of EnKF in field cases. In the proposed research, a couple of ways to make EnKF viable in terms of computing cost are implemented. Related literature review and methodology are described in the upcoming chapters.

1.1.2 Real-Time Production Optimization of SAGD Reservoirs

Once the reservoir model with minimum uncertainty in unknown parameters is obtained through assisted history matching, it is used further to optimize various input parameters in reservoir management with a view to maximize oil recovery and achieve better economics. At distinct decision-making levels that are typically distinguished based on time-scale, optimizations with different objective functions and variables are carried out. *Figure 1.4* describes various types of optimization and the corresponding time scale for which decisions can be made. Arrows in the figure indicate the typical flow of execution for each level, however, seldom is the whole exercise performed in an integrated manner. As shown in the figure, long-term and medium-term

optimization are generally implemented before day-to-day operations of the reservoir start. Initially, at the reservoir development stage, future field plans are designed using long-term optimization that involves decisions related to surface facilities and drainage strategy. Mid-term optimization is performed to decide the well placements and their target injection-production rates after the end of exploration phase. However, only long-term and mid-term optimizations are not sufficient for the efficient and dynamic routine field operations as they involve many assumptions regarding well operations (for e.g. injection well is operated at a constant rate for a particular time interval) and small-scale heterogeneities, which cannot be captured by history-matched model due to its higher grid resolution. Also, due to inherent errors in several parameters used to create the numerical reservoir model, decisions of long-term and mid-term optimizations won't be effective enough for reservoir operations with shorter time-scale. As a result, short-term optimization, commonly referred as "real-time production optimization" in the literature that involves supervisory and regulatory control of well operations has become popular in the latest field practices.

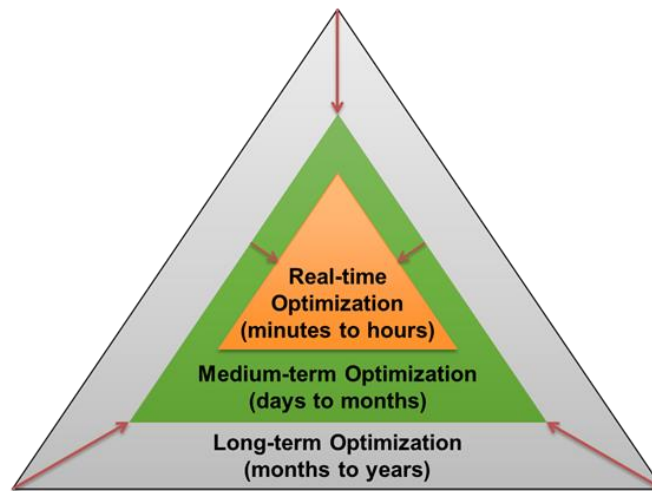


Figure 1.4 – *Different types of optimization carried out at various decision-making levels in field development.*

As per the definition proposed by Saputelli et al. (2003), real-time production optimization consists of measuring real-time data, calculating the production parameters for the next control interval and then implementation of the calculated controls at a particular frequency. Advancement in field monitoring technology over the last decade has led the oil industry towards the development of "intelligent oil

fields" (also known as "smart fields" or "i-field" or "e-field"). Such fields are equipped with modern sensing and control devices such as permanent downhole sensors, fiber-optic sensor arrays and inflow/outflow control devices that can measure and regulate various parameters in real-time; making the implementation of real-time optimization possible. Frequency or time-scale in real-time production optimization is generally decided based on the maximum time that can be afforded between the measurement of the data and control of the variables. However, time-scale for real-time optimization is much shorter as compared to long or mid-term optimization, normally spanning from sec/minutes to hours/day. Since real-time data depicts the current reservoir conditions, well parameters are optimized such that a variable can be maintained at a specified target. Ultimately, this practice results into the maximum efficiency of the oil recovery process for that particular control interval and when it is continued for a longer period, real-time optimization can provide a considerable benefit in terms of the economics of the process.

The primary objective of the real-time production optimization is to improve efficiency and hence the economics of the oil recovery process. In SAGD, it immensely depends on the amount of steam injected and its conformance in the reservoir. Uniform growth of steam chamber along the wellbore is important as it leads to the improved steam delivery in the reservoir, ultimately increasing bitumen recovery. However, as shown in *Figure 1.5*, steam conformance near the wellbore region in SAGD is restricted by numerous parameters like heterogeneity in geological properties (i.e. porosity and permeability), fluid composition and their properties as well as saturations. These heterogeneities may lead to different steam conformance in well pairs as close as 100 meters (Gotawala and Gates 2012) mostly due to variable injectivity along the wellbore, different mobility ratio, and the distinct temperature-viscosity relationship of bitumen. Also, wellbore geometry creates a significant pressure drop in the annulus of the injector well due to lower density and high flow rates of steam. It allows the injection of varying steam quality and amount injected along the wellbore (Edmunds and Gittins 1993) that contributes to the heterogeneous steam chamber development. Since non-conformance of steam may lead to suboptimal usage of steam, it will affect the bitumen recovery and economics of SAGD adversely. It can be mitigated by controlling the liquid pool around producer well (Gates and Leskiw 2010), the process commonly known as steam trap control.

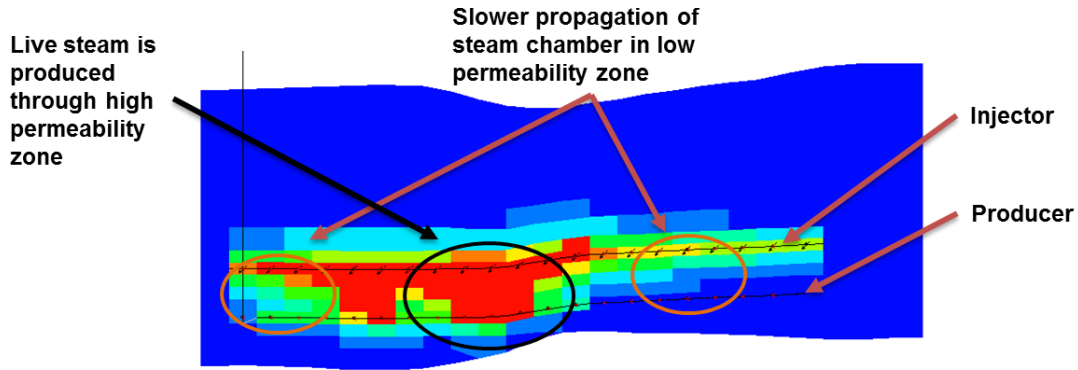


Figure 1.5 – *Non-uniform steam chamber growth along the wellbore in SAGD.*

Working principle of steam trap control in SAGD is analogous to that of thermodynamic traps used for steam heating control in the process industry. However, in SAGD, liquid pool acts as a steam trap that directs the live steam away from the producer due to its lower temperature. The liquid pool is basically a mixture of mobilized bitumen and steam condensate accumulated near the producer well because of convective heat transfer (between steam and reservoir at the edge of the steam chamber) and gravity drainage. The height of liquid pool is controlled by changing the liquid production rate of the producer well. If the liquid is produced at a lower rate, the liquid pool may rise well above the producer. It can reduce the exposure of steam chamber to the bitumen, a consequence detrimental to oil recovery. In contrast, when the height of liquid pool is significantly reduced by producing more fluid, most of the injected steam may directly be produced instead of heating the bitumen in the reservoir. The phenomenon is known as steam breakthrough which reduces the thermal efficiency of SAGD. As the height of liquid pool cannot be measured directly, subcool (or interwell subcool) is considered. It can be defined as the temperature difference between injected steam and produced liquid (Le Ravalec et al. 2009).

Figure 1.6 depicts optimization of injection-production parameters in real-time, which is often of very high importance due to relatively higher production cost in SAGD. By maintaining the subcool at a predefined optimum set-point with the help of adequate control strategy, production of live steam can be avoided without undermining the steam chamber development.

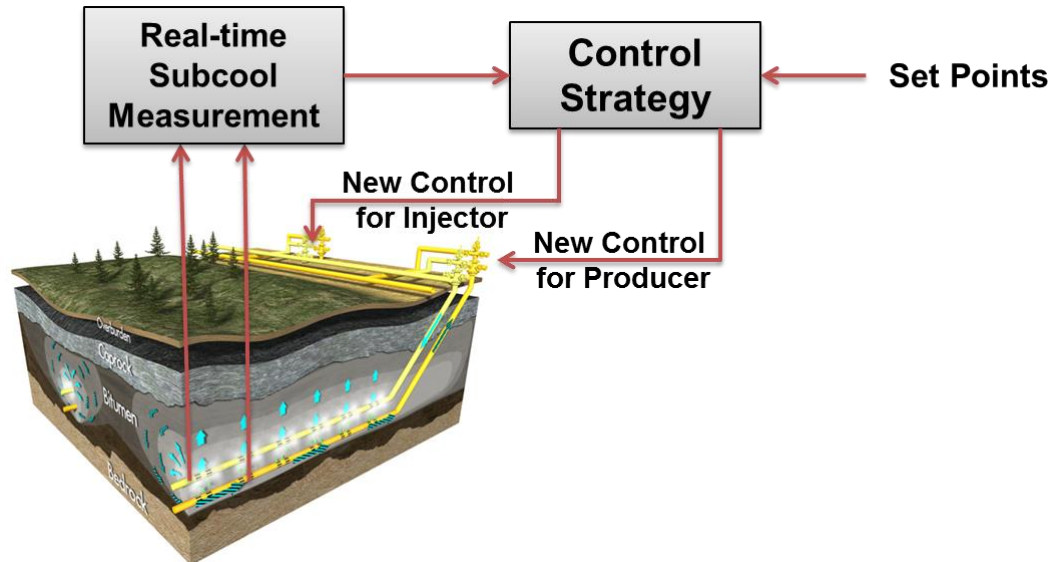


Figure 1.6 – Workflow for real-time production optimization of SAGD reservoirs.

1.2 Problem Statement

As noticed before, the primary limitation for assisted history matching of field-scale reservoir models is impractical computational cost, making them less prone to sequential updating of the reservoir properties. Likewise, Model Predictive Control (MPC) has been used for real-time production optimization, yet with confined capabilities due to lack of proper approaches to handle the nonlinearity of the reservoir dynamics. Limitations offered by current methods are described in this section that can lead to several hypotheses stated at the end of the section.

For effectual EnKF performance with a smaller ensemble size, the subset selected using a ranking/selection method should retain three important characteristics of the initial ensemble i.e. span, variability, and unbiasedness. Solution space of EnKF algorithm is bound by the span of the ensemble (Evensen 2009). Therefore, if the span of the subset chosen is smaller than initial ensemble then solution space for the subset will also be smaller and hence there will be chances of ensemble moving in unrealistic domains after updates (Chitrlekha et al. 2010). The subset should have maintained the same variability among the realizations as the initial ensemble because if the variability of the subset is limited then after few assimilation steps in EnKF, the ensemble will be collapsed (Myrseth et al. 2012). Also, Kalman gain calculated from

such ensemble may introduce spurious correlations and update state parameters in impractical regions (Chen and Oliver 2010). In addition, realizations should be selected from all quantiles of the initial ensemble so that subset will be unbiased. If the subset is biased, then the solution may lie outside of the space covered by the subset and hence it will create the convergence problem (Jensen 2007). A comprehensive ranking/selection method that considers all these aspects and is computationally efficient requires further attention for history matching applications.

Most of the proxy/meta/surrogate models in literature have been utilized for history matching of a single reservoir model with few undiagnosed reservoir parameters. Primary reasons can be either the complexity current proxy models create when used for a higher number of realizations or its inability to incorporate a higher number of parameters. In addition, when the proxy model is used in history matching, it might not be able to represent the physical process since it is purely a mathematical model, expressing the relationship between input and output parameters. Therefore, proxy models may not serve as intended in uncertainty assessment if applied without proper care (Goodwin 2015), which can lead to the poor estimation of history matching parameters. Such restraints offered by current techniques create a scope for an improved metamodel that can be incorporated in the framework of latest assisted history matching methods while reducing computing cost. The effect of forecast model uncertainty on data assimilation also requires additional consideration.

MPC controller is flawless if a mismatch between output predicted by a dynamic model and physical plant is zero. Such controller can predict the outputs with no error, leading to exact cost function calculation and hence, the foolproof change in input variables to achieve the prescribed target. Dynamic models based on first principles generally give accurate estimates. However, for complex systems like SAGD reservoirs, such models are in form of differential equations that can be solved using computationally intensive numerical solvers. So far in the literature, reservoir dynamics in MPC is mostly represented using either linear step response model or one-dimensional ordinary differential equation (ODE). Although MPC is robust enough to handle minor plant/model mismatch, use of such simplified models may undervalue the capability of MPC in controlling SAGD reservoirs as it is more complex and highly nonlinear process. Therefore, an all-inclusive control framework that addresses the nonlinear behavior of SAGD over an extended control period, and also comply with constraints

of surface facilities is necessary for efficacious real-time production optimization. It can eventually render maximum NPV of bitumen asset while minimizing the environmental footprints.

Scopes of improvement in current methods as well as research gap explained in this section led to following hypotheses:

H1 – *Subset of realizations with similar statistical characteristics as a large initial ensemble can reduce the required simulations without compromising the quality of assisted history matching results.*

H2 – *Mathematical model that handles a large number of unknown parameters can be built using few full physics simulations and integrated easily into current assisted history matching frameworks to replace commercial reservoir simulator.*

H3 – *Real-time production optimization can be improved using strategies that can correctly represent nonlinear reservoir dynamics in MPC, which will ensure faster convergence and better subcool control.*

Considering the 168 billion barrels of estimated reserves of bitumen in Alberta, the invention of viable methods and approaches for real-time model updating and production optimization will be of practical interest to petroleum industries while improving production, reducing fuel costs and mitigating environmental footprints.

1.3 Key Objectives of Research

To address the above described problems and test the proposed hypotheses, the proposed research is divided into 4 sequential components. Research objectives and corresponding questions to be answered for each of them can be outlined as follows:

1) Formulate optimal sampling/screening method for subset selection based on probability distance minimization.

- ✓ How to provide a unique identity to each realization?
- ✓ How to compare and minimize dissimilarity between two ensembles?
- ✓ How is the performance of proposed sampling method as compared to other well-known methods after sampling as well as history matching?

2) Develop a workflow for computationally efficient assisted history matching using appropriate proxy model.

- ✓ Can a large number of unknown geological parameters be parameterized?
- ✓ How to build a versatile proxy model for SAGD reservoirs?
- ✓ How to integrate the proxy model with the EnKF framework?
- ✓ How are the history matching results as compared to conventional EnKF workflow?

3) Implement Adaptive MPC and Gain-Scheduled MPC for effective real-time subcool control in SAGD reservoirs.

- ✓ How to find a proper linear model structure based on system identification theory?
- ✓ How to incorporate recursive estimation of coefficients in control workflow?
- ✓ Can multiple controllers with different configurations handle the challenging control situations during the life-cycle of SAGD reservoirs?
- ✓ How is the performance of proposed approaches as compared to Linear MPC?

4) Employ nonlinear system identification model in MPC for precise representation of reservoir dynamics.

- ✓ Which nonlinear dynamic model should be used?
- ✓ How to comprise nonlinear model in MPC?
- ✓ Does nonlinear system model make a positive impact on subcool control as compare to linear model?

In addition, all proposed objectives of research are verified using a field-scale reservoir model of Underground Test Facility (UTF) Phase B1, a SAGD reservoir located 60 km north of Fort McMurray in northeastern Alberta, Canada. Reservoir model was built in-house using operational data and well logs provided by Alberta Oil Sands Technology and Research Authority (AOSTRA), currently known as Alberta Energy Research Institute (AERI).

1.4 Thesis Outline

The organization of this dissertation is summarized below with a brief explanation of each chapter:

Chapter 2: Literature review

Chapter 2 contains the detailed review of the previous work done to improve the computational cost of the assisted history matching as well as real-time production optimization. In literature, two approaches are discussed that are either to reduce the number of realizations in the initial ensemble or replace simulator with a mathematical model. Subsection 2.1 comprises different techniques for screening/ranking/sampling of the initial ensemble proposed by various authors while next subsection contains details about distinct proxy models used in place of commercial reservoir simulator for assisted history matching. Similarly, in the last subsection, various attempts made to improve control strategy used in production optimization of SAGD reservoirs are reviewed.

Chapter 3: Initial sampling of ensemble for SAGD reservoir history matching

In this chapter, a novel sampling method based on the probability distance minimization is discussed to generate an initial ensemble of reduced size. The method considers multiple static measures and geological properties, and uses Kantorovich distance to quantify the probability distance between original ensemble and reduced ensemble, which is then optimized using mixed integer linear programming (MILP) technique. To show the effectiveness of the method, we have shown history matching of a SAGD reservoir using the smaller size initial ensemble derived from the proposed method and compared with the original ensemble.

Chapter 4: Polynomial-Chaos-Expansion based integrated dynamic modeling workflow for computationally efficient reservoir characterization

In this chapter, we take the opportunity to evaluate and compare the performance of EnKF and MCMC using Polynomial Chaos Expansion (PCE) based forecast model. Proposed forecast model relies on reducing parameter space using Karhunen–Loeve (KL) expansion that preserves the two-point statistics of the given random field. Random variables from KL expansion and orthogonal polynomials corresponding to the

prior probability density function (pdf) constitute the set of input parameters in PCE. Further, non-intrusive probabilistic collocation method (PCM) is used to compute PCE coefficients. PCE forecast model is then used in EnKF and MCMC to calculate the likelihood of the samples in place of high fidelity full physics simulation runs. Performance of both assimilation techniques is assessed under forecast model uncertainty using rigorous qualitative and quantitative analysis as well as posterior distribution characterization.

Chapter 5: SAGD real-time production optimization using adaptive and gain-scheduled model predictive control

In this chapter, two novel workflows are proposed to handle nonlinear reservoir dynamics in MPC. The first approach is adaptive MPC that includes continuous re-estimation of the model at each control interval. It allows the evolution of the coefficients of a fixed model structure such that the updated system identification model in MPC controller reflects current reservoir dynamics adequately. Another approach, gain-scheduled MPC, decomposes the subcool control problem in a parallel manner and uses a bank of multiple controllers rather than only one controller. It ensures effective control of the nonlinear reservoir system even in adverse control situations by employing appropriate variations in input parameters based on the operating region.

Chapter 6: Nonlinear Model Predictive Control of SAGD Well Operations for Real-Time Production Optimization

Two completely novel approaches to implement nonlinear plant model in MPC are proposed in *Chapter 6*. First approach includes linear approximation of nonlinear dynamic model using structurally similar linear model. Approximations is used to estimate nonlinear dynamics of the system in local neighbourhood of the input signals used for linearization. Cost function in the MPC can be minimized using quadratic programming (QP) over the specified prediction horizon using linear approximation. Another approach is to use nonlinear dynamic model for prediction of the plant states and/or outputs, which makes the cost optimization problem nonconvex. Interior point algorithm is implemented to minimize the nonlinear cost function and thereby, to obtain the optimum input parameters.

Chapter 7: Concluding remarks and recommendations

Final outcomes are summarized and possible directions for future research are discussed in this chapter.

Finally, this is a paper-based thesis and hence some information may repeat in the different chapters, especially in the "Introduction" section and reservoir model description.

Chapter 2

Literature Review

2.1 Screening/Ranking/Sampling Methods

Various authors have presented different methods that use either dynamic or static measures to rank/select the subset of realizations from the initial ensemble. Ballin et al. (1992) first proposed the idea of ranking stochastic realizations. Instead of using comprehensive flow simulator for all realizations, they used tracer model as a fast simulator to first rank the realizations by preserving the quantiles and then applied fine-scaled simulations to only those ranked realizations. Saad et al. (1996) used 3D streamtube tracer simulator and ranked the geological realizations based on the results of single phase tracer simulations. Streamline simulation based ranking criterion was proposed by Idrobo et al. (2000) in which realizations were ranked on the basis of time-of-flight connectivity calculated for each realization using streamline simulator. Ates et al. (2003) presented a field example using the method proposed by Idrobo et al. (2000) and selected optimistic, most likely and pessimistic realizations for history matching. Though streamline simulation is much faster than the conventional simulation with finite difference approaches, it might not capture the gist of simultaneous flow of fluid and heat in the case of thermal recovery processes. In addition, various simplified fluid flow assumptions are made in streamline simulation (Gilman et al. 2002). Such limitations of dynamic ranking measures make it inappropriate to select geological realizations of SAGD reservoirs from the original ensemble in an efficient manner; a necessity for computationally effective assisted history matching using EnKF.

Ranking methods based on static measures were also proposed by numerous authors. Deutsch and Srinivasan (1996) proposed a ranking method based on the static measures like net-to-gross ratio, net pore volume and average permeability where a cell is considered to be a net cell based on some combination of lithofacies, porosity, and permeability threshold. Deutsch (1999) used geo-object connectivity, connectivity to a well location and connectivity between multiple wells as static ranking measures. Hird and Dubrule (1998) tried to predict the reservoir performance based on reservoir connectivity characteristics. They defined a connectivity parameter named 'resistivity index' for each grid block where the minimum cumulative value of the parameter shows the path that offers minimum resistance. Reservoir performance parameters such as secondary recovery efficiency and drainable hydrocarbon pore volume were

estimated using the connectivity parameter. McLennan and Deutsch (2005) proposed four different types of static measures, volumetric, statistical, global connectivity and local connectivity measures, to rank the geological realizations of SAGD reservoirs. Fenik et al. (2009) also used the connected hydrocarbon volume (CHV) as a ranking measure for SAGD reservoir cases. Li et al. (2012) proposed a new static quality measure for a particular well distribution and geological model. By comparing the results of ranking using static quality measure and CHV, they concluded that static quality measures give better results as they account for permeability and distance of productive cells from production wells. Yazdi and Jensen (2014) suggested a new $(k_H)_A$ method to rank realizations in which harmonic average of permeability of the grid blocks within a search radius considering producer as a center is calculated. However, Deutsch and Srinivasan (1996) remarked that no ranking measure is perfect and unique and hence they must be chosen very carefully. If these measures have poor correlation with output parameters from the field, then the realizations selected will not be an efficacious representation of initial ensemble. Also, even if the ranking methods based on static measures might be able to identify high, low and intermediate performing realizations, the ability of these methods to maintain diversity within the subset selected is not verified, which is again the much-needed characteristic to apply EnKF successfully.

Various other methods, widely known as sampling strategies are also proposed by several authors to reduce the size of the initial ensemble for the application of assisted history matching. Evensen (2004) proposed the sampling scheme in which ensemble with fewer realizations is generated by selecting the required number of dominant singular values from the singular value decomposition (SVD) of the initial ensemble. In this method, the subspace denoted by first few eigenvectors does not actually cover the entire space spanned by the original ensemble, which in turn may affect the variability of ensemble and ultimately the results of EnKF history matching. Another sampling method known as importance sampling is used extensively in communication theory (Lu and Yao 1988). In this method, a weighting factor is used to derive new probability density from the prior one such that it will include an important region of the sample space. The issue with this method is the selection of proper weighting factor for reservoir applications. It is difficult to have a single weighting factor that has good correlation with different reservoir output parameters. Scheidt and Caers (2009)

proposed distance-based kernel clustering method to select the subset of realizations. They parameterized the realizations through a distance function calculated using a streamline simulator and modeled a multi-dimensional space using kernel principal component analysis that allows the selection of subset from the larger initial ensemble. Though this method can give a robust representation of original ensemble, use of streamline simulation to calculate distance function may undermine the flow responses in case of SAGD reservoirs. Also, computing cost for streamline simulation of 3D model increases by the cube of third dimension times as compare to 2D model when direct methods are used and to a lower power (still greater than one) of the third dimension in case of using iterative methods (Aziz and Settari 1979). As streamline simulation of each realization is required, it would increase the total computing cost significantly, making EnKF computationally less efficient in large-scale real field cases.

2.2 Proxy Models Used in Assisted History Matching

For later approach, i.e. to replace computationally demanding reservoir simulators in history matching and optimization, different techniques have been proposed. A type of proxy model, commonly known as "Response Surface Model" (RSM) is studied by several authors. Li and Friedmann (2007) generated response surfaces using thin-plate spline interpolant in order to approximate objective function in history matching of two waterflooded reservoirs. Two separate proxy models, one to calculate production parameters and another to distinguish good and bad reservoir models in the initial parameter space were developed by Yu et al. (2007) using genetic programming based symbolic regression for history matching and uncertainty analysis of a large oil field in West Africa. For uncertainty assessment of a mature field in Norway, Slotte and Smorgrav (2008) also designed a couple of proxy functions based on polynomial regression and multidimensional kriging to determine production parameters and importance of each unknown parameter respectively where the convergence of proxy models was achieved through iterative sampling. Zubarev (2009) presented the comparative study of different proxy models and explained several pros and cons of both, proxy models and full reservoir simulations in history matching. An integrated approach with RSM and a genetic algorithm was suggested

by Monfared et al. (2012) where the one-factorial experimental design was used to select proper experiments while p-value associated with each coefficient was calculated to discard insignificant terms in the proxy model. Though RSMs are very attractive due to the lower computational cost of the fitting process, they do not honor the basic assumption of random error that may lead to poor least-squares regression (Jurecka 2007). Also, a large number of unknown parameters in history matching cannot be handled by such proxy models, an important attribute required to integrate a proxy model in the EnKF framework.

Recently, Artificial Neural Network (ANN) based proxy models have gained much popularity due to its extreme versatility. Queipo et al. (2000) presented surrogate modeling based on neural network, Design and Analysis of Computer Experiments (DACE) modeling and adaptive sampling for optimization of the objective function in reservoir characterization. A small set of numerical simulations obtained from experimental design was used to create a nonlinear proxy neural network by Cullick et al. (2006), which was then implemented in history matching to find the solution set for unknown parameters. For uncertainty assessment of estimated ultimate recovery (EUR), Jeong et al. (2013) built a neural network using only high-quality history matched models of basement fracture reservoir located in Vietnam. Bruyelle and Guerillot (2014) demonstrated the superior predictive capability of neural networks as compare to second order polynomials and kriging method with the help of PUNQ-S3 reservoir history matching case study and concluded that first and second order derivatives of the neural network can be computed with gradients and Hessian in the learning process. Application of ANN in history matching of a synthetic water flooded reservoir is discussed by Costa et al. (2014), mostly considering multipliers and exponents as unknown reservoir parameters. A newly developed proxy model, named as "Smart Proxy" is a combination of one or more interconnected Neuro-Fuzzy systems and capable to learn fluid flow behavior in multi-well, multilayer reservoir model. It has been utilized for continuous model updating in history matching by He (2016). Overall, ANN-based proxy models have been successfully implemented in history matching workflows, however, due to their nested layout, the imagination of the process is restricted to the graphical representation of outputs. In addition, inexperience in setting up network architecture may lead to overfitting of the data,

ultimately resulting in the unstable proxy model. Also, ANN's ability to forecast outside the trained parameter space needs further investigation.

In proxy modeling, some other approaches based on statistical methods have also been proposed by numerous authors. Sarma and Xie (2011) applied Polynomial Chaos Expansion (PCE) for uncertainty quantification of water flooded reservoirs while considering limited reservoir parameters as unknown and using Non-Intrusive Spectral Projection (NISIP) to estimate PCE coefficients. Similarly, Bazargan et al. (2015) used PCE for uncertainty quantification of a synthetic 2D model with fluvial channels, however, used regression-based Probabilistic Collocation Method (PCM) to calculate dynamic coefficients. He concluded that it is feasible to construct a proxy based on PCE and its precision improves as PCE order and hence the corresponding number of initial simulation runs increases. He et al. (2011) proposed reduced-order models that consider Trajectory Piecewise Linearization (TPWL) and incorporated them into EnKF for history matching of the synthetic reservoir model. An innovative approach was presented by Sayarpour et al. (2010) that involves Capacitance-Resistance Model (CRM) and Buckley-Leverett-based fractional flow model to obtain equiprobable history matched solutions using only past injection-production data. However, none of these methods are tested for thermal reservoirs yet.

In case of thermal recovery processes, in addition to purely data-driven proxy models, several authors have discussed the application of analytical or semi-analytical proxy models for history matching. Akram (2011) considered a simple linear or quadratic polynomial regression model determined by least square fit for optimization of a test model with 5 facies. Also, a proxy model that used Green's functions was suggested by Fedutenko et al. (2012) for production forecasting in SAGD reservoirs. In order to add some physical meaning to proxy models, Vanegas et al. (2008) developed a semi-analytical proxy model based on Butler's SAGD theory to predict time profile of oil flow rate, cumulative oil production and cumulative steam injection for SAGD reservoirs. Application of physics-based analytical models for fast history matching of field cases is demonstrated by Azad and Chalaturnyk (2013). However, Shi and Leung (2013) pointed out that many assumptions and approximations are associated with physics-based proxy models, which undermine their capability in assisted history matching of complex thermal reservoirs.

2.3 Strategies Used for Real-Time Production Optimization

As discussed before, real-time production optimization is primarily achieved by maintaining the subcool to an optimum set-point. In order to obtain the optimal target, several attempts have been made to understand the effect of different subcool values. Ito and Suzuki (1999) conducted a series of parametric numerical simulations using a 2D reservoir model and concluded that 36°C is the optimum subcool as it provided minimum cumulative Steam-Oil-Ratio (cSOR). Edmunds (2000) performed different simulations to investigate the effect of steam trap constraints by varying it between 5 to 50°C in a prototype 2D & 3D Athabasca reservoir and also discussed its economic consequences. He demonstrated that optimum subcool for 2D reservoir was 20 to 30°C and supply cost would be reduced by 2 \$/bbl if 20°C subcool is maintained over the life cycle of well pair. Effect of different subcool targets on oil production rates at distinct operational pressures was studied by Das (2005) and based on the results of numerical simulations, he determined that subcool plays a significant role if it exceeds a critical value that appeared to be 20 °C for the Athabasca reservoir model he considered. Vander Valk and Yang (2007) carried out several sensitivity analyses using a reservoir model with typical rock and fluid properties of Athabasca oil sands to evaluate the combined effect of frictional pressure drop and subcool on bitumen production. They mentioned couple of remarks: 1) productivity, as well as cSOR, were optimal near 20°C subcool and 2) oil production rate is very sensitive to subcool when frictional pressure drop in wellbore is significant, from which it can be inferred that not only liquid production rate but also steam injection rate (which causes high frictional pressure drop) should be taken into account to determine overall effect of subcool on oil recovery. Using commercial optimizer, Bao et al. (2010a) optimized target subcools for different time intervals in a SAGD reservoir life cycle with an objective to minimize cSOR and concluded that initially higher subcool target, followed by the lower value provided better economic performance. Gates and Leskiw (2010) analyzed the effect of different liquid production rates on subcool profile with time at multiple locations of a 3D reservoir model and concluded that critical subcool value that should be maintained for energy efficient SAGD operation was about 20 °C. Using history matched the model of Surmont pilot study area, Bao et al. (2010b) examined the effect

of different subcool values on 3 different well pairs and concluded that 15°C is the optimum value of subcool at 1500 kpa injection pressure for a particular well pair since it yielded higher cumulative bitumen production and minimum cSOR. Though literature suggests a range of optimum subcool between 5 to 40°C, as Edmunds and Gittins (1993) mentioned, optimum liquid drawdown (or subcool) changes during the life-cycle of SAGD well pair. Also, as critical subcool value depends on average reservoir properties (Gates and Leskiw 2010) between wells, due to heterogeneity, it may vary from well pair to well pair and obviously, reservoir to reservoir.

Several authors have made efforts to achieve steam chamber conformance by implementing state-of-the-art well completion technology in the field. Kisman (2003) designed two-stage artificial lift system called ELift to maintain low subcool values at lower pressures, as standard bottom hole pump cannot be used due to a lower liquid level that does not provide enough net positive suction head (NPSH). As reported by Clark et al. (2010), a well pair in Orion SAGD field was divided into 4 segments using Interval Control Valves (ICV) for differential steam trap control and hence better steam injection conformance, which resulted into improved injectivity in poorer zones and almost 20% lower cSOR. Stalder (2013) concluded that flow-distribution-control (FDC) liners installed in Surmont field provided uniform temperature profiles along the wells without toe strings and appeared to achieve steam trap control regardless of the vertical spacing between wells. Banerjee et al. (2013a) and Banerjee et al. (2013b) discussed the use of autonomous Inflow Control Devices (ICD) and hybrid-geometry Passive ICDs as a secondary level of steam trap control that restricts steam breakthrough by choking behavior when a shift in Reynolds number regime is observed. Similarly, Shad and Yazdi (2014) used nozzle-based ICD and compared the simulation results with the case where no ICDs were installed and determined that due to uniform pressure distribution, lower subcool values can be maintained while producing no live steam in the case where ICDs were used. A simple approach of blanking off the part of the injection or production liner strings according to the SAGD well trajectory was mentioned by Taubner et al. (2015) to avoid steam breakthrough. Though these permanent downhole technologies can enhance steam chamber conformance and maintain low subcool, significant fiscal investment is required for their development and installation. Also, workover and maintenance of such systems are costly and disrupts the SAGD operations. Therefore, control strategies which can

be implemented without any change in SAGD well pair design as shown in figure 3, has attracted researchers' attention in recent times.

Different control strategies have been explored by intellectuals to optimize operational parameters of SAGD, thereby maintaining optimum subcool level for real-time production optimization. Gotawala and Gates (2009) presented a dynamic injection strategy in which steam injection pressure of 6 intervals of the well was controlled using Proportional-Integral-Derivative (PID) feedback control algorithm to retain subcool at a particular set-point, leading to better cSOR, higher cumulative oil production, and uniform steam conformance. Guyaguler et al. (2010) proposed a generic feedback-based controller and employed it to maintain an average temperature in a particular region of the heavy oil reservoir, results of which were obtained using both PI and fuzzy controller and comparison was made with the base case, indicating improvement in cSOR. A simplistic theory which uses material balance and heat balance was formulated by Gotawala and Gates (2012) for estimation of PID controller parameters, demonstrating the capability of PID controller to ensure the optimum liquid pool above producer. Two single-loop PID controllers were designed by Khaledi et al. (2012) to control chamber pressure and temperature of the produced liquid in SAGD where the open-loop dynamic response of the process was determined by inducing series of step changes and fitting a first order plus dead-time (FOPTD) model. Performance of a SAGD well pair with ICD equipped producer and dual tubing strings, steam injection rates of which were controlled by two separate PID controllers was examined by Stone et al. (2013), exhibiting improvement in cSOR as well as cumulative oil production while maintaining toe and heel subcool near the predefined target value. Stone et al. (2014a) also demonstrated the ability of identical feedback based PID controllers to control steam injection rates at both injection points (i.e. toe and heel) in SAGD fields with varying degrees of heterogeneity and concluded that improved steam conformance could be achieved. PID controllers with configurations similar to previous work were used by Stone et al. (2014b) to optimize the NPV of the bitumen asset using Radial Basis Function (RBF) scheme while controlling optimum subcool by manipulating SAGD operational parameters, specifically, initial circulation period, maximum injection rate as well as water production limit of each tubing string and proportionality constant (K_p) of the controllers. Though the use of PID controllers has been extensively studied for subcool control, they are Single Input Single Output

(SISO) control strategy, meaning that it cannot consider the interaction between different manipulated and controlled variables. Also, it does not have the predictive capability, which may result in underrated subcool control and steam conformance, ultimately affecting the oil recovery and economics of the SAGD reservoir.

More advanced and Multi Input Multi Output (MIMO) control method, Model Predictive Control (MPC) is also considered by several authors in which system to be controlled is mimicked using either physical or empirical dynamic model. Use of empirical model based on system identification theory is not strange to the petroleum industry as Nikolaou et al. (2006) employed state space model identified using parametric system identification approach for short-term prediction where parameters were updated on a daily basis using continuously available field data over the moving horizon. Likewise, MPC has also been used in petroleum engineering before. For example, Van Essen et al. (2013) proposed two-level optimization strategy for waterflooding reservoir in which MPC was used for lower level optimization with a view to tracking the injection profiles obtained in life-cycle optimization and reported that performance drop of 6.4% in NPV was reduced to 0.5% when MPC was used for tracking optimized injection profiles. For subcool control, MPC was first exercised by Patel et al. (2014) considering a combination of many linear empirical step-response models as plant model. They successfully tested the capability of MPC for stable SAGD operations in general as well as while transitioning between a set of targets. However, the methodology for subcool control was implemented using proprietary software called SEPTIC (Strand and Sagli 2004). Vembadi et al. (2015) implemented MPC with 2nd order ARX model as a plant model to manipulate injection/production rates of both tubing strings for better subcool control where varying subcool targets were obtained from NPV optimization over the life-cycle of SAGD reservoir. An adaptive-predictive control approach comprised of neural network based ARMAX model and MPC was applied by Guevara et al. (2015) for subcool control as well as Net Present Value (NPV) optimization of a synthetic reservoir, results of which outperformed those obtained using decentralized PID control. Purkayastha et al. (2015) also practiced MPC to calculate steam injection rate using recursive parameter estimation of the model proposed by Gotawala and Gates (2012) in order to achieve better steam conformance. It was concluded that oil recovery was improved by 35.7% for a synthetic reservoir, however, such one-dimensional ODE plant model is computationally expensive (Vembadi 2014),

potentially enforcing larger control intervals, which is an undesirable characteristic for an efficient MPC controller.

Chapter 3

Initial Sampling of Ensemble for SAGD Reservoir History Matching ¹

¹ A version of this chapter has been published in the proceedings of the *World Heavy Oil Congress 2015* and *Journal of Canadian Petroleum Technology*, 54(6): 424-441.

3.1 Introduction

In this chapter, a new method based on probability distance minimization, earlier proposed by Rahim et al. (2014), is used to select a subset of realizations. The method calculates multiple static measures for each realization of the initial ensemble and along with geological properties, uses them to differentiate each realization from others. Kantorovich distance is defined to quantify probability distance between the initial ensemble and reduced ensemble. An MILP model with appropriate constraints is suggested in the work, which can be solved using an appropriate MILP solver. The objective of the MILP model is to minimize the Kantorovich distance between initial ensemble and reduced ensemble by optimally selecting realizations for the reduced ensemble. The main goal of the proposed method is to select the subset of realizations such that it has same statistical characteristics as an initial ensemble and also serves as an ideal smaller size ensemble for history matching in terms of spread, variability, and unbiasedness.

Section 3.2 and 3.3 describe other ranking/selection methods briefly and the pedagogy of the proposed method in detail respectively. Also, the conventional EnKF procedure is shown in the next section. In order to verify the proposed method, it is applied to a real SAGD reservoir field case and history matched using EnKF. The results are compared with other existing sampling methods. A detailed explanation of case study and application of each screening method to the field case is provided in section 3.5. Section 3.6 comprises results of the case study and discussion about the performance of the proposed method in comparison with other realization selection methods in terms of statistical characteristics of selected subset and results obtained after applying EnKF history matching on the reduced ensemble. At the end, a summary of the results of the case study is presented in section 3.7.

3.2 Contemporary Sampling Techniques

In this section, different ranking/selection methods proposed by various authors are described briefly with which results of the proposed method is compared.

3.2.1 Orthogonal Ensemble Members

Evensen (2004) proposed an improved sampling scheme to reduce the direct computation of eigenvectors in case of a large ensemble. He used singular value decomposition (SVD) to resample the members from the initially larger ensemble. A similar approach can be applied in the screening of realizations to reduce the size of the initial ensemble of model parameters. Steps to be carried out to apply this sampling method are as follows:

- 1) Generate large ensemble of reservoir model parameters with $N_e (= \beta N_s)$ members and assign them to $\hat{\mathbf{Z}}' \in \mathfrak{R}^{N_c \times \beta N_s}$, where size of initial ensemble is β times (value greater than 1) the required size of reduced ensemble.
- 2) Compute the SVD, $\hat{\mathbf{Z}}' = \hat{\mathbf{U}} \hat{\mathbf{\Sigma}} \hat{\mathbf{V}}^T$.
- 3) Retain only $N_s \times N_s$ quadrant of $\hat{\mathbf{\Sigma}}$ and assign them to $\mathbf{\Sigma} \in \mathfrak{R}^{N_s \times N_s}$, where diagonal values of $\hat{\mathbf{\Sigma}}$ are non-zero singular values of original ensemble.
- 4) Scale the non-zero singular values by $\sqrt{\beta}$ to maintain the correct variance.
- 5) Generate a random orthogonal matrix \mathbf{V}_1^T by SVD of a random $N_s \times N_s$ matrix $\mathbf{Z}_1 = \mathbf{U}_1 \mathbf{\Sigma}_1 \mathbf{V}_1^T$.
- 6) Choose only first N_s singular vectors from $\hat{\mathbf{U}}$ and assign them to \mathbf{U} .
- 7) Generate reduced ensemble using singular vectors stored in \mathbf{U} , non-zero singular values stored in $\mathbf{\Sigma}$ and orthogonal matrix \mathbf{V}_1^T .

The equation used here to create reduced ensemble with only N_s members is,

$$\mathbf{Z} = \mathbf{U} \frac{1}{\sqrt{\beta}} \mathbf{\Sigma} \mathbf{V}_1^T \quad (3.1)$$

3.2.2 Importance Sampling

The main objective of importance sampling is, instead of taking samples from the original pdf, identifying another distribution that is more heavily weighted and samples are taken from that pdf so that some important regions of sample space gets more samples. As Oliver and Chen (2009) noted if $p(m)$ is the prior probability density and $\tilde{p}(m)$ is related to prior probability density by the weighting factor $w(m)$, then relation of those pdfs can be shown as,

$$\tilde{p}(m) = \tilde{c}w(m)p(m) \quad (3.2)$$

Now, as $\tilde{p}(m)$ is also a probability density, it should also be licit.

$$\int \tilde{p}(m)dm = \int \tilde{c}w(m)p(m)dm = 1 \quad (3.3)$$

To implement importance sampling in reservoir application stepwise procedure can be written as follows:

- 1) Generate initial ensemble of model parameters (e.g. porosity, permeability) with N_e members that serves as a prior probability density $p(m)$.
- 2) Select the computationally inexpensive weighting factor $w(m)$, since it is evaluated for each ensemble member.
- 3) Calculate the normalization constant \tilde{c} in Eq. (3.2), and approximate the integral in Eq. (3.3):

$$\tilde{c} = \frac{N_e}{\sum_{i=1}^{N_e} w(m_i)} \quad (3.4)$$

- 4) Compute the weighting factor w_i for each realization in the large ensemble.
- 5) Using $w_i/\sum_{i=1}^{N_e} w_i$ as the resampling probability density, resample N_s realizations from the large ensemble.

3.2.3 K-Means Clustering

Scheidt and Caers (2009) proposed a distance-based kernel clustering method that depends on a realization-based model of uncertainty, parameterized by distances. The workflow of this method can be explained as follows:

- 1) Generate a larger ensemble of geological realizations with N_e members initially.
- 2) Calculate the dissimilarity distances between realizations by use of the distance function and construct the dissimilarity-distance matrix \mathbf{D} .
- 3) Map the dissimilarity matrix \mathbf{D} into Euclidean space \mathbf{R} by use of multidimensional scaling.
- 4) Transform Euclidean space \mathbf{R} into featured space \mathbf{F} using kernel functions so that points mapped in space behaves linearly. In general, Gaussian kernel (radial basis function) is used, equation for which can be given as

$$K(X, Y) = \exp\left(-\frac{\|X - Y\|^2}{2\sigma^2}\right) \quad \text{with } \sigma > 0 \quad (3.5)$$

- 5) Apply a clustering algorithm, a standard linear pattern recognition tool that assigns points in a featured space \mathbf{F} to a cluster by minimizing the expected squared distances between the points of cluster (x_g) and its center μ_u :

$$G = \sum_{u=1}^{N_k} \sum_{x_g \in H_u} |x_g - \mu_u|^2 \quad (3.6)$$

where S_i denotes initial clusters and number of clusters generated here is equal to number of realizations (N_s) we want to select from initial ensemble.

- 6) Select one realization from each cluster that is nearest to the centroid of that cluster to select N_s realizations.

3.3 Proposed Scenario Reduction Method

The proposed method consists of two important steps. The first step is to calculate multiple static measures and use them to quantify dissimilarity between geological realizations in the initial ensemble, which is described in subsection 3.3.1. In the next step, Kantorovich distance is computed that is used to quantify disparity between pdf of model parameters in the initial ensemble and reduced ensemble elaborated in section 3.3.2. The proposed method follows similar steps to select realizations as optimization based uncertainty quantification method by Rahim et al. (2014) except some changes in static measures.

3.3.1 Static Measures and Quantification of Dissimilarity in Realizations

As Hovadik and Larue (2007) discussed, static measures are important links between reservoir characterization and simulation studies. Also, they are simple in concept with minimal computing costs as compared to dynamic measures or flow simulation. In order to use the static measures efficiently, it should be confirmed that static measures being used have good correlation with the output parameters. Sometimes, one single static measure does not show good correlation with several different output parameters. In such cases, multiple static measures must be used in order to give each realization a unique identification. McLennan and Deutsch (2005) used four different kinds of static measures i.e. volumetric, statistical, global connectivity and local connectivity.

In the proposed method, three types of static measures are used i.e. statistical, fractional and volumetric measures. Total 7 separate static measures are used in the method out of which 3 are statistical, 1 is fractional and 3 are volumetric measures. Statistical measures are usually calculated by arithmetic average and are computed only for net cells. A grid block with very low permeability and porosity in reservoir model does not contain much oil or gas and hence it will not contribute to any production parameter. So, to increase the correlation between measure and output parameter, it is necessary to differentiate between producing and non-producing cells in reservoir model and as a result, the concept of the net cell is introduced. Any cell

or grid block in the geological realization that has higher permeability and porosity value than the threshold value is considered as a net cell. Binary indicator I_c^{net} is used to identify whether the cell is net cell or not. In other words, I_c^{net} equal to 1 show that cell c in particular realization is a net cell and vice versa. In mathematical notations, indicator I_c^{net} can be defined as (McLennan and Deutsch 2005),

$$I_c^{net} = \begin{cases} 1, & \text{when } \phi_c \geq \phi_0 \text{ and } k_c \geq k_0 \\ 0, & \text{otherwise} \end{cases} \quad (3.7)$$

where ϕ_c and k_c are porosity and horizontal permeability value of cell c respectively in a particular realization while ϕ_0 and k_0 are threshold porosity and threshold horizontal permeability respectively. Any cell in reservoir is not a net cell only if it has either lower porosity than ϕ_0 or lower permeability than k_0 .

First statistical measure, average net permeability (K_{net}) for each realization can be defined as,

$$K_{net} = \frac{\sum_{c=1}^{N_c} k_c I_c^{net}}{\sum_{c=1}^{N_c} I_c^{net}} \quad (3.8)$$

Similarly, average net porosity (ϕ_{net}) for each realization can be calculated using equation,

$$\phi_{net} = \frac{\sum_{c=1}^{N_c} \phi_c I_c^{net}}{\sum_{c=1}^{N_c} I_c^{net}} \quad (3.9)$$

Also, average net irreducible water saturation (S_{net}) for each realization can be given as,

$$S_{net} = \frac{\sum_{c=1}^{N_c} S_c I_c^{net}}{\sum_{c=1}^{N_c} I_c^{net}} \quad (3.10)$$

where S_c is irreducible water saturation of cell c for particular realization. Here, in all three equations of static measures, I_c^{net} is introduced to make sure that only net cells are being used to calculate the measures. Also N_c is total number of cells in a reservoir model in all equations.

Fractional static measures are good candidates to identify the quality of reservoir model. Fraction of net cells (F_{net}) is the only fractional static measure used in the method. It is a ratio of net cells to the total number of cells in reservoir model, hence it is also known as a net to gross ratio. Equation of F_{net} can be given as,

$$F_{net} = \frac{\sum_{c=1}^{N_c} I_c^{net}}{N_c} \quad (3.11)$$

Higher F_{net} value shows that a particular realization has more number of net cells and therefore higher chances for good SAGD production performance.

Another type of static measure we used is volumetric static measures. These measures are being considered as global properties of a realization. As Hovadik and Larue (2007) noticed, these measures are most important discriminator to differentiate realizations. Also, there is a strong correlation between reservoir volume and cumulative recovery. Three different volumetric measures are used in the proposed method.

Net pore volume (PV_{net}) is the volumetric measure that represents total pore volume of net cells in a particular realization. It can be calculated by summation of multiplication of porosity and volume of each net cell in a realization. Mathematically, it can be shown as,

$$PV_{net} = \sum_{c=1}^{N_c} V_c \phi_c I_c^{net} \quad (3.12)$$

where V_c is volume of cell c in a reservoir model.

Original oil-in-place ($OOIP$) is another volumetric measure used in proposed method. It is the simplest summary of reservoir in terms of hydrocarbon volume. Equation to calculate $OOIP$ can be shown as,

$$OOIP = \sum_{c=1}^{N_c} V_c \phi_c (1 - S_c) \quad (3.13)$$

Net original oil-in-place ($OOIP_{net}$) is the final volumetric measure used. As only net cells have a considerable ϕ_c and k_c , amount of hydrocarbon possessed by those cells is important in terms of production performance. Therefore, $OOIP_{net}$ must be having a better correlation with SAGD production parameters as compare to $OOIP$. Net original oil-in-place can be computed using the formula,

$$OOIP_{net} = \sum_{c=1}^{N_c} V_c \phi_c (1 - S_c) I_c^{net} \quad (3.14)$$

Now, to differentiate two realizations, we need to define a function that can quantify the dissimilarity between them. The function should be also simple in terms of computing cost. A function that considers static measures and geological properties is defined to calculate the difference between two realizations. As discussed, static measures are simple non-iterative equations that can be computed very easily and hence computing of proposed dissimilarity function also becomes cost efficient. To quantify dissimilarity between two realizations i and i' , the function used can be shown as,

$$c_{i,i'} = \sum_{j=1}^{N_s} |s_{ij} - s_{i'j}| + \sum_{p=1}^{N_{gp}} \sum_{l=1}^{N_c} \gamma |\theta_{ilp} - \theta_{i'lp}| \quad \forall i, i' \quad (3.15)$$

where s_{ij} is the value of static measure j for realization i , N_s is total number of static measures, θ_{ilp} denotes value of geological property p of cell l of realization i and N_{gp} stands for total number of geological properties used to calculate the dissimilarity function. Also, γ denotes the weight given to the geological properties while quantifying dissimilarity between two realizations. As static measures are better indicator of dissimilarity and also calculated using geological properties, more importance is given to them by adjusting γ equal to 0.01 in proposed work.

3.3.2 Kantorovich Distance and its Minimization

The principal objective of the proposed method is to identify the subset of realizations which is as similar as an initial ensemble so that EnKF can be applied successfully on

a subset. In order to select a subset that has similar characteristics as an initial ensemble, it is necessary to quantify dissimilarity between initial ensemble and subset selected. Kantorovich distance is used in a proposed method to quantify dissimilarity between initial ensemble and subset selected and by minimizing it, we can select the subset that can represent initial large ensemble effectively in terms of reservoir production performance.

Kantorovich distance is basically a probabilistic measure to distinguish two probability distributions i.e. initial ensemble and reduced ensemble in our case. It was first introduced in transportation problem in 1942 and since then it has been used in many applications such as mining (Armstrong et al. 2013), image compression (Alexopoulos and Drakopoulos 2012), stochastic programming (Dupacova et al. 2003) etc. In our case, for realization reduction problem, Kantorovich distance between original ensemble and reduced ensemble can be defined by optimal value of a linear transportation problem which can be shown as,

$$\begin{aligned}
 D_{Kan} = \min_{\eta_{i,i'}} & \sum_{i \in I} \sum_{i' \in S} \eta_{i,i'} c_{i,i'} \\
 \text{s.t.} & \sum_{i \in I} \eta_{i,i'} = p_i^{new} \quad \forall i' \in S \\
 & \sum_{i' \in S} \eta_{i,i'} = p_i^{orig} \quad \forall i \in I \\
 & \eta_{i,i'} \geq 0 \quad \forall i \in I \quad \forall i' \in S
 \end{aligned} \tag{3.16}$$

where i and i' are realizations, $\eta_{i,i'}$ is the decision variable that represents probability mass transportation plan, $c_{i,i'}$ is dissimilarity between realizations explained in Eq. (3.15), I is initial ensemble and S is reduced ensemble and p_i^{new} is the probability of realization i' in reduced ensemble while p_i^{orig} denotes the probability of realization i in initial ensemble. In our case, it is considered that all realizations in initial ensemble are equiprobable, so p_i^{orig} is equal to $1/N_e$ where N_e is total number of realizations in initial ensemble.

Dupacova et al. (2003) proved that optimal objective value for the minimization problem shown in Eq. (3.16) is,

$$D_{Kan} = \sum_{i \in I-S} p_i^{orig} d_i \quad (3.17)$$

where $d_i = \min_{i' \in S} c_{i,i'} \forall i \in I - S$ is the cost of removing realization i . Also, it is the minimum dissimilarity distance between a removed realization i and all the realizations selected in subset $i' \in S$. If we consider $p_{i'}^{new}$ as a decision variable, optimal solution for problem in Eq. (3.16) can be shown as,

$$p_{i'}^{new} = p_{i'}^{orig} + \sum_{i \in J(i')} p_i^{orig} \quad \forall i' \in S \quad (3.18)$$

where $J(i') = \{i \mid i \in I - S, c_{i,i'} \leq c_{i,i''}, \forall i'' \in S\}$. Eq. (3.18) shows that new probability of a selected realization is equal to the sum of its original probability and all probabilities of removed realizations which are nearest to it.

Now, the objective value of Eq. (3.17) needs to be minimized in order to select a better reduced ensemble. To specify whether a particular realization is selected in a reduced ensemble or not, a binary variable for each realization in the initial ensemble is defined where 0 and 1 indicate selection and rejection of particular realization respectively. Since our optimization model consists both binary and continuous variables, a constrained mixed integer linear optimization algorithm is used to minimize the Kantorovich distance between original ensemble and reduced ensemble. Constraints for the optimization problem in the proposed scenario reduction method are explained in detail by Rahim et al. (2015) and detailed proofs are described in Li and Floudas (2014).

Mixed Integer Linear Optimization (MILP) is well-known since 1960s and commercial solvers (e.g. CPLEX, Gurobi, PICO) are available to solve the optimization problems (Bixby 2012). Mathematically, MILP problem can be generally defined as,

$$\begin{aligned} z &= \min_{x,y} f^T x + g^T y \\ s.t. \quad & Ax + Ey \leq b \\ & x_{min} \leq x \leq x_{max}, \quad y \in \mathbb{Z} \end{aligned} \quad (3.19)$$

where z is the optimal value of the linear objective function comprising continuous and integer variables with f^T and g^T being the coefficients. Here, x denotes continuous variable defined between lower bound x_{min} and upper bound x_{max} while y represents the integer variable that belongs to \mathbb{Z} (i.e. set of integers in general). As Kostuik et al. (2013) noted, MILP can guarantee an optimal solution for any mixed integer optimization problem with linear objective function and constraints. Various algorithms are available to solve the above MILP problem shown in Eq. (3.19), e.g., branch and bound, branch and cut, branch and price and dynamic search algorithm. As the minimization of Kantorovich distance is modeled as an MILP optimization problem, it can be solved using any MILP solver.

3.4 Ensemble Kalman Filter

After selecting a reduced ensemble using different methods discussed in previous sections, EnKF is implemented to perform assisted history matching on reduced ensemble in proposed work. EnKF is a data assimilation technique for large-scale systems, based on theory of Kalman filters and sequential Monte Carlo methods. Evensen (2009) has a well documented theoretical basis for various aspects of EnKF. Also, Aanonsen et al. (2009) have reviewed the application of EnKF in reservoir engineering, specifically for estimation of reservoir parameters. To apply the traditional EnKF for history matching, the stepwise procedure is provided here with necessary explanations.

- 1) Create an initial ensemble consisting N_e independent ensemble members primarily using data available from well logs, core analysis, seismic analysis and other prior information available. Simulation techniques like Sequential Gaussian Simulation (SGS), Sequential Indicator Simulation (SIS), etc. are used to generate multiple stochastic realizations.
- 2) In forecast step of EnKF, forward each member of initial ensemble separately to a next time step using a state transition function (f) that relates current state of system to the previous or initial state of system. In reservoir applications, commercial reservoir simulators are used to propagate realizations that solve nonlinear differential equations using finite element or

finite difference method. Eq. (1.2) shows the forecast step of EnKF in mathematical terms. It can be considered here while keeping the notations consistent.

- 3) Construct a state vector for each realization in the initial ensemble by combining interested parameters (commonly known as state variables) of it. State vector z at time step k for a particular realization j can be defined as,

$$z_k^j = \begin{bmatrix} m_k^j \\ u_k^j \\ d_k^j \end{bmatrix} \quad \forall j \in [1, N_e] \quad (3.20)$$

where typically, model parameters m_k^j can be logarithmic of permeability, porosity, state parameters u_k^j can be time dependent parameters like pressure, water saturation and production data d_k^j can be oil rate, water rate, steam oil ratio, etc. at all or selected wells in the reservoir model.

- 4) Introduce initial ensemble in a matrix form by combining state vector z_k^j of each realization. Mathematically, it can be written as,

$$Z_k = [z_k^1, z_k^2, \dots, z_k^j, \dots, z_k^{N_e}] \quad (3.21)$$

- 5) Calculate ensemble mean $\overline{Z_k}$ of the prediction ensemble using equation,

$$\overline{Z_k} = [\overline{z_k^1}, \overline{z_k^2}, \dots, \overline{z_k^j}, \dots, \overline{z_k^{N_e}}] = Z_k W_k \quad (3.22)$$

where w_k is the $N_e \times N_e$ matrix with each element of it equal to $1/N_e$.

- 6) Next, compute ensemble perturbation matrix ΔZ_k by subtracting ensemble mean from state vector of each realization, equation of which can be shown as,

$$\Delta Z_k = Z_k - \overline{Z_k} \quad (3.23)$$

- 7) Determine ensemble covariance matrix $C_{Z_k}^p$ of an initial ensemble Z_k shown in Eq. (3.21) using standard statistical formula that can be written as,

$$C_{Z_k}^p = \frac{\Delta Z_k (\Delta Z_k)^T}{N_e - 1} \quad (3.24)$$

where superscript p symbolizes predicted (before update) state of particular matrix. Here, from Eq. (3.24) it can be said that calculation of covariance matrix $C_{Z_k}^p$ only requires data available at time step k , providing EnKF an edge over standard Kalman filter (Gu and Oliver 2006).

- 8) Prepare N_e perturbed observations by adding a random Gaussian noise (also known as measurement error) $v_k \sim N(0, R)$ to original observation d_k^{obs} at time step k as follows,

$$d_k^{j,obs} = d_k^{obs} + v_k^j \quad \forall j \in [1, N_e] \quad (3.25)$$

where v_k follows a zero mean Gaussian distribution with measurement noise covariance matrix R and $E[v_k v_k^T] = R$ assuming that R is known. Observations calculated after adding random measurement error in Eq. (3.25) can be considered as random variables, a necessity to maintain variance of updated ensemble (Burgers et al. 1998).

- 9) In order to update state vector in analysis step, Kalman gain K_g needs to be calculated using ensemble covariance matrix, equation for which can be written as,

$$K_g = C_{Z_k}^p H^T (H C_{Z_k}^p H^T + R)^{-1} \quad (3.26)$$

where H is a measurement operator which relates state vectors to theoretical observations. Generally, it has only 0 and 1 as its elements. Mathematically it can be shown as,

$$H = [0 \mid I] \quad (3.27)$$

- 10) Finally, state vector of each realization in the predicted ensemble is updated using Kalman update equation in the analysis step. Mathematically, it can be shown as,

$$z_k^{j,a} = z_k^{j,p} + K_g(d_k^{j,obs} - Hz_k^{j,p}) \quad \forall j \in [1, N_e] \quad (3.28)$$

where superscript a denotes analyzed (after update) state vector. If uncertainty in production forecast of updated state vector $z_k^{j,a}$ is high then repeat step 2 to 10 considering updated ensemble as a predicted ensemble until it is reduced to a level that firm decisions related to field development can be taken.

3.5 Application to a SAGD Reservoir

In order to verify the proposed sampling method and also to compare it with other methods, we applied all 4 methods to a SAGD reservoir located in northern Alberta. A workflow using MATLAB® (release R2014a) was developed in-house, which consists several user-defined functions in order to implement different screening methods and EnKF explained in the previous section. It also integrates different software like CMG STARS™ (CMG 2013a) for reservoir simulations, Results Report™ (CMG 2013b) to export data once simulations are done and CPLEX® (IBM 2010) for solving MILP optimization model in proposed scenario reduction method. In section 3.5.1, general description of reservoir model is provided. Also, application of different methods, including the proposed method on real reservoir model is discussed in section 3.5.2 to 3.5.5. In section 3.5.6, application of EnKF on reduced ensemble derived using all four different methods is discussed.

3.5.1 Description of the Reservoir Model

Reservoir model was built from the ground up by use of the various data available from the field. Different types of well logs from the vertical core holes near a particular horizontal well pair were used to build a static model in Petrel exploration and production software platform from Schlumberger. The corner point grid was generated in which dimensions of each grid block are $25 \times 2 \times 1.5$ m and number of grid blocks are $25 \times 50 \times 16$ in i (East), j (North) and k (Elevation) direction respectively. The porosity of the grid blocks containing vertical core holes was obtained using the well logs and also permeability was calculated for those grid blocks (*Figure 3.1*). Sequential Gaussian simulation (SGS) was performed to generate 100 realizations of permeability

using the data at the wells as conditioning data. Bitumen viscosity at initial reservoir temperature (7 °C) was 625,000 cp and at a higher temperature of 216 °C, it was 10 cp. Also, rock type with appropriate relative permeability curves was used in the model detail of which is not provided due to confidentiality. A horizontal well pair of length 500 m and 6 m spacing between injector at top and producer at the bottom was modeled. Also, different constraints of both wells from the field data were used in the simulation model. Permeability values range from 1525 md to 7150 md in the realizations. Porosity values range from 31.5 to 41.5% while irreducible water saturation ranges from 0.16 to 0.2 in 100-member initial ensemble. Realizations were simulated for 1355 days in order to compare results of various sampling methods with proposed method by use of the thermal simulator CMG STARS™ (CMG 2013a).

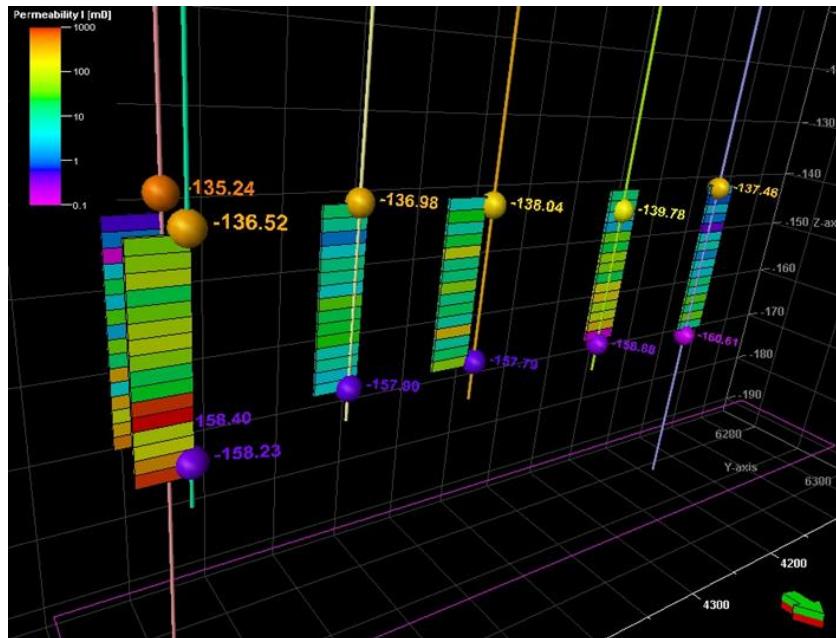


Figure 3.1 – Permeability values (in *i*-direction) of grid blocks containing core holes that were used as conditional data in Sequential Gaussian Simulation.

3.5.2 Application of Orthogonal Ensemble Members Method

The ensemble containing 100 realizations was used as an initial ensemble. Smaller size ensemble with only 50 members was created by following the steps described in section 3.2.1. Singular value decomposition was calculated much faster and reduced ensemble was generated using Eq. (3.1).

3.5.3 Application of Importance Sampling

To select the smaller ensemble of 50 realizations using importance sampling, steps explained in section 3.2.2 is followed. As pointed out in step 2 of the method, weighting factor needs to be selected in order to give more importance to the certain region of prior model space. As we need to calculate weighting factor for each realization in the original ensemble, it must be simple and inexpensive to compute. Though there is no particular guideline to select a weighting factor, it should represent the realization fairly i.e. value of the weighting factor for a realization should be small when the value of production parameter to be predicted is small for the same realization or vice versa (Oliver and Chen 2009). In SAGD, oil recovery is highly affected by the vertical permeability of the reservoir. Edmunds and Best (1989) has discussed the effect of anisotropy on the growth of steam chamber in detail. Hence, vertical permeability can be a good weighting factor. However, before using the weighting factor, the correlation between the parameter and weighting factor should be ensured.

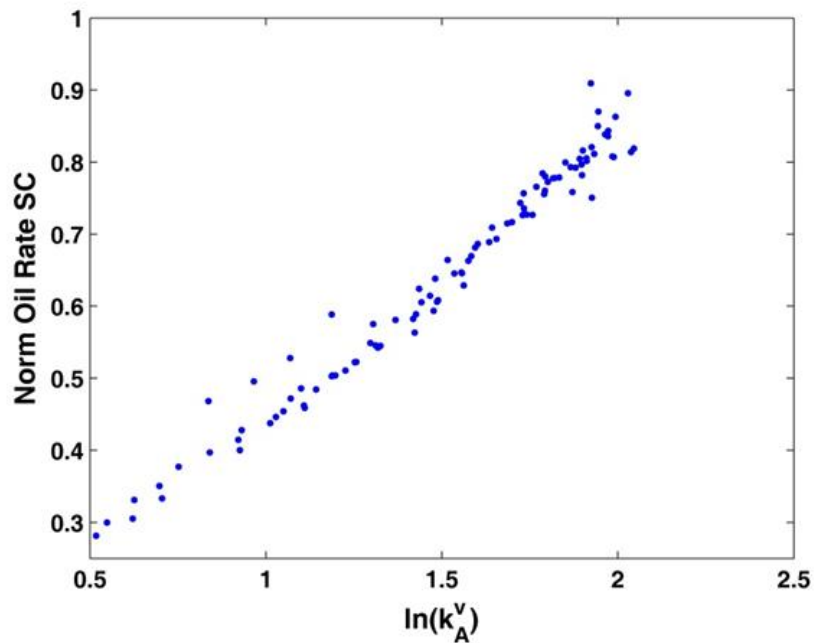


Figure 3.2 - Proportionality between $\ln(k_A^v)$ and normalized oil rate at 1200 days.

As shown in *Figure 3.2*, the plot of oil rate at 1200 day and the natural logarithm of the arithmetic average of vertical permeability of each cell of realization is proportional.

However, in our case, multiple production parameters need to be predicted and therefore instead of using $\ln(k_A^v)$ as a weighting factor, we use

$$w_i = \frac{\lambda \times \ln(k_A^v)}{1 + \lambda \times \ln(k_A^v)} \quad (3.29)$$

where k_A^v is arithmetic average of vertical permeability of each grid block of realization i in units of μm^2 . λ is an empirical constant in Eq. (3.29) and is equal to 10.8 in the case study considered. For *Figure 3.2*, we simulated all 100 realizations of initial ensemble. However, in practical application, one can run few simulations and identify the appropriate weighting factor. Once the weighting factor is decided, the computational cost to select realizations with higher probability density is quite low.

3.5.4 Application of K-Means Clustering

In order to select 50 member reduced ensemble using k-means clustering method, steps described in section 3.2.3 were followed.

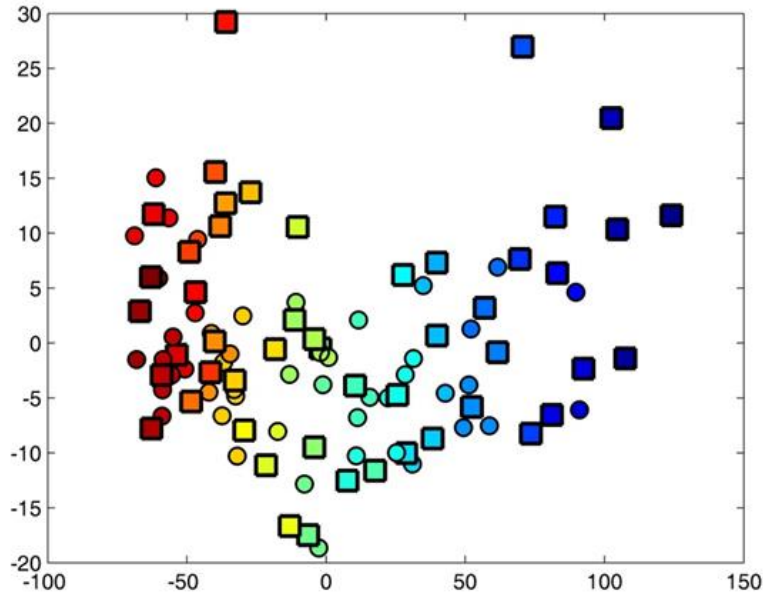


Figure 3.3 – Realizations in multidimensional space where square box shows realizations selected by K-Means clustering.

To implement the method, codes available publicly by Stanford Center for Reservoir Forecasting (SCRF) were modified. As authors Scheidt and Caers (2009) proposed to use oil rate or cumulative oil production at a particular time interval as a distance function, we used oil rate at 5 different time steps to calculate the distance function. After calculating distance matrix, classical multidimensional scaling was applied to map realizations on 2D Euclidean space. In order to apply standard linear pattern recognizing tools, Gaussian radial basis function kernel (Eq. (3.5)) with $\sigma = 250$ was used to transform Euclidean space into featured space and clustering algorithm was applied. 50 clusters were generated and realizations nearest to the centroid of the clusters were selected as a subset. The realizations mapped in 2D space are shown in *Figure 3.3* where square box represents selected realizations.

3.5.5 Application of Scenario Reduction Method

To apply proposed method, initially, we identified net cells in each realization in the initial ensemble using criteria explained in Eq. (3.7). Threshold porosity (ϕ_0) and threshold permeability (k_0) were considered as half of mean of the porosity and permeability of a particular realization respectively. Then static measures explained in Eq. (3.8) to Eq. (3.14) were calculated for each realization. Also, dissimilarity distance between realizations was calculated using Eq. (3.15). Next, to select reduced ensemble, Kantorovich distance was calculated between two distributions and a constrained MILP model was defined to minimize the objective value defined in Eq. (3.17). The optimization model was solved using CPLEX solver and 50 realizations were selected when Kantorovich distance between initial distribution and reduced distribution was minimum. Solving the optimization model took even less than a second, which shows computational efficiency of the proposed method. It is important to note that proposed scenario reduction method can also be effective in case of reservoir with multimillion grid blocks since the MILP based scenario reduction method only needs static measure that is calculated for the whole reservoir and irrespective of the total number of grid blocks in a particular realization. The static measures provide exclusive identification to each realization in the initial ensemble and ultimately form a basis for ensemble reduction.

3.5.6 Application of EnKF

In order to check the performance of reduced ensemble selected using all four different methods in history matching, EnKF was applied on each of them. The model parameter used here is natural logarithm of permeability in order to fulfill Gaussian statistics assumption of EnKF and production parameters used are oil rate and steam oil ratio. Hence, state vector for all realizations together can be shown as,

$$Z_k = \begin{bmatrix} \{\ln(\text{permeability})\}_{N_c \times N_s} \\ \{\text{Oil Rate}\}_{1 \times N_s} \\ \{\text{Steam Oil Ratio}\}_{1 \times N_s} \end{bmatrix}_{20002 \times N_s} \quad (3.30)$$

where N_c is number of cells in reservoir model i.e. 20000 and N_s is number of realizations in reduced ensemble i.e. 50. Reduced ensemble with even less number of realizations could be selected using other screening methods as well as proposed scenario reduction method. However, small ensemble in EnKF update converge to the same ensemble member (Sarma and Chen 2013), ultimately resulting into ensemble collapse and poor uncertainty quantification. Therefore, to obtain credible results in history matching using EnKF, reduced ensemble with 50 realizations was sampled. State parameters are not used in Eq. (3.30) as they are time dependent and can cause potential inconsistency (Gu and Oliver 2006). All the forward simulations were run using thermal simulator CMG STARS. State vector was assimilated at 760 days and results in the forecast period (761 days to 1355 days) were obtained by simulating the updated ensemble. Performance of each method was verified by analyzing decrease in average data mismatch and closeness of mean of ensemble to the true value.

3.6 Results and Discussions

As discussed before, our main intention is to select reduced ensemble such that it has same statistical distribution as initial ensemble after sampling/screening and to check the performance of the reduced ensemble in history matching using EnKF. To analyze results in a lucid manner, they are divided into two subsections. In section 3.6.1, only results after sampling/screening are discussed while in section 3.6.2, results after applying EnKF is compared. Note that all the production parameters presented in proposed work are normalized by a target value of respective production parameter.

3.6.1 Screening for reduced initial ensemble

To compare the results after initial screening, simulations were carried out for each realization in the reduced ensemble as well as an initial ensemble. For uncertainty assessment after the screening, oil rate, cumulative oil production, and steam oil ratio (all normalized) of the reduced ensemble are superimposed on the results of original ensemble. Also, a histogram of each production parameter at 1200 days are plotted to verify the statistical characteristics of both distributions, original and after screening. In addition, detailed quantitative analysis of production parameters obtained from simulation of the reduced ensemble is shown and compared with the original ensemble in *Table 3.1*. The true expected mean values of the original ensemble for oil production rate, cumulative oil produced and SOR are 0.513, 0.594, and 0.271, respectively. The standard deviation of the estimates of mean values, minimum and maximum values of these production parameters of screened ensembles are also compared with the original ensemble in *Table 3.1*.

If the method estimates mean and standard deviation close to those estimated by the original ensemble, it is considered as an unbiased method. It is also important to retain variability among ensemble members. The loss of ensemble variability could severely underestimate the underlying uncertainties of the geological models (Devegowda et al. 2007). Because of loss of variability in the prior model (after initial sampling in our case), the sample-derived covariance could become negligible (i.e. uncertainties in prior models are negligible) and therefore ensemble loses the ability to assimilate new observations. It can lead to spurious errors and unrealistic updates of state vectors referred as "ensemble collapse" (Chen and Oliver 2010). A method of screening whether retains variability among the ensemble members or not can be seen by superimposing their forecast on the original ensemble forecast and observing the spread or subspace spanned by the ensemble. Similarly, if the spread of ensemble is maintained after initial sampling/screening, the maximum and minimum values of the production parameters from the forecast of the method should be closer to that of original ensemble. If the spread is underestimated, filter divergence will occur in the analysis step with analysis result far away from the true observations (Anderson 2010).

Table 3.1 – Quantitative analysis of production data at 1200 days after sampling

	Original Ensemble	Scenario Reduction	Orthogonal Ensemble Members	K-Means Clustering	Importance Sampling
Normalized Oil Rate SC					
Mean	0.513	0.468	0.552	0.463	0.621
Std Dev	0.127	0.136	0.029	0.128	0.046
Min	0.225	0.225	0.484	0.225	0.530
Max	0.728	0.728	0.623	0.696	0.728
R²	-0.408	-0.230	-0.132	-0.168	-1.102
RMSE	0.146	0.136	0.137	0.133	0.186
Normalized Cumulative Oil Production					
Mean	0.594	0.549	0.645	0.546	0.689
Std Dev	0.117	0.128	0.017	0.125	0.026
Min	0.306	0.306	0.605	0.306	0.627
Max	0.734	0.734	0.687	0.718	0.734
R²	0.859	0.842	0.939	0.848	0.846
RMSE	0.073	0.077	0.053	0.075	0.084
Normalized Cumulative Water Production					
Mean	0.271	0.295	0.239	0.296	0.225
Std Dev	0.066	0.074	0.007	0.073	0.009
Min	0.212	0.212	0.224	0.215	0.212
Max	0.490	0.490	0.253	0.490	0.247
R²	0.296	-0.001	0.808	0.010	0.716
RMSE	0.050	0.061	0.031	0.060	0.038

The oil production rate of reduced ensembles (blue lines) superimposed on the oil rate of the original ensemble (green lines), and the actual field oil rate (red line) are shown in *Figure 3.4*. Similarly, the comparisons for cumulative oil production are shown in *Figure 3.7*. Improper weighting factor could lead to bias in screening in importance sampling. As shown in *Figure 3.2*, the weighting factor selected for the case study has a good correlation with production parameter. Therefore, the bias in screening is not due to the weighting factor. Rather, it is due to the fact that the orthogonal ensemble members and importance sampling methods are screening the realizations only having

higher oil rate. A similar bias in terms of cumulative oil production was also evident for the ensemble screened using these methods. On the other hand, the proposed scenario reduction method and k-means clustering cover the entire spread of oil rate and cumulative oil production displayed by the original ensemble. The distribution histograms of oil production rate and cumulative oil production are plotted in *Figure 3.5* and *Figure 3.6* respectively. The proposed scenario reduction method has a similar distribution as that of original ensemble. Also, from *Table 3.1*, minimum and maximum of oil production parameters for original ensemble and reduced ensemble using scenario reduction method show the similar values. Therefore, it is evident that the screened realizations using scenario reduction method correctly represent the original ensemble in terms of oil rate.

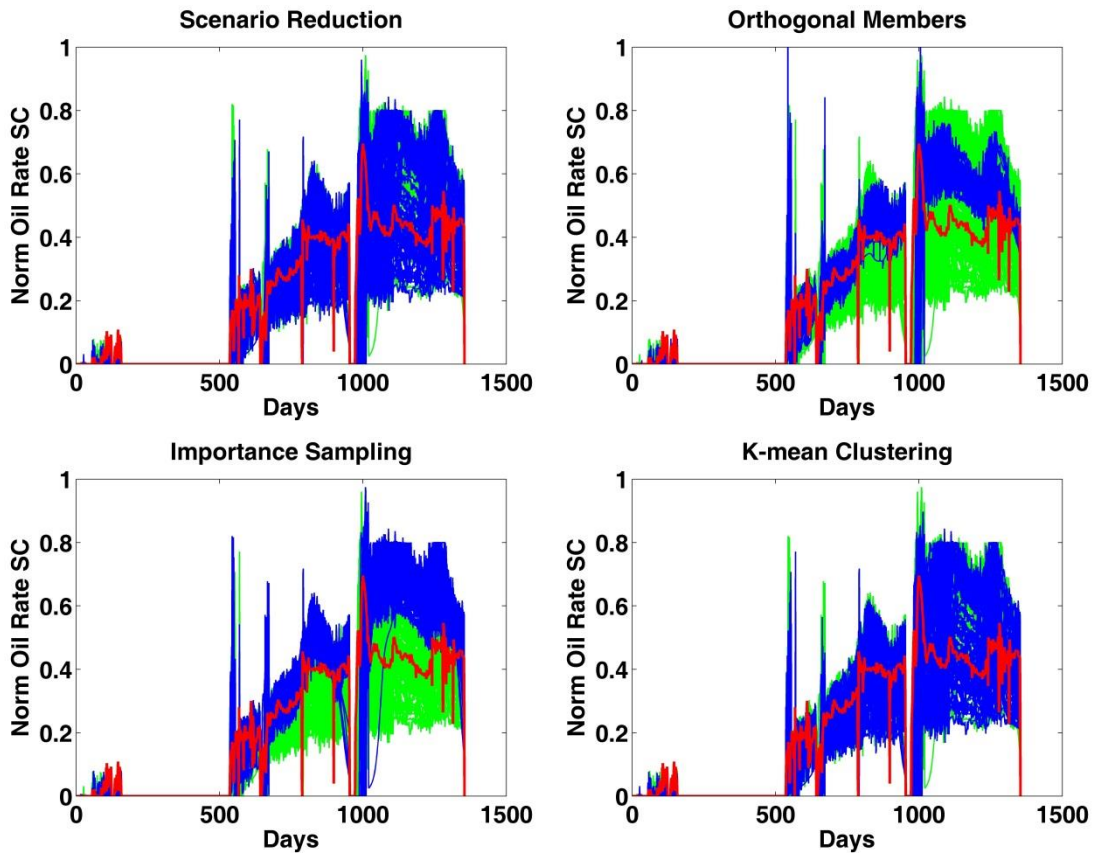


Figure 3.4 – Normalized oil rate of reduced ensembles (blue lines) obtained using different sampling methods, superimposed on normalized oil rate of the initial ensemble (green lines). Red line shows history from field data. SC = surface conditions.

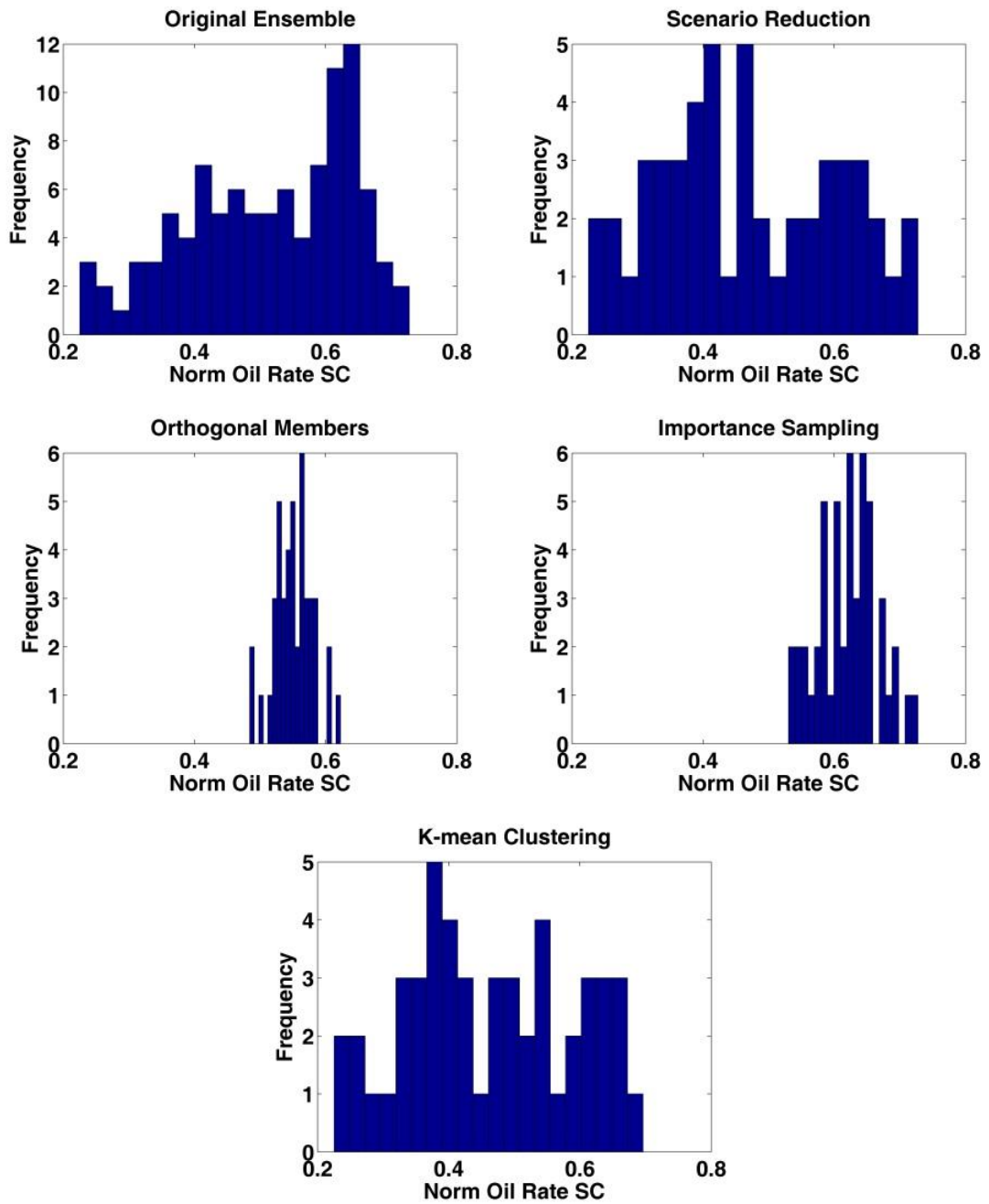


Figure 3.5 – Histogram of normalized oil rate at 1200 days for realizations obtained using different sampling methods and the original ensemble. SC = surface conditions.

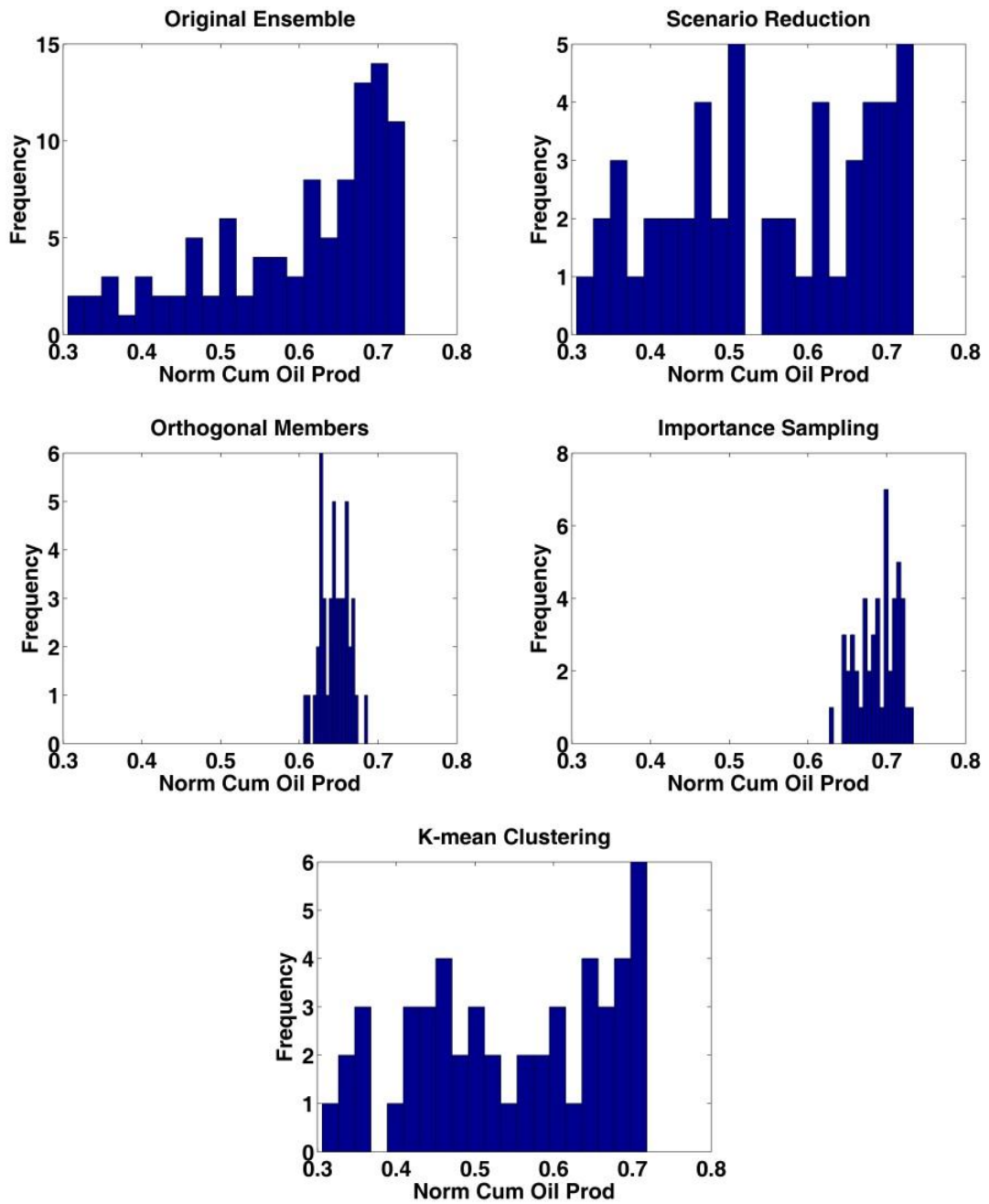


Figure 3.6 – Histogram of normalized cumulative oil production at 1200 days for realizations obtained using different sampling methods and the initial ensemble.

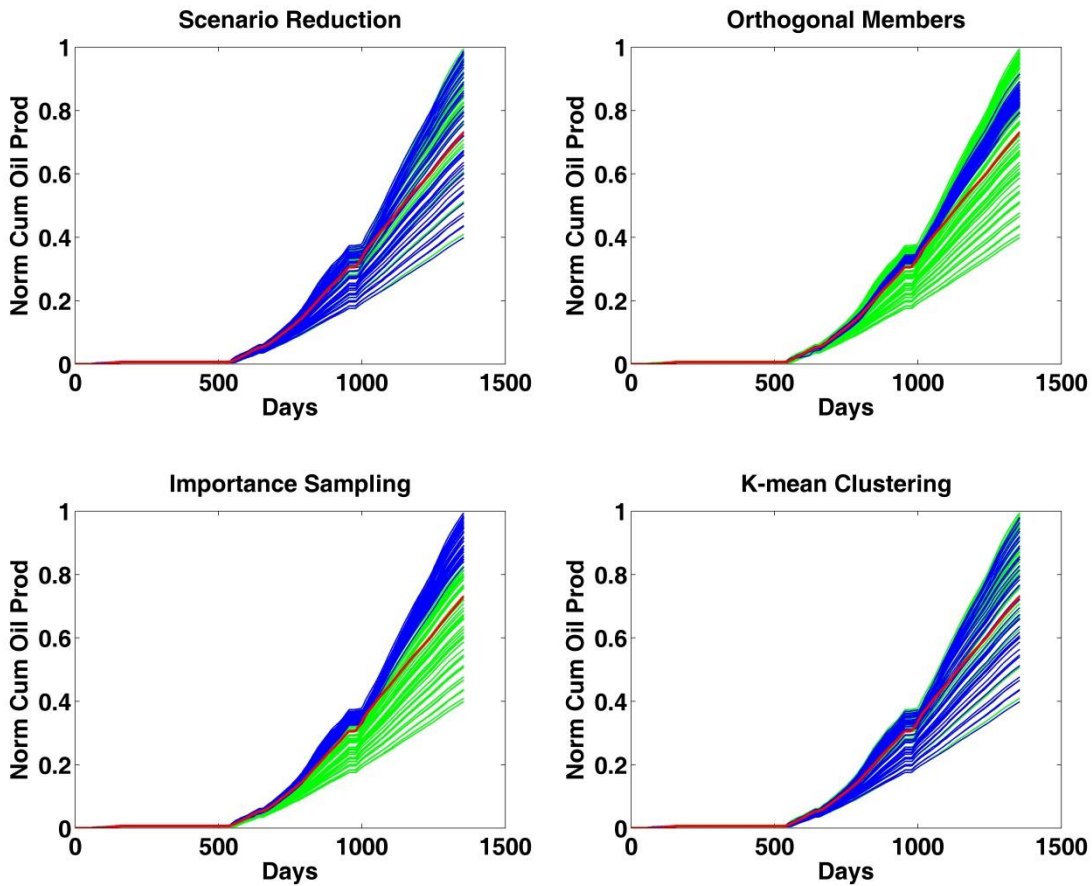


Figure 3.7 – Normalized cumulative oil production of reduced ensembles (blue lines) obtained using different sampling methods, superimposed on normalized cumulative oil production of the initial ensemble (green lines). Red line shows history from field data.

An important production parameter that depicts efficiency of the SAGD process, steam oil ratio (SOR) is also plotted in *Figure 3.9*. As no oil is produced in circulation phase, steam oil ratio will be very high. To see the difference in output of different realizations, SOR is plotted for 700 days to 820 days. The proposed scenario reduction method and k-means clustering method both show similar SOR predictions as the original ensemble. However, the scenario reduction method identifies the high-frequency and low-frequency areas of distribution of original ensemble precisely in case of SOR than other methods (*Figure 3.8*). Likewise, for scenario reduction method the minimum and maximum values of SOR, and the values of mean and standard deviation are similar to those of initial ensemble (*Table 3.1*).

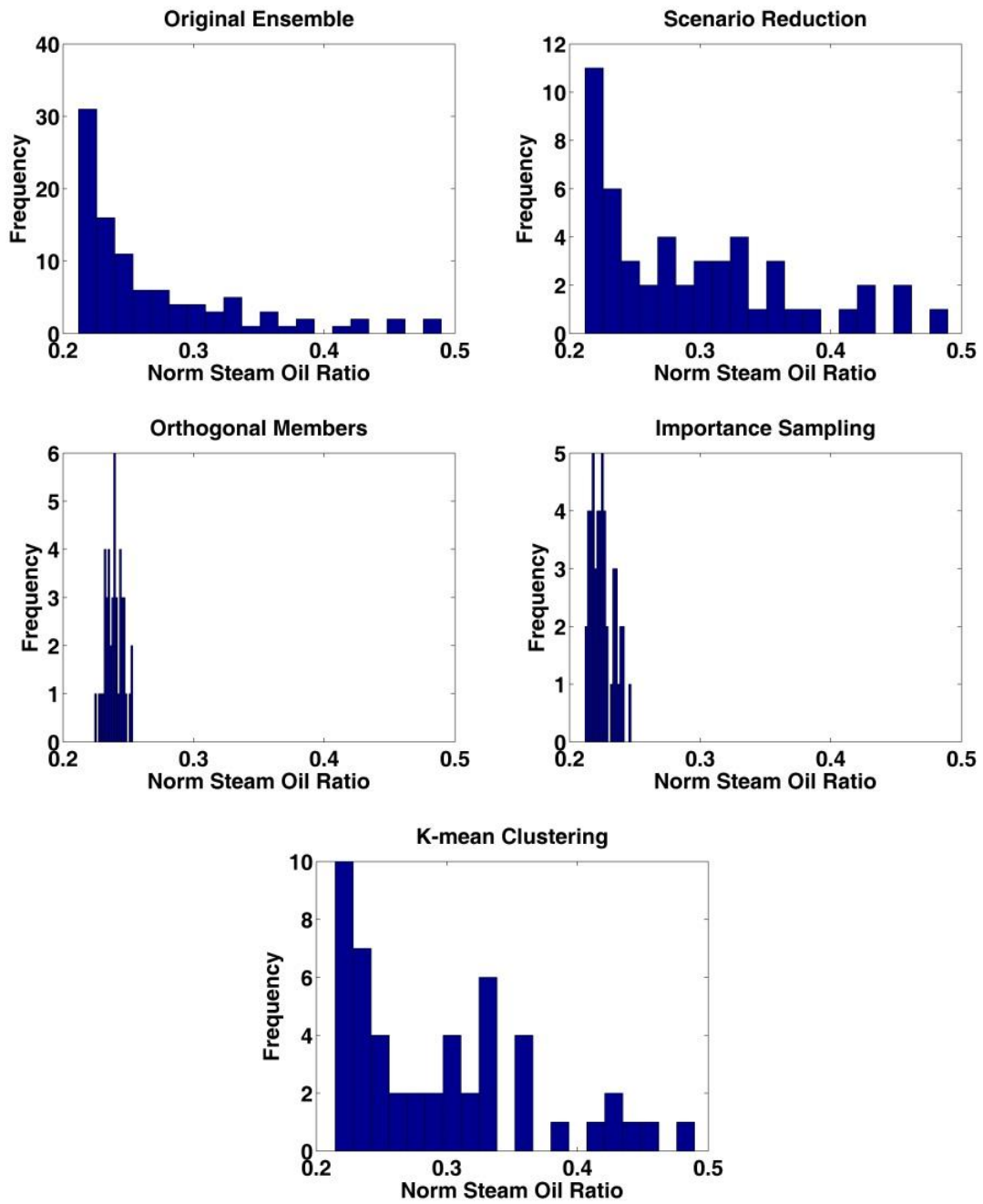


Figure 3.8 – Histogram of normalized steam oil ratio at 1200 days for realizations obtained using different sampling methods and the initial ensemble.

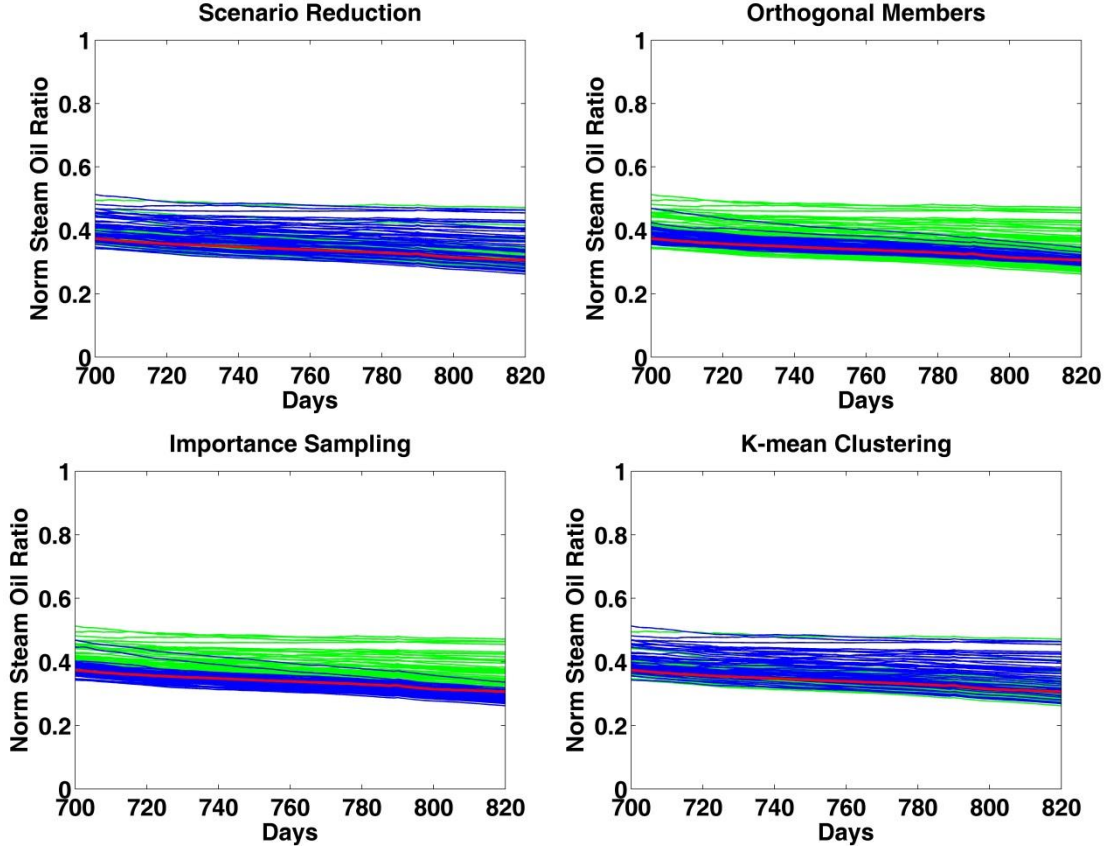


Figure 3.9 – Normalized steam oil ratio of reduced ensembles (blue lines) obtained using different sampling methods, superimposed on normalized steam oil ratio of the initial ensemble (green lines). Red line shows history from field data.

The R^2 and RMSE for each ensemble are calculated where R^2 represents the quality of ensemble as compare to original data while RMSE stands for Root Mean Square Error that represents average data mismatch. R^2 of any realization i for any particular production parameter can be defined as (Chitralekha et al. 2010),

$$R_i^2 = 1 - \frac{\sum_{k=t_1}^{t_n} (\hat{x}_i - \hat{x}_{obs})^2}{\sum_{k=t_1}^{t_n} (\hat{x}_{obs} - \bar{x}_{obs})^2} \quad (3.31)$$

where R_i^2 is the R^2 for i^{th} realization, \hat{x}_i and \hat{x}_{obs} are the simulated value and observed true value from the field of a production parameter for i^{th} realization respectively and

\bar{x}_{obs} is time average of a production parameter, averaged over time interval t_1 to t_n . To calculate R^2 of ensemble, equation can be shown as,

$$R^2 = \frac{1}{N_e} \sum_{i=1}^{N_e} R_i^2 \quad (3.32)$$

Value of R^2 in Eq. (3.32) can vary from $-\infty$ to 1 where $R^2 = 1$ represents a perfect match. To calculate RMSE of realization i for any production parameter, equation can be shown as (Gu and Oliver 2006),

$$RMSE_i = \sqrt{\frac{1}{t_n} \sum_{k=1}^{t_n} (\hat{x}_i - \hat{x}_{obs})^2} \quad (3.33)$$

By averaging the root mean square error of each realization, average data mismatch of ensemble can be calculated equation for which can be shown as,

$$RMSE = \frac{1}{N_e} \sum_{i=1}^{N_e} RMSE_i \quad (3.34)$$

where $RMSE$ equal to 0 shows that ensemble has no data mismatch and it has exact value of the parameter as true data.

Table 3.1 indicates R^2 and RMSE for all production parameters of the reduced ensemble as well as an initial ensemble. If a subset of realizations selected shows same statistical characteristics and distribution as an original ensemble, then R^2 and RMSE of the reduced ensemble should also be same as that of original ensemble. In case of oil rate, R^2 for the original ensemble is -0.408 while for proposed scenario reduction method it is -0.230, closer than any other sampling method. R^2 for oil rate is negative because of high fluctuation in daily oil rate as constraints are not constant with time. Also, the trend of oil rate changes in SAGD with a change in permeability (Marianayagam 2012) and hence output differs with respect to original data from the field at a particular time, which leads to negative R^2 values.

Box and whisker plots for all production parameters are also shown in *Figure 3.10*. In this figure, the box spans from the 0.25 quantile to 0.75 quantile and the whiskers span the entire range of the set. The horizontal red line in this figure shows the median of the distribution. It is evident from the figure that reduced ensemble sampled using orthogonal ensemble members method and importance sampling method are biased and with less variability than an original ensemble, hence these methods are not suitable for sampling/screening of realizations for the reservoirs with nonlinear processes such as SAGD. K-Means clustering shows comparable results except for distributions of some production parameters like steam oil ratio in this case. On the other hand, *Figure 3.10* confirms promising results of proposed scenario reduction method for all production parameters studied here.

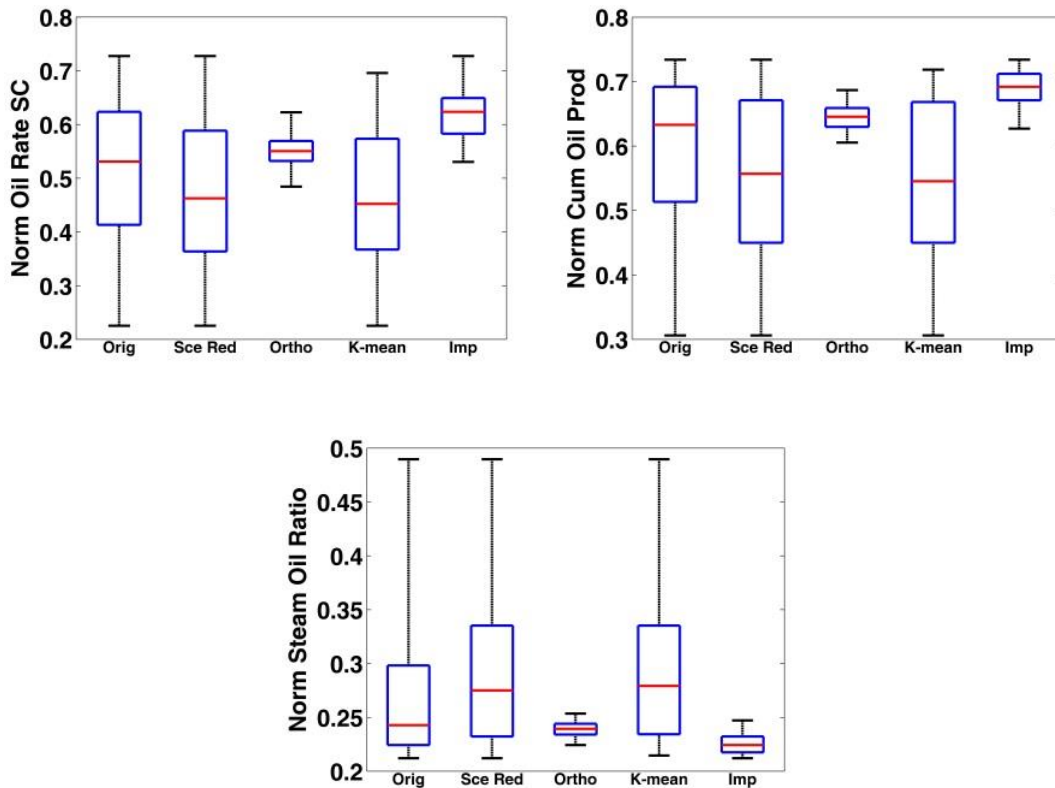


Figure 3.10 – Box and whisker plots representing distributions of different normalized production parameters at 1200 days obtained using simulations of all realizations of the original ensemble as well as reduced ensembles obtained using different sampling methods. Red line shows the median of each distribution.

3.6.2 Effect of initial screening/sampling on EnKF

After selecting reduced ensemble using four different methods, EnKF was applied on each of them in order to study their performance for history matching. To compare the results of different reduced ensemble after applying EnKF, simulations were rerun using updated reduced ensembles and production parameters were plotted. Also, the detailed quantitative analysis was performed in terms of data mismatch, standard deviation, and closeness of mean of the updated ensemble to the true value.

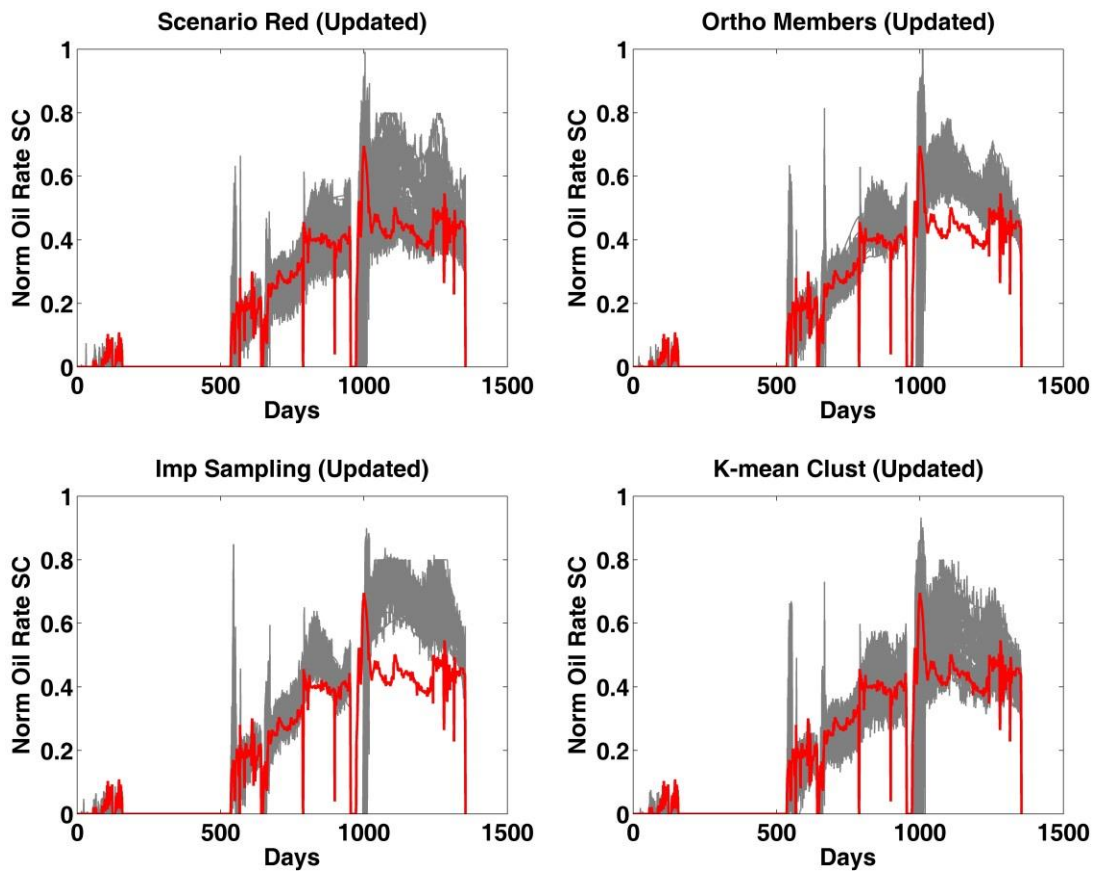


Figure 3.11 – Normalized oil rate of reduced ensembles (grey lines) obtained after EnKF update. Red line shows history from field data. History up to 760 days was used in EnKF and subsequent period from 761 days to 1355 days constitutes the forecast region.

Table 3.2 – Quantitative analysis of production data at 1200 days after update

	Scenario Reduction	Orthogonal Ensemble Members	K-means Clustering	Importance Sampling
Normalized Oil Rate SC (True Value = 0.398)				
Mean	0.490	0.555	0.494	0.636
Std Dev	0.084	0.029	0.072	0.039
Min	0.377	0.487	0.367	0.557
Max	0.733	0.613	0.641	0.702
R²	0.142	-0.145	0.142	-1.280
RMSE	0.115	0.138	0.116	0.195
Normalized Water Rate SC (True Value = 0.6)				
Mean	0.705	0.710	0.703	0.702
Std Dev	0.012	0.015	0.014	0.023
Min	0.664	0.667	0.668	0.652
Max	0.724	0.754	0.735	0.756
R²	-0.131	-0.419	-0.150	-0.595
RMSE	0.161	0.181	0.162	0.193
Normalized Cumulative Oil Production (True Value = 0.562)				
Mean	0.580	0.646	0.593	0.695
Std Dev	0.071	0.017	0.068	0.021
Min	0.475	0.602	0.460	0.646
Max	0.689	0.678	0.698	0.733
R²	0.948	0.938	0.949	0.831
RMSE	0.045	0.053	0.046	0.089
Normalized Steam Oil Ratio (True Value = 0.268)				
Mean	0.269	0.240	0.263	0.222
Std Dev	0.032	0.006	0.030	0.007
Min	0.223	0.226	0.221	0.210
Max	0.320	0.255	0.334	0.237
R²	0.679	0.845	0.692	-1.280
RMSE	0.039	0.028	0.038	0.038

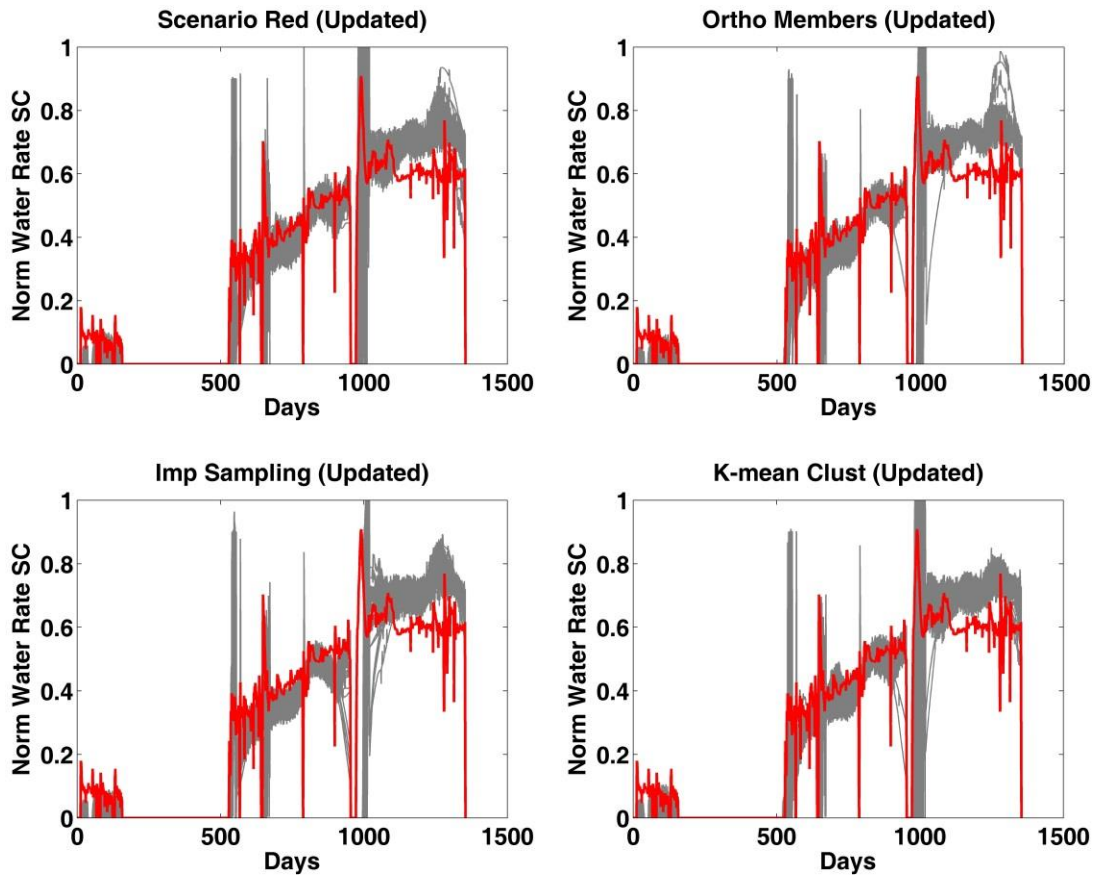


Figure 3.12 – Normalized water rate of reduced ensembles (grey lines) obtained after EnKF update. Red line shows history from field data.

The oil production rates and cumulative oil production of the updated reduced ensemble (plotted in grey lines) and the original oil rates from the field data (red line) are shown in *Figure 3.11* and *Figure 3.13* respectively. By comparing the ensembles after sampling (blue lines in *Figure 3.4* and *Figure 3.7*) and ensemble after update (grey lines in *Figure 3.11* and *Figure 3.13*), it can be seen that the uncertainty represented by ensemble spread after the update has decreased considerably compared to prior. However, ensembles selected using orthogonal ensemble members method and importance sampling method did not converge towards the true data after EnKF update because of the bias introduced during sampling step. The narrow ensemble spread for these two methods is a sign of ensemble collapse and may lead to underestimation of predicted uncertainty in the model variables. Also, mean of updated reduced ensemble obtained using scenario reduction method is the closest to

the true value from the field as compared to other methods (*Table 3.2*). The average data mismatch is lowest for scenario reduction method. In addition, R^2 value has increased from -0.408 to 0.142 that shows improvement in the quality of history matching after EnKF update. Also, the standard deviation in oil production rate and cumulative oil production decreased for the ensemble screened using scenario reduction, which depicts the convergence of reduced ensemble towards the true data after history matching.

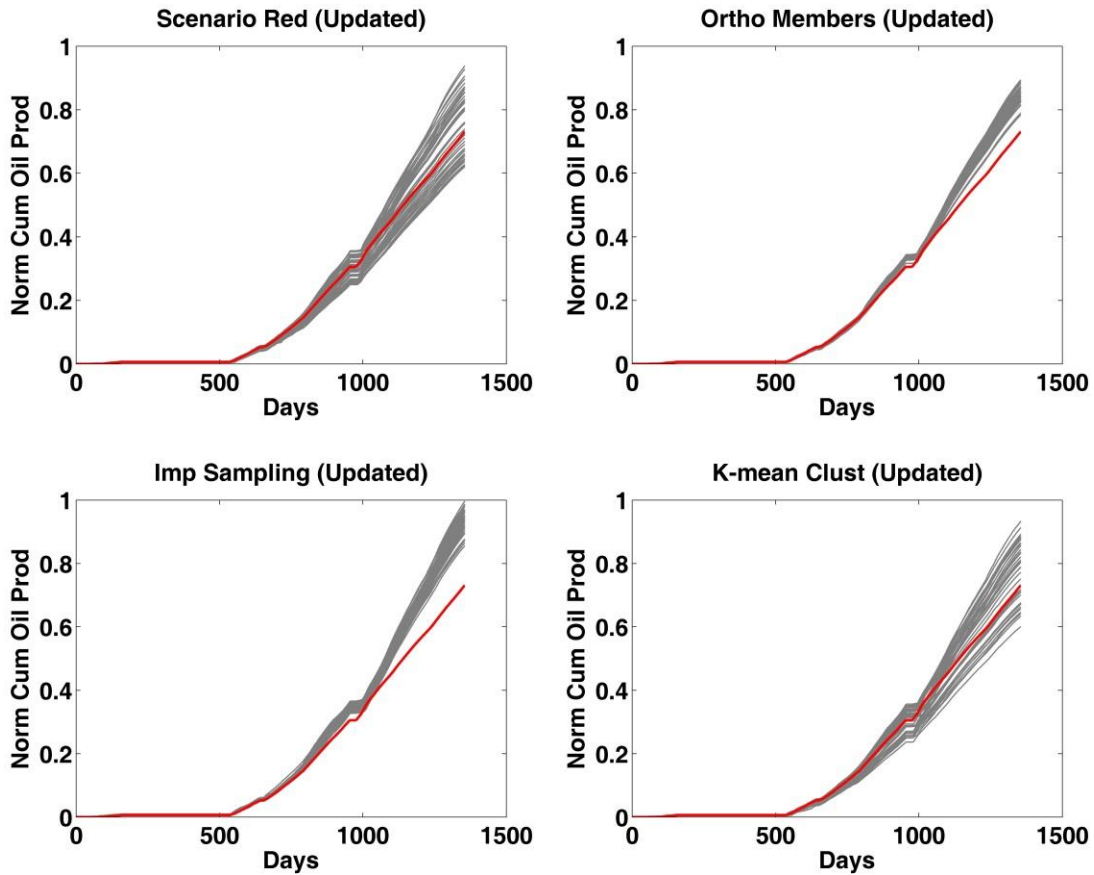


Figure 3.13 – Normalized cumulative oil production of reduced ensembles (grey lines) obtained after EnKF update. Red line shows history from field data.

The water production rate from simulations of updated reduced ensembles (grey lines) and original water rate from the field data (red line) is shown in *Figure 3.12*. After the update, water rate converged to the lowest standard deviation (equal to 0.012) for the reduced ensemble obtained using scenario reduction among all other methods studied here (*Table 3.2*). The RMSE in updated ensemble selected using k-means clustering is

also lower than those selected using orthogonal and importance sampling, however RMSE for ensemble selected using scenario reduction method was lowest.

In addition, to confirm the performance of proposed scenario reduction method in history matching using EnKF, steam oil ratio obtained from simulations of updated reduced ensembles are plotted and compared with original data in *Figure 3.14*. The standard deviation in case of orthogonal ensemble members and importance sampling is lower but the mean of the updated reduced ensemble did not converge to the true value. K-Means clustering method shows mean closer to the true value, however, mean of ensemble screened using scenario reduction method is same as a true value, which shows the superiority of proposed method over other techniques studied in this case study.

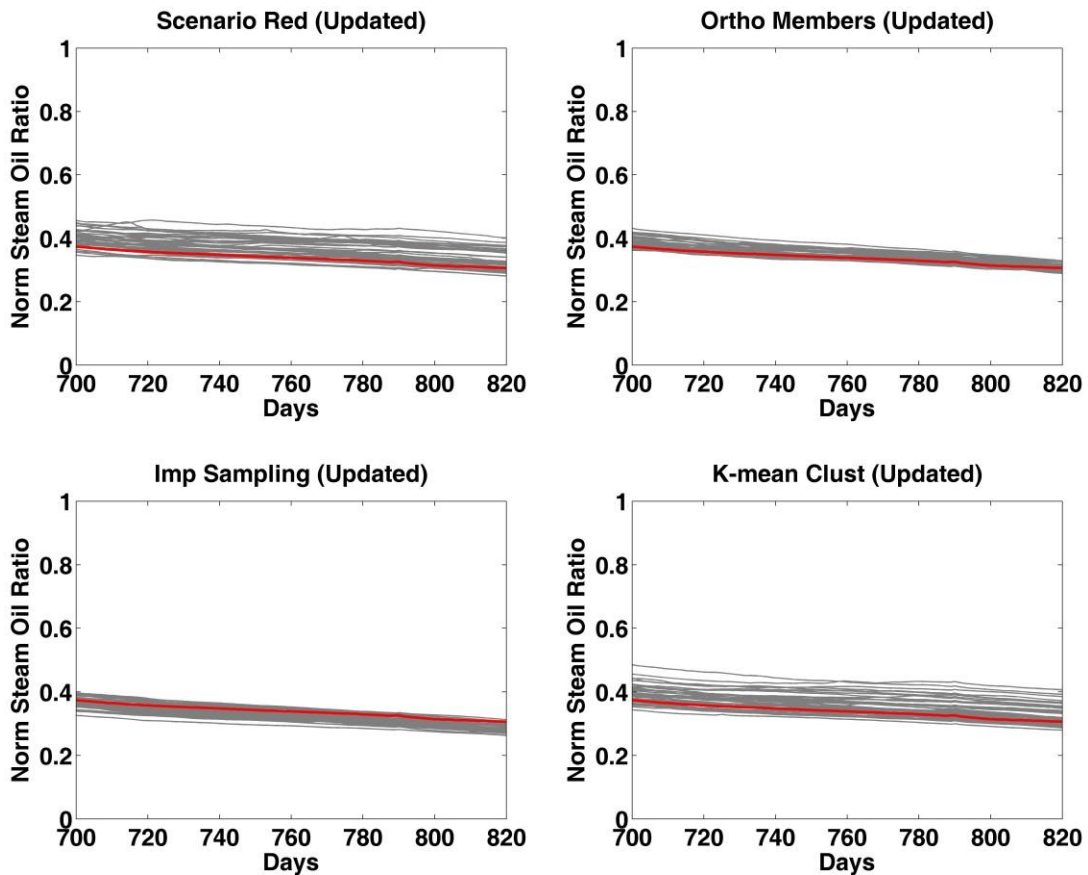


Figure 3.14 – Normalized steam oil ratio of reduced ensembles (grey lines) obtained after EnKF update. Red line shows history from field data.

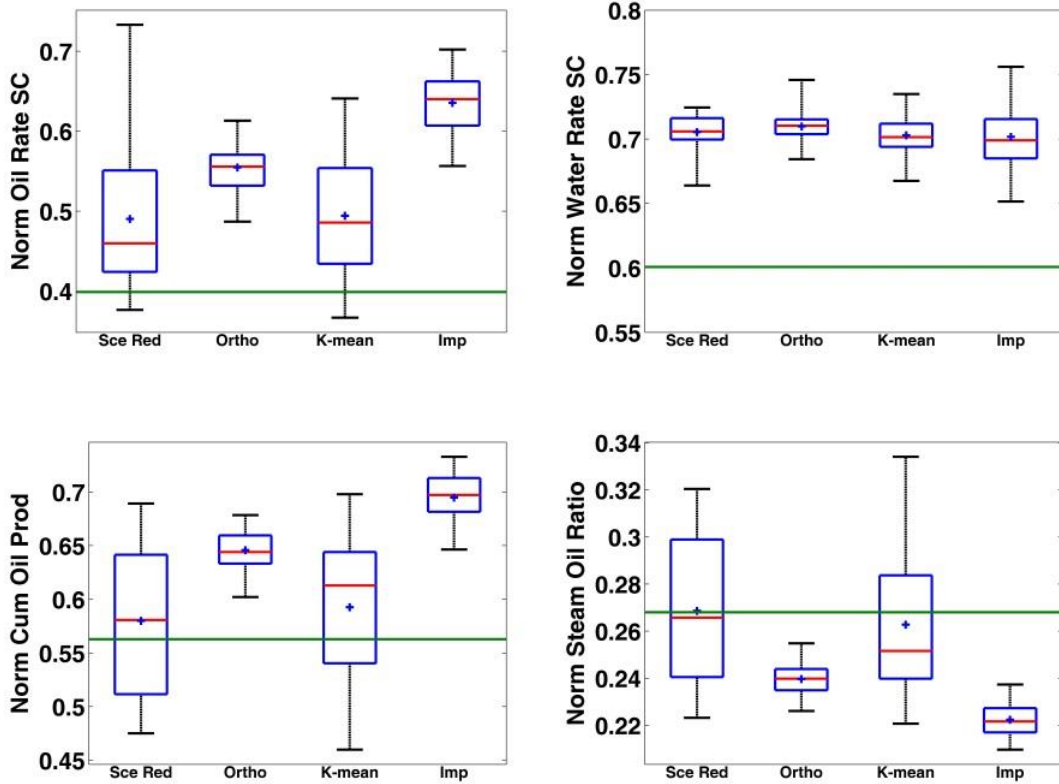


Figure 3.15 – Box and whisker plots representing distributions of different production parameters at 1200 days, obtained using simulations of all realizations of reduced ensembles obtained after EnKF update, red line shows median of each distribution while green continuous horizontal line shows true value of particular production parameter at 1200 days and '+' mark shows mean of each ensemble.

The box and whisker plots for all production parameters (obtained from a rerun of updated reduced ensembles) are shown in *Figure 3.15*. In the figure, the red line shows the median of the distribution, '+' sign in interquartile range shows the mean of the distribution while the green horizontal line represents the true value of a particular parameter from the field. It can be noticed that performance of importance sampling is poorer as compare to other methods with low standard deviation but biased ensemble means for all production parameters. Similar results can be observed for orthogonal ensemble member method. The reason for the poor performance of both methods is the smaller subspace spanned by the reduced ensembles due to which ensemble variability is not maintained, ultimately resulting into poor convergence in

the assimilation of data using EnKF. K-Means clustering shows comparable results in both sampling and updating using EnKF. However, streamline simulation model needs to be reformulated if numbers of wells or well locations are changed in the model. Also, streamline simulation takes significant time as compared to the time required to compute simple static measures in the proposed method. Facts explained here using various figures and tables endorse that ensemble selected using proposed scenario reduction method performs well in data assimilation, honoring the observations, and at the same time preserves variability in the prior.

3.7 Summary

We have presented a novel method with a primary objective of screening realizations from a large initial ensemble such that selected ensemble correctly represents the uncertainty of initial ensemble by maintaining model variability, preventing ensemble collapse and filter divergence, and gives good performance in history matching using EnKF even with less number of ensemble members. Proposed scenario reduction method is based on probability distance minimization in which dissimilarity between initial ensemble and subset selected is quantified using Kantorovich distance. In order to minimize it, a constraint-based mixed integer linear optimization model is used that assigns a new probability to each of those selected realizations. Moreover, this method uses multiple static measures relevant to the reservoir and the process. We have applied the scenario reduction method on a real field SAGD reservoir. The scenario reduction method maintained the variability in the screened ensemble, which is important for avoiding ensemble collapse, whereas the orthogonal ensemble and importance sampling methods introduced bias. During the history match, the spread of ensemble results is reduced significantly for all the methods demonstrating uncertainty reduction in geological models due to the assimilation of production data. However, EnKF was unable to correct the bias introduced due to orthogonal and importance sampling methods. Therefore, true observations did not fall within the ensemble results for these two methods. Scenario reduction method significantly reduced the computing cost without compromising uncertainty in forecast model that allows real-time updating of large-scale SAGD reservoirs at smaller time intervals.

Chapter 4

Polynomial-Chaos-Expansion Based Integrated Dynamic Modeling Workflow for Computationally Efficient Reservoir Characterization ²

² A version of this chapter has been published in the proceedings of the *SPE Europec featured at 79th EAGE Conference and Exhibition* and submitted to *Journal of Petroleum Science and Engineering*.

4.1 Introduction

Reservoir simulation is an important tool for optimal decision making and risk management in reservoir operations, however, not all the petrophysical properties are known in the reservoir model. A prior distribution of the geological properties conditioned to static data can be generated using various geostatistical techniques (Deutsch 2002). Also, different subsurface flow measurements (y) pertinent to unknown model parameters (θ) are available from surface and downhole sensors. From probabilistic perspective, Bayesian inference provides an excellent platform to compute the posterior probability density function (pdf) $p(\theta|y)$ conditioned to available data. Bayes' rule in the context of this work can be shown as follows (Robert and Casella 2004, Kaipio and Somersalo 2005):

$$p(\theta|y) = \frac{p(y|\theta) p_{pr}(\theta)}{p(y)} \quad (4.1)$$

where $p_{pr}(\theta)$ is the prior distribution, $p(y)$ is the density function of all the measurements used for conditioning and $p(y|\theta)$ is the likelihood function for obtaining y given the model parameters θ . From Eq. (4.1), it can be inferred that problem of uncertainty quantification is now reduced to sampling from pdf $p(\theta|y)$. However, thorough characterization of density is prohibitively expensive and not possible in most practical cases (Tarantola 2005).

Markov chain Monte Carlo (MCMC) is a standard sampling technique to implement Bayes' theorem. Given the conditioning data and likelihood function, it allows rigorous sampling of prior by performing a random walk constrained to some probabilistic rules such as Metropolis-Hastings algorithm (Metropolis et al. 1953). However, obtaining posterior in MCMC is not a finite-dimensional problem except in strictly linear and Gaussian cases (Iglesias et al. 2013). Therefore, evaluation of likelihood function – which commonly includes the use of reservoir simulator – may be required for thousands or millions of times to characterize the posterior, especially in reservoir applications that are highly nonlinear and non-Gaussian. Higher dimensions of unknown model parameters make this problem only worse. For computationally efficient implementation of MCMC, several workflows are developed to increase the

probability of acceptance of new proposals in Markov chain using discretization (Cotter et al. 2013), error modelling (Efendiev et al. 2009), linear approximation (Ma et al. 2008), and state vector covariance (Emerick and Reynolds 2012). However, longer chains required for legitimate posterior characterization has mostly restricted the MCMC applications for data assimilation in reservoir models to toy models (Efendiev et al. 2009, Emerick and Reynolds 2010, Liu and Oliver 2003, Oliver et al. 1997).

Currently, there is a growing interest in sequential ensemble-based methods, particularly the ensemble Kalman filter (EnKF). Initially introduced as an extension to the linear Kalman filter for state estimation in nonlinear systems (Evensen 1994), it is widely used for model parameter estimation. It approximates the solution space using few samples and updates the unknown parameters through state space augmentation, given a perturbed set of observations. To obtain an updated empirical estimate of posterior, Kalman gain (similar to weighting matrix in particle filter) is calculated using mean and covariance of prior pdf and cross-covariance between parameters and observations. Since computational cost is independent of the dimensions of model parameters and measurements in EnKF, its applications can be found in various engineering and science fields, including oceanography and atmospheric science (Anderson 2001, Houtekamer and Mitchell 1998, Evensen and van Leeuwen 1996), hydrology (Chen and Zhang 2006), and petroleum engineering (Lorentzen et al. 2001, Naevdal et al. 2003, Oliver and Chen 2011). However, when high fidelity simulation is used in EnKF, the overall computational cost is dominated by the forward model runs (Jafarpour and McLaughlin 2008). Various sampling/screening techniques (Oliver and Chen 2009, Patel et al. 2015) are proposed to reduce the size of ensemble, however, it may affect the quality of covariance estimates (Oliver and Chen 2011) and in turn the estimation of model variables.

Another approach for efficient data assimilation would be to implicate computationally less demanding data-driven meta/surrogate/proxy model as the forward model. These metamodels are essentially linear/nonlinear functions or their combinatorial with specified regressors. Using an available set of input-output data, unknown regressors (for e.g., coefficients, weights, biases) can be regressed or trained to forecast observations in EnKF. In section 2.2, ample studies have been reported employing different metamodels for various petroleum applications. Since architecture and underlying training algorithms are different for each metamodel, pros and cons offered

by them vary. However, a common drawback offered by the use of metamodel is the compromised accuracy. In the context of this work, deviation of metamodel responses from grid-based simulation introduces uncertainty in the forecast model, essentially motivating the proposed study.

While several comparative studies evaluating the uncertainty quantification properties of data assimilation techniques are reported in literature (Barker et al. 2001, Liu and Oliver 2003, Gao et al. 2006, Tavakoli and Reynolds 2011, Emerick and Reynolds 2013), it would be relevant to mention the work of Iglesias et al. (2013) and Jafarpour and Tarrahi (2011). Iglesias et al. (2013) evaluated the Gaussian approximations in ad-hoc techniques based on linearization around the maximum a posteriori estimate (LMAP), randomized maximum likelihood (RML) and EnKF methods. Using posterior distribution characterization, they concluded that Gaussian approximations provided the suboptimal estimations, for e.g., converged Gaussian approximation in EnKF with sufficient ensemble size was at least 10% off both in mean and variance as compared to the posterior obtained using MCMC. Jafarpour and Tarrahi (2011) investigated the performance of EnKF under the varying level of variogram uncertainty. They showed that overestimating uncertainty in variogram parameters was a better choice rather than introducing bias by use of incorrect initial values. From both the studies, it can be concluded that data assimilation algorithms are sensitive to uncertainties induced from different sources and neglecting them may lead to erroneous estimations. However, to the best of our knowledge, consequences of uncertainty in forecast model on the outcomes of various sampling/data-assimilation algorithms has not been systematically understood yet.

In this chapter, the performance of EnKF and MCMC is studied under uncertainty in the forecast model. The metamodel is based on cost-effective PCE that can handle nonlinearity and integrating high-dimensional state vectors through Karhunen-Loeve (KL) parameterization (Patel et al. 2017). KL expansion represents the initial ensemble in terms of uncorrelated random variables using eigen decomposition of covariance function, while PCE based mathematical model relates the random variables and production parameters using orthogonal polynomials and deterministic coefficients. As shown in *Figure 4.1*, the metamodel is comprised in the EnKF framework by utilizing PCE model to predict production parameters in forecast step and updating random variables obtained by KL expansion instead of permeability of each grid block in

analysis step of EnKF. Significant contributions of this work can be summarized as (1) assessing the ability of EnKF and MCMC to recover the quantities of interest (QoI) within a confidence interval under forecast model uncertainty, (2) evaluating the impact of PCE forecast model on EnKF and MCMC performance at distinct phases, and (3) illustrating the advantage of using MCMC with PCE metamodel through posterior distribution characterization. Results and analysis reported in this chapter will be instrumental in designing computationally efficient reservoir characterization, uncertainty quantification and real-time data assimilation workflows for improved closed-loop reservoir management.

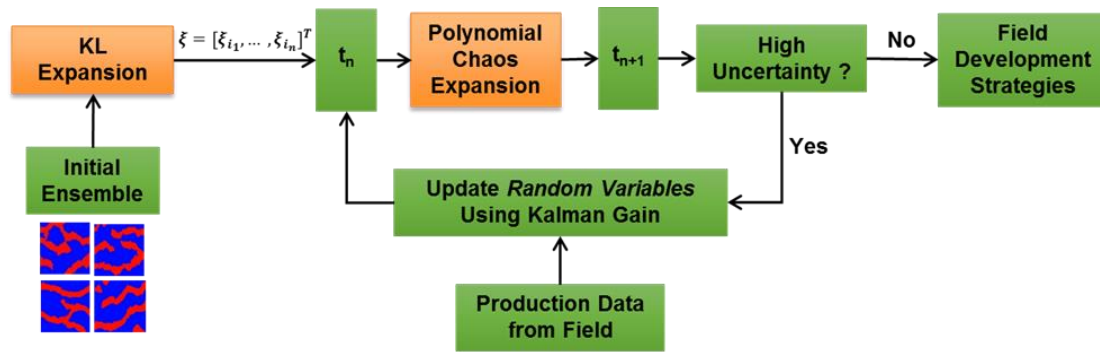


Figure 4.1 – Proposed idea of comprising PCE metamodel in the EnKF framework.

Section 4.2 and 4.3 comprises parameter inference methodologies MCMC and EnKF respectively. The explanation of the metamodel including KL, PCE and their integration in EnKF framework is given in section 4.4. Section 4.5 elaborates the application setup for the study including details of the reservoir model, PCE metamodel development and design of numerical experiments. In section 4.6, we report the inference results and analyze them qualitatively and quantitatively to discuss and compare different numerical cases considered in this work. Summary of this numerical study is presented in section 4.7.

4.2 Markov Chain Monte Carlo (MCMC)

MCMC is an iterative sampling algorithm (Gamerman and Lopes 2006) for Bayesian inference of the posterior distributions that are often difficult to obtain analytically. As the name suggests, it is a conjugation of two properties: Monte Carlo and Markov chain. In Monte Carlo approach, samples are randomly drawn from a distribution with

known density while Markov chain is a probabilistic sequential process that gives the sampling process a formal direction to make it more efficient. Assuming prior distribution with mean $\bar{\theta}$ and covariance C , the algorithm shown below can be followed to obtain the posterior distribution.

Algorithm 4.1 [MCMC]

1. Set proposal index $i = 0$ and initial model $\theta_0 \sim \mathcal{N}(\bar{\theta}, C)$.
2. Generate a proposal $\theta' = \theta_i + \epsilon$ where $\epsilon \sim \mathcal{N}(0, \beta^2 I)$.
3. Calculate the probability of acceptance using likelihood function $L(\theta)$ for proposal θ' and original sample θ_i :

$$r = \frac{L(\theta')}{L(\theta_i)}, \quad \text{where } L(\theta) \doteq \pi(\theta|y) \quad (4.2)$$

4. Select the new model in Markov chain as per the following rule:

$$\theta_{i+1} = \begin{cases} \theta', & \text{if } r > \alpha \quad (\text{ACCEPT}) \\ \theta_i, & \text{Otherwise} \quad (\text{REJECT}) \end{cases} \quad (4.3)$$

5. $i \mapsto i + 1$ and repeat from step 2.
-

In the algorithm, ϵ is the local perturbation, β^2 is the variance of proposal distribution, and α is the random sample such that $\alpha \in \mathcal{U}(0,1)$. To obtain a well-mixed chain, acceptance rate should be far from both 0 and 1. Recently, considerable theoretical and empirical support has been given to the notion of optimal acceptance rate between 0.2 and 0.3 (Gelman et al. 1996, Roberts et al. 1997, Roberts and Rosenthal 2001). β^2 can be scaled by trial and error or adaptively to achieve the optimal acceptance rate; higher the β^2 , lower the acceptance rate and vice versa.

4.3 EnKF Algorithm

EnKF is an alternative filtering approach to obtain the posterior $p(\theta|y)$ by assimilating new observations sequentially in a Bayesian framework. It has found applications in

distinct nonlinear inverse problems for parameter estimation including subsurface characterization due to its reasonable computational cost, ability to incorporate higher dimensional state space, and ease of implementation. We refer the readers monograph by Aanonsen et al. (2009) in which application of EnKF in reservoir engineering is reviewed.

Joint EnKF estimation comprises two steps: prediction (forecast) step and analysis step. Augmented state vectors containing model parameters (θ) and system states (u) are propagated in the future using a forecast (forward) model in prediction step and latest observations (y) are assimilated using the analysis equation to estimate the unknown parameters. With Gaussian approximations, standard perturbed observation version of EnKF used in this study to understand the effect of uncertainty in forecast model is discussed below. The method is similar to the one in section 3.4, except that it is presented in the form of algorithm in the current context.

Algorithm 4.2 [EnKF]

1. Create N_e independent samples of $\theta_0^{a,j}$ and $u_0^{a,j}$ from their respective priors to form an initial state vector:

$$z_0^{a,j} = \begin{Bmatrix} \theta_0^{a,j} \\ u_0^{a,j} \end{Bmatrix}, \quad \forall j \in [1, N_e] \quad (4.4)$$

2. Integrate the state vector from timestep t_n to t_{n+1} using forward model $F(\cdot)$.
3. Construct an augmented state vector at timestep t_{n+1} where $n = 0, 1, \dots, N_t$ by adding the observations measured using measurement operator Ψ_{n+1} :

$$z_{n+1}^{p,j} = \begin{Bmatrix} \theta_{n+1}^{p,j} \\ u_{n+1}^{p,j} \\ y_{n+1}^{p,j} \end{Bmatrix} = \begin{Bmatrix} \theta_n^{a,j} \\ F(u_n^{a,j}, \theta_n^{a,j}) \\ \Psi_{n+1}(F(u_{n+1}^{p,j}, \theta_n^{a,j})) \end{Bmatrix} \in \mathbb{R}^{N_\theta + N_u + N_y}, \quad \forall j \in [1, N_e] \quad (4.5)$$

4. Calculate first- and second-order moments using Monte Carlo integration as follows:

$$\bar{Z}_{n+1}^p = Z_{n+1}^p W \quad (4.6)$$

$$C_{n+1}^{p,ZZ} = \frac{1}{N_e - 1} (Z_{n+1}^p - \bar{Z}_{n+1}^p)(Z_{n+1}^p - \bar{Z}_{n+1}^p)^T \quad (4.7)$$

where

$$Z_{n+1}^p = \{z_{n+1}^{p,1}, \dots, z_{n+1}^{p,j}, \dots, z_{n+1}^{p,N_e}\} \in \mathbb{R}^{(N_\theta + N_u + N_y) \times N_e} \quad (4.8)$$

5. Update the ensemble using analysis equation,

$$z_{n+1}^{a,j} = z_{n+1}^{p,j} + K_{n+1} (d_{n+1}^j - H z_{n+1}^{p,j}), \quad \forall j \in [1, N_e] \quad (4.9)$$

where

$$K_{n+1} = C_{n+1}^{p,zy} (C_{n+1}^{p,yy} + R)^{-1} \quad (4.10)$$

and

$$d_{n+1}^j \sim \mathcal{N}(d_{n+1}^{obs}, R) \quad (4.11)$$

6. $n \mapsto n + 1$ and repeat from step 2.

In the algorithm, K_{n+1} (see Eq. (4.10)) is the Kalman gain for the whole ensemble. Since model parameters and system states are not observed in the reservoir applications (Gu and Oliver 2006), observation operator $H = [0, 0, I]$ is used in the Eq. (4.9). Dimensions of model parameters, state variables, and observations (predicted data) are denoted as N_θ , N_u , and N_y respectively. Accordingly, in Eq. (4.10), $C_{n+1}^{p,zy}$ and $C_{n+1}^{p,yy}$ are the cross-covariance between forecast state vector and observations and auto-covariance between observations with dimensions $(N_\theta + N_u + N_y) \times N_y$ and $N_y \times N_y$, respectively. R is the $N_y \times N_y$ measurement noise covariance matrix while W is the $N_e \times N_e$ matrix with each element of it equal to $1/N_e$. True observations at current timestep $n + 1$ are denoted using d_{n+1}^{obs} in Eq. (4.11) based on which perturbed measurements d_{n+1}^j are created. Superscript p and a represent the prediction or analysis step of EnKF. From Eq. (4.10), it is clear that data obtained in the prediction

step is sufficient to calculate both covariance matrices. Also, computing cost of updating ensemble (step 5) is trivial as compared to propagation of each ensemble member (step 2) in prediction step using nonlinear forward model $F(\cdot)$ (typically a reservoir simulator).

4.4 PCE Metamodel

Constructing KL-PCE based mathematical model comprises several steps that are described in following subsections. The first step includes the reduction in dimensionality of geological parameters using KL expansion, which is described in subsection 4.4.1. Then PCE is described in next subsection that ultimately substitutes full physics simulation in assisted history matching. Also, details about Probabilistic Collocation Method (PCM) used to determine time-dependent coefficients in PCE is provided. The last subsection delineates the integration of KL, PCE, and EnKF which can be further used for history matching of SAGD reservoirs.

4.4.1 Karhunen-Loeve Parameterization

KL parameterization/transformation/expansion is the most popular parameterizing technique to represent a random field in the form of series expansion. It uses deterministic basis functions and uncorrelated random variables for linear approximation of spatial properties. KL transformation can retain two-point statistics of a random field (Bazargan 2014), which is one of the unique properties responsible for its extensive use in different applications. In addition, Huang et al. (2001) mentioned that if deterministic basis functions, as well as random coefficients, are orthogonal, then such bi-orthogonal property of KL transformation ensures that it epitomizes the maximum information about the random field in the form of random variables. Furthermore, random variables in KL expansion can be treated as a reduced number of differentiable parameters of original high dimensional random field (permeability realizations in our case).

In this study, to tackle the curse of dimensionality in PCE metamodel, prior distribution is honored by obtaining the model parameters in terms of an optimal L^2 basis through KL expansion. By truncating the KL series, prior can be parameterized in terms of few

stochastic variables. A random field $M(\theta)$ with first-order moment $E[M(\theta)] = \bar{M}(\theta)$ and $E \int_{\Omega} M^2(\theta) d\theta < \infty$ can be expanded using orthogonal basis $\{\phi_l\}$ as,

$$M(\theta) = \bar{M}(\theta) + \sum_{l=1}^{\infty} \omega_l \phi_l(\theta) \quad (4.12)$$

where random variables ω_l can be expressed as,

$$\omega_l = \int_{\Omega} (M(\theta) - \bar{M}(\theta)) \phi_l(\theta) d\theta \quad (4.13)$$

Following Mercer's theorem, spectral decomposition of covariance function $C(\theta_1, \theta_2)$ is,

$$C(\theta_1, \theta_2) = \sum_{l=1}^{\infty} \lambda_l f_l(\theta_1) f_l(\theta_2) \quad (4.14)$$

where λ_l is the eigen values of prior covariance ordered as $\lambda_1 \geq \lambda_2 \geq \dots$ and $f_l(\theta)$ are eigen functions, which is a special case of orthogonal basis $\{\phi_l\}$ in $L^2(\Omega)$.

Denote $\xi = \frac{\omega_l}{\sqrt{\lambda_l}}$ with $E[\xi_l] = 0$ and $E[\xi_{l_1} \xi_{l_2}] = \delta_{l_1 l_2}$ where $\delta_{l_1 l_2} = 1$ if $i = j$ and zero otherwise. As Eq. (4.12) and (4.14) entails each other, it follows the well-known KL expansion (truncated by N_s terms) that can be expressed as,

$$M(\theta) = \bar{M}(\theta) + \sum_{l=1}^{N_s} \sqrt{\lambda_l} \xi_l f_l(\theta) \quad (4.15)$$

where λ_l and $f_l(\theta)$ satisfy the homogeneous Fredholm equation of second kind that can be given as,

$$\int_{\Omega} C_{\theta} f(\theta) d\theta = \lambda f(\theta) \quad (4.16)$$

L^2 basis functions in Eq. (4.15) are deterministic and resolves spatial variance of random field, enabling parameterization of the model parameters.

If ensemble size is large enough then covariance matrix calculated using Eq. (4.14) is bounded, symmetric and positive definite. Eigen values for such covariance matrix are calculated using standard methods like singular value decomposition that gives square roots of eigen values diagonally in a singular matrix. In addition, due to the symmetry of covariance matrix, monotonic reduction in eigen values is guaranteed (Saad 2007) as represented in *Figure 4.2*. In KL parameterization truncated by N_S larger eigen values, the rate of reduction in eigen values depends on the correlation length of the initial ensemble (Bazargan et al. 2015). Higher the spatial change in field variance is, slower the rate of monotonic reduction in eigen value will be. Hence, more eigen values should be considered in such cases to absorb the maximum information of the original random field. Contrary to that, reduction in eigen values with highly correlated random field happens much faster and the small number of eigen values will be sufficient to represent the random field. Ghanem and Spanos (1991) demonstrated that even the truncated KL expansion is optimal in the sense that mean square approximation error is converged and minimized.

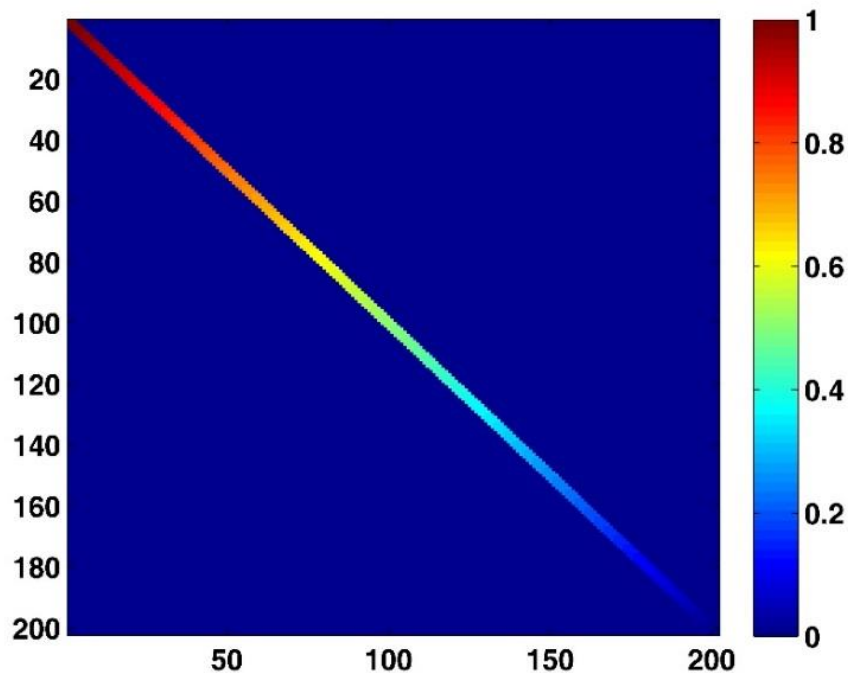


Figure 4.2 – *Monotonic reduction in eigen values of covariance matrix obtained using singular value decomposition.*

The stepwise procedure used in this work to implement KL expansion is as follows:

Algorithm 4.3 [KL]

1. Calculate the covariance matrix $C_\theta \in \mathbb{R}^{N_\theta \times N_\theta}$ using samples from prior as shown below:

$$C_\theta = \frac{1}{N_e} (\theta_0 - \bar{\theta}_0)(\theta_0 - \bar{\theta}_0)^T \quad (4.17)$$

2. Obtain the eigenvalues $\lambda \in \mathbb{R}^{N_\theta \times N_\theta}$ and eigen functions $f(\theta) \in \mathbb{R}^{N_\theta \times N_\theta}$ by solving the following discretized equation:

$$C_\theta f(\theta) = \lambda f(\theta) \quad (4.18)$$

3. Retain the N_s leading eigen values such that energy ratio (e) is as close to 1 as possible.

$$e = \frac{\sum_{l=1}^{N_s} \lambda_l}{\sum_{l=1}^{N_\theta} \lambda_l} \quad (4.19)$$

4. Generate the model parameters by substituting distinct ξ_l in Eq. (4.15).
-

For rapid reduction rate of $\lambda_l, \forall l \in [1, N_\theta]$, truncated KL can be optimal in the L^2 sense. When analytical covariance function is not known priori, number of samples considered to calculate it should be carefully chosen so that converged covariance function yields (Bazargan 2014). KL expansion reproduces the second-order statistics, proof of which is given by Huang et al. (2001).

4.4.2 Polynomial Chaos Expansion (PCE)

PCE is an efficient way to represent computationally prohibitive dependent differential equations of nonlinear subsurface systems by including nonlinearity in stochastic analysis through fast converging polynomials in probability space. It is a spectral expansion of stochastic quantities using orthogonal polynomials and weights associated with a specific probability density (Debuschere et al. 2004). Among several advantages offered by PCE, the most significant benefit is that convergence in

probability space is assured as the order of PCE increases (Babaei et al. 2015). In fact, Li et al. (2011) concluded that PCE converges with a faster rate as compared to other polynomials for a particular type of probability density function of input variables. Hence, PCE is an appropriate choice as a forward model in this study.

Since its inception in 1938 by Wiener, PCE has been used in numerous engineering applications. Especially, implementation of truncated Hermite polynomials in stochastic finite element methods by Ghanem and Spanos (1991) re-established the popularity of PCE. For numerical model of form $y = g(\xi)$, in a probability space Ω , PCE can be written as (Wiener 1938),

$$\begin{aligned} \hat{y} = c_0 \Gamma_0 + \sum_{k_1=1}^{\infty} c_{k_1} \Gamma_1(\xi_{k_1}(\Omega)) + \sum_{k_1=1}^{\infty} \sum_{k_2=1}^{k_1} c_{k_1 k_2} \Gamma_2(\xi_{k_1}(\Omega), \xi_{k_2}(\Omega)) \\ + \sum_{k_1=1}^{\infty} \sum_{k_2=1}^{k_1} \sum_{k_3=1}^{k_2} c_{k_1 k_2 k_3} \Gamma_3(\xi_{k_1}(\Omega), \xi_{k_2}(\Omega), \xi_{k_3}(\Omega)) + \dots \end{aligned} \quad (4.20)$$

where $\xi_k \in \Omega \subseteq \mathbb{R}^d$ are independent random variables, c_k are the deterministic coefficients, and Γ_k are the d-variate orthogonal basis set, chosen as per the pdf of the random variables. Typically, type of orthogonal polynomials in PCE depends on the probability distribution of input random variables. It is recommended to use specific orthogonal polynomials with a particular kind of probability distribution to achieve better convergence rate in chaos expansion for e.g. Legendre polynomials for uniform distribution, Hermite polynomials for Gaussian distribution, Laguerre polynomials for gamma distribution and Jacobi polynomials for beta distribution (Li et al. 2011).

In our case, random variables used in PCE are identical to those employed in KL transformation, i.e. $\xi \sim \mathcal{N}(0,1)^d$. Therefore, Γ_k are Hermite polynomials in chaos expansion as they form best orthogonal basis for Gaussian independent random variables (Ghanem and Spanos 1991). Hermite polynomial of n^{th} order (H_n) can be calculated using the following equation (Li and Zhang 2007):

$$H_n(\xi_{k_1}, \xi_{k_2}, \dots, \xi_{k_n}) = (-1)^n e^{\left(\frac{1}{2}\xi^T \xi\right)} \frac{\partial^n}{\partial \xi_{k_1} \partial \xi_{k_2} \dots \partial \xi_{k_n}} e^{-\left(\frac{1}{2}\xi^T \xi\right)} \quad (4.21)$$

where ξ is a vector of n Gaussian random variables that can be shown as,

$$\xi = [\xi_{k_1}, \xi_{k_2}, \dots, \xi_{k_n}]^T \quad (4.22)$$

After obtaining one-dimensional Hermite polynomials of different orders using Eq. (4.21), higher order polynomials ($n > 2$) can be derived using lower order polynomials. Relationship between them can be expressed as (Bazargan 2014),

$$H_n(\xi) = \xi H_{n-1}(\xi) - (n-1)H_{n-2}(\xi) \quad (4.23)$$

Like KL parameterization, it is not pragmatic to implement PCE with an infinite number of terms. Furthermore, the number of coefficients to be computed increases as the order of PCE increases. Hence, if PCE is truncated to N_s number of terms, then using term-based indexing in Eq. (4.20), it can be shown mathematically as follows:

$$\hat{y}(\xi) = \sum_{k=0}^{N_s} c_k \Gamma_k(\xi) \quad (4.24)$$

Here, each term in Eq. (4.24) corresponds on one to one basis with the terms of Eq. (4.20) if the total number of terms in the later equation is limited to N_s . The complexity of truncated PCE should also be considered to determine its feasibility in practical application. It is defined by the total number of terms in polynomial, which ultimately depends on the order of PCE and dimensions of random variables. Maximum number of terms (P) in the d -variate PCE of order m can be determined using the equation shown below (Augustin et al. 2008):

$$P = \frac{(d+m)!}{d! m!} \quad (4.25)$$

From Eq. (4.25), it can be said that as order and/or a number of random variables increases, complexity in PCE increases immensely. Also, a number of summands for different orders of PCE and random variables dimensions is plotted in *Figure 4.3* from which it can be said that the number of terms in PCE increases exponentially with increment in either of two responsible parameters. As the number of polynomial terms increases, coefficients to be computed will also increase, creating the need for additional numerical simulations. To alleviate this issue, KL expansion is used in this

work to decrease the dimensions of random numbers as discussed in the previous subsection. Furthermore, Li et al. (2011) demonstrated that by considering only pure terms, a reasonable estimate can be obtained for slightly nonlinear problems. However, neglecting cross terms is only valid if the true model contains only pure terms.

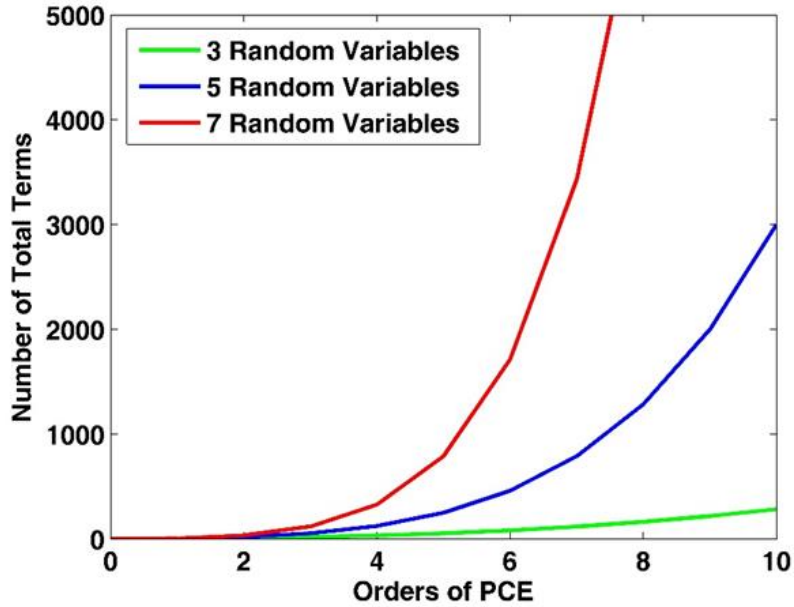


Figure 4.3 – Number of total terms (P) for different orders and dimensions of random variables in PCE.

The algorithm used to formulate PCE forecast model is presented below.

Algorithm 4.4 [PCE]

1. Construct a truncated, d -variate polynomial chaos of (initially lowest) order m as follows:

$$\hat{y}(\xi) = \sum_{k=0}^P c_k \Gamma_k(\xi) \quad (4.26)$$

2. Using zeroes of $(m + 1)^{th}$ order $\Gamma(\xi)$, sample the N_q quadrature nodes with higher probability, set of which can be shown as:

$$\mathcal{L} = \{\xi_k\}_{k=1}^{N_q} \subset \Omega \quad (4.27)$$

3. Compute $y(\xi_q)$ for $\forall \xi_q \in \mathcal{L}$ using high fidelity forward model $F(\cdot)$.
4. Discretize polynomial chaos in form of system of equations to obtain unique c_k as shown below:

$$\begin{Bmatrix} c_0 \\ c_1 \\ \cdot \\ \cdot \\ c_P \end{Bmatrix} = \begin{Bmatrix} \Gamma_0(\xi_1) & \Gamma_1(\xi_1) & \dots & \Gamma_P(\xi_1) \\ \Gamma_0(\xi_2) & \Gamma_1(\xi_2) & \dots & \Gamma_P(\xi_2) \\ \cdot & \cdot & \cdot & \cdot \\ \cdot & \cdot & \cdot & \cdot \\ \Gamma_0(\xi_q) & \Gamma_1(\xi_q) & \dots & \Gamma_P(\xi_q) \end{Bmatrix}^{-1} \begin{Bmatrix} y(\xi_1) \\ y(\xi_2) \\ \cdot \\ \cdot \\ y(\xi_q) \end{Bmatrix}, \quad q = P \quad (4.28)$$

5. Determine responses $\hat{y}(\xi_q)$ using Eq. (4.26) for $\forall \xi_q \in \mathcal{L}$.
6. Calculate the approximation error as follows:

$$E_m = \sum_{k=1}^{N_q} |y(\xi_k) - \hat{y}(\xi_k)| \quad (4.29)$$

7. If $E_m > \tau$, $m \mapsto m + 1$ and repeat the procedure.

In the algorithm, τ represents the tolerance in PCE responses that varies for distinct applications. In Eq. (4.28), rank of the matrix containing $\Gamma(\xi)$ should be equal to the number of coefficients (P) to ensure the unique solutions. Probabilistic collocation method (PCM) is used in algorithm to calculate PCE coefficients as explained in detail in section 4.4.3. As mentioned before, use of PCM is restricted by the dimensionality of ξ and PCE order m since required numerical simulation runs (step 3) increase exponentially. Non-intrusive spectral projection (NISP) can be used in such cases, which is almost independent of the dimensionality (Sarma and Xie 2011). As evident from Eq. (4.26), both pure terms and cross terms are considered in this study since subsurface dynamics of thermal oil recovery processes exhibits highly nonlinear behaviour.

4.4.3 Probabilistic Collocation Method (PCM)

After obtaining Hermite polynomials (or orthogonal polynomials in general), next step in constructing PCE is to determine coefficients (steps 2-4 in algorithm 4.4). Though convergence in PCE is guaranteed, there is an underlying assumption that coefficients are accurate (Bazargan 2014). Hence, computing coefficients is a crucial task to achieve the convergence and obtain efficacious PCE. Several methods to calculate coefficients of polynomial chaos can be classified broadly into two categories: Intrusive methods and Non-intrusive methods. Intrusive methods determine the polynomial chaos coefficients considering that residuals are always orthogonal to the subspace spanned by polynomial basis. Galerkin projection approach is a well-known intrusive method in which coefficients are calculated by solving weighted residual integral. Mathematical formulation of weighted residual for a random field can be shown as,

$$\int_{\xi} R_{PS}(\{c_i\}, \xi) W_i(\xi) p(\xi) d\xi = 0 \quad i = 1, 2, \dots, N \quad (4.30)$$

where R_{PS} denotes residual defined as difference between approximated output obtained using PCE and output of full physics simulation while $p(\xi)$ represents joint pdf of random variables ξ . Weighting function W_i in Eq. (4.30) is considered same as basis function of the approximation (orthogonal polynomials in our case). Such choice of weighting function in Galerkin approach requires the manipulation of governing equations to solve the integral in Eq. (4.30). On the other hand, as name suggests, non-intrusive methods do not need any access to governing equations and simulators can be considered as a black-box (Sarma 2006). Due to this essential benefit of non-intrusive methods, probabilistic collocation method (PCM) proposed by Tatang (1995) is used in this proxy model to calculate PCE coefficients.

PCM (Tatang et al. 1997) is the most used non-intrusive method to calculate PCE coefficients. Several full physics simulation runs are required to apply PCM. Outputs obtained from simulation runs are then used as a training data and PCE coefficients are achieved by solving the system of equations. In other words, collocation method forces residual to be zero for selected random variables. Also, delta function is used as a weighting function in PCM, which is the reason original model can be considered as a black-box model. Now, full physics simulations with different input random

parameters (widely known as collocation points or collocation nodes) will give different results and consequently the coefficients of PCE. Therefore, it is necessary to select such collocation points that encompass maximum information about the domain of interest. Otherwise stated, chosen collocation points should give a better representation of the high probability region in order to achieve better performance in PCM (Lin and Tartakovsky 2009). Selecting collocation points randomly may not provide a proper estimation of coefficients.

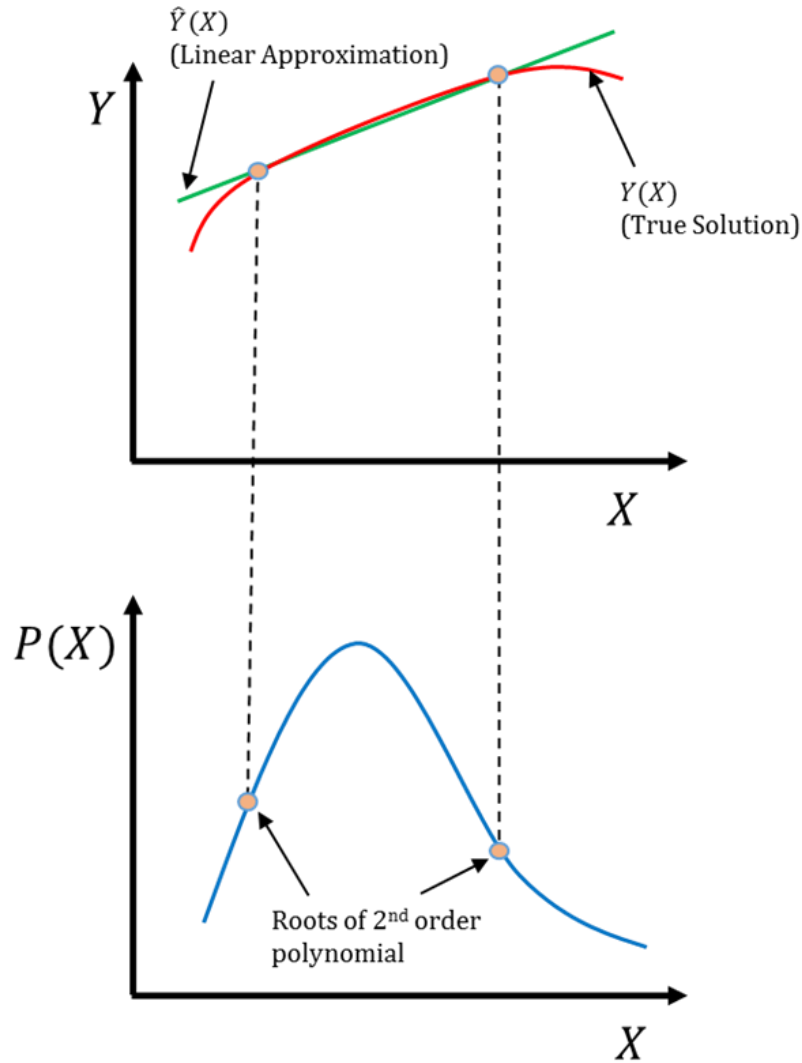


Figure 4.4 – Representation of Gaussian quadrature technique where roots of the 2nd order polynomial span high probability region of $P(X)$ and gives good linear approximation of output $Y(X)$.

As Webster et al. (1996) noted, Gaussian quadrature technique gives the estimate of an integral with zero error when roots of next higher order polynomials are utilized. As shown in *Figure 4.4*, if the linear function is to be approximated for any pdf of random variable X , then we need to define two points that cover high probability region of given pdf $P(X)$. As per Gaussian quadrature technique, these two points are set same as two roots of 2nd order polynomial. Once these two points which cover maximum area under pdf are specified, the output variable \hat{Y} can easily be approximated with negligible error. As shown in *Figure 4.4*, linear approximation that gives zero error between two roots of higher order polynomial may deviate from the correct solution in low probability region. However, it contributes very less to the cumulative approximation error as chances of variable X to occur from the low probability region is very less. A similar method is followed in proposed proxy model to obtain collocation nodes i.e. if coefficients of m^{th} order PCE is to be determined, roots of $(m + 1)^{th}$ order orthogonal polynomial are used as collocation nodes. Generally, number of roots of polynomials are more than number of collocation points required. Therefore, among all the collocation points obtained, N_q collocation points with higher probability are selected (Bazargan 2014).

Once N_q collocation nodes of input random variables ξ are selected, by use of N_q full physics simulations, output for each collocation point is obtained. By substituting the N_q outputs and N_q collocation points in truncated PCE equation (Eq. (4.26)), system of equations (similar to the Eq. (4.28)) can be obtained. In matrix form, it can be written as follows:

$$[Y] = [\Gamma(\xi)][C] \quad (4.31)$$

where $[Y]$ is the vector of dimension $N_q \times 1$ containing correct responses at each collocation point while $[\Gamma(\xi)]$ denotes the space-independent matrix of dimension $N_q \times N_q$ consists of orthogonal polynomials computed at each collocation node. As both matrices $[Y]$ and $[\Gamma(\xi)]$ are known, matrix $[C]$ of dimension $P \times 1$ containing coefficients can be easily calculated by solving system of N_q equations in Eq. (4.31). As noted before, a unique solution for coefficients can be obtained if and only if the

rank of matrix equals the number of variables. Hence, collocation points in PCM should be selected such that the total number of collocation nodes are equal to number of deterministic coefficients.

4.4.4 Integration of PCE Metamodel in EnKF Framework

In the last step, PCE metamodel is integrated with the conventional iterative EnKF framework. The workflow that shows how three different mathematical techniques are associated and stepwise procedure to be followed to implement assisted history matching with reasonable computing cost is provided in *Figure 4.5*. The starting point of proposed integrated dynamic modeling workflow is to represent initial ensemble in terms of eigen values and corresponding eigen functions of covariance matrix along with random variables using Eq. (4.15). As stated before, Gaussian random variables with standard normal pdf are used and accordingly, Hermite polynomials are employed in polynomial chaos. Using Gaussian quadrature technique, quadrature nodes are obtained. Considering each set of random variables as separate input, full physics simulations using commercial reservoir simulator are run and output data is collected. The system of equations is developed using each input-output pair and coefficients are determined. If the error in approximation using PCE is not significant, then the same polynomial model is used in forecast step of EnKF.

The only loop in proposed assisted history matching workflow is of EnKF. It starts with the construction of a state vector. Since initial ensemble is represented by random variables in KL parameterization, they are used as model parameters. Then using PCE metamodel in forecast step, production parameters are computed considering the random variables in state vector as input parameters. Uncertainty in production forecast is analyzed and if it is high then state vector is updated using true production data from the field and Kalman gain in analysis step of EnKF loop. The loop is repeated using random variables from updated state vector and when uncertainty in production parameters is less enough, realizations can be generated by substituting latest updated random variables into Eq. (4.15). Best realization from the ensemble then can be used further to outline future field development strategies.

Similarly, to implement MCMC with PCE metamodel, the EnKF loop in *Figure 4.5* is replaced by the algorithm 4.1.

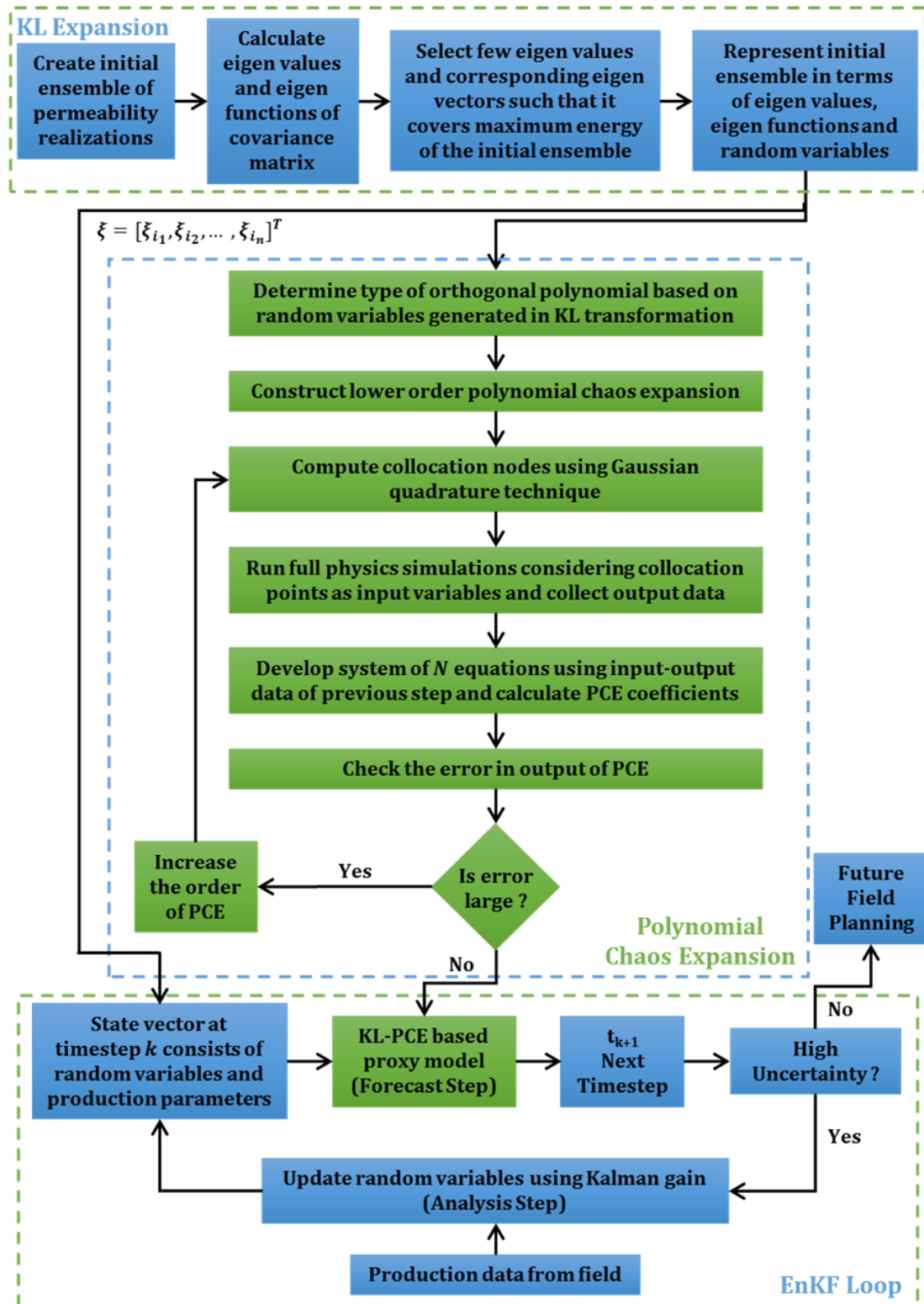


Figure 4.5 – Reservoir characterization workflow using PCE metamodel with EnKF.

4.5 SAGD Field Case Study

Realistic performance assessment of EnKF and MCMC under forecast model uncertainty is made possible in this case study by considering the oil sands reservoir located in northern Alberta, Canada. Several routines and subroutines were developed using MATLAB® (release R2014a) to create a platform that integrates CMG STARS™ (CMG 2013a) and Results Report™ (CMG 2013b) in order to implement the proposed workflow. In this section, we discuss the 3D reservoir model, development of the PCE forward model, and three numerical experiments designed for this work.

4.5.1 SAGD Reservoir Model

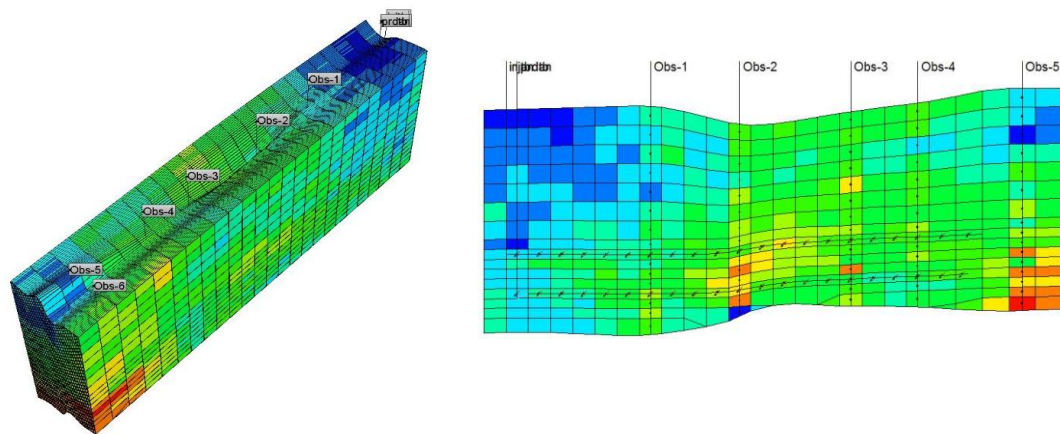


Figure 4.6 – 3D view of the field-scale reservoir model (left) and trajectories of all wells (right).

The test problem considered in this case study is a field-scale 3D reservoir model, representing a segment of the oil sands reservoir with one horizontal well pair and six vertical observation wells. Thermal oil recovery process steam-assisted gravity drainage (SAGD) is employed to extract the bitumen. Well logs are used to determine reservoir top and a bottom surface and the domain is discretized spatially on an optimal corner point grid (Shin et al. 2012) containing 20000 cells. Prior information about the permeability at well locations is used as conditioning data to generate an ensemble of 100 models using geostatistical simulation. A 3D view of the reservoir model (left) and well trajectories (right) are shown in *Figure 4.6*. The detailed

information regarding simulation inputs is given in *Table 4.1*. The objective is to sample the model parameters – permeability of each cell of the reservoir model – from the posterior distribution conditioned to data observed in the field using PCE metamodel.

Table 4.1 – *Reservoir model parameters for the case study*

Variable	Description
Phases	Oil/water
Grid system	25×50×16
Cell dimensions	25×2×1.5 m
Reservoir depth	135 m
Reservoir thickness (net)	22 m
Well spacing	6 m
Rock porosity	0.315 to 0.41
Horizontal permeability	1525 to 7150 md
Vertical permeability	1144 to 5362 md
Initial oil saturation	0.8
Initial pressure	650 kpa
Oil viscosity	625000 cp (at 7 °C), 10 cp (at 216 °C)
Bitumen heat conductivity	11500 J/(m.day.C)
Rock heat conductivity	660000 J/(m.day.C)
Overburden heat conductivity	172800 J/(m.day.C)
Geostatistical simulation	Sequential Gaussian simulation
Injection well constraints	Steam injection rate*
Production well constraints	Well bottom-hole pressure*
Field history	45 months

* varies on daily basis as per field measurements

4.5.2 PCE Forward Model

PCE forward model essentially integrates two mechanisms: parameterization and prediction. Following the algorithm 4.3, uncertainty in model parameters is reproduced

using lower dimensional subspace. In our field case study, it is challenging since prior parameterization is not available for any reference case. Therefore, we start with the 100 ensemble members to calculate the covariance matrix, and corresponding eigenvalues and eigenfunctions are obtained using Cholesky factorization. *Figure 4.7* depicts 100 initial eigenvalues (normalized by the highest component) ordered $\lambda_1 \geq \lambda_2 \geq \dots$ and energy associated with them (see Eq. (4.19)). From the swift reduction in eigen values, it can be inferred that spatial change in field variance is moderate. The same is also evident from the energy plot in which energy corresponding to 60 eigen values is almost 98%. Though discarding small eigen values will smoothen out the high-frequency changes in variance, few eigen values should be sufficient to parameterize the field effectively. In this work, we have considered 3 eigen values – resolving more than 90% of the field variance spatially – in KL parameterization for the minimal cost of generating PCE forward model.

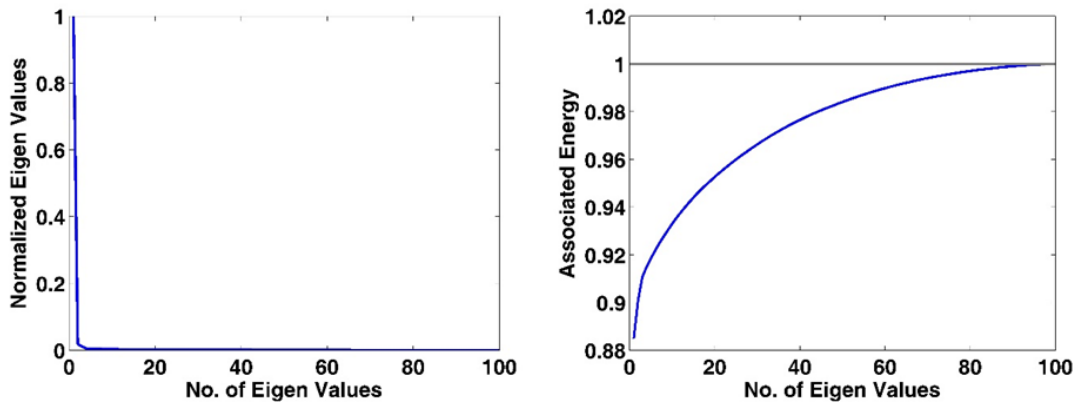


Figure 4.7 – First 100 normalized eigen values of the covariance matrix (left) and energy associated with each of them (right).

Uncertainty in model parameters is reflected in PCE through stochastic variables $\xi \in \mathbb{R}^{N_s}$ sampled from $\mathcal{N}(0,1)$. We follow the algorithm 4.4 to first create a 2nd order PCE. Collocation nodes are determined using roots of 3rd order Hermite polynomial $H_3 = \xi^3 - 3\xi$. With three stochastic dimensions, the construction of PCE metamodel requires 10 full physics simulation runs. Hence, from total $3^3 = 27$ collocation nodes, 10 nodes (ξ_q) with higher probability are selected to obtain $y(\xi_q)$ that corresponds to

any QoIs, particularly, oil rate, cumulative oil/water production and steam-oil ratio (SOR) in this study.

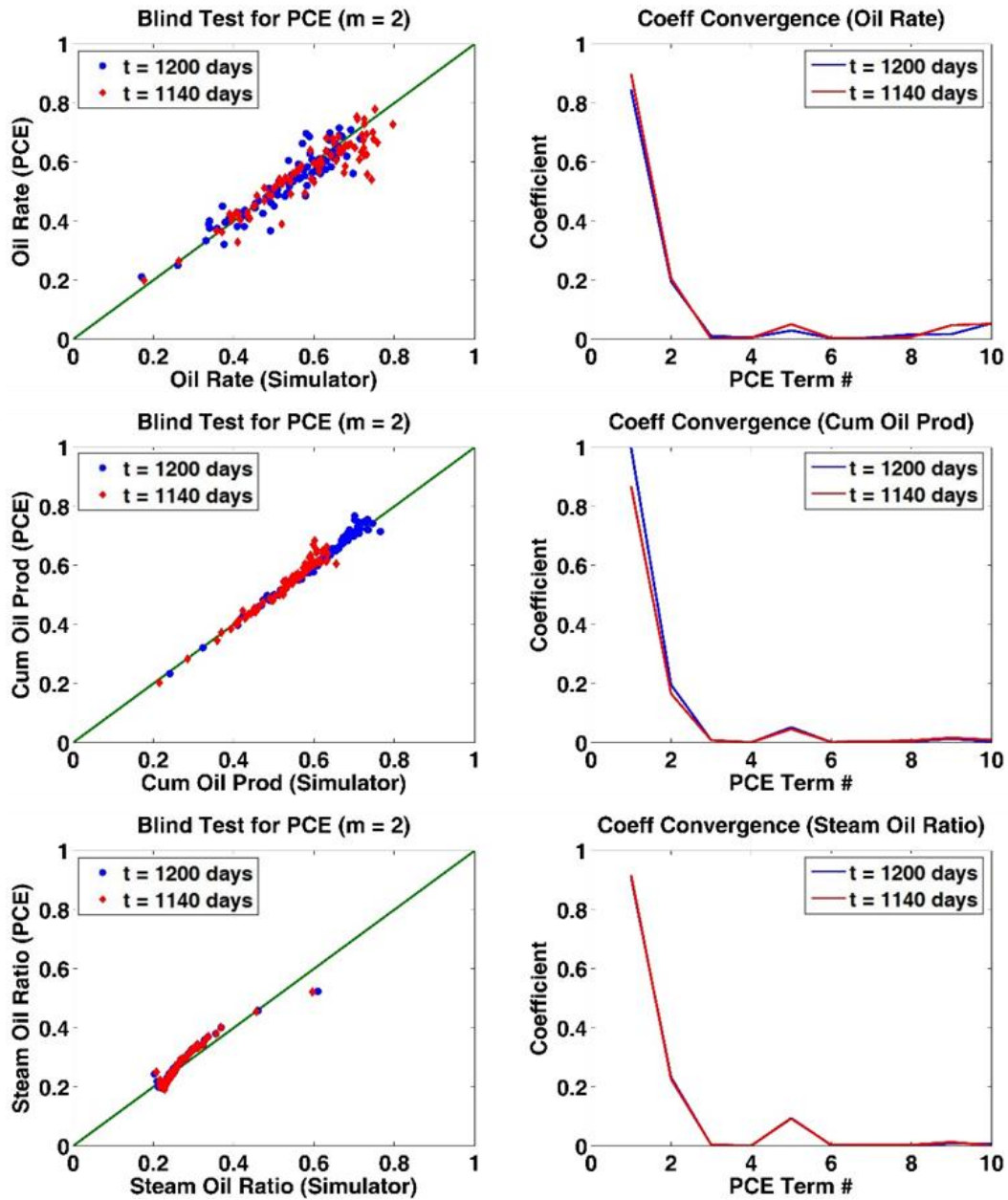


Figure 4.8 – Blind test results of 2nd order PCE metamodel using 100 random vectors (left) and convergence of PCE coefficients for each QoI (right).

To evaluate convergence and accuracy of PCE surrogate, a blind test is performed by generating 100 random vectors (not used before in PCE construction) and predicting

corresponding QoIs. Approximation error is calculated against the simulator outputs and results for selected timesteps are plotted in *Figure 4.8*. Also, the convergence of PCE coefficients is shown in the same figure. According to these results, 2nd order PCE is sufficient for the given problem with most of the data points forming the cloud near the 45-degree line and converging coefficients. In addition, all the QoIs are estimated with less than 10% error. However, to confirm this, 3rd order PCE model is created using 21 collocation nodes and results are compared with the previous model for all the QoIs. Various quantitative measures are shown at a particular timestep in *Table 4.2* to summarize the comparison. It can be concluded that 3rd order model marginally deteriorates the prediction accuracy possibly due to the no third order terms in the true model or better performance of even order PCM as compared to next higher odd order (Li and Zhang 2007). Therefore, 2nd order model is used as the forecast model in numerical experiments of the case study. Note that in the assessment of PCE model, input parameters are sampled from all the regions of prior distribution to avoid the notion of inferior metamodel performance in low probability regions. In addition, uncertainty introduced in the prediction of QoIs is due to not only lower order PCE but also parameterization.

Table 4.2 – Quantitative assessment of QoI approximated using 2nd and 3rd order PCE model at $t = 1200$ days

Quantitative Measures	Normalized Oil Rate		Normalized Cumulative Oil Production		Normalized Steam Oil Ratio	
	$m = 2$	$m = 3$	$m = 2$	$m = 3$	$m = 2$	$m = 3$
Mean	0.532	0.482	0.628	0.556	0.255	0.22
Std Dev	0.107	0.177	0.103	0.197	0.063	0.083
Min	0.212	0.037	0.234	0.013	0.195	0.017
Max	0.717	0.8	0.768	0.829	0.524	0.39
RMSE	0.073	0.151	0.016	0.178	0.019	0.111

4.5.3 Numerical Experiments

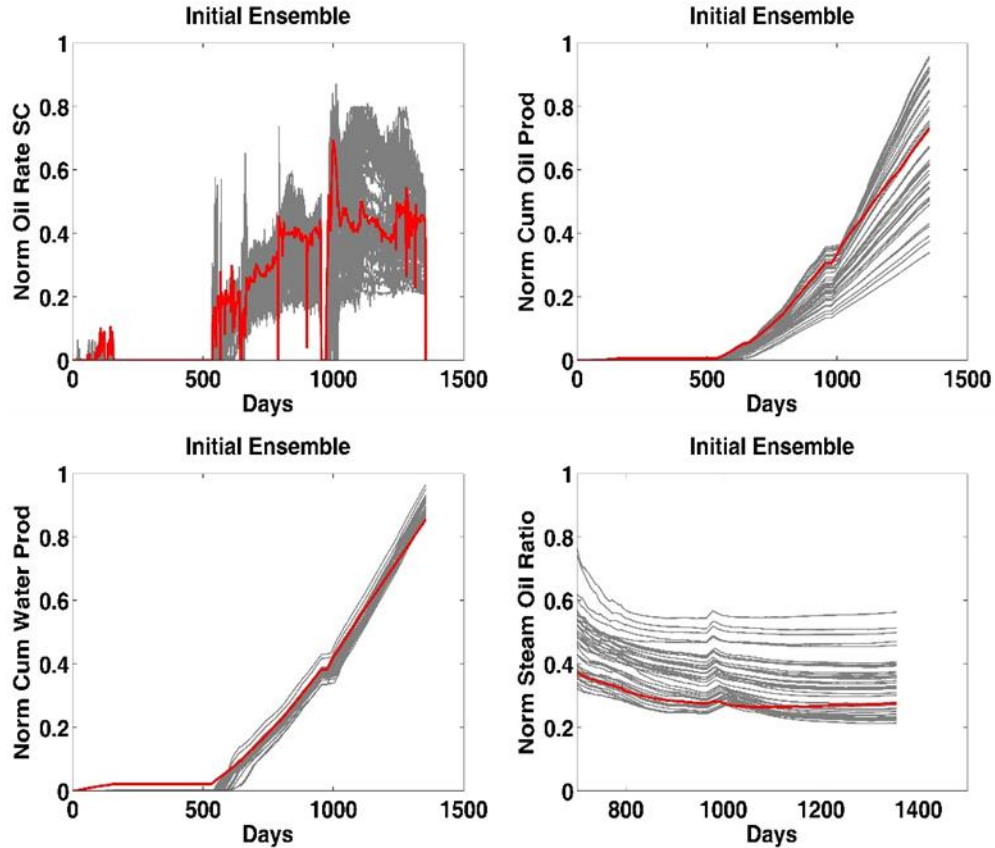


Figure 4.9 – QoIs for initial ensemble (grey lines) in traditional EnKF demonstrating sufficient solution space mapped by the prior distribution. The red curve shows the history obtained from the field.

In this study, three different experiments are composed to assess the effect of uncertainty in PCE forecast model on posterior inference. To set up a benchmark, we consider the traditional iterative EnKF acknowledging the nonlinear propagation of time-dependent system states. Model parameters for this experiment are log permeability ($\ln(k)$) of grid blocks. The prior distribution for model parameters is assumed to be Gaussian and error covariance matrix to be an identity matrix. From the 100 samples (realizations) created initially (as explained in section 4.5.1), 50 are retained in the initial ensemble using mixed-integer linear optimization (MILP) based screening technique (Patel et al. 2015). The technique ensures adequate solution space even with the smaller ensemble, making EnKF pragmatic for the field-scale

problem considered in this case study. The same is evident from the *Figure 4.9* as ensemble spread of QoI displays overestimated uncertainty in the prior distribution. State vector Z_n for the benchmark case can be written as,

$$Z_n = \begin{bmatrix} \{\ln(k)\}_{20000 \times 50} \\ \{Oil\ Rate\}_{1 \times 50} \\ \{Steam\ Oil\ Ratio\}_{1 \times 50} \end{bmatrix}_{20002 \times 50} \quad (4.32)$$

Logarithmic permeability in Eq. (4.32) is necessary to fulfill Gaussian statistics assumption of EnKF. Furthermore, state parameters are not used in the state vector since their time dependency can cause potential inconsistency (Gu and Oliver 2006). Measured data includes daily oil rate and SOR that are assimilated after 20, 25, 28 and 38 months. Subsequently, production parameters are predicted up to 45 months and compared against the field history. Thermal reservoir simulator CMG STARS™ (CMG 2013a) is used as the high fidelity forecast model in this study.

For the second experiment, we consider 2nd order PCE model in the prediction step of EnKF to evaluate its performance under forecast model uncertainty. Since PCE accepts random variables with standard Gaussian prior to inputs, their posterior distributions are estimated. State vector used in this experiment can be expressed as,

$$Z_n = \begin{bmatrix} \{Random\ Variables\ (\xi)\}_{3 \times 50} \\ \{Oil\ Rate\}_{1 \times 50} \\ \{Steam\ Oil\ Ratio\}_{1 \times 50} \end{bmatrix}_{5 \times 50} \quad (4.33)$$

To evaluate the results against a benchmark, we used the identical measured data, assimilation time steps, and ensemble size ($N_e=50$) in this experiment. However, the computational cost of forecast step is decreased significantly with the use of PCE forecast model and hence, the large ensemble is recommended in practice. Note that ensemble size in this experiment is much larger than the stochastic variable dimensions. Therefore, amendments such as covariance inflation (Evensen 2009) and covariance localization (Houtekamer and Mitchell 1998, Sakov and Bertino 2011) applied to mitigate effects of sampling errors and singularity of covariance matrices are not utilized. Also, the study of such ad hoc fixes is not the primary interest of this work.

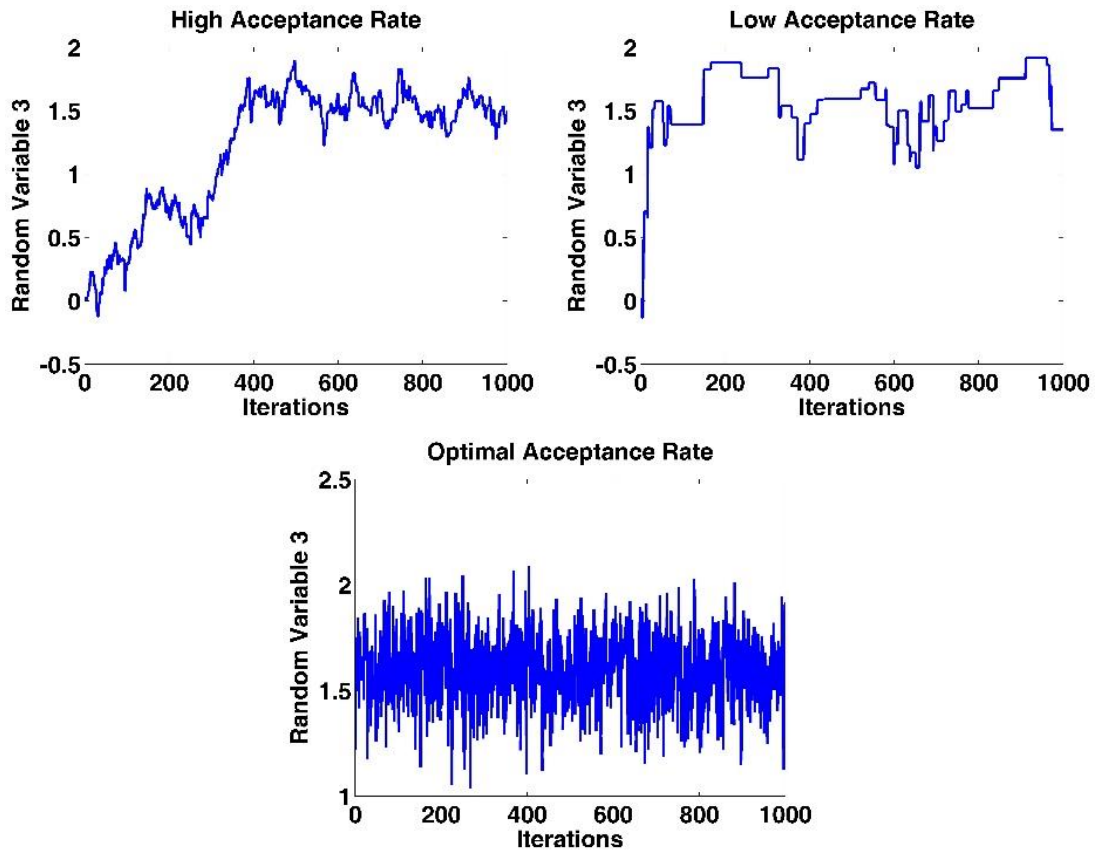


Figure 4.10 – Experimentation for scaling of proposal variance in MCMC. Top left: high acceptance rate (65.03%). Top right: low acceptance rate (9.9%). Bottom: optimal acceptance rate (23.6%).

The last experiment includes inference of stochastic variables using PCE forward model in MCMC. The posterior distributions are estimated with long Markov chain of 10 million proposals assuming that they are enough to provide samples from the converged posterior. To obtain a well-mixed chain, variance of proposal distribution (β^2) should be scaled properly. Higher the β^2 , lower the acceptance rate and vice versa. We did some experimentation using different values of proposal variance as shown in *Figure 4.10* and finally chose $\beta^2 = 0.15$ for this case. It provides the acceptance rate of 23.6% which is within the optimal range (refer section 4.2). For the initial approximation (θ_0) of model parameters, mean of the corresponding variables in initial ensemble after KL parameterization is used. Despite the distant guess in random variables, burn-in period

is not more than 1000 iterations as shown in *Figure 4.11*. Likelihood function used to calculate probability of acceptance in this experiment is as follows (Nejadi et al. 2014):

$$L(\theta) = [\hat{y}(\xi) - d^{obs}]^T R^{-1} [\hat{y}(\xi) - d^{obs}] \quad (4.34)$$

where $y(\xi)$ is the response obtained using PCE forecast model, d^{obs} is the true observations from the field, and R is the noise covariance matrix used in EnKF.

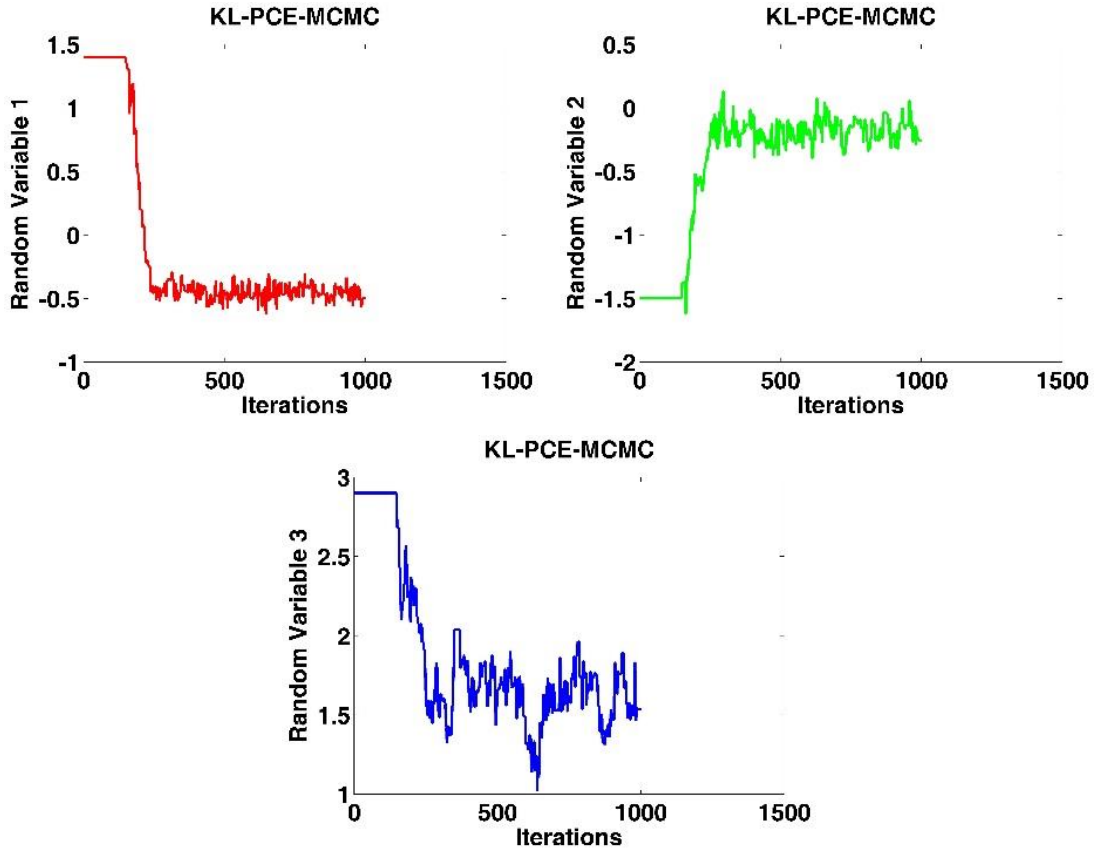


Figure 4.11 – First 1000 proposals displaying smaller burn-in period for model parameters in Markov chain with 10 million samples.

4.6 Results and Discussion

We present the outcomes of numerical experiments to evaluate the effect of uncertainty in forecast model on various aspects of data assimilation. In the three subsections, we present the (1) qualitative analysis to examine the distribution of QoI,

(2) quantitative analysis to investigate the performance of MCMC and EnKF after each assimilation step, and (3) posterior characterization in terms of their ability to produce converged pdf using PCE metamodel.

4.6.1 Distribution of QoI

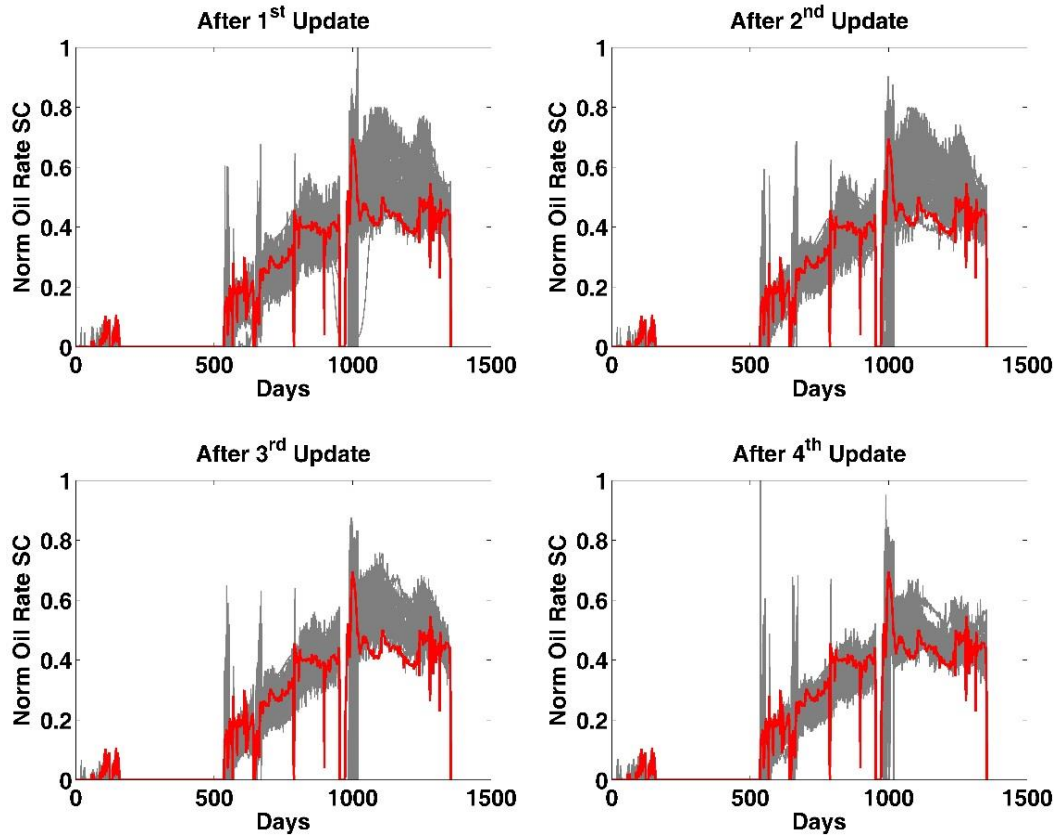


Figure 4.12 – Normalized oil rate after each data assimilation step in numerical experiment 1 (benchmark case). Red curve represents the field history and grey-shaded area corresponds to the ensemble predictions. History up to 1160 days was used in data assimilation and subsequent period from 1161 days to 1355 days constitutes the forecast region.

In subsurface flow applications, one of the objectives of obtaining the posterior distribution is to forecast the relevant quantities accurately such that they can add value in decision making. To assess the performance of each numerical experiment in reproducing the truth, we compute and plot the QoI using the samples from the parameter posterior and respective forecast model after every step in sequential

assimilation. Note that all the plots are normalized by a corresponding target value that is consistent throughout the analysis. For benchmark case, we plot the oil rate and cumulative oil production in *Figure 4.12* and *Figure 4.13* respectively. Ensemble spread of predictions (grey-shaded area) in both figures is converging towards field history as more data is assimilated, as one might expect. Especially, after the 1st update, a significant reduction in variance of ensemble predictions is observed as compared to the initial ensemble (*Figure 4.9*). Likewise, we notice the decreasing uncertainty in predictions of steam oil ratio in *Figure 4.15*. Contrarily, estimates of cumulative water production in *Figure 4.14* is pretty much unchanged throughout the experiment. It is due to the direct proportionality between the amount of produced water and injected steam in SAGD. It is worthy to mention that amount of injected steam is in line with the field observations and kept same across the ensemble.

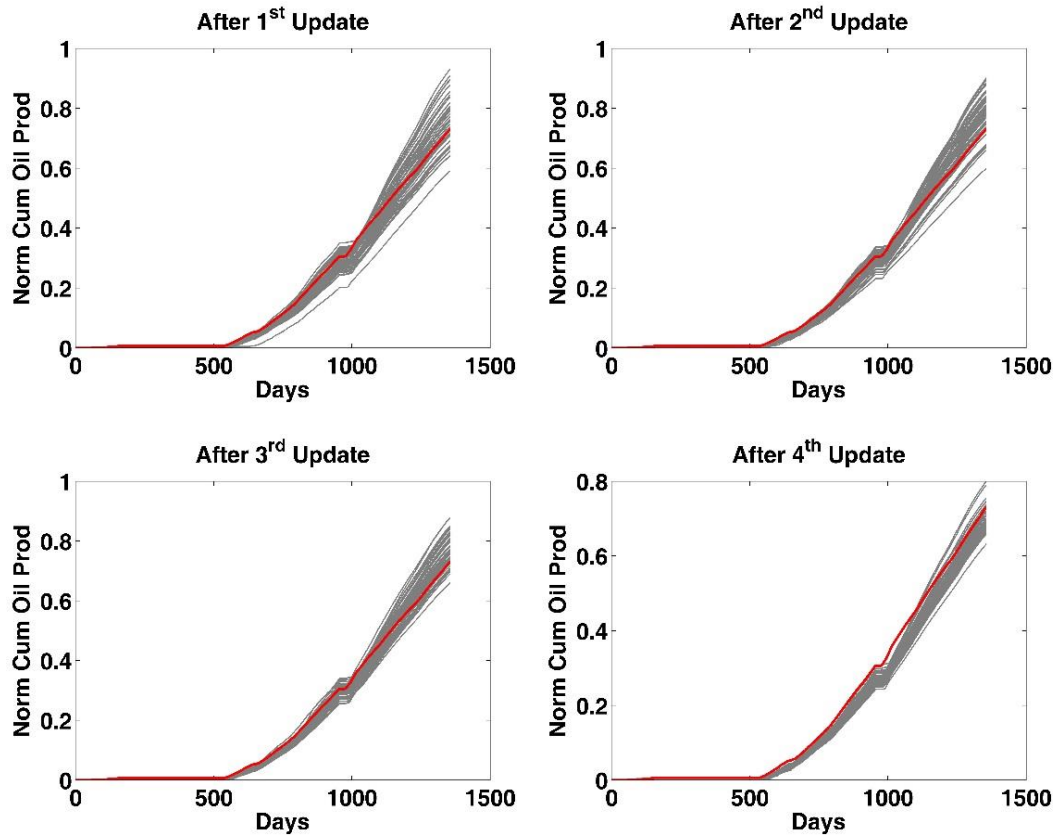


Figure 4.13 – Normalized cumulative oil production after each data assimilation step in numerical experiment 1 (benchmark case). Legends in this figure can be described similarly as *Figure 4.12*.

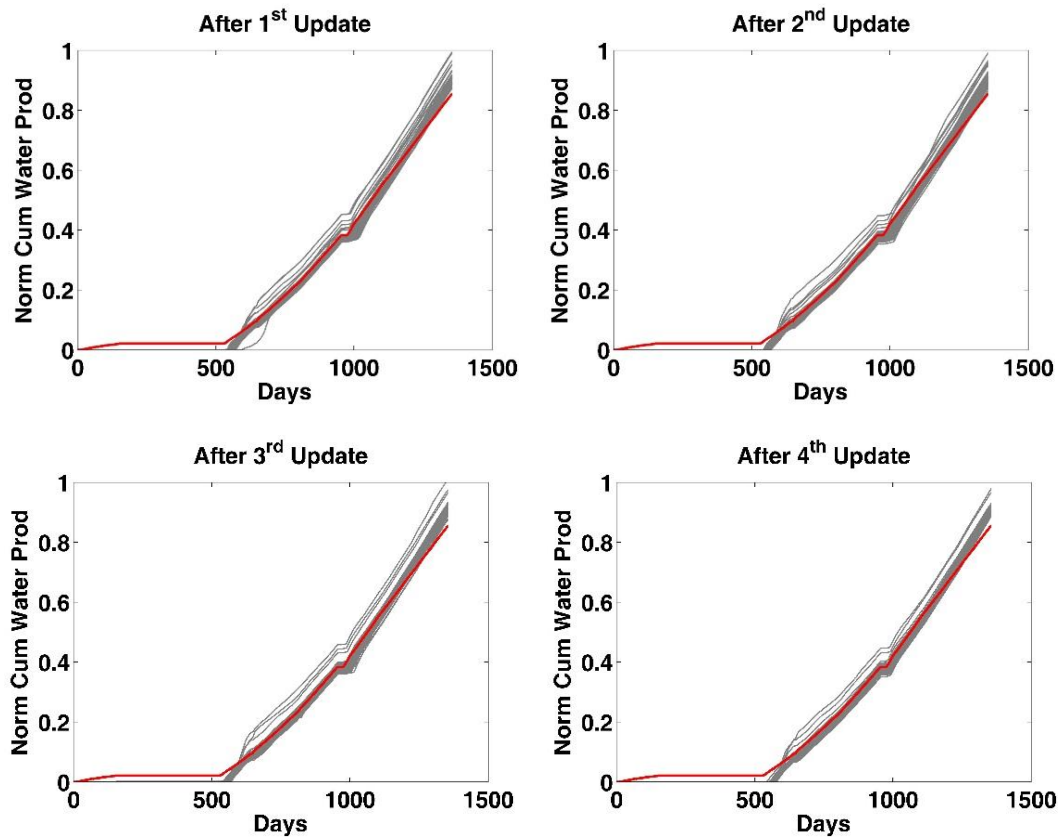


Figure 4.14 – Normalized cumulative water production after each data assimilation step in numerical experiment 1 (benchmark case). Legends in this figure can be described similarly as Figure 4.12.

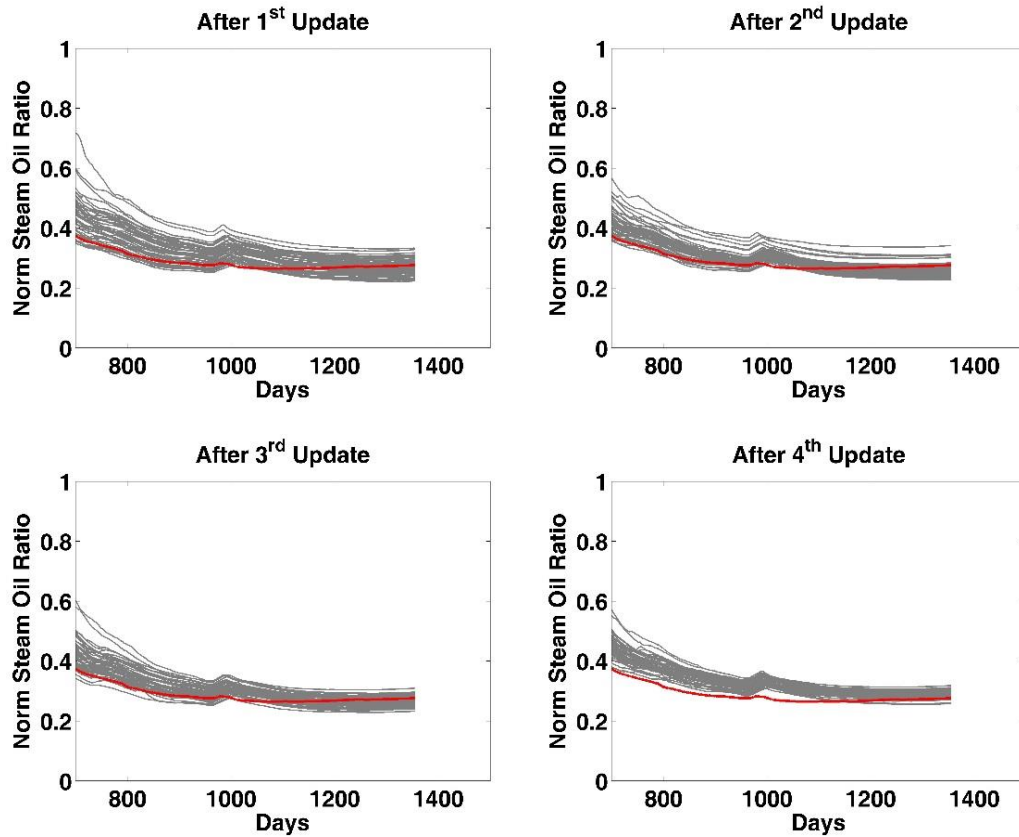


Figure 4.15 – Normalized steam oil ratio after each data assimilation step in numerical experiment 1 (benchmark case). Legends in this figure can be described similarly as Figure 4.12.

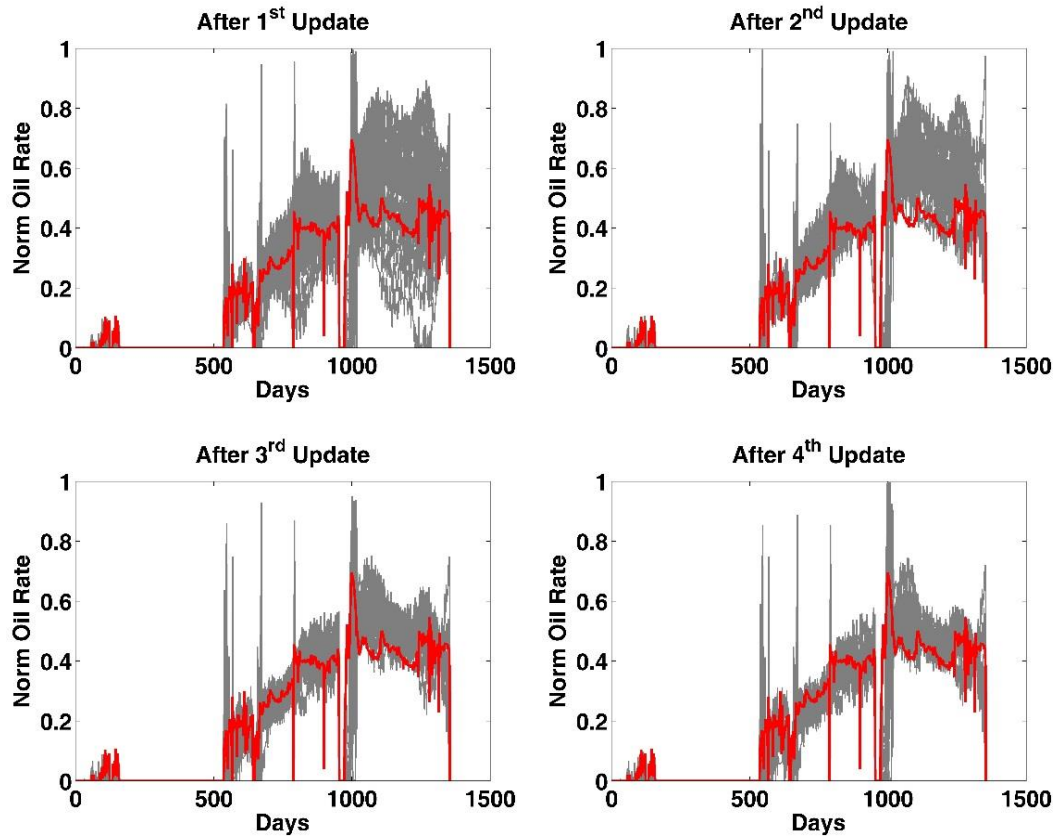


Figure 4.16 – Normalized oil rate after each data assimilation step in numerical experiment 2 (EnKF under PCE uncertainty). Legends in this figure can be described similarly as Figure 4.12.

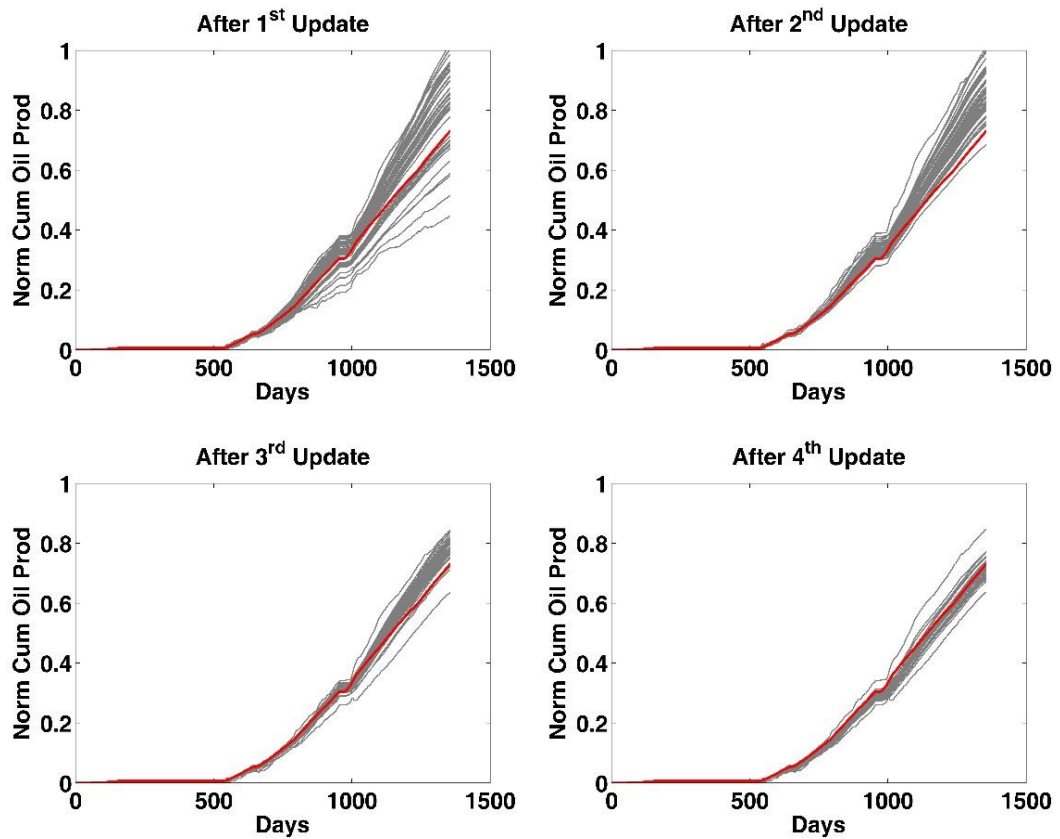


Figure 4.17 – Normalized cumulative oil production after each data assimilation step in numerical experiment 2 (EnKF under PCE uncertainty). Legends in this figure can be described similarly as Figure 4.12.

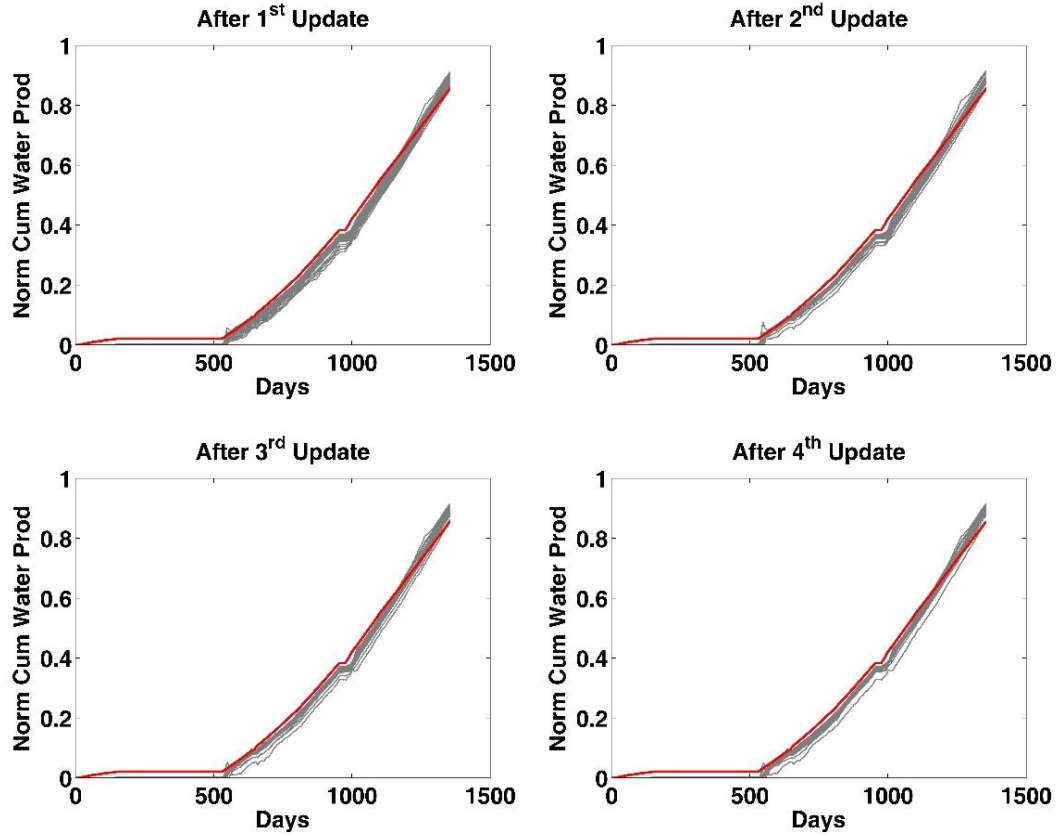


Figure 4.18 – Normalized cumulative water production after each data assimilation step in numerical experiment 2 (EnKF under PCE uncertainty). Legends in this figure can be described similarly as Figure 4.12.

Accurate estimates of observations provide accurate estimates of model variables and vice versa (Siripatana et al. 2017). With the use of PCE model in experiments 2 and 3, the estimation performance is expected to be altered due to the forecast uncertainty; however, encouraging results are achieved overall, especially with MCMC in experiment 3. To compare the predictions with benchmark case, a similar qualitative analysis is performed for both experiments. It is clear from the *Figure 4.16* that uncertainty reduced in the oil rate predictions after the 1st update is not as good as the benchmark case. Likewise, cumulative oil production and steam oil ratio in *Figure 4.17* and *Figure 4.19* respectively, depict larger span of ensemble predictions in the first two assimilation steps. It is because of the uncertainty introduced by the PCE forecast model which led to the different update of model parameters than the

experiment 1. Nevertheless, the effect of forecast model uncertainty diminishes with the sequential assimilation as almost all QoI are converging towards the truth like benchmark case after the final analysis step. As expected, no significant change is observed in predictions of cumulative water production in *Figure 4.18*.

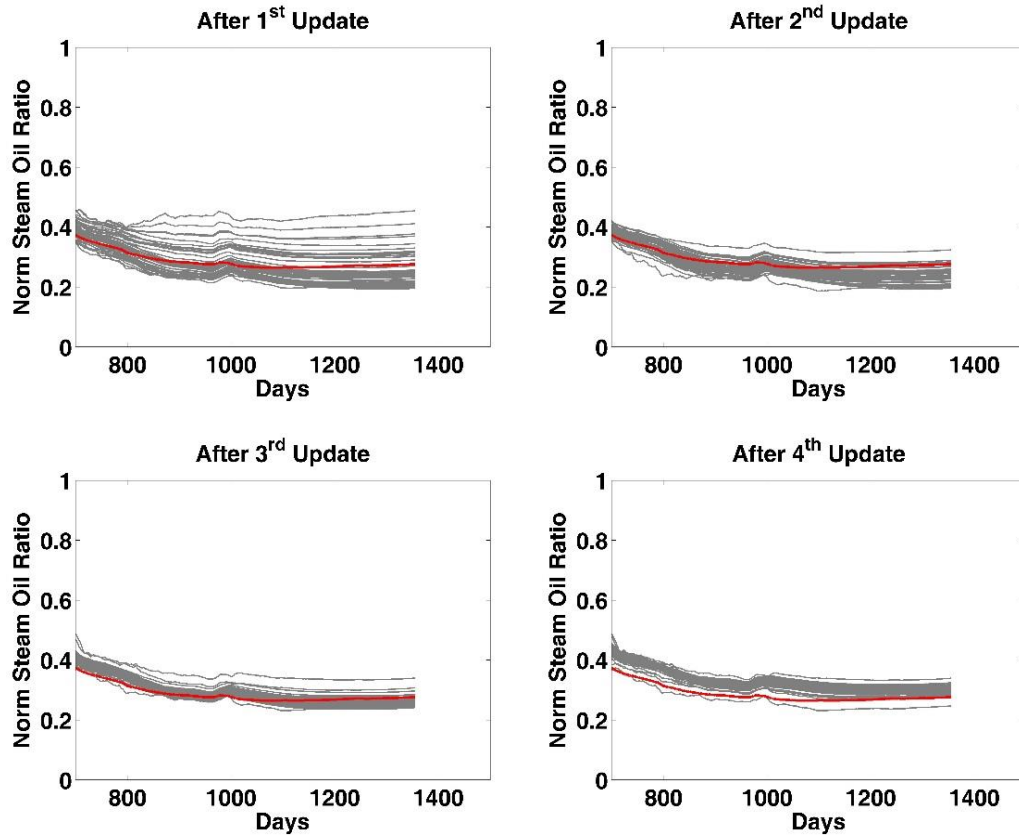


Figure 4.19 – Normalized steam oil ratio after each data assimilation step in numerical experiment 2 (EnKF under PCE uncertainty). Legends in this figure can be described similarly as *Figure 4.12*.

In *Figure 4.20*, we display all four QoI for experiment 3 using every 1000th sample (i.e., 10,000 samples from the total 10 million proposals) of the Markov chain shown in *Figure 4.22*. Despite the forecast model uncertainty, improvement in estimates of all the relevant quantities in terms of variance and accuracy is clearly evident from the figure. Also, overestimation of uncertainty in QoI forecast is observed in the benchmark case as compared to MCMC with PCE forecast model, consistent with the study of Oliver and Chen (2011). Further, we assess the predicting distribution of QoI in *Figure 4.21* at arbitrarily selected time instant outside of the assimilation bounds.

Notice that both EnKF based experiments 1 and 2 provide the reasonable estimations of all four quantities' distributions in terms of mean, median, P25 and P75 values, and ensemble span; however, their characterization of predicting distributions is poor as compared to MCMC in experiment 3. In addition, experiment 2 exhibits similar predicting distributions of oil rate and steam oil ratio as benchmark case while better in both cumulative oil and water production with mean closer to the truth. For the test problem considered, it suggests the capability of EnKF to reproduce the truth under reasonable uncertainty in the forecast model.

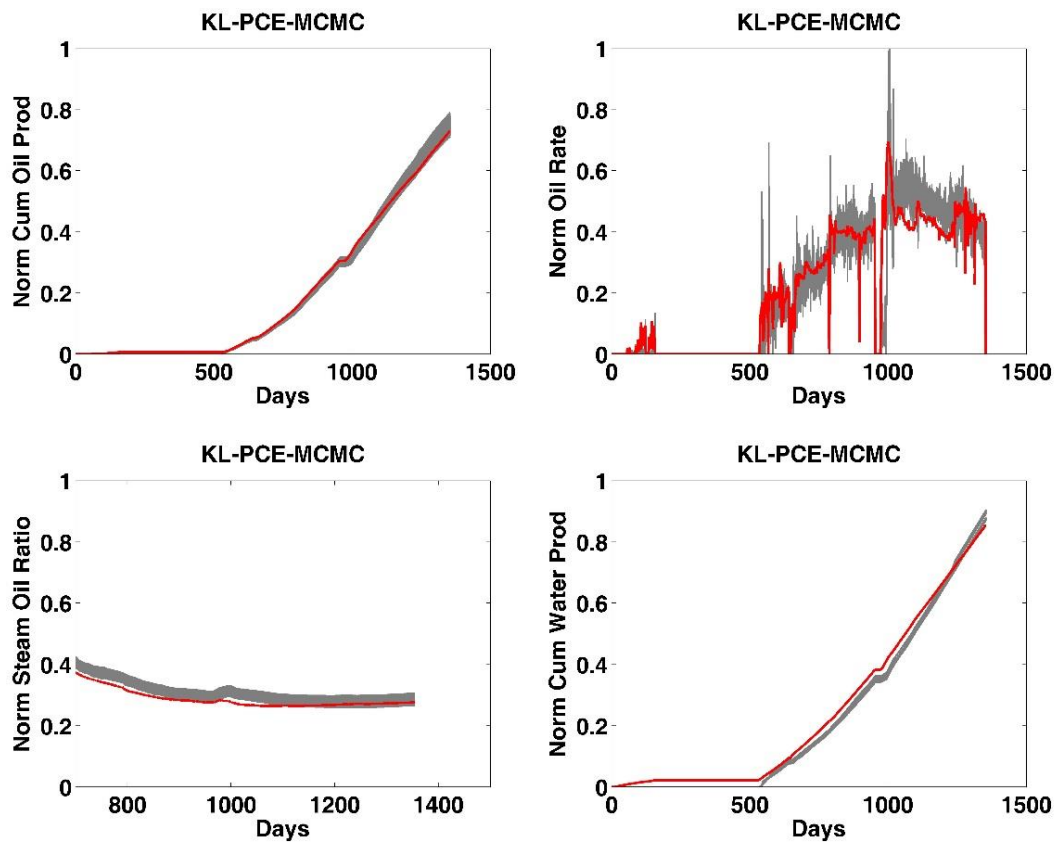


Figure 4.20 – Normalized QoI for every 1000th sample of Markov chain in numerical experiment 3 (MCMC under PCE uncertainty). Legends in this figure can be described similarly as Figure 4.12.

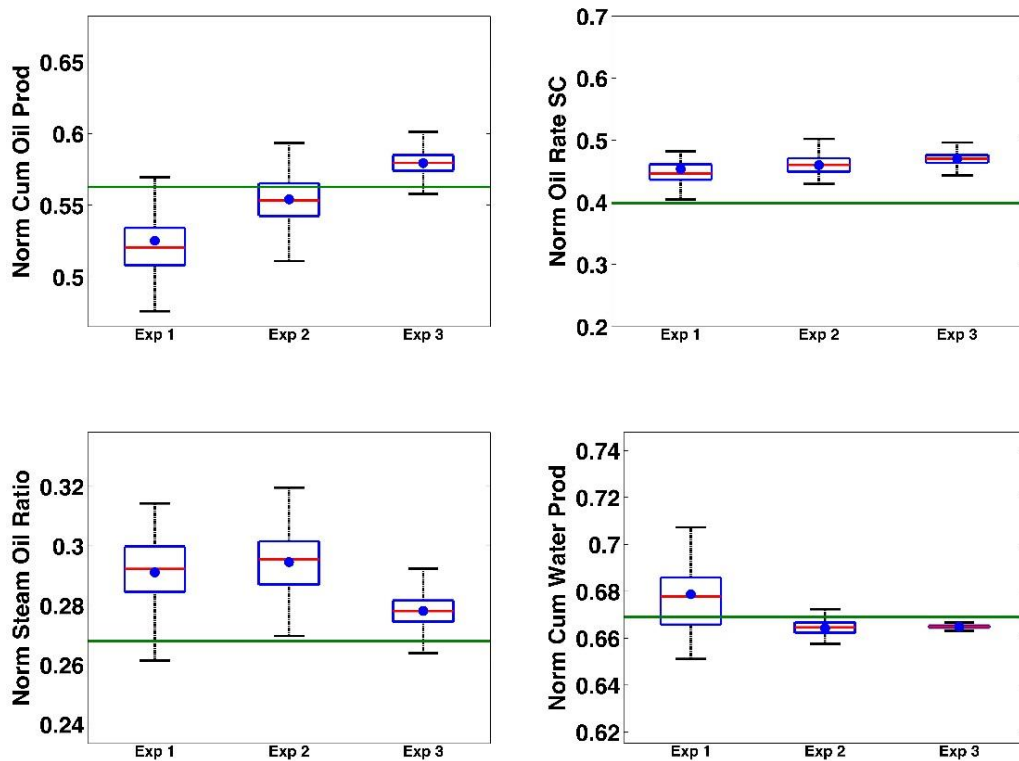


Figure 4.21 – Box plots comparing the distribution of QoI at 1200 days for all numerical experiments. Red line and blue dots show median and mean of each distribution respectively while continuous green line depicts true value of the QoI . The top and bottom of every box correspond to percentiles $P25$ and $P75$ and end points of the whisker represent the minimum and maximum values.

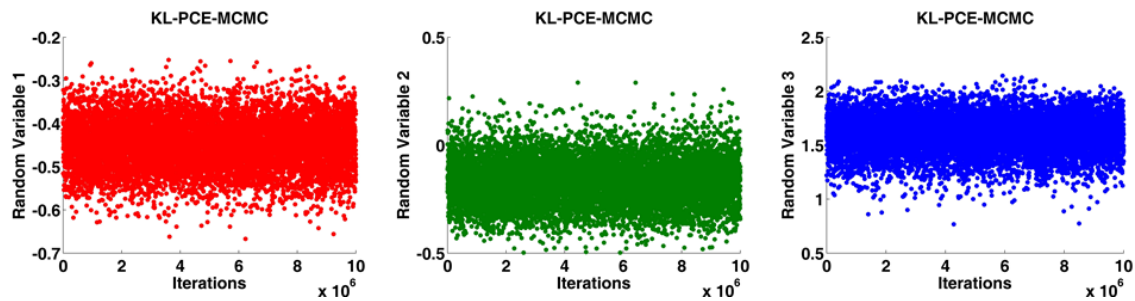


Figure 4.22 – Every 1000^{th} sample of well-mixed Markov chain in numerical experiment 3 (MCMC under PCE uncertainty).

4.6.2 Sensitivity of QoI to Forecast Model Uncertainty

We explore how sensitive QoI are to forecast model uncertainty in different numerical experiments. Time instant chosen for this analysis is same as the one used for box plots in *Figure 4.21*. In *Table 4.3*, *Table 4.4*, and *Table 4.5*, we display several quantitative measures for every production variable obtained in experiments 1, 2, and 3 respectively. Root-mean-square-error (RMSE) and R^2 (coefficient of determination or Nash-Sutcliffe coefficient) of a quantity (y) are defined by

$$RMSE(y) = \frac{1}{N_e} \sum_{k=1}^{N_e} \sqrt{\frac{1}{t} \sum_{l=1}^t (y_{l,k} - d_l^{obs})^2} \quad (4.35)$$

and

$$R^2(y) = \frac{1}{N_e} \sum_{k=1}^{N_e} \left[1 - \frac{\sum_{l=1}^t (y_{l,k} - d_l^{obs})^2}{\sum_{l=1}^t (d_l^{obs} - \bar{d}^{obs})^2} \right] \quad (4.36)$$

where t is the time horizon and $y_{l,k}$ is the predicted observation for k^{th} sample at time l . We reiterate that N_e is the ensemble size, d_l^{obs} is the field observation (or truth) at time l and \bar{d}^{obs} is its time average. Since all the quantities are normalized, RMSE reported here is scale-independent.

Quantitative analysis of initial ensemble predictions in *Table 4.3* and *Table 4.4* demonstrates some mismatch. It is expected due to the uncertainty introduced by KL parameterization in the initial ensemble of experiment 2. Lower the energy captured by eigen values, higher the difference in initial ensemble predictions will be. Despite this difference in the initial ensemble, experiment 2 displays improved error statistics for steam oil ratio, which can be attributed to its accurate forecast by PCE metamodel as evident in the blind test results (*Figure 4.8*). Further, ensemble predictions for cumulative oil production are better in the 1st and 2nd update of benchmark case when compared to experiment 2 in terms of mean, standard deviation, R^2 and RMSE. However, results after final assimilation step are very similar in both experiments, supporting our previous qualitative observation that update of model parameters and therefore, predictions of QoI are least sensitive to forecast model uncertainty in

sequential data assimilation. In other words, assimilation of more data helps to offset the uncertainty in forecast model predictions. Consistent results with qualitative analysis (i.e. no major changes throughout the assimilation) are observed for cumulative water production in both EnKF based experiments.

Table 4.3 – Quantitative analysis of QoI at $t = 1200$ days in numerical experiment 1

	Initial Ensemble	After 1st Update	After 2nd Update	After 3rd Update	After 4th Update
Normalized Oil Rate SC (Truth = 0.404)					
Mean	0.458	0.510	0.530	0.519	0.454
Std Dev	0.131	0.063	0.059	0.046	0.029
Min	0.214	0.403	0.394	0.419	0.405
Max	0.672	0.665	0.654	0.613	0.551
R²	-0.306	-0.048	-0.153	0.053	0.476
RMSE	0.143	0.129	0.136	0.124	0.093
Normalized Cumulative Oil Production (Truth = 0.562)					
Mean	0.513	0.568	0.590	0.586	0.525
Std Dev	0.132	0.055	0.047	0.038	0.024
Min	0.253	0.433	0.453	0.503	0.476
Max	0.701	0.684	0.664	0.668	0.600
R²	0.801	0.960	0.966	0.976	0.968
RMSE	0.085	0.040	0.037	0.032	0.038
Normalized Cumulative Water Production (Truth = 0.67)					
Mean	0.672	0.678	0.677	0.681	0.679
Std Dev	0.022	0.025	0.024	0.022	0.018
Min	0.631	0.648	0.640	0.649	0.651
Max	0.737	0.761	0.766	0.767	0.742
R²	0.987	0.987	0.988	0.988	0.989
RMSE	0.026	0.025	0.025	0.024	0.024
Normalized Steam Oil Ratio (Truth = 0.268)					
Mean	0.318	0.274	0.263	0.264	0.291
Std Dev	0.087	0.026	0.021	0.017	0.012
Min	0.219	0.229	0.233	0.230	0.259
Max	0.553	0.337	0.338	0.305	0.314
R²	-1.914	-0.198	0.301	0.288	-0.051
RMSE	0.102	0.069	0.052	0.053	0.069

Table 4.4 – Quantitative analysis of QoI at $t = 1200$ days in numerical experiment 2

	Initial Ensemble	After 1st Update	After 2nd Update	After 3rd Update	After 4th Update
Normalized Oil Rate SC (Truth = 0.404)					
Mean	0.511	0.525	0.556	0.500	0.460
Std Dev	0.119	0.116	0.061	0.020	0.017
Min	0.157	0.165	0.392	0.439	0.430
Max	0.726	0.770	0.725	0.542	0.506
R²	-0.400	-0.362	-0.337	0.161	0.401
RMSE	0.148	0.146	0.147	0.118	0.099
Normalized Cumulative Oil Production (Truth = 0.562)					
Mean	0.611	0.625	0.653	0.601	0.554
Std Dev	0.112	0.091	0.048	0.030	0.028
Min	0.266	0.366	0.535	0.474	0.475
Max	0.756	0.748	0.777	0.672	0.672
R²	0.863	0.886	0.906	0.978	0.987
RMSE	0.070	0.066	0.060	0.030	0.022
Normalized Cumulative Water Production (Truth = 0.67)					
Mean	0.659	0.658	0.659	0.662	0.664
Std Dev	0.010	0.011	0.010	0.010	0.009
Min	0.635	0.627	0.622	0.621	0.621
Max	0.678	0.682	0.684	0.687	0.687
R²	0.988	0.988	0.990	0.991	0.991
RMSE	0.026	0.026	0.023	0.023	0.023
Normalized Steam Oil Ratio (Truth = 0.268)					
Mean	0.265	0.255	0.235	0.263	0.295
Std Dev	0.070	0.056	0.025	0.017	0.015
Min	0.194	0.197	0.197	0.237	0.238
Max	0.498	0.438	0.317	0.334	0.334
R²	0.259	0.518	0.738	0.807	0.586
RMSE	0.053	0.046	0.036	0.031	0.046

In *Table 4.5*, we perform the similar analysis for MCMC under forecast model uncertainty with the same 10,000 samples used to plot *Figure 4.20*. Final estimates of oil rate and cumulative oil production for the given time instance in experiment 3 are slightly away from the truth when compared to other two experiments. In contrast,

improved error metrics for all production variables that are calculated over the time horizon (see Eq. (4.35) and (4.36)) prove the superiority of MCMC in data assimilation under uncertainty in predictions. Also, lower standard deviations in experiment 3 suggest reduced uncertainty in QoI estimations.

Table 4.5 – Quantitative analysis of QoI at $t = 1200$ days in numerical experiment 3

	Normalized Oil Rate (Truth = 0.404)	Normalized Cum Oil Production (Truth = 0.562)	Normalized Cum Water Production (Truth = 0.67)	Normalized Steam Oil Ratio (Truth = 0.268)
Mean	0.470	0.579	0.665	0.278
Std Dev	0.010	0.008	0.001	0.005
Min	0.434	0.549	0.645	0.260
Max	0.509	0.607	0.668	0.298
R²	0.476	0.995	0.991	0.808
RMSE	0.094	0.015	0.024	0.032

4.6.3 Characterization of Posterior Distribution

Appreciating the data assimilation techniques by their ability to reproduce the QoI within a confidence interval only is not sufficient because it does not affirm the convergence of model parameters in nonlinear inverse problems, like the one considered in this study. Therefore, we present the characterization of posterior distributions of model parameters for both the experiments performed using PCE metamodel. Note that model parameters are referred as the random variables here; however, we reiterate that except in creating the samples for initial ensemble, they are not stochastic in nature throughout the data assimilation.

In *Figure 4.23*, we display the prior and posterior pdfs of all three model variables after each assimilation step in experiment 2. Relatively significant convergence is observed after 3rd and 4th updates in the approximations of model variables, which is also reflected by the reduction in standard deviation and RMSE of several QoI predictions in *Table 4.4*. Further, evolution in posterior of random variable 1 is conspicuous as

compared to other model parameters. It can be explained by the maximum energy associated with the eigen value (see *Figure 4.7*) corresponding to random variable 1.

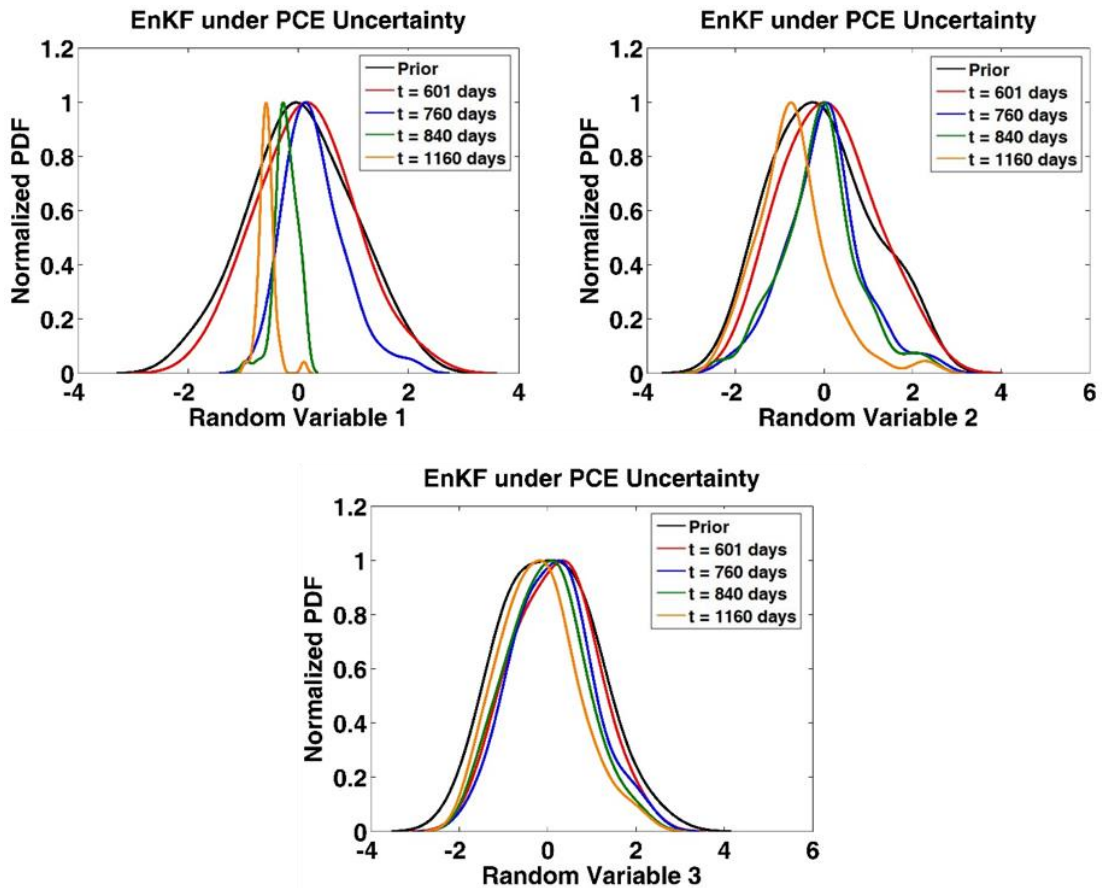


Figure 4.23 – Posterior characterization of model parameters after each assimilation step in numerical experiment 2 (EnKF under PCE uncertainty).

Figure 4.24 compares the posterior pdfs inferred from experiments 2 and 3 with the prior distributions. Notice that reference (or truth) for model parameters is unknown as our test problem is a field case. In such cases, many studies (Liu and Oliver 2003, Iglesias et al. 2013) consider the MCMC as a gold standard to obtain the true posteriors. Based on the similar notion, we found that EnKF using PCE metamodel overestimates the uncertainty in parameter space as evident from the wider spread of pdfs in *Figure 4.24*. Also, the accuracy of the inference results is poor in experiment 2. *Table 4.6* shows that both mean and variance are offset by at least 14% as compared to MCMC with the similar initial guess. The deficient characterization here indicates that nonunique relation between model variables and subsurface

observations is difficult to explain using second-order moments of EnKF analysis equation under forecast model uncertainty.

Table 4.6 – Final estimates and pdf variance of model parameters estimated in experiments 2 and 3

Model Parameters	Initial Guess	Final Estimate		Variance	
		Exp 2	Exp 3	Exp 2	Exp 3
Rand Var 1	1.4	-0.575	-0.449	0.149	0.056
Rand Var 2	-1.5	-0.707	-0.161	0.832	0.161
Rand Var 3	2.9	-0.194	1.588	0.849	0.216

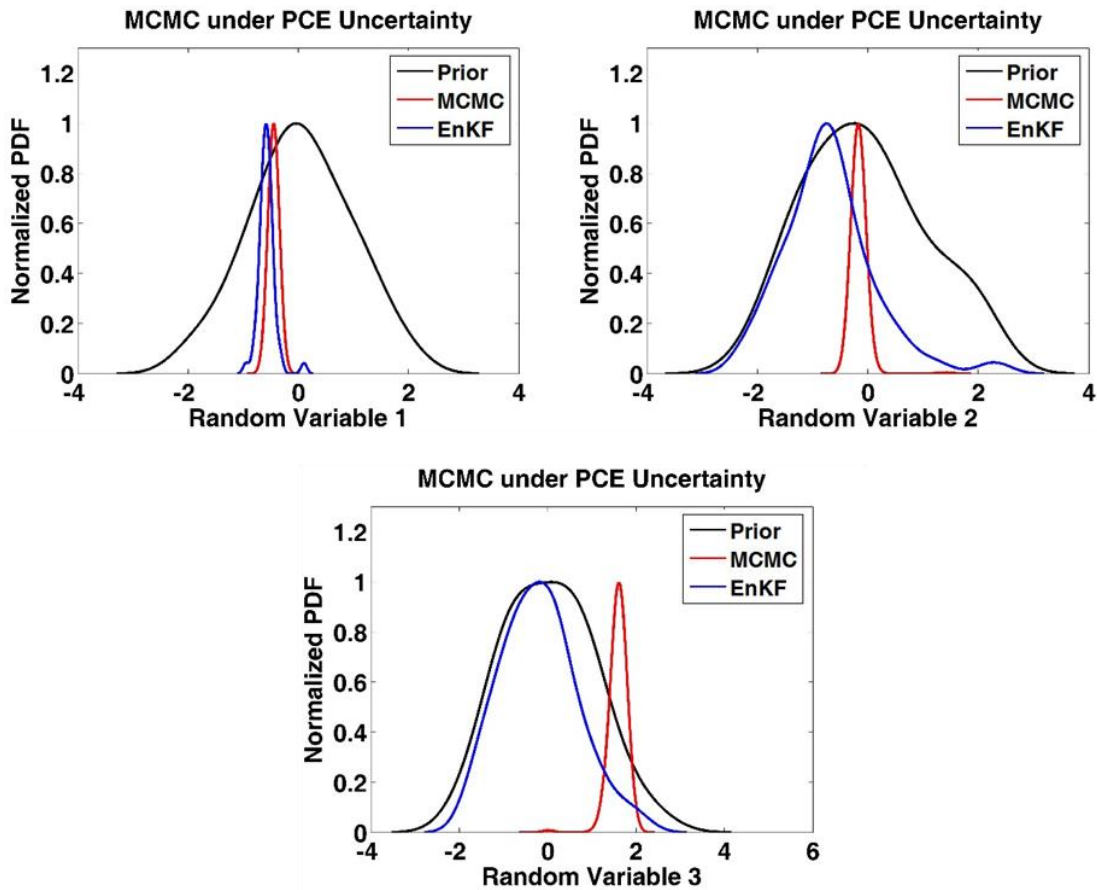


Figure 4.24 – Posterior density estimate of stochastic variables obtained in numerical experiments 2 and 3. The prior is $\mathcal{N}(0,1)$ for all model parameters.

At this point, it is important to discuss the practical implications of both EnKF and MCMC approaches under forecast model uncertainty. As observed, the overall performance of EnKF is not as good as MCMC. Also, aspects such as ensemble size, assimilation time interval, iterative/non-iterative implementation, and bias in initial ensemble affect the final estimates of model parameters and QoI (Wen and Chen 2007, Jafarpour and Tarrahi 2011). On the other hand, MCMC is a rigorous assimilation method and requires only the density of model parameter distribution. Further, the summary of computational cost in *Table 4.7* confirms that the cost of MCMC is higher than EnKF only by an order of the magnitude (10^2 sec for EnKF and 10^3 sec for MCMC). Therefore, MCMC with PCE metamodel would be a learned choice to characterize uncertain parameters. The only limitation for MCMC is the high dimensionality of model parameters that may increase with longer correlation lengths in subsurface inverse problems. In such cases, EnKF would be a preferred option as it can provide reasonable estimations – if not perfect – with the assimilation of sufficient data. Finally, computational cost for both experiments 2 and 3 is less by two orders of magnitude (see *Table 4.7*) as compared to benchmark case. Together with reliable inference under forecast model uncertainty, it advocates the use of metamodels in practical data assimilation cases.

Table 4.7 – *Computational cost of different numerical experiments*

Numerical Experiment	Number of Simulation Runs	Execution Time (sec)
Traditional Iterative EnKF	400	4.573×10^5
EnKF with PCE metamodel	10	3.051×10^2
MCMC with PCE metamodel	10	6.073×10^3

Routines and subroutines are written in MATLAB® (MathWorks 2014) and codes are executed on Intel Core™ i7-2600 CPU @ 3.40 GHz × 8 processor with the memory of 12.0 GiB. Computational cost of PCE construction is not included.

4.7 Summary

In essence, our study throws light on the role of the forecast model uncertainty in estimating high dimensional posterior distributions of geological properties. We used PCE metamodel with two most popular data assimilation methods: EnKF and MCMC. Through qualitative and quantitative characterization of posterior pdfs and QoI predictions in the field case study, we list the important outcomes as follows:

1. PCE metamodel is suitable to forecast relevant flow properties within a confidence interval in highly nonlinear subsurface problems.
2. EnKF can provide reliable estimations of model parameters and observations under PCE model uncertainty. Also, assimilation of additional data reduces the effect of forecast uncertainty in posterior estimation.
3. With accurate mean and variance of posterior distributions, MCMC is more robust than EnKF against the forecast model uncertainty.
4. High computational cost of data assimilation can be avoided in practical applications by use of forecast model providing reasonable approximations.

In our opinion, this kind of assessments can be significant in the evolution of the future subsurface characterization workflows. Further evaluation of different forecast models suggested in the literature (see section 2.2) may be useful to understand the performance and tolerance of assimilation techniques under various conditions and sources of uncertainty respectively.

Chapter 5

SAGD Real-Time Production Optimization Using Adaptive and Gain-Scheduled Model Predictive Control ³

³ A version of this chapter has been published in the proceedings of the *SPE Western Regional Meeting* and submitted to *SPE Production & Operations*.

5.1 Introduction

In this chapter, two novel control workflows based on adaptive and gain-scheduled MPC are proposed for real-time production optimization of SAGD reservoirs. In the first one, rather than using only a single linear model for the whole control period, re-estimation of coefficients at each control interval based on system identification theory is included in the control workflow. In the other, the operating range of the controlled variable is divided into multiple control regions and a separate controller is designed for each of them, rather than using only one controller for the entire range of operation of the SAGD process. Switching between controllers is incorporated in the workflow by considering output variables of the previous interval as the scheduling variable. The main goal is to maintain subcool near the predefined optimum set-point along the well pair, which will eventually result in maximum NPV of the SAGD asset while minimizing the environmental and carbon footprint.

Section 5.2 covers various aspects of system identification while section 5.3 explains MPC including adaptive and gain-scheduled MPC. It also includes control workflows to implement the proposed ideas in SAGD reservoirs. Details of the field-scale reservoir model used to verify the suggested approaches are given in the section 5.4 along with the specific details related to the application of adaptive and gain-scheduled MPC. Results explaining the impact of the proposed approaches on real-time production optimization are then presented and discussed. They are also compared with linear MPC and the true field case where no control strategy was used. Section 5.6 provides the summary of the study.

5.2 Identification of Dynamic Systems

The primary objective of identifying a dynamic model here is to predict the future behaviour for process control. Physical, empirical and semi-empirical models can be considered (Seborg et al. 2011) to represent the process. Physical models are derived analytically considering first principles of the process. However, for many complex systems, physics is not known explicitly. Similarly, semi-empirical models involve use of first principles in which unknown parameters are determined empirically. Such models are typically in form of ordinary and/or partial differential equations that are

difficult to develop and computationally expensive to solve. In contrast, empirical models, also known as black box models, can easily be identified by fitting the input-output data available. Also, computational time required to solve these models is very less, which enables the real-time prediction of the system. Considering their suitability for application in control engineering (Foss et al. 1998), we choose to develop empirical models based on system identification using input-output data.

A dynamic system can be represented using an empirical linear time invariant (LTI) model as follows (Ljung 1999):

$$y(t) = G_p(z^{-1}, \theta)u(t) + G_l(z^{-1}, \theta)e(t) \quad (5.1)$$

where $y(t)$, $u(t)$ and $e(t)$ are the output, input, and disturbance (Gaussian white noise), respectively at current time step t . G_p in Eq. (5.1) is a process model representing the relationship between output and input while G_l is a disturbance (or noise) model that relates the output and unmeasured disturbances in the system. Process and disturbance models are defined in terms of z , the time-shift operator and θ , the vector of parameters to be estimated.

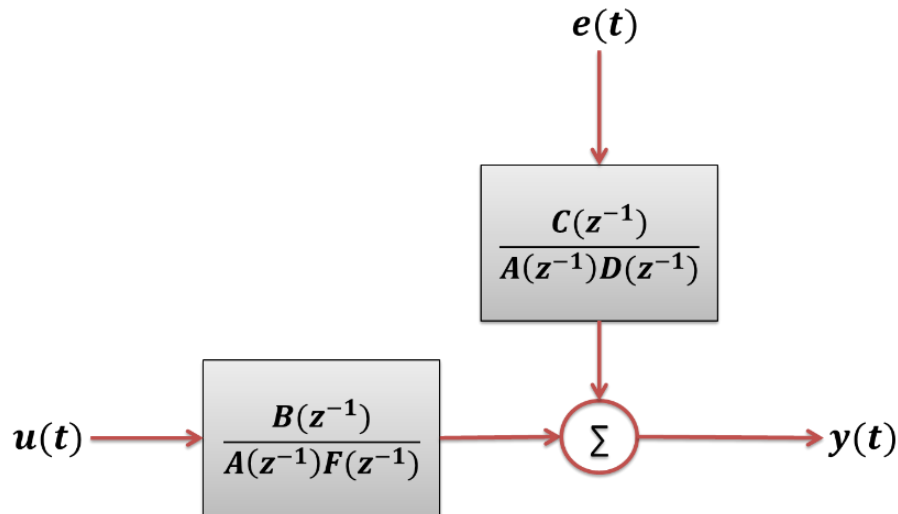


Figure 5.1 – Structure of Prediction Error (PE) model in System Identification.

Different process and disturbance models can be implemented in Eq. (5.1). As a result, numerous different model structures are possible. The prediction error (PE) model is

the most common model structure used in linear system identification models (*Figure 5.1*). Mathematically, it can be expressed as (Huang et al. 2013),

$$A(z^{-1})y(t) = \frac{B(z^{-1})}{F(z^{-1})}u(t) + \frac{C(z^{-1})}{D(z^{-1})}e(t) \quad (5.2)$$

where $A(z^{-1}), B(z^{-1}), C(z^{-1}), D(z^{-1})$ and $F(z^{-1})$ are polynomials of the time-shift operator z .

$$\begin{aligned} A(z^{-1}) &= 1 + a_1z^{-1} + \dots + a_{na}z^{-na} \\ B(z^{-1}) &= b_1z^{-1} + \dots + b_{nb}z^{-nb} \\ C(z^{-1}) &= 1 + c_1z^{-1} + \dots + c_{nc}z^{-nc} \\ D(z^{-1}) &= 1 + d_1z^{-1} + \dots + d_{nd}z^{-nd} \\ F(z^{-1}) &= 1 + f_1z^{-1} + \dots + f_{nf}z^{-nf} \end{aligned} \quad (5.3)$$

Note that in Eq. (5.3), polynomial $B(z^{-1})$ starts from negative power of time-shift operator unlike zero power in other polynomials in order to reinforce the fact that process has delay of at least one sampling interval. Various linear model structures like ARX (autoregressive with exogenous input), ARMAX (autoregressive moving average with exogenous input), OE (output error) and BJ (Box-Jenkins) can be obtained by considering different polynomials in numerator and denominator (see *Table 5.1*) of PE model shown in Eq. (5.2) (Huang et al. 2013). In addition, state-space model structure which considers system states is widely used to model dynamic processes, especially MIMO systems. It can be defined as,

$$\begin{aligned} x(t+1) &= A(\theta)x(t) + B(\theta)u(t) + K(\theta)e(t) \\ y(t) &= C(\theta)x(t) + e(t) \end{aligned} \quad (5.4)$$

where $x(t)$ is a state vector comprising system states at time t while A, B, K and C are system matrices/vectors in terms of model parameters θ . All the model structures shown in *Table 5.1* can easily be converted to state-space model and vice versa (Yao

et al. 2015). Therefore, state-space model is also suitable for designing modern control algorithms.

Table 5.1 – Various linear model structures in System Identification

Model Structure	Process Model		Disturbance Model	
	Numerator	Denominator	Numerator	Denominator
ARX	$B(z^{-1})$	$A(z^{-1})$	1	$A(z^{-1})$
ARMAX	$B(z^{-1})$	$A(z^{-1})$	$C(z^{-1})$	$A(z^{-1})$
OE	$B(z^{-1})$	$F(z^{-1})$	1	1
BJ	$B(z^{-1})$	$F(z^{-1})$	$C(z^{-1})$	$D(z^{-1})$

Model parameters θ (the coefficients of polynomials shown in Eq. (5.3)) can be estimated using different techniques like subspace identification, least squares method and Prediction Error Method (PEM). Though subspace identification method is non-iterative and avoids local minima, it cannot obtain maximum likelihood like PEM (Huang et al. 2013). Also, unlike least squares method, PEM can be used to estimate parameters of almost whole family of model structures (Ljung 2002). Due to such advantages, PEM that minimizes difference between original observation and predicted output is used in the proposed work. The technique exploits dynamic structure of the system explicitly to get the accurate prediction. The procedure to calculate the parameters of the process and the disturbance model using PEM is shown below:

1. Derive an optimal one-step ahead predictor in terms of past outputs and inputs for the selected model structure. For the generic system identification model shown in Eq. (5.1), an optimal predictor denoted by $\hat{y}(t|t-1)$ can be determined as (Ljung 1999),

$$\hat{y}(t|t-1) = G_l^{-1}(z^{-1}, \theta)G_p(z^{-1}, \theta)u(t) + [I - G_l^{-1}(z^{-1}, \theta)]y(t) \quad (5.5)$$

2. Substitute input values recorded from the process and corresponding output measurements in Eq. (5.5) and calculate the one-step ahead prediction in terms of model parameters θ .

3. Compute the one-step ahead prediction error (or residual) for the entire dataset. The prediction error at time step t is

$$\varepsilon(t) = y(t) - \hat{y}(t|t-1) \quad (5.6)$$

4. Calculate the loss function, which is the sum of squared one-step ahead prediction errors for each pair of the input-output data. It can be calculated using the following equation:

$$J(\theta) = \sum_{t=1}^N \varepsilon^2(t) \quad (5.7)$$

where N is the total number of samples in the dataset.

5. Finally, minimize the loss function by considering model parameters θ as regressors.

$$\theta^* = \underset{\theta}{\operatorname{argmin}} J(\theta) \quad (5.8)$$

where θ^* represents the optimum model parameters. In general, the optimization problem shown in Eq. (5.8) is nonlinear and iterative numerical algorithms are required to obtain optimal model parameters.

Model validation is performed using four distinct criteria: autocorrelation and cross-correlation tests, cross-validation and Akaike's Information Criterion (AIC). Initially, autocorrelation test is conducted in which autocorrelation of residuals defined in Eq. (5.6) is calculated. An autocorrelation is a normalized autocovariance given by

$$\rho_{\varepsilon}(\tau) = \frac{r_{\varepsilon}(\tau)}{r_{\varepsilon}(0)} \quad (5.9)$$

where $r_{\varepsilon}(\tau)$ is the autocovariance of residuals respectively at lag τ . Initially, in Eq. (5.1), it was assumed that $e(t)$ is a white noise, and therefore, if process model and disturbance model are estimated accurately then residual should be equal to the white noise. If more than 99% of the autocorrelation values lie within $\left[-\frac{3}{\sqrt{N}}, \frac{3}{\sqrt{N}}\right]$, the residuals can be considered as white noise (Huang et al. 2013) and hence the model is valid. The cross-correlation between residuals and the input is

$$\rho_{\varepsilon u}(\tau) = \frac{r_{\varepsilon u}(\tau)}{\sqrt{r_{\varepsilon}(0)r_u(0)}} \quad (5.10)$$

where $r_{\varepsilon u}(\tau)$ represent the cross-covariance between residuals and input at lag τ and $r_u(0)$ is the autocovariance of the input. If 99% of the cross-correlations at different lags lie within $\left[-\frac{3}{\sqrt{N}}, \frac{3}{\sqrt{N}}\right]$ while displaying no significant trend, the model is considered to be valid. Note that for OE model structure, autocorrelation test is not applicable since noise model is considered as unity.

In cross-validation, the model fit on a separate validation dataset (which is not used in model identification) is calculated (Ljung 2016):

$$\text{Model Fit (\%)} = \left[1 - \frac{|y - \hat{y}|}{|y - \bar{y}|}\right] \times 100 \quad (5.11)$$

where y is the observed output, \hat{y} is predicted output while \bar{y} denotes the mean of output. Model fit equals to 100% refers to a perfect model while 0% indicates that predicted output is no better than a speculation equal to the mean value.

Finally, the AIC is given by (Soderstrom and Stoica 1989):

$$AIC = N \log J(\theta^*) + 2p \quad (5.12)$$

where p represents number of model parameters. Since the AIC penalizes the number of parameters and a larger number of parameters leads to an increase in the degrees of freedom and usually a reduction in the loss function, the AIC provides a metric to choose between models with different numbers of parameters. While comparing different models, one with lower AIC should be chosen as it provides best trade-off between accuracy and model dimensions.

The most important and time consuming task in system identification is to select the appropriate model order; too low an order may result into inaccurate prediction while unnecessarily high orders may lead to overfitting of the data. *Figure 5.2* demonstrates the workflow used in our work to determine model orders in linear system identification. First, we choose a simple model structure (e.g., ARX) and try to identify a lower order model. If the model fails the residual analysis or cross-validation tests, the order of the noise model is increased and if this does not provide a satisfactory fit,

the order of the process model is increased. The procedure is repeated until an acceptable model is found. It is also repeated with other model structures, and the AIC is used to select the best system identification model. It is observed that same order for numerator and denominator of noise model provides encouraging results and hence, order for both should be increased simultaneously keeping in mind the model structure. In case of process model, order of the numerator should be given first preference since increasing the denominator order will increase the overall order of dynamic model.

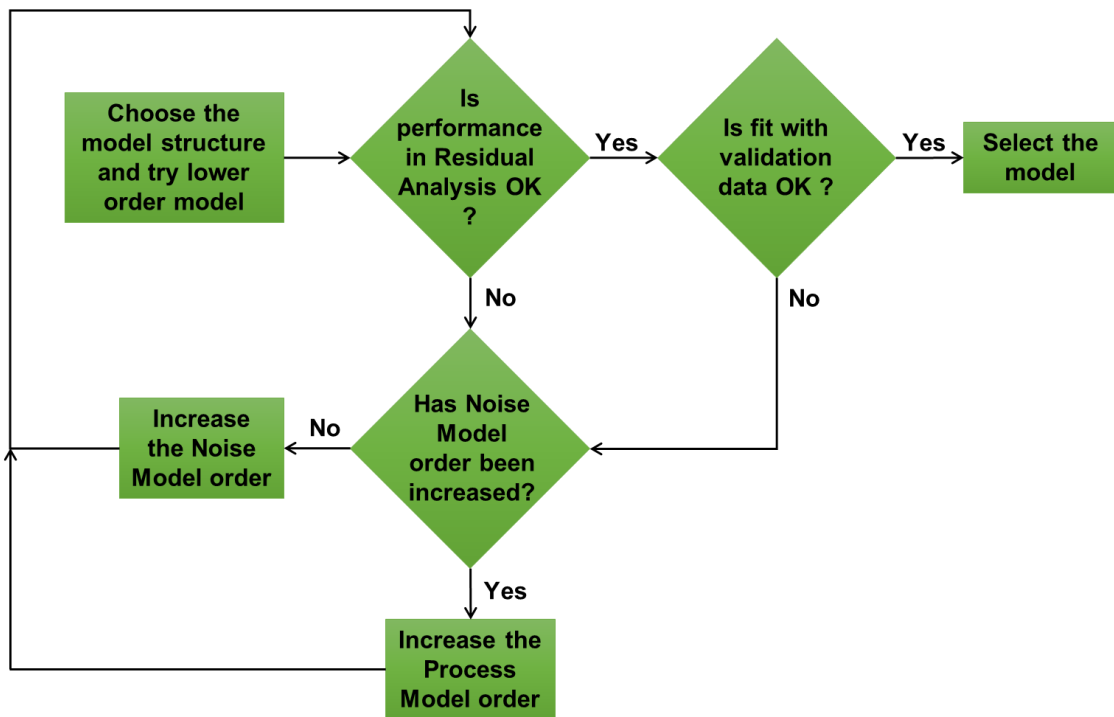


Figure 5.2 – Workflow for linear model order selection in System Identification.

5.3 Model Predictive Control

In real-time production optimization, controlling subcool at a set-point is the central intention to achieve uniform steam chamber along the wellbore. Various control methods are available including manual, PID or fuzzy control to fulfill this objective. Though such methods have simple control laws and easy practical applications, they are not suitable for controlling complex MIMO systems (Richalet 1993). In contrast,

MPC is an advanced multivariable control strategy that considers internal dynamics of the system while defining interaction between distinct output and input variables by means of physical or empirical models. In addition, such internal models provide predictive capability to MPC controller due to which it can anticipate future contraventions and take corrective measures at current time interval (Seborg et al. 2011). Various equality and inequality constraints can also be handled explicitly by MPC, which is one of its key characteristics (de Oliveira and Biegler 1994). Further, feedback nature of the algorithm compensates for the offset in model predictions up to some extent, which ensures robust control of a given process (Camacho and Bordons 2007). Considering its versatility and suitability to the problem of subcool control, MPC is an excellent control technique to optimize the performance of SAGD process by manipulating input variables.

Concept of model based predictive control started evolving in late 1960s (Lee and Markus 1967) and initial applications were reported in 1970s by Richalet et al. (1978) and Cutler and Ramaker (1979). Since then it has been applied to more than 4600 control problems (Qin and Badgwell 2003). It comprises mainly two components i.e. dynamic model and cost function optimization. Details regarding types of dynamic models which can be used in MPC as well as how an empirical model is identified in proposed work is given in previous section. Another component involves minimization of a cost function (also known as an objective function) that ultimately provides the inputs for next sampling interval. Therefore, cost function should be defined such that it considers the necessary control effort required by an output variable to follow the reference trajectory. Equation of the cost function used in this work can be given as (Bemporad et al. 2015),

$$C = C_y + C_u + C_{\Delta u} \quad (5.13)$$

where C represents the total cost. For simplicity, each term on right hand side of the Eq. (5.13) is explained separately. C_y that denotes cost due to error in output reference tracking can be explained as follows:

$$C_y = \sum_{j=1}^{N_y} \sum_{i=1}^P \{w_j^y [r_j(t+i|t) - y_j(t+i|t)]\}^2 \quad (5.14)$$

where r_j and y_j are reference set-point and predicted output value from dynamic model respectively for output j . Here, $t + i|t$ suggests values at time interval $t + i$ as MPC calculations are being done at current time interval t . w_j^y refers to the tuning weight associated with output j while N_y denotes total number of outputs. Number of future sampling intervals to be considered in calculations of MPC is known as prediction horizon, which is represented by P in Eq. (5.14).

Similarly, equation for cost corresponding to input variable mismatch that is referred as C_u in Eq. (5.13) can be written as,

$$C_u = \sum_{j=1}^{N_u} \sum_{i=1}^{P-1} \{w_j^u [u_j(t + i|t) - u_j^{opt}(t + i|t)]\}^2 \quad (5.15)$$

where u_j represents input value while u_j^{opt} denotes optimum target value obtained from the mid-term optimization for j^{th} input variable. N_u and w_j^u in Eq. (5.15) refer to total number of inputs and tuning weight for input j respectively.

Finally, last term $C_{\Delta u}$ in Eq. (5.13) that addresses rate of change (or adjustments) in input variables can be expressed as,

$$C_{\Delta u} = \sum_{j=1}^{N_u} \sum_{i=1}^{P-1} \{w_j^{\Delta u} [u_j(t + i|t) - u_j(t + i - 1|t)]\}^2 \quad (5.16)$$

where $w_j^{\Delta u}$ is the tuning weight related to rate of change of input j . Note that in both Eq. (5.15) and (5.16), summations are done only till $P - 1$ sampling intervals. Since it is assumed that process has delay of at least one sampling interval, output at sampling interval P will not be affected by input at the same sampling interval and hence it is not considered in the cost function.

Minimization of Cost function C in Eq. (5.13) is subjected to following constraints:

$$\begin{aligned}
y_j^{min} &\leq y_j(t + i|t) \leq y_j^{max} \\
u_j^{min} &\leq u_j(t + i|t) \leq u_j^{max} \\
\Delta u_j^{min} &\leq \Delta u_j(t + i|t) \leq \Delta u_j^{max} \\
\Delta u(t + M|t) &= 0
\end{aligned}
\tag{5.17}$$

where y_j^{min}, u_j^{min} and Δu_j^{min} are the lower bounds of output, input, and rate of change of input j respectively. Similarly, y_j^{max}, u_j^{max} and Δu_j^{max} are the upper bounds of output, input, and rate of change of input j respectively. Here, last constraint signifies that in optimization, inputs up to only M (control horizon) sampling intervals are manipulated and after that, inputs are held constant.

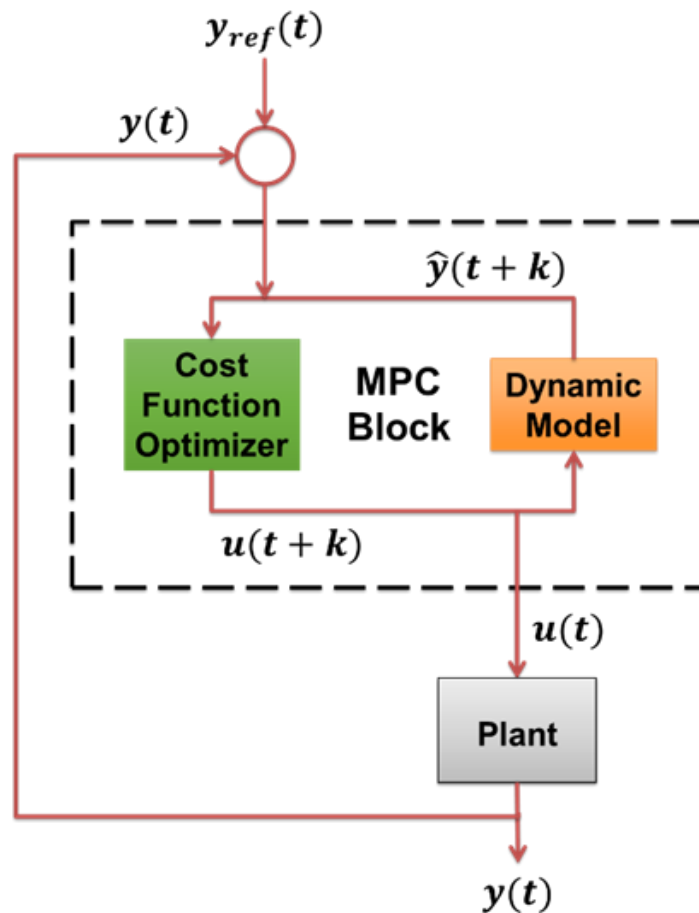


Figure 5.3 – Control framework of Model Predictive Control.

Control framework of MPC is explained in *Figure 5.3* using block diagrams. Set-point or reference trajectory y_{ref} for output variables are available from the supervisory control or mid-term optimization. Also, constraints for cost function optimizer are decided according to surface facilities available and safe operation of the system. Then predefined cost function is calculated where future outputs are estimated using dynamic model for the given prediction horizon. Suitable optimization algorithm is used to minimize the cost function by changing the input variables for the given control horizon. Input for the next control interval that corresponds to minimum cost function is then implemented in the physical plant. Output $y(t)$ at current time step is recorded in the plant and then fed back to the MPC controller to calculate input of the next control interval. The process is repeated at each sampling interval, which depicts the moving horizon nature of MPC. Note that input (IV) and output variables (OV) can also be referred as manipulated (MV) and controlled variables (CV) respectively.

5.3.1 Adaptive MPC

Primary concern in model based control strategies is the availability and accuracy of the process model (Kozak 2014). Especially in case of empirical models which does not involve any physics and are trained using only required range of operating conditions, estimations may not be accurate enough when extrapolated (Seborg et al. 2011). If output predictions from dynamic model are erroneous then cost function optimization will be inappropriate, which ultimately leads to incorrect calculation of future inputs by MPC controller. In addition, Fukushima et al. (2007) noted that there are always uncertainties present in the model that can significantly affect the controller performance. Therefore, only an LTI empirical model would not be sufficient to represent the continuously changing states of nonlinear SAGD process in real-time production optimization using MPC.

Adaptive model predictive control, a variant of MPC is proposed in this work to incorporate time varying plant characteristics in real-time production optimization. One of the well-known adaptive schemes, widely recognized as generalized predictive control (GPC), was proposed by Clark et al. (1987) for control applications utilizing long range predictive controllers. Also, Genceli and Nikolaou (1996) suggested a control framework that performs simultaneous MPC calculations and model

identification such that process is least interrupted. A similar approach has been employed in this work schematic representation of which is shown in figure 7. Instead of using linear model with fixed coefficients in MPC controller, new coefficients are identified online at each control interval. The model with new coefficients is then used to determine inputs for next control interval in MPC. Corresponding outputs are recorded from the plant and an input-output dataset is prepared, which represents the latest plant behaviour. It is further used to estimate coefficients of the plant model for next control interval and the loop goes on. Since PEM explained in section 5.2 can be used to calculate new coefficients online while keeping the linear model structure same, empirical models used in this work are suitable for Adaptive MPC. In addition, time required for online calculation of coefficients is much less as compared to the sampling interval with commonly available computational resources, a key feature due to which Adaptive MPC has become prominent (Karra et al. 2008) from the implementation point of view. Such evolution of coefficients represents current states of the reservoir that allows for better prediction of outputs and in turn better control of the SAGD process.

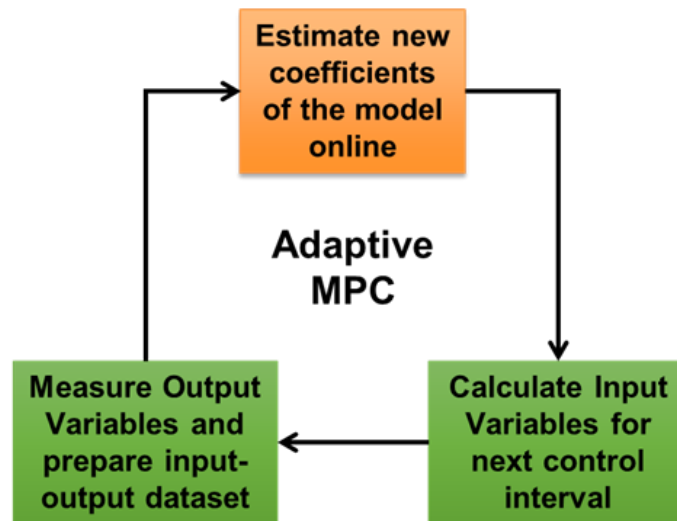


Figure 5.4 – Schematic representation of Adaptive MPC.

5.3.2 Gain-Scheduled MPC

Gain scheduling is an effective method to design controllers for nonlinear systems by employing linear control techniques. As the name suggests, controller gains are

adjusted (scheduled) for the different operating regions of the plant based on the current value of scheduling variables. Several approaches such as switching or blending of controllers or their parameters or plant models can be practiced to achieve gain scheduling. Rugh and Shamma (2000) has reviewed latest development in the gain scheduling methods including classical linearization-based scheduling as well as linear parameter varying (LPV) approaches. Main advantage of gain scheduling is the properties that it inherits from linear control methods, making it computationally efficient as compare to other nonlinear control approaches. As Ilka (2015) noted, gain scheduling basically facilitates the nonlinear control problem by parallel decomposition of the whole system into numerous sub-problems where communication between sub-problems is defined by scheduling variables. It allows the aggressive variation in control parameters, ultimately leading to tighter and efficient control of the system even in adverse situations like beginning of the SAGD production phase that depicts substantially offset subcool values from the optimum target.

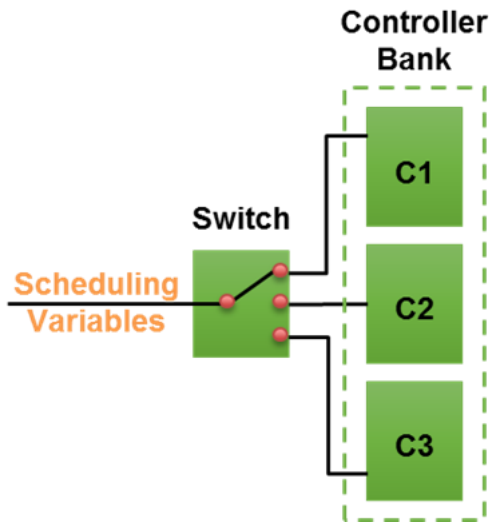


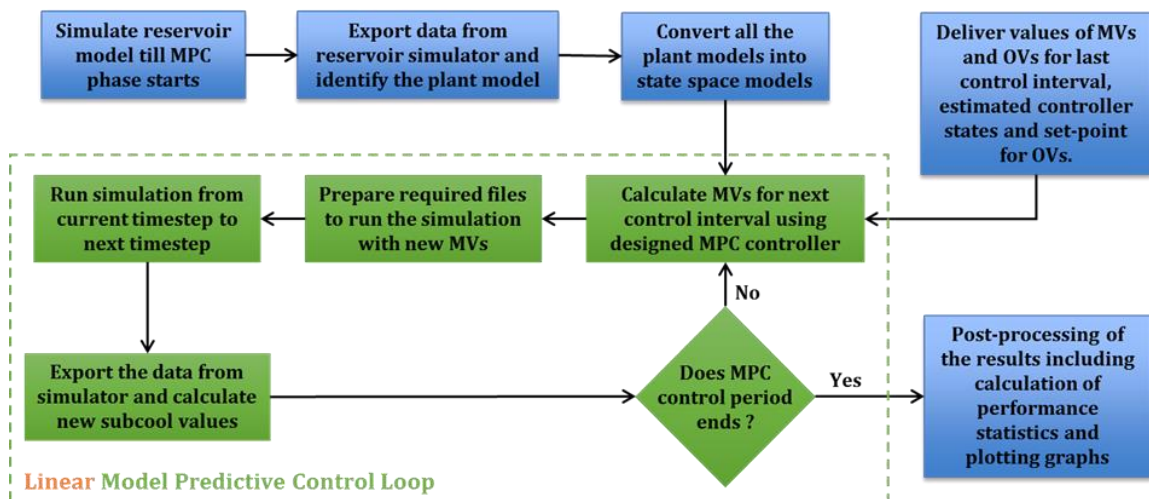
Figure 5.5 – Schematic representation of Gain-Scheduled MPC.

We have implemented gain-scheduled MPC for real-time subcool control by constructing a family of linear controllers as shown in *Figure 5.5*. The operating range of the SAGD reservoir is divided into numerous control regions and a separate controller is designed for each of the control region, with constraints being set according the operating region. Minimum subcool is considered as the scheduling variable to switch between the controllers. Several measures are considered for

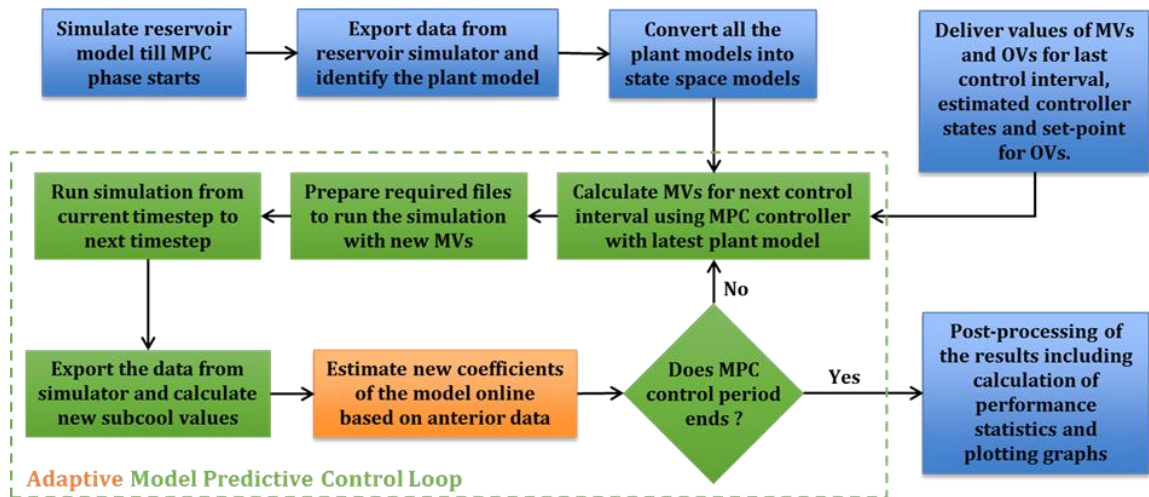
smooth transfer between controllers such as limiting the maximum allowable change in manipulated variables for a particular timestep, tuning the operating range of each controller and specifying the priority of the controller based on the physics of SAGD. In addition, as in adaptive MPC, the coefficients of the plant model are updated after each control interval to account for changes in reservoir dynamics while calculating optimum input parameters for the next control interval.

5.3.3 Control Framework for Real-Time Production Optimization Using MPC

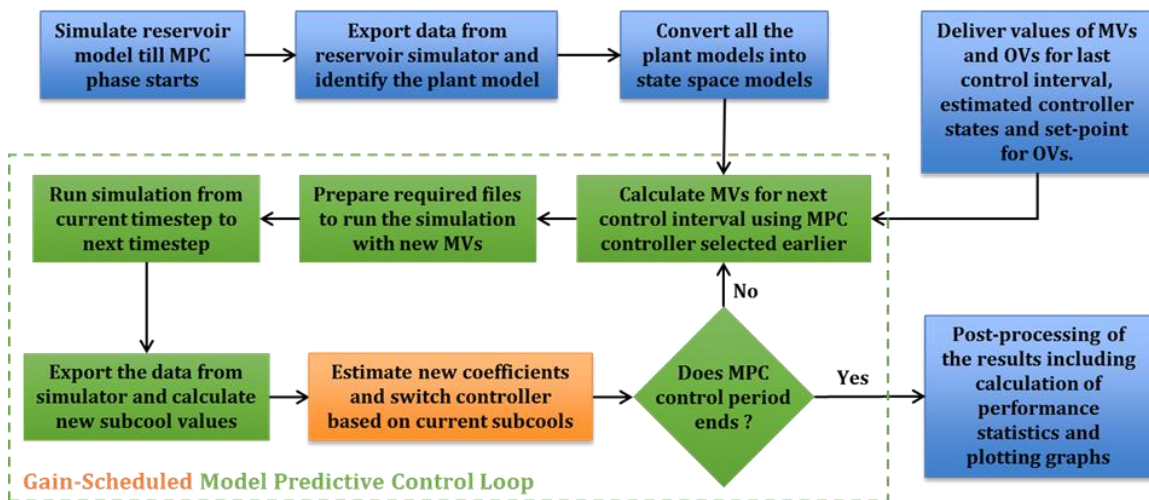
Workflows to implement the different variants of MPC are shown in *Figure 5.6*. The history-matched reservoir model is used as a virtual plant in proposed workflows. *Figure 5.6(a)* depicts the control framework for linear MPC that uses only one controller. Since determination of the model based on system identification requires a training dataset, the reservoir model is simulated up to the date when the MPC phase is set to begin. Then, linear empirical models are identified by following the procedure discussed in section 5.2. All the dynamic models are then converted to state space formulations. The conversion includes transformation of identified model parameters into a state space canonical realization (Ljung 1999), which is followed by balancing and rescaling of state space matrices to improve numerics and accuracy of the model (Ljung 2016).



(a)



(b)



(c)

Figure 5.6 – Control framework for real-time subcool control using (a) Linear MPC (b) Adaptive MPC and (c) Gain-Scheduled MPC.

An appropriately designed controller which considers MVs and OVs from the last control interval along with estimated controller states and set-point for OVs is used to calculate optimum values of MVs for next control interval. The necessary input files for the reservoir simulator used are then prepared using the MPC-recommended MVs for the next control interval; this is equivalent to supplying the MV to the real process in industrial implementation. The reservoir model is simulated up to the next sampling

interval, following which real-time measurements are collected and used to calculate OV_s in the next step of the workflow. Workflows for adaptive and gain-scheduled MPC are presented separately in *Figure 5.6(b)* and *Figure 5.6(c)* respectively with orange blocks indicating the additional steps to be carried out.

5.4 Application to the SAGD Field: A Case Study

To assess the effectiveness of suggested ideas in real-time production optimization, all three variants of MPC have been applied to a SAGD reservoir located in northern Alberta. A bidirectional link between the MPC controller developed using the Model Predictive Control Toolbox™ (Bemporad et al. 2016) and the virtual process plant, i.e. the thermal reservoir simulator CMG STARS™ (CMG 2013a), was established using routines written in MATLAB® (MathWorks 2014). In addition, Results Report™ (CMG 2013b) is integrated in the workflow to facilitate import-export of the data between the controller and the plant.

5.4.1 Details of History-Matched Reservoir Model

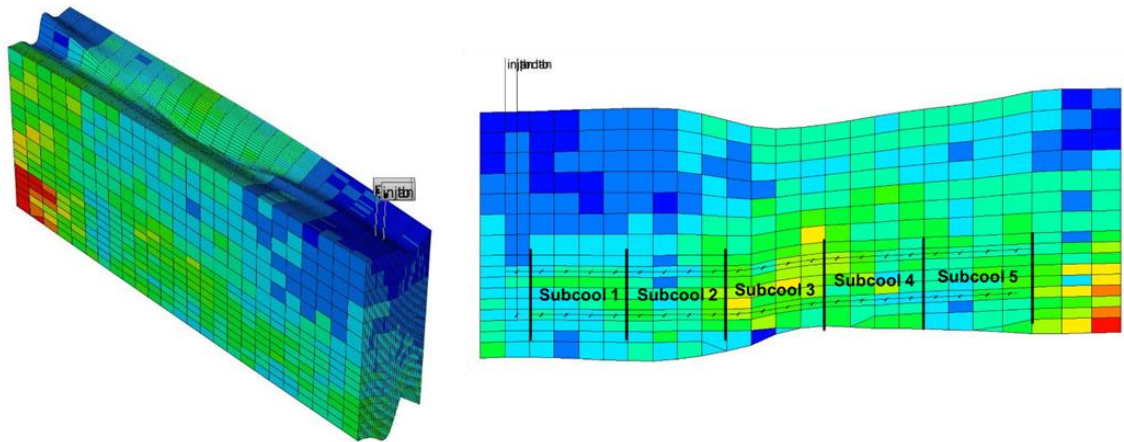


Figure 5.7 – 3D view (left) and IK view for plane 26 along j -direction with well pair divided in five sections (right) of history-matched reservoir model.

As noted before, a history-matched reservoir model of a SAGD field is used as a virtual process plant in this work. In history matching (Oliver and Chen 2011), unknown reservoir parameters are estimated by matching the production outputs of reservoir

model with field history. In our work, permeability values of all the grid blocks of the reservoir model were considered as unknown parameters and history matching was performed using the EnKF as explained in *Chapter 3* and *Chapter 4* (Patel et al. 2015, Patel et al. 2017). The reservoir model depicting the best match with field data was chosen from the updated ensemble for real-time production optimization. *Figure 5.7* presents the 3D view of the selected model while history matching results of the same are shown in *Figure 5.8*, which clearly indicate that the reservoir model used in this work meticulously represents the actual oilfield.

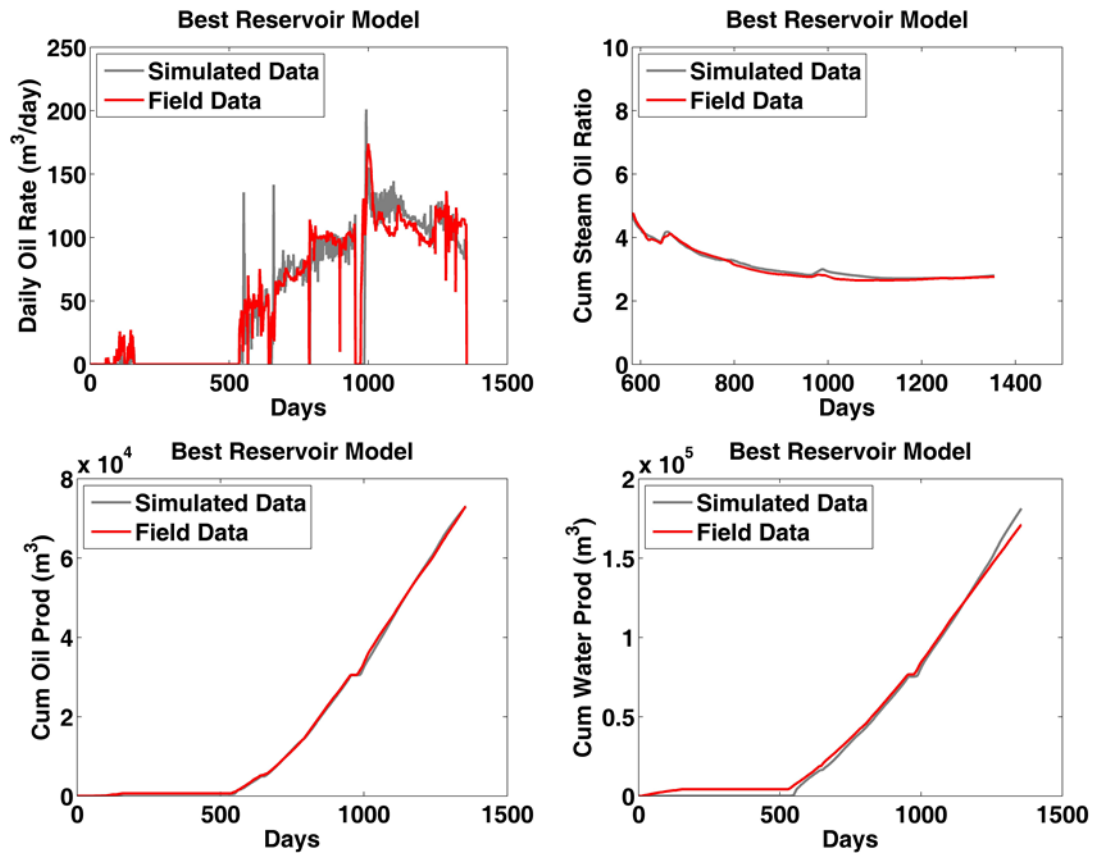


Figure 5.8 – History matching results of reservoir model selected for real-time production optimization.

Grid dimensions of the reservoir model shown in *Figure 5.7* can be given as 25×50×16 with size of each grid being 25 m, 2 m and 1.5 m in i (East), j (North) and k (Elevation) direction respectively. Like the true SAGD reservoir, the history-matched model also demonstrates heterogeneity with horizontal permeability values ranging from 1561 md

to 7765 md and porosity values varying from 31.6 % to 42.6 %. The initial average reservoir pressure and temperature are set at 650 kpa and 7 °C, respectively, while the oil saturation is estimated to be 0.8 with no solution gas present in the reservoir. The fluid model is developed using a typical viscosity-temperature relationship of bitumen where the viscosity is around 625,000 cp at initial reservoir temperature and decreases to 10 cp at operating temperature of 216 °C. The rock type is defined using appropriate relative permeability curves that indicate the usual water-wet behaviour. Note that relative permeability and viscosity vs. temperature curves are not provided here because of the confidentiality of that data. A horizontal well pair with injector consisting long and short tubing strings is modeled, while the producer comprised of only annulus. Both wells are 500 m long and placed 6 m apart, and well constraints are assigned to be the same as for the field history. The model is simulated for 1355 days using the CMG STARS™ thermal reservoir simulator. The results obtained from the simulation of history-matched model are considered as the base case where no control algorithm is used and the performance of the proposed approaches is compared to it.

5.4.2 Application of System Identification Techniques

System Identification Toolbox™ (Ljung 2016) was used in this work to estimate the behaviour of the system in MPC. To simplify the control problem, well pair was divided in 5 sections as shown in *Figure 5.7* and subcool of each section was considered as an output variable. Steam injection rate of long and short tubing as well as liquid production rate that directly affect subcool were considered as input variables. Separate model was identified for each of the five multiple input single output (MISO) systems that considers one subcool as an output and all three input variables. Such decoupling of the system introduces an assumption that OVs do not interact with each other, which is reasonable in our case since subcool is influenced by input variables rather than adjacent subcool.

To consider the practical situation that would arise in the field, it was decided to identify model based on data available from the field if it is persistently excited. Since temperature measurements from the DTS were not consistent in the field, IVs recorded on daily basis were implemented in history-matched reservoir model explained in

previous subsection to obtain the subcool data. Temperature measurements of the respective grid blocks were averaged to calculate subcool for a section of the well pair. In total, 250 samples of input-output data with sampling interval of 1 day were obtained from the simulation. Roughly 2/3rd of the data i.e. 165 samples were used for identification of the model while rest 85 samples were used to cross-validate the estimated model. Time delay is estimated for each MISO system, which can be different for each input variable considered in the model.

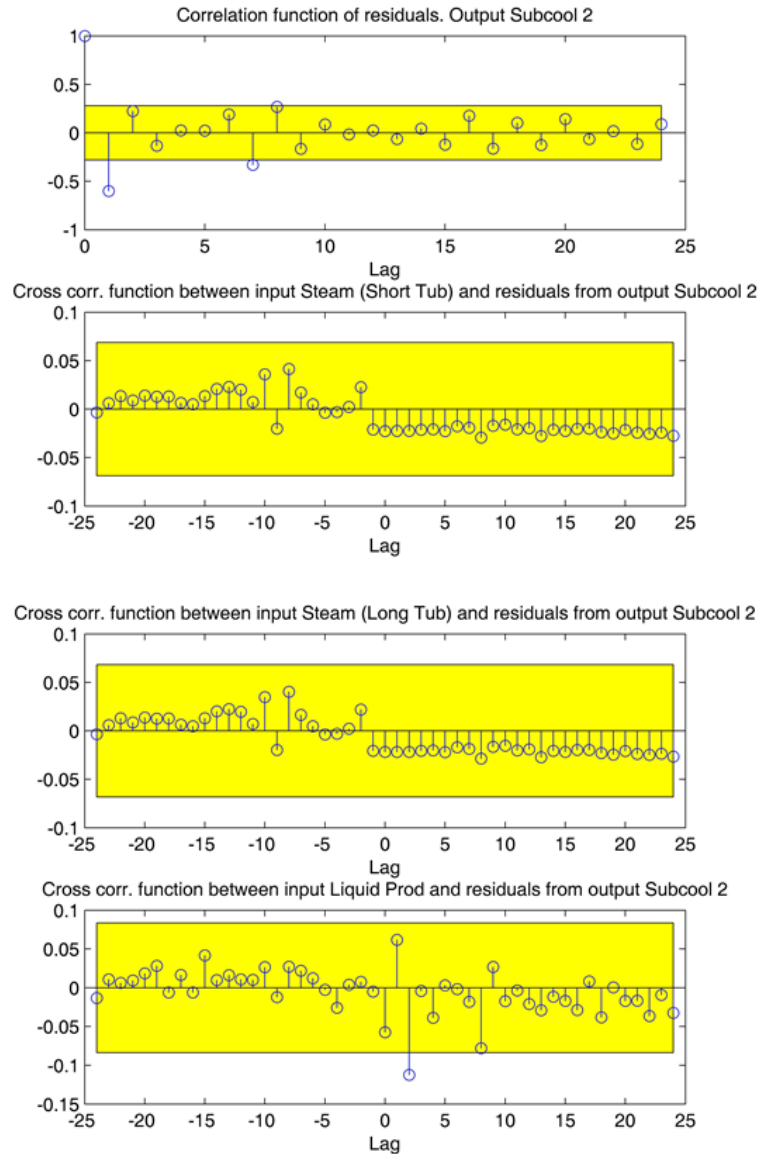


Figure 5.9 – Results of autocorrelation and cross-correlation tests for Subcool 2. Yellow rectangle box shows 99% confidence interval.

More than 50 models were investigated in the system identification procedure for each MISO system. Residual tests and cross-validation were performed to select the best model for each subcool. Results of autocorrelation and cross-correlation tests for Subcool 2 are shown in *Figure 5.9*. It can be observed that residuals are well within the 99% confidence interval indicated by yellow rectangle box. Also, there is no trend in the residuals for different lags, which confirms that models are legitimate. The performance of the models for all subcools in cross-validation is shown in *Figure 5.10*, and the models perform well in infinite-step ahead prediction. Specifications of the system identification models including its structure, delay, order, fit and AIC are presented in *Table 5.2* for each subcool. Orders of polynomials $B(z^{-1})$, $C(z^{-1})$, $D(z^{-1})$ and $F(z^{-1})$ in Eq. (5.3) are shown using nB , nC , nD and nF , respectively, in *Table 5.2*. Models identified separately for each subcool were then combined by replacing scalar coefficients in polynomials $A(z^{-1})$, $B(z^{-1})$, $C(z^{-1})$, $D(z^{-1})$ and $F(z^{-1})$ (refer Eq. (5.3)) with matrices A , B , C , D and F , respectively. After vertical concatenation of the MISO systems, the dimension of the matrix A is $N_y \times N_y$ while matrices B and F are of dimension $N_y \times N_u$ and matrices C and D are of dimension $N_y \times 1$ (Vembadi 2014). In addition, the noise variance of each system was preserved by creating a separate $N_y \times N_y$ matrix in the combined MIMO system. Finally, as explained in the workflow to implement MPC (*Figure 5.6*), the combined MIMO model was converted to a state space formulation. Current states of the state space models were obtained using the training data such that model fit with output signal is maximum.

Table 5.2 – *Specifics of system identification models identified for each subcool*

Output Variables	System Identification Models							Fit (%)	AIC
	Structure	Delay	Order						
			nB	nC	nD	nF			
Subcool 1	BJ	[1 2 1]	[1 3 1]	3	3	[1 3 1]	59.98	1.66	
Subcool 2	BJ	[1 1 1]	[1 4 1]	8	8	[1 4 1]	73.73	0.53	
Subcool 3	OE	[1 2 1]	[1 1 1]	-	-	[1 1 1]	62.77	2.63	
Subcool 4	BJ	[1 1 1]	[1 2 1]	2	2	[1 2 1]	60.26	2.0	
Subcool 5	BJ	[1 1 1]	[1 4 1]	8	8	[1 4 1]	80.19	1.27	

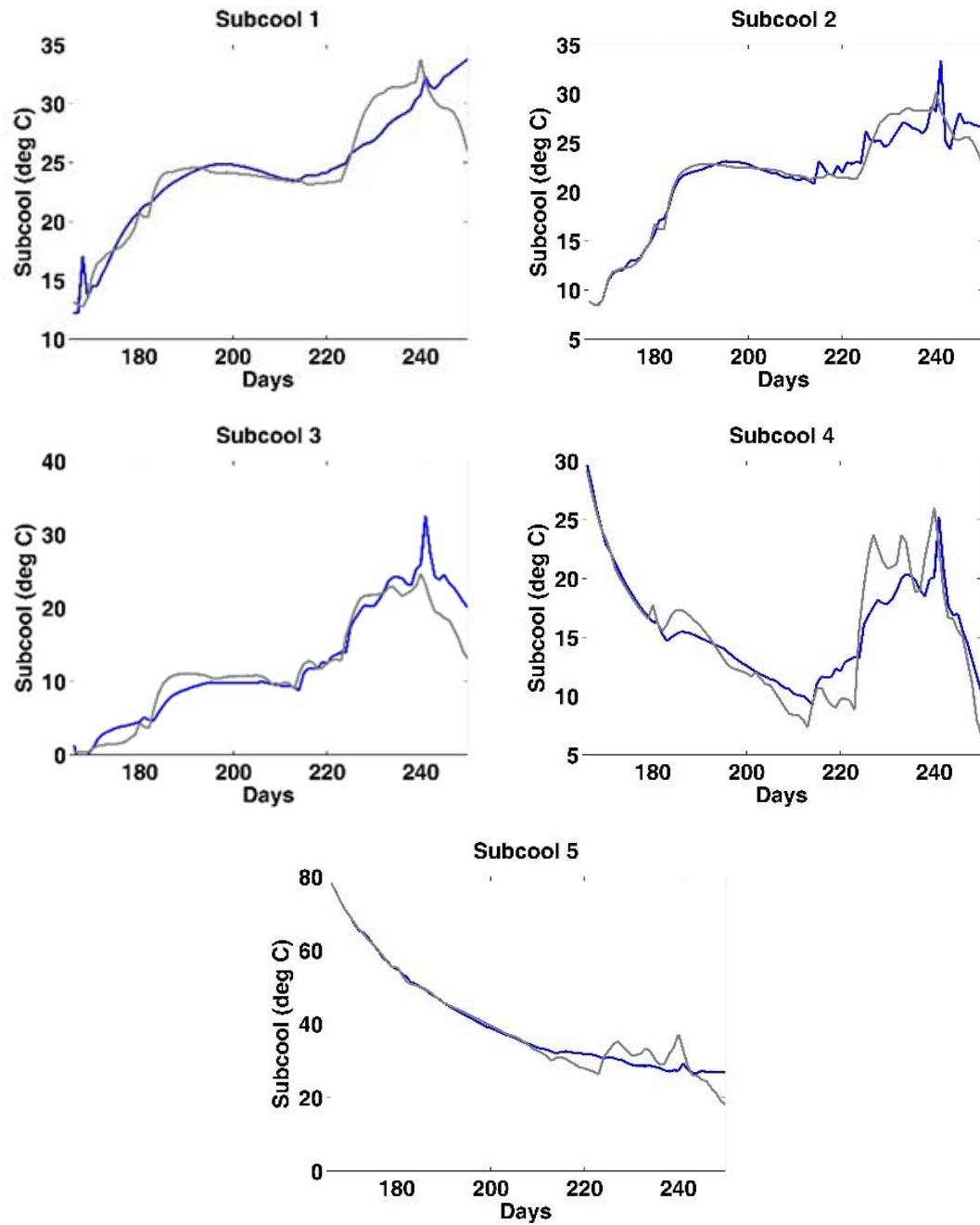


Figure 5.10 – Results of cross-validation for all subcools. Blue line represents predicted output from the model while grey line depicts validation data.

5.4.3 Application of Linear MPC

For stable control of the process, constraints should be defined properly while having some physical meaning. The constraints applied for this case study are shown in *Table 5.3*. The upper bounds (u_j^{max}) for IVs were decided based on the available surface facilities (e.g., capacity of steam generator and separator). Since a small amount of steam is required to be injected to keep the SAGD reservoir alive, lower bounds (u_j^{min}) for steam injection in both short and long tubing were set at 20 m³/day. The lower bound for the liquid production rate was fixed at 50 m³/day. Since a high frequency of change in IVs leads to wear and tear of actuators such as valves, a smaller rate of change in IVs is desired; this is incorporated by specifying lower values (10 m³/day for both steam injection rates and 5 m³/day for liquid production rate) for Δu_j^{max} and Δu_j^{min} . Next, optimum targets (u_j^{opt}) for IVs were determined by performing several trial simulations runs. However, they are available from the mid-term optimization in reality. Lower tuning weight of 0.25 and 0.1 are specified for all IVs (w_j^u) and rate of change of IVs ($w_j^{\Delta u}$), respectively. Higher weights for input parameters results into conservative approach, which is not desirable when OVs are away from the set-point. Sampling time was selected same as that of dynamic model to be consistent. Furthermore, longer the prediction horizon (P) is, higher the computational cost will be. After conducting a few trials in which P was kept higher initially and decreased gradually, the control horizon (M) and prediction horizon were chosen to be 3 and 6 sampling intervals, respectively.

As Patel et al. (2014) noted, the maximum number of OVs that can be controlled is equal to the number of IVs (also known as degree of freedom of the controller). In our case, there are 5 subcools and only 3 input variables and therefore not all the subcools can be controlled near target. As minimum subcool below target value implies steam breakthrough, maintaining it near the specified set-point should be prioritized. To incorporate this in MPC, weights for OVs were specified in a hierarchy where subcool values were sorted in ascending order after each sampling interval and a higher weight (0.9) was assigned to the first 3 subcools and a lower weight (0.1) was assigned to the rest of the subcools. Though the optimum subcool varies from well pair to well pair

and reservoir to reservoir, the literature suggests that it is between 20 to 30 °C for most SAGD reservoirs studied (Edmunds 2000, Vander Valk and Yang 2007, Gates and Leskiw 2010). Hence, the optimum target for subcool was specified as 20 °C. In this case study, the SAGD production phase started from 550 days and data from the initial 250 days was used for model identification, with the MPC being implemented from 800 days onwards up to 1355 days.

Table 5.3 – Design of MPC controller for real-time production optimization

Parameters	Input Variables		
	Steam Inj Rate (Short Tub)	Steam Inj Rate (Long Tub)	Liquid Prod Rate
u_j^{max} (m ³ /day)	250	70	400
u_j^{min} (m ³ /day)	20	20	50
Δu_j^{max} (m ³ /day)	10	10	5
Δu_j^{min} (m ³ /day)	-10	-10	-5
u_j^{opt} (m ³ /day)	115	35	275
w_j^u	0.25	0.25	0.25
$w_j^{\Delta u}$	0.1	0.1	0.1
Sampling Time (Day)		1	
Control Horizon (M)		3	
Prediction Horizon (P)		6	
Output Variables			
r_j (°C)		20	
w_j^y		0.9 (for three minimum subcool)	
		0.1 (for other subcool)	

5.4.4 Application of Adaptive MPC

We have used dynamic models with the same structures and orders as linear MPC in adaptive MPC. The input-output data recorded for the immediate past 50 days were used to estimate the new coefficients and the model was used in MPC to calculate the optimum input parameters for the next control interval. Since the latest available data is used to identify model parameters, the current reservoir conditions will be reflected in model predictions when used in MPC. The time required to calculate new coefficients was much shorter than the sampling interval, which indicates that practical implementation of the proposed approach is feasible at the field scale. Since the model structure and order are not altered with time, it is not necessary that model with latest coefficients computed online will pass the validation tests. However, to ensure that the model is acceptable, predicted values obtained from the model were compared with training data by calculating the model fit (specified in Eq. (5.11)). It was observed that for more than 90% of the control intervals, the model fit was above 60% for all subcools. The controller design is the same as for linear MPC. Also, adaptive MPC was applied from 800 days to 1355 days to create a common basis of comparison with linear MPC.

5.4.5 Application of Gain-Scheduled MPC

Practical aspects of gain-scheduled MPC are pretty much similar to those of adaptive MPC except the segmentation of operating region into multiple sub-regions and designing controller for each of them. As shown in *Figure 5.11*, operating range of subcool is divided into three control regions in this case study. Region 1 is defined for the higher subcool values of more or equal to 35 °C and corresponding controller is denoted as C1 in *Figure 5.11*. Hence, if any of the five subcools goes above the specified range then controller C1 is switched and used in MPC to calculate optimum IVs for next control interval. Similarly, region 2 comprises subcool values between 18 °C and 35 °C with corresponding controller C2. Since set-point for subcool is 20 °C, smaller lower window is provided for C2 as subcool below the target should be avoided as soon as possible. The last control region 3 handles the subcool below 18 °C, meaning that when any of the subcool goes below stated limit, controller C3 will be utilized for necessary responses.

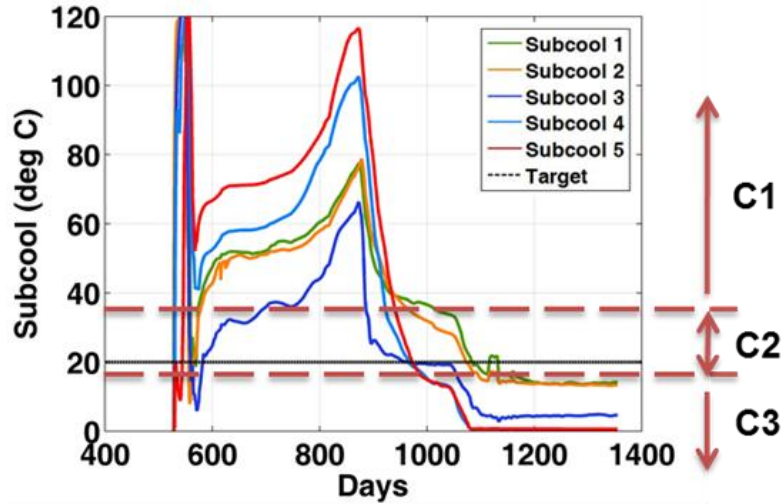


Figure 5.11 – Segmentation of operating range of subcool in real-time production optimization using gain-scheduled MPC.

The design of all three controllers is similar to the one shown in *Table 5.3* except for some changes in constraints for the liquid production rate. As discussed before, higher subcool values indicate a higher liquid level above the producer and to avoid that, the controller should be allowed to produce more fluid. Hence, u_j^{max} for controller C1 was increased to 600 m³/day. Also, a higher value of u_j^{opt} (500 m³/day) was fixed for controller C1 while for controller C2 and C3, it was specified as 220 and 150 m³/day, respectively. Also, higher rates of change in liquid production were permitted when subcools are very far away from the target value by removing Δu_j^{min} and Δu_j^{max} constraints for the liquid production rate in controller C1 and C3. As mentioned before, the subcool is used as the scheduling variable. Since there are multiple subcools and higher subcool hampers steam chamber growth, C1 is given the highest priority, meaning that the first condition checked while selecting the controller is whether any of the subcools are within the range of its operating region. The second check is performed on controller C3 since subcool values lower than the target increase the chances of steam breakthrough; finally, controller C2 is selected only if all the subcools are within its operating range. Gain-scheduled MPC is tested by implementing it at 600 days since subcools are generally away from the target at the start of SAGD production phase and this makes for a challenging control problem.

5.5 Results and Discussion

Consequences of implementing proposed approaches are discussed and results are compared with base case as well as linear MPC in this section. The effectiveness of proposed approaches in controlling subcool as well as behaviour of MVs for different control algorithms is presented. Effects of adaptive and gain-scheduled MPC on different production parameters is also assessed. Finally, statistical measures are used to verify the performance of proposed approaches.

5.5.1 Performance in Real-Time Subcool Control

Control strategy is successful if it can maintain all the OVs within acceptable operating range near specified target. Also, faster convergence rate of OVs towards the set-point demonstrates capability of the control method to quickly regain the optimum operating states of the system. Furthermore, an ideal control method contemplates and treats various uncertainties (for e.g. measurement noise) in the system appropriately to provide the robust control. In addition, control method should be such that stability of the process is not disturbed to achieve optimum set-points, meaning that IVs estimated for the future control interval should be bounded. Keeping in mind these key aspects, performance of proposed approaches in subcool control is analyzed.

The subcool of all segments of the well pair are plotted against time in *Figure 5.12* for all the control methods considered. For the base case, it can be seen clearly that steam breakthrough occurs along the length of the well pair since subcools are almost zero after 800 days. Linear MPC demonstrates better performance than the base case as subcool values for all sections are around the given target; however, frequent changes in subcool profiles can be noticed around 1100 days. Also, near the end of the SAGD process, all subcools are below the target in linear MPC with two of them being almost equal to zero, indicating failure of the controller to maintain subcool. In the case of gain-scheduled MPC, a rapid decrease in subcool values can be observed at the start of the MPC period as controller C1 was active for aggressive control action against higher subcool values. Though subcool in the first four sections of the well pair are very low initially, they increased eventually as all the subcool values fell in the operating range of controller C2 and remained within 19 to 33 °C as desired. Adaptive MPC provided robust subcool control as it depicts smooth subcool profiles after its

implementation. In addition, offset in subcool values from target is minimum (7 °C) in adaptive MPC, which shows its superiority in real-time production optimization.

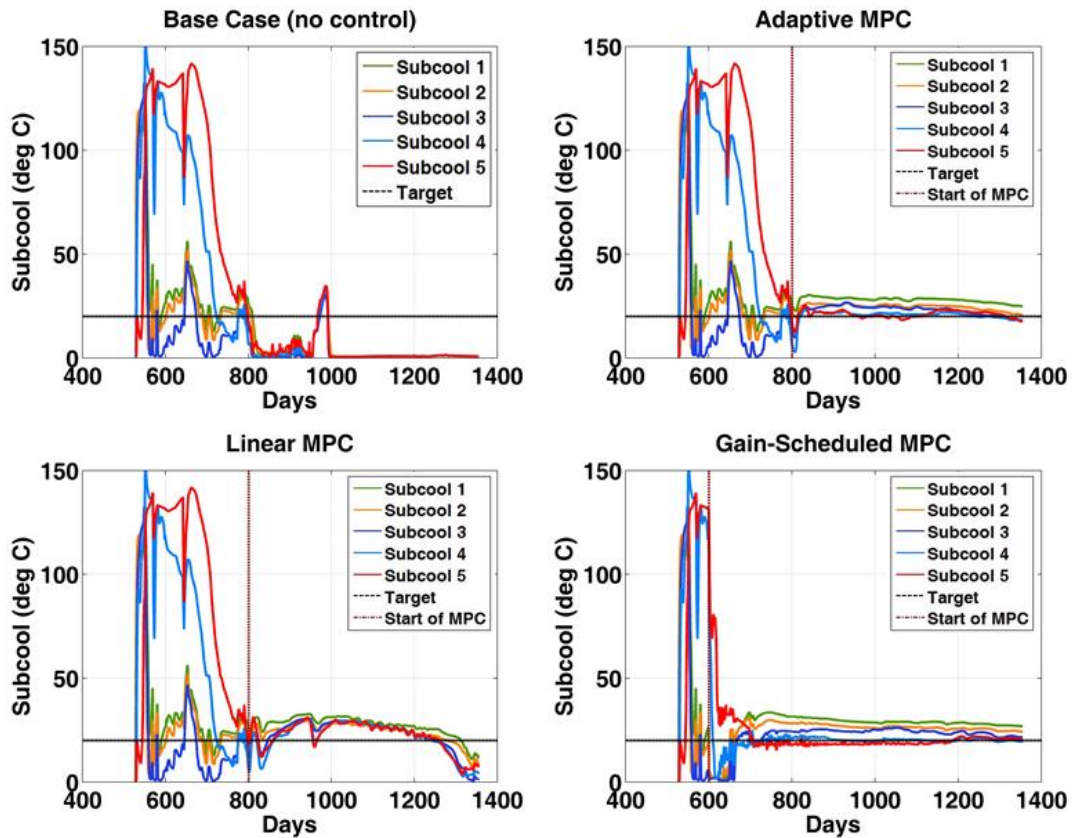


Figure 5.12 – Subcool of all segments of the well pair obtained using different control methods in real-time production optimization.

As explained before, not all the subcools can be maintained near the set-point due to a lack of sufficient degrees of freedom. Therefore, the minimum subcool among all sections of the well pair is the most important parameter to evaluate the proposed methods, and it is plotted in Figure 11. The ability of gain-scheduled MPC to maintain minimum subcool near the target value is apparent except in the initial period when subcools in some sections were very high. The minimum subcool in the case of adaptive MPC is close to the target with a maximum error of 2 °C. Also, a swift increase in minimum subcool after the start of the control period is evident in the same figure, which results in effective control with adaptive MPC. In contrast, the minimum subcool in linear MPC does not remain near the set-point over the control period potentially due to the inefficient dynamic model. An additional observation is that the minimum

subcool is in sections 4 and 5 for most control intervals in all the control methods. It indicates higher probability of steam breakthrough in the toe sections of the reservoir; this may be due to higher permeability between well pairs or a relatively high amount of steam injection due to wellbore geometry in those sections.

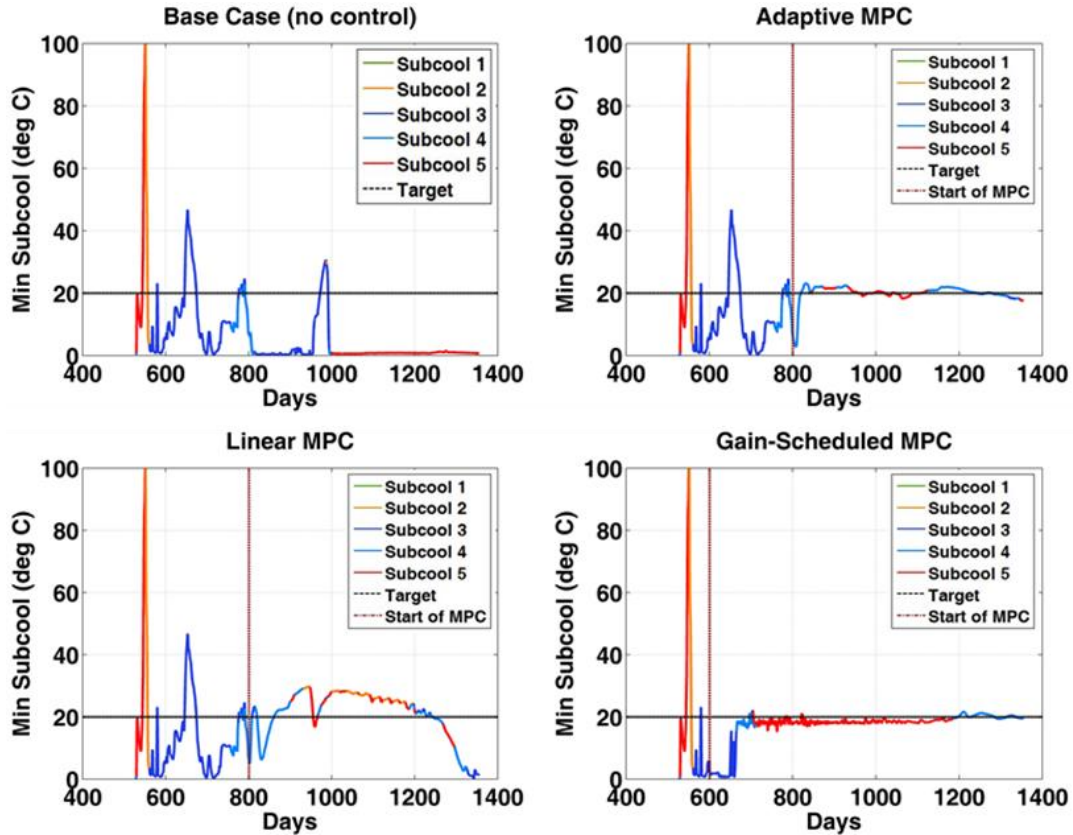


Figure 5.13 – Minimum subcool of the well pair obtained using different control methods in real-time production optimization.

5.5.2 Impact on Input (Manipulated) Variables

To ensure that IVs calculated using proposed approaches are legitimate and bounded, steam injection rate for short tubing, long tubing and liquid production rate are plotted against time and compared with linear MPC as well as base case in *Figure 5.14*, *Figure 5.15*, and *Figure 5.16* respectively. All the IVs are within the defined constraints for the MPC controller and follow the optimum target in all cases; however, they display different behaviour for the different control strategies. From *Figure 5.14*, it is seen that the lowest fluctuations in the steam injection rate for short tubing are for adaptive

MPC, while gain-scheduled MPC shows some more variation in the beginning, though it is still within the acceptable range. Linear MPC displays frequent changes that results into continual opening and closing of valves, ultimately causing damage to the actuators. Also, the rate of convergence towards the optimum target is slower in linear MPC. The steam injection rate of long tubing, shown in *Figure 5.15*, shows higher variation for all controllers; this may be due to the relatively higher order of polynomials used in the dynamic model (specified in *Table 5.2*) for this specific IV. The liquid production rate, shown in *Figure 5.16*, is almost constant for adaptive MPC while linear MPC exhibits minor variations around the specified target. In contrast, gain-scheduled MPC presents the highest fluctuation until the subcools are stabilized due to frequent switching of controllers. Also, the operating range of the multiple controllers is decided such that changes in liquid production rate do not exceed a certain fraction of the overall operating range to avoid damage to the actuators. In our case study, changes in liquid production rate are around 12.5% of the total operating range (0 to 600 m³/day), which is tolerable. Further, frequent variations in gain-scheduled MPC are not visible after approximately 1100 days, which endorses the ability of the proposed approach to control subcool in adverse control situations.

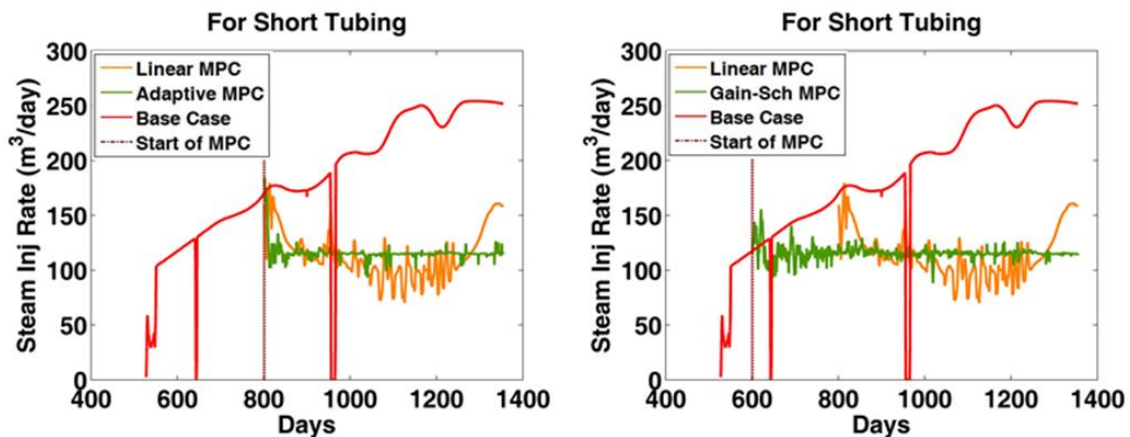


Figure 5.14 – Performance of steam injection rate (short tubing) in adaptive MPC (left) and gain-scheduled MPC (right) when compared with base case and linear MPC.

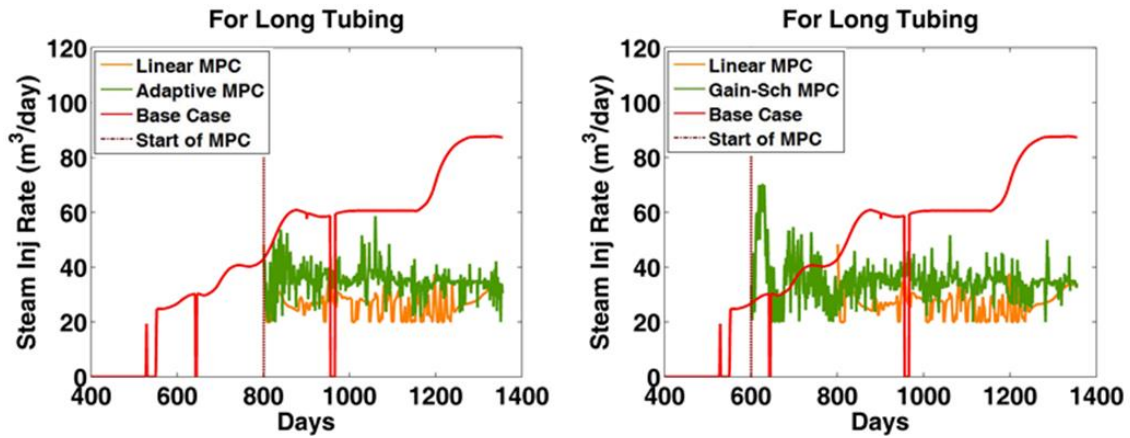


Figure 5.15 – Performance of steam injection rate (long tubing) in adaptive MPC (left) and gain-scheduled MPC (right) when compared with base case and linear MPC.

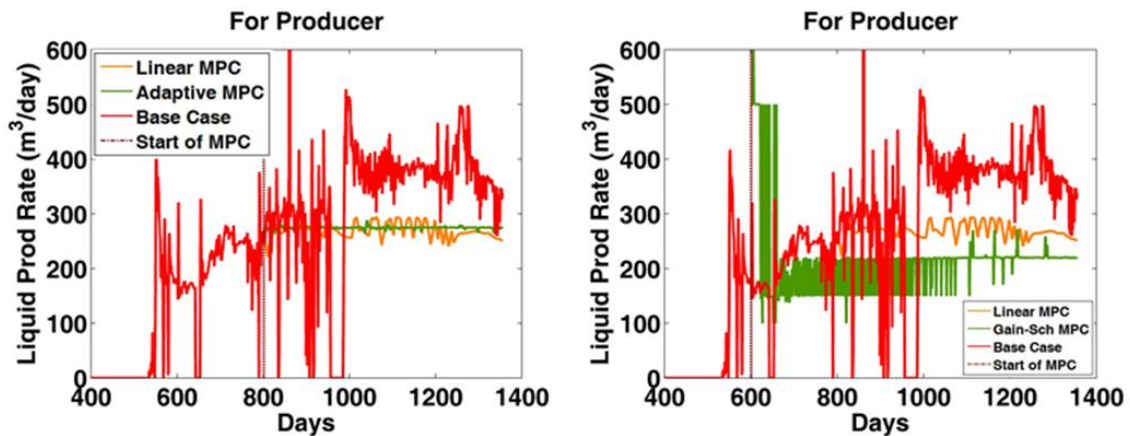


Figure 5.16 – Performance of liquid production rate in adaptive MPC (left) and gain-scheduled MPC (right) when compared with base case and linear MPC.

5.5.3 Effect on Production Parameters

The impact of these approaches on various production parameters has also been assessed qualitatively. *Figure 5.17*, *Figure 5.18*, and *Figure 5.19* present the daily oil rate, cumulative oil production and cSOR, respectively, for the different control algorithms. A common observation is the higher production parameters for the base case, which is due to the higher amount of steam injected in the reservoir irrespective of the subcool values, ultimately resulting into higher cSOR; this can be observed in *Figure 5.19*. Since the base case represents the current practice in the field, it suggests

that the efficiency of the SAGD process can be improved by controlling the subcool in real-time. Due to infrequent changes in IVs, adaptive MPC shows the lowest fluctuation in oil production rate (see *Figure 5.17*). Also, a slightly higher cumulative oil production is evident for adaptive MPC in *Figure 5.18* as compared to linear MPC. Here, it seems that the maximum oil production is restricted by the predefined target subcool since not only is it the case that more steam than required cannot be injected but also more liquid cannot be produced. Hence, the target subcool should be chosen carefully in order to obtain as high an oil production as possible.

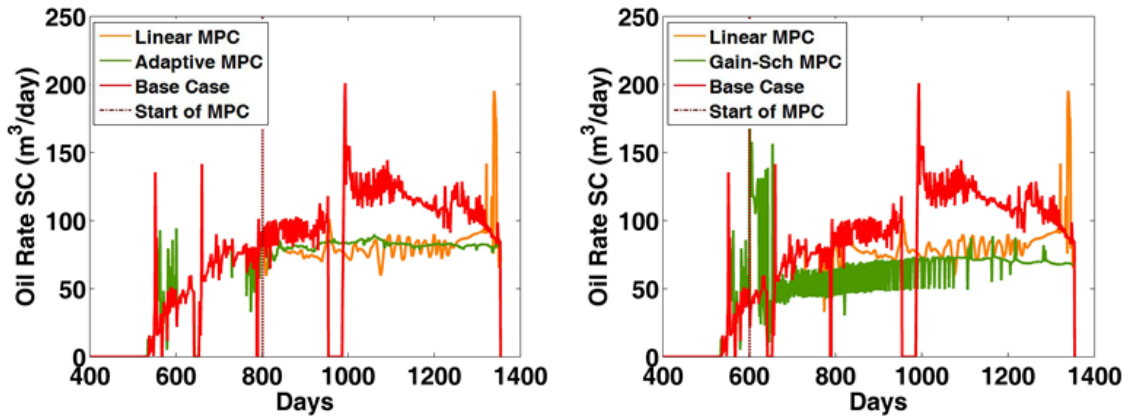


Figure 5.17 – Effect of adaptive MPC (left) and gain-scheduled MPC (right) on oil production rate. SC = surface conditions.

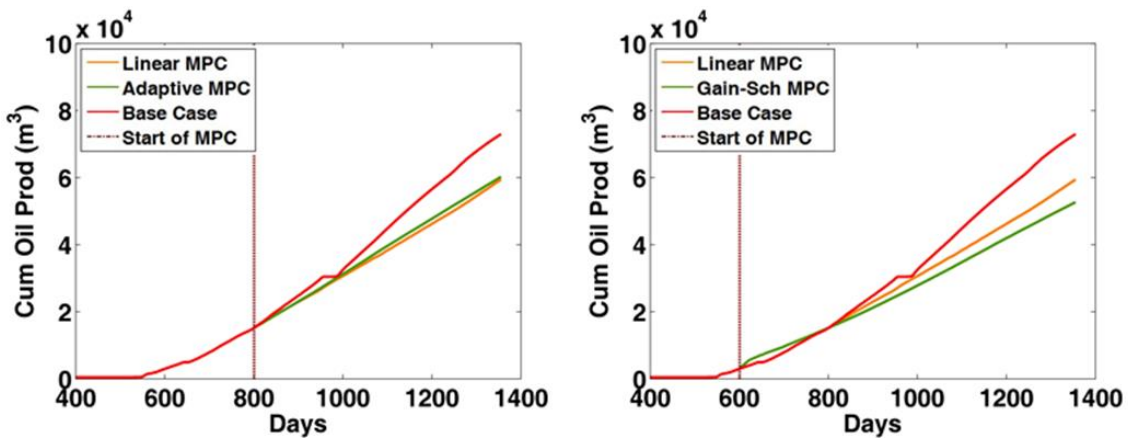


Figure 5.18 – Effect of adaptive MPC (left) and gain-scheduled MPC (right) on cumulative oil production.

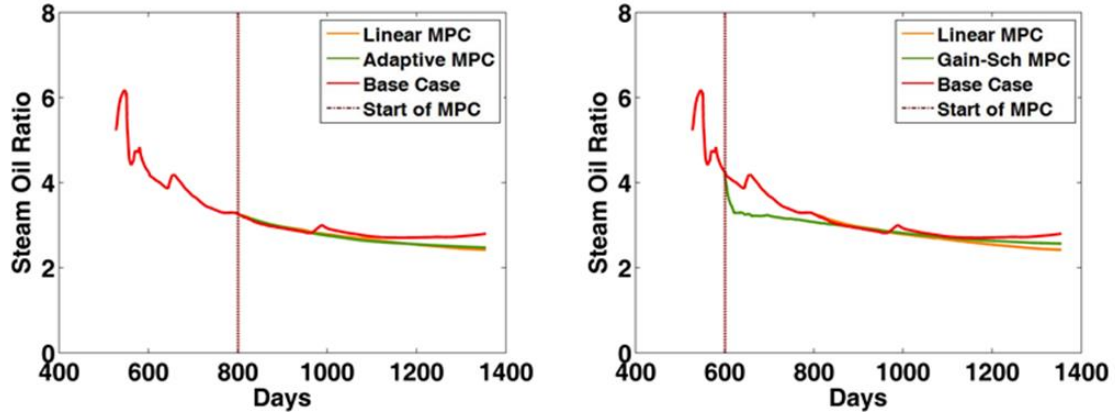


Figure 5.19 – Effect of adaptive MPC (left) and gain-scheduled MPC (right) on cumulative steam oil ratio.

From Figure 5.19, it is seen that cSOR (which is a measure of the efficiency of SAGD) is lower for variants of MPC compared to base case. At the end of the control period, the cSOR is almost equal for adaptive and linear MPC. Since subcools away from the target were handled effectively in gain-scheduled MPC, a sharp decrease in cSOR can be observed at start of MPC; however, it increased slightly at later stages due to fluctuations in IVs. Overall, the proposed approaches have been successful in achieving higher oil production while maintaining lower cSOR.

5.5.4 Quantitative Analysis Using Statistical Performance Measures

Quantitative analysis of the performance of adaptive and gain-scheduled MPC is performed by evaluating the net present value (NPV) and root mean square error (RMSE) (Table 5.4). NPV is obtained by discounting the cash flow on a daily basis as shown below:

$$NPV = \sum_{i=t_{start}}^{t_{end}} \frac{q_o^i p_o - q_w^i p_w}{(1 + DF)^{(i-t_{ref})/365}} \quad (5.18)$$

where q_o and q_w represent oil produced and steam injected in STB/day, respectively, and p_o and p_w are the oil price and steam generation cost in \$/STB (specified as 50 \$/STB and 12 \$/STB), respectively. DF is the discount factor (10% a year) and t_{ref} is

the reference time to which NPV is discounted (the start of the production phase, i.e. day 527) while the summation is from the start to end of the MPC control period.

RMSE which quantifies data mismatch has also been calculated to analyze the ability of proposed approaches in controlling subcool near the set-point. For a particular output j , it can be defined as,

$$RMSE_j = \sqrt{\frac{1}{t_{end} - t_{start}} \sum_{i=t_{start}}^{t_{end}} (m_j^i - r_j)^2} \quad (5.19)$$

where m_j^i refers to the measured value of output j at control period i while r_j is the set-point for j^{th} output. The values for RMSE for all subcools reported in *Table 5.4* were obtained by averaging RMSE of each subcool.

Table 5.4 – *Quantitative analysis of various control algorithms used for real-time production optimization*

Case	Performance Statistics		
	Net Present Value	RMSE	RMSE
	(in million \$)	(Min Subcool)	(All Subcool)
Base Case (no control)	5.623	18.035	32.367
Linear MPC	7.239	11.652	28.963
Adaptive MPC	6.956	9.897	28.523
Gain-Scheduled MPC	6.201	9.024	22.705

From *Table 5.4*, it can be stated that SAGD performance in the base case is not optimal, because of which its NPV is the lowest and its RMSE the highest for minimum and all subcools. Linear MPC achieves the highest NPV; however, this is due to ineffective controller performance that allowed more steam injection in short tubing at later stages (see *Figure 5.14*) irrespective of the offset exhibited by subcools (see *Figure 5.12*). Higher values of RMSE in linear MPC is most probably due to the poor predictions of fixed linear model. Adaptive MPC shows satisfactory performance with its NPV being much higher than the base case and lower RMSE for both minimum and

all subcools. The lowest RMSE was obtained for gain-scheduled MPC, but with slightly lower NPV than adaptive MPC due to frequent switching of controllers. Thus, quantitative analysis using these statistical measures also endorses the superiority of the proposed control methods.

5.6 Summary

In this work, two advanced control methods are presented for better subcool control in SAGD. The first, adaptive MPC, involves continuous re-estimation of model coefficients while the other, gain-scheduled MPC, uses multiple controllers in different operating regions. Control workflows are developed to validate these approaches using a history-matched numerical reservoir model of a SAGD field. The results have been assessed qualitatively and quantitatively, leading to the following conclusions:

1. Identification of new coefficients in adaptive MPC leads to better subcool predictions, ultimately resulting into effective subcool control with lower fluctuations in manipulated variables.
2. Gain-scheduled MPC can maintain subcools near target values, resulting in lower mismatch for a variety of control situations.
3. NPV is increased by more than 23% and 10% with adaptive and gain-scheduled MPC, respectively, when compared to the base case.
4. By implementing the proposed approaches, lower cSOR and higher oil production can be achieved simultaneously if the target subcool is defined properly.

Thus, both the proposed control approaches can be utilized successfully for real-time production optimization of SAGD reservoirs, consequently reducing energy consumption and minimizing the CO₂ footprint.

Chapter 6

Nonlinear Model Predictive Control of SAGD Well Operations for Real-Time Production Optimization ⁴

⁴ A version of this chapter was presented at the *66th Canadian Chemical Engineering Conference* and manuscript is in progress for submission to *Journal of Process Control*.

6.1 Introduction

In this chapter, a state-of-the-art control framework using nonlinear model predictive control (NMPC) is presented for efficient subcool control and optimal SAGD well operations in real-time. In the first NMPC workflow, linear approximation of a nonlinear dynamic model in mean-square-error sense is implemented, which provides reasonable prediction of output variables (OVs) in the neighbourhood of the input signal used for linearization. Due to linear representation of nonlinear plant dynamics, standard QP algorithm can now be used for minimization of cost function in MPC. In the second one, nonlinear plant models are directly used for estimation of different OVs, enforcing the use of nonlinear optimization algorithm to calculate the optimum input parameters (IVs) for the next control interval. Interior point algorithm is used in the proposed workflow. Primary objective of this study is to improve the real-time subcool control by manipulating IVs in SAGD well operations, ultimately leading to better financial consequences and minimal environmental impact while considering available surface facilities and well configurations.

Various nonlinear dynamic models in system identification are explained in section 6.2. In section 6.3, NMPC formulation is discussed including linearization, interior-point algorithm and advanced control workflows designed for the SAGD application considered in this study. Section 6.4 provides the details regarding the application of both NMPC workflows comprising identification of nonlinear models, controller design, linearization of nonlinear system identification models as well as nonlinear optimization. Effect of NMPC on subcool control, MVs, OVs is reported and analyzed in section 6.5 along with the economic evaluation of the proposed approaches. Finally, summary of this study is given in section 6.6.

6.2 Nonlinear Dynamic Models

In reality, input-output relationships in almost all of the industrial systems are nonlinear. Linear models can provide estimations with desired accuracy in case of the weakly nonlinear systems; however, when nonlinear nature of the systems is explicitly known, nonlinear dynamic models are preferred to represent the systems. Dynamics of fluid flow in porous media is highly nonlinear (Wang and Li 2011), especially in case

of complex thermal oil recovery processes such as SAGD. Further, the operating range is different in distinct phases (i.e., circulation, production ramp-up, production decline, and wind-down) of the SAGD lifecycle and to capture the dynamic behavior of the output variable in different phases, nonlinear model should be utilized. Also, lower-than-expected model fit in case of linear models for different subcools (see *Table 5.2*) suggests the need of nonlinear black box models in MPC of SAGD well operations to improve the steam conformance and performance in real-time production optimization.

Like LTI model in Eq. (5.1), general form of a discrete nonlinear dynamic model for a given system can be shown as follows (Ljung 2016):

$$y(t) = f(u(t-1), y(t-1), u(t-2), y(t-2), \dots) \quad (6.1)$$

where $f(\cdot)$ is the unknown nonlinear function demonstrating the relationship between output ($y(t)$) and input ($u(t)$) respectively, at current time interval t . Considering the characteristics of nonlinearity, different kinds of nonlinear dynamic models are used to capture behaviour of a nonlinear process.

The simplest way to construct a nonlinear model structure is to consider the nonlinear input-output relationship in different linear model structures (see *Table 5.1*). For example, using nonlinear function $f(\cdot)$ shown in Eq. (6.1) and linear ARX model, nonlinear ARX (NARX) model of order m can be defined as,

$$y(t) = f(y(t-1), \dots, y(t-m), u(t-d), \dots, u(t-d-m)) + e(t) \quad (6.2)$$

where d is the delay of the system. From Eq. (6.2), it can be said that coefficients of the polynomials of time-shift operator in ARX model are replaced by the nonlinear function in NARX model. Similar to NARX model, more details about the family of nonlinear ARMAX (NARMAX) models is explained by Huang et al. (2013). Such models are commonly referred as "external dynamics" model as they directly uses input-output data to estimate nonlinear function of the model regardless of unknown system states, giving them an upper hand as compared to nonlinear state space models. Though NARX model is capable enough to model many of the nonlinear systems, it cannot represent certain type of nonlinearities for example, hysteresis and backlash, restricting its application in modern nonlinear systems.

Volterra-Series model, like the linear impulse response (IR) model, is a nonlinear model without output feedback and can be used to represent a nonlinear “fading memory” system (system with negligible effect of distant past on present) using polynomials. It can be represented as (Huang 2013),

$$\begin{aligned}
 y(t) = & y_0 + \sum_{k_1=1}^{\infty} a_{k_1} u(t - k_1) + \sum_{k_1=1}^{\infty} \sum_{k_2=1}^{\infty} b_{k_1, k_2} u(t - k_1) u(t - k_2) \\
 & + \sum_{k_1=1}^{\infty} \sum_{k_2=1}^{\infty} \sum_{k_3=1}^{\infty} c_{k_1, k_2, k_3} u(t - k_1) u(t - k_2) u(t - k_3) + \dots
 \end{aligned} \tag{6.3}$$

Here, the first term in Eq. (6.3) is an offset. The Volterra-Series model needs to be truncated in practical applications, which is known as “finite Volterra-Series models”. Since no feedback is involved in this model structure, it is guaranteed to be stable (Nelles 2001). Another variant of this model structure that considers nonlinearity only for inputs while incorporating linear feedback is known as “parametric Volterra-Series models”. Mathematically, it can be expressed as (Nelles 2001),

$$y(t) = f(u(t - d), \dots, u(t - d - m)) - a_1 y(t - 1) - \dots - a_m y(t - m) \tag{6.4}$$

The parametric Volterra-Series model with larger order m can be considered as an extension of the Eq. (6.3). Linear feedback in the variant would help in reducing the dynamic order of the model (Nelles 2001). However, the system in which nonlinearity due to the output variable is dominant cannot be replicated using parametric Volterra-Series model shown in Eq. (6.4).

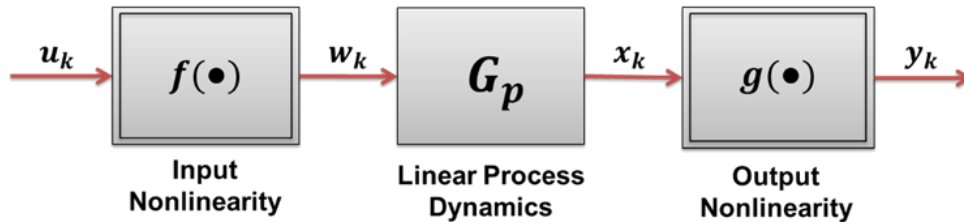


Figure 6.1 – Hammerstein-Wiener model structure in nonlinear model identification.

Hammerstein-Wiener model structure is a special subclass of the Volterra approach and belongs to the family of widely used block-oriented nonlinear models. It assumes both input $f(\cdot)$ and output $g(\cdot)$ nonlinearities as static and independent from the linear

process dynamics as shown in *Figure 6.1*. Mathematically, the structure can be expressed as,

$$\begin{aligned}x(t) &= G_p(z^{-1}, \theta)f(u(t)) + G_l(z^{-1}, \theta)e(t) \\y(t) &= g(x(t))\end{aligned}\tag{6.5}$$

where G_p and G_l are the linear process and noise model respectively (see Eq. (5.1)). Due to the independent nature of nonlinearities in this model, it provides flexibility to model actuator nonlinearities and sensor nonlinearities separately, resulting into better representation of a nonlinear system. In addition, stability of the system depends only on the process dynamics represented using a linear model in the structure, which makes it suitable for controlling the process (Nelles 2001). Furthermore, if needed, Hammerstein model (input nonlinearity with linear process dynamics) and Wiener model (output nonlinearity with linear process dynamics) can also be used separately according to the nature of the process.

To represent the first principles model of a nonlinear system, state space equation can be easily written in a discretized form if the states of the systems are measurable. Like Eq. (5.4), $y(t)$ can be determined using nonlinear state space model as follows:

$$\begin{aligned}x(t+1) &= f(x(t), u(t)) \\y(t) &= g(x(t))\end{aligned}\tag{6.6}$$

where $x(t)$ is a vector of system states. Since exact and complete knowledge of states of the system is typically uncommon, identification of nonlinear state space model using only experimental data is very difficult (Camacho and Bordons 2007), which ultimately confines use of such "internal dynamics" model.

As mentioned earlier, nonlinear functions are not known priori in the black box nonlinear models. A common approach to solve this issue is to parameterize nonlinear function through series expansion of basis functions which can be shown as follows:

$$f(\phi(t)) = \sum_{l=1}^n \alpha_l \kappa(\beta_l(\phi(t) - \gamma_l))\tag{6.7}$$

where $\phi(t)$ is the set of regressors, κ denotes the basis function while α_l are the coordinates that assigns weight to individual basis functions in series expansion. In Eq. (6.7), β_l and γ_l are the scaling and relocation factor of the standardized basis functions. Examples of the basis functions are sigmoid function, piecewise (PW) linear function, wavelet function, Fourier series, one-dimensional polynomial function and neural networks. In general, higher the number of basis function is, better the representation of nonlinearity will be. However, it will increase the number of model parameters to be estimated. Selection of a proper basis function that incorporates nonlinearity of the process is very critical in identification of a nonlinear model as Huang et al. (2013) explained the analogy between construction of a building using bricks of various shapes as well as sizes and identification of nonlinear model using scaling and shifting of basis functions.

Due to nonlinearity induced by basis functions, estimation of model parameters in nonlinear dynamic models becomes complex. PEM (explained in section 5.2) used in case of LTI models can be utilized only for NARX model in nonlinear system identification. For parameter estimation in Hammerstein model structures, linear optimization techniques can be used with generalized model structure. In contrast, straightforward linear parameterization is not possible in Wiener model structures as output nonlinearity should be invertible. Therefore, nonlinear optimization algorithms such as Gauss-Newton method, gradient method, Levenberg-Marquardt method are required for estimation of model parameters in Hammerstein-Wiener model.

To validate the empirical nonlinear models, all four criteria (i.e., autocorrelation and cross-correlation tests, cross-validation and AIC) explained in section 5.2 for linear models can be used because all nonlinear models contain the process model and noise model. Further, the workflow displayed in *Figure 5.2* can also be implemented to determine the orders of process and noise model in nonlinear system identification.

6.3 Nonlinear Model Predictive Control

NMPC is the most advanced control framework that can be used for real-time subcool control and production optimization. It is an extension of linear MPC as conceptually, it is possible to integrate the nonlinear models in MPC framework. NMPC incorporates

nonlinear dynamics of the process through nonlinear models in time-domain to predict the OV and computes the optimum input sequence for the next control interval. Due to the efficient representation of process dynamics, improved and stable control performance can be achieved in NMPC (Camacho and Bordons 2007). It can handle various constraints effectively – especially the nonlinear ones – and hence, ensures the robust control performance. Therefore, short-term optimization of SAGD well operations using NMPC can potentially improve the steam conformance and process economics while reducing the carbon footprints.

Like any other MPC strategy, NMPC includes two primary elements: 1) prediction of the process outputs and 2) constrained minimization of objective/cost function to calculate the future input control sequence. In the previous section, nonlinear models which can be used to predict OVs are discussed in detail. A cost function similar to linear MPC (see Eq. (5.13)) can be implemented in NMPC to ensure that process outputs follow the reference trajectory. Formulation of the cost function minimization problem in NMPC can be written as (Camacho and Bordons 2007),

$$\begin{aligned} \min_{u(t|t), \dots, u(t+M-1|t)} J = & \sum_{i=1}^P \|\hat{y}(t+i|t) - y_{ref}(t+i|t)\|_{W_y}^2 \\ & + \sum_{i=1}^{P-1} \|u(t+i|t) - u_{ref}(t+i|t)\|_{W_u}^2 + \sum_{i=1}^{P-1} \|\Delta u(t+i|t)\|_{W_{\Delta u}}^2 \end{aligned} \quad (6.8)$$

subject to

$$\begin{aligned} y_{min} &\leq \hat{y}(t+i|t) \leq y_{max} && \forall i \in [1, P] \\ u_{min} &\leq u(t+i|t) \leq u_{max} && \forall i \in [1, P-1] \\ \Delta u_{min} &\leq \Delta u(t+i|t) \leq \Delta u_{max} && \forall i \in [1, P-1] \\ \Delta u(t+i|t) &= 0 && i \geq M \end{aligned} \quad (6.9)$$

where $u(t|t), \dots, u(t+M-1|t)$ is the future control sequence determined at current time step t . Variables y_{ref} and u_{ref} are reference trajectories for OV and IV respectively while \hat{y} denotes the output predicted by the dynamic model. Adjustment in the input variable Δu can be defined as $\Delta u(t+i|t) = u(t+i|t) - u(t+i-1|t)$ in Eq. (6.8). Like linear MPC, P and M represents prediction and control horizon

respectively while W_y , W_u , and $W_{\Delta u}$ are weighting matrices corresponding to OVs, IVs, and rate of adjustment, respectively. The cost function shown here is quadratic, however, it can be linear as well in some cases.

Minimization of objective function is subjected to various constraints, which are presented in Eq. (6.9). Lower bounds for outputs, inputs, and rate of change of input are denoted with y_{min} , u_{min} , and Δu_{min} while upper bounds for the same are denoted with y_{max} , u_{max} , and Δu_{max} respectively. The last constraint enforces no change in input variables beyond the control horizon. Input constraints are generally “hard constraints” which must be satisfied while output constraints can be considered as “soft constraints” where deviation from the constraints are penalized for feasible optimization problem. Soft constraints can be considered in the problem formulation (Eq. (6.8)) by adding the penalty term $\|s\|_{W_s}^2$ where W_s is the weighting matrix corresponding to the slack variable s . In this case, the new constraint for the output variable in Eq. (6.9) will be,

$$y_{min} - s \leq \hat{y}(t + i|t) \leq y_{max} + s \quad \forall i \in [1, P] \quad (6.10)$$

Note that in case of fundamental models based on first-principles, there can be some additional constraints corresponding to the nonlinear equations. Also, NMPC formulation discussed so far is for the SISO system and to consider the multiple OVs and IVs, variables in the equations should be replaced with the vectors.

If nonlinear state space models (see Eq. (6.6)) are used in NMPC, a state observer should be introduced when system states are not measurable (which is the case in most nonlinear systems). Algorithms based on Kalman Filter theory like extended Kalman filter (EKF) and unscented Kalman filter (UKF) can be used as state observer to update the controller states. Also, using moving horizon approach, optimization-based online estimations of the current states of the NMPC controller can be obtained.

Like linear MPC, solution of the optimization problem in Eq. (6.8) is not possible by the well-studied QP algorithm since nonlinear dynamics considered in NMPC will make the optimization problem nonlinear and nonconvex that may exhibit multiple minima. It introduces additional complexities in terms of control quality, stability, and computational cost. Especially, the computational cost increases by a fair margin,

prohibiting the online solution of the optimization problem at each control interval. Several alternative formulations with better computational efficiency are suggested by various authors to handle nonconvex optimization problems in NMPC (Henson 1998, Camacho and Bordons 2007). In this work, two different approaches, i.e. linearization and nonlinear optimization are implemented for real-time subcool/production control using NMPC. Performance of the proposed workflows is analyzed and compared to current field practices as well as linear MPC.

6.3.1 Linearization

Subsurface flow systems are highly nonlinear and hence, NMPC is desired for real-time production optimization in SAGD reservoirs. However, as mentioned earlier, optimization of cost function in NMPC is a nonlinear nonconvex optimization problem, solution of which is more difficult and complex to obtain. A simple and efficient way to solve this issue is to use linear approximations of nonlinear dynamic model for prediction of process outputs in NMPC. The approach essentially reduces the NMPC problem to linear MPC in which QP can be used (if the cost function is quadratic) to obtain global minimum and optimum future input sequence at each control interval.

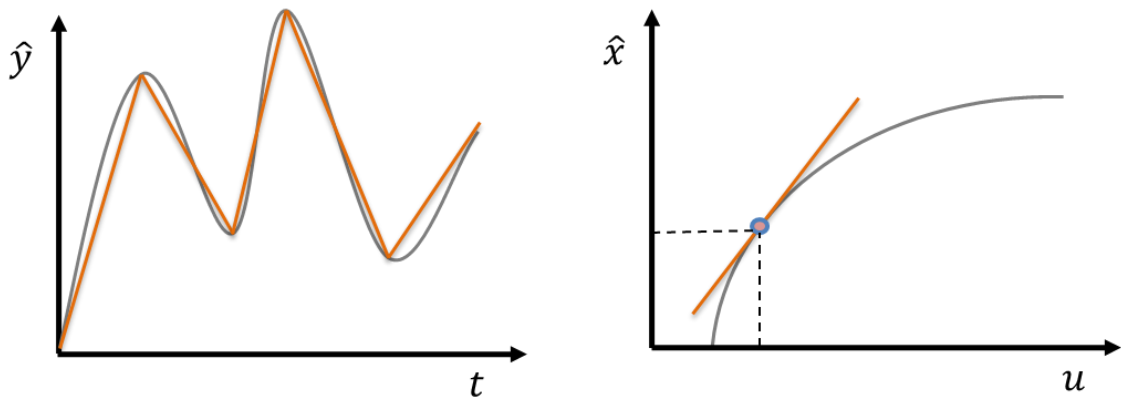


Figure 6.2 – Linearization of a nonlinear model for a given input signal (left) and in the neighbourhood of an operating point (right).

In literature, various types of linearization schemes such as feedback linearization (Kurtz and Henson 1997, Nevistic and Morari 1995), successive linearization (Henson 1998), and local models network (Camacho and Bordons 2007) have been reported as an alternative formulation to NMPC. For linearization of nonlinear black box models,

two methods are discussed by Ljung (2016) i.e., tangent linearization and linearization for a given input. As shown in *Figure 6.2*, the nonlinear dynamics is approximated using a first-order Taylor series expansion about a nominal operating point (also known as equilibrium point or reference point) in tangent linearization. Operating point consists of a constant input and corresponding model states values. To illustrate the concept, consider a nonlinear system $y(t) = f(x(t), u(t))$. Corresponding Taylor series expansion about an operating point $(x_0(t), u_0(t))$ can be written as,

$$f(x(t), u(t)) = f(x_0(t), u_0(t)) + \left(\frac{\partial f}{\partial x}\right)_{(x_0(t), u_0(t))} \Delta x(t) + \left(\frac{\partial f}{\partial u}\right)_{(x_0(t), u_0(t))} \Delta u(t) + \dots \quad (6.11)$$

where $\Delta x(t) = x(t) - x_0(t)$ and $\Delta u(t) = u(t) - u_0(t)$ are the deviation variables. Truncating higher order terms and considering derivatives with respect to x and u as coefficients c and d respectively in Eq. (6.11), approximation of the output for given nonlinear model can be calculated as,

$$\hat{y}(t) = y_0(t) + c\Delta x + d\Delta u \quad (6.12)$$

where $\hat{y}(t)$ is the linear approximation of the output while $y_0(t)$ is the output obtained using the nonlinear model at the operating point. As higher order terms are neglected in Eq. (6.12), such linear models are accurate only in the local neighbourhood of the operating point. Typically, current operating point is used in tangent linearization. Note that tangent linearization is more suitable for nonlinear models in state space form as updated states of the model can be approximated through similar series expansion.

Linearization using an input signal involves the estimation of the best linear model (refer *Table 5.1*) that is structurally similar to the nonlinear black box model. The identified linear model provides best fit with the simulated response of a nonlinear model for the given input signal in a mean-square-error sense (see *Figure 6.2*). Any random input signal can be utilized in this linearization method. Like tangent linearization, linear approximation in this method is accurate only for the input signals similar to the one used for linearization. In addition, linearization for a given input signal is convenient for input-output nonlinear models rather than state space

formulations. According to the nonlinear model used in NMPC, either of the linearization technique can be employed.

6.3.2 Interior Point Algorithm

As Henson (1998) noted, control performance can be improved in NMPC if nonlinear model is directly used in cost function minimization, although at higher computational cost. To solve the optimization problem in NMPC, various nonlinear programming techniques (refer Nelles 2001 for more details) can be utilized keeping in mind their pros and cons and suitability to the optimization problem.

In this work, interior point method is utilized for nonlinear optimization of the cost function in NMPC. Its nature of outlining the optimal path while restricting the search in interior space gives an upper hand in terms of computational efficiency and complexity of the problem, especially in large-scale problems. Several variants of this method have been developed over the time for different types of optimization problems, which are reviewed in Potra and Wright (2000). Basic idea behind the interior point algorithm implemented in this work is to integrate inequality constraints of the optimization problem into the objective function by adding the barrier term which also restricts the search within the feasible region. A set of equations is then created using Karush-Kuhn-Tucker (KKT) first order optimality conditions, which can be solved by employing Newton's method or conjugate gradient method based on the availability of the Hessian of the objective function. As the dominance of the barrier decreases, the optimum follows a smooth path to the optimum of the original problem. For the solution of an optimization problem given as

$$\begin{aligned} & \min_x f(x) \\ & s.t. \quad h_i(x) \geq 0, \quad i = 1, \dots, m \end{aligned} \tag{6.13}$$

interior point algorithm implemented in this work is presented below.

Algorithm 6.1 [Interior Point Method]

1. Add slack variable (s) for each inequality constraint and rewrite the optimization problem in eq. (6.13) as follows:

$$\begin{aligned} \min_x f(x) \\ \text{s.t. } h(x) - s = 0, \quad s \geq 0 \end{aligned} \quad (6.14)$$

2. Introduce barrier term in the objective function and for $\mu > 0$, reformulate the optimization problem as shown below by denoting $g(x) = h(x) - s$:

$$\begin{aligned} \min_{x,s} f_\mu(x) = f(x) - \mu \sum_{i=1}^m \ln(s_i) \\ \text{s.t. } g(x) = 0 \end{aligned} \quad (6.15)$$

3. Apply KKT conditions to the objective function as follows:

$$\begin{aligned} \nabla f(x) + \nabla g(x)\lambda - \mu \sum_{i=1}^m \frac{1}{s_i} = 0 \\ g(x) = 0 \end{aligned} \quad (6.16)$$

4. By denoting $z_i = \frac{\mu}{s_i}$, modify KKT conditions as,

$$\begin{aligned} \nabla f(x) + \nabla g(x)\lambda - z = 0 \\ g(x) = 0 \\ SZe - \mu e = 0 \end{aligned} \quad (6.17)$$

5. For iteration $l = 1$, initialize x_0, λ_0 and z_0 .
6. If the Hessian (H) is available for the objective function, follow the steps below to solve the search directions using Newton's method:

- a) Formulate the system of equations to find the KKT solution.

$$\begin{bmatrix} H_l & \nabla g(x_l) & -I \\ \nabla g(x_l)^T & 0 & 0 \\ Z_l & 0 & S_l \end{bmatrix} \begin{bmatrix} p_l^x \\ p_l^\lambda \\ p_l^z \end{bmatrix} = \begin{bmatrix} \nabla f(x_l) + \nabla g(x_l)\lambda_l - z_l \\ g(x_l) \\ S_l Z_l e - \mu e \end{bmatrix} \quad (6.18)$$

where

$$H_l = \nabla_{xx}^2 L(x_l, \lambda_l, z_l) = \nabla_{xx}^2 (\nabla f(x_l) + \nabla g(x_l)^T \lambda_l - z_l) \quad (6.19)$$

and

$$Z_l = \begin{bmatrix} z_1 & 0 & 0 \\ 0 & \ddots & 0 \\ 0 & 0 & z_m \end{bmatrix}, \quad S_l = \begin{bmatrix} s_1 & 0 & 0 \\ 0 & \ddots & 0 \\ 0 & 0 & s_m \end{bmatrix} \quad (6.20)$$

- b) Rearrange the Eq. (6.18) to obtain the linear reduced KKT system as follows and solve for p_l^x as well as p_l^λ :

$$\begin{bmatrix} H_l + S_l^{-1}Z_l & \nabla g(x_l) \\ \nabla g(x_l)^T & 0 \end{bmatrix} \begin{bmatrix} p_l^x \\ p_l^\lambda \end{bmatrix} = - \begin{bmatrix} \nabla f(x_l) + \nabla g(x_l)\lambda_l \\ g(x_l) \end{bmatrix} \quad (6.21)$$

- c) Calculate p_l^z explicitly using the equation below:

$$p_l^z = \mu S_l^{-1}e - z_l - S_l^{-1}Z_l p_l^x \quad (6.22)$$

7. Otherwise, calculate search directions using conjugate gradient method in a trust region as shown below:

- a) Obtain Lagrange multipliers ($\lambda > 0$) by approximately solving KKT equations (see Eq. (6.17)) in least-squares sense.

- b) Compute search directions p_l^x and p_l^z by solving following problem:

$$\begin{aligned} \min_{p_l^x, p_l^z} \nabla f(x_l)^T p_l^x + \frac{1}{2} (p_l^x)^T \nabla_{xx}^2 L(p_l^x) + \mu e^T S_l^{-1} p_l^z + \frac{1}{2} (p_l^z)^T S^{-1} \Lambda p_l^z \\ \text{s. t. } g(x_l) + J_g(p_l^x) + p_l^z = 0 \end{aligned} \quad (6.23)$$

8. Determine the optimal step size (α_l) according to reduction in the merit function shown below:

$$\phi(x) = f_\mu(x) + \nu \sum_{i=1}^m |g_i(x)| \quad (6.24)$$

9. Estimate the new value of the optimum as follows:

$$\begin{aligned} x_{l+1} &= x_l + \alpha_l p_l^x \\ \lambda_{l+1} &= \lambda_l + \alpha_l p_l^\lambda \\ z_{l+1} &= z_l + \alpha_l p_l^z \end{aligned} \quad (6.25)$$

10. Check the convergence criteria by evaluating the following KKT conditions:

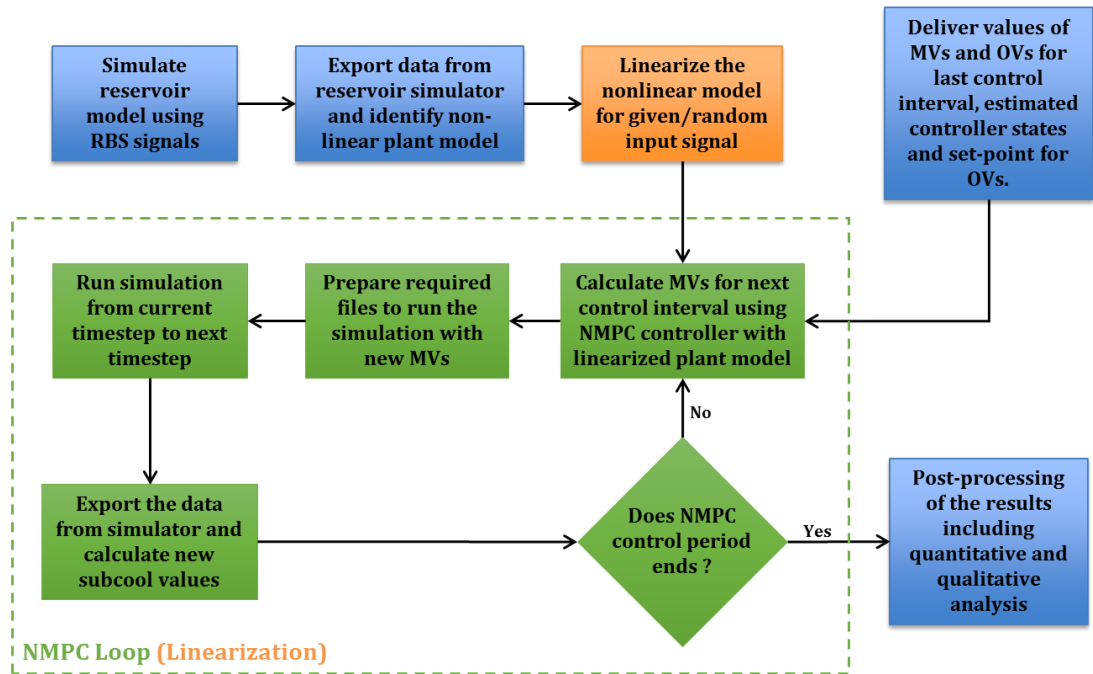
$$\begin{aligned}
 \max |\nabla f(x_{l+1}) + \nabla g(x_{l+1})\lambda_{l+1} - z_{l+1}| &\leq \epsilon_{tol} \\
 \max |g(x_{l+1})| &\leq \epsilon_{tol} \\
 \max |SZe - \mu e| &\leq \epsilon_{tol}
 \end{aligned} \tag{6.26}$$

11. If convergence is not achieved, $l \mapsto l + 1$ and repeat from step 6.
-

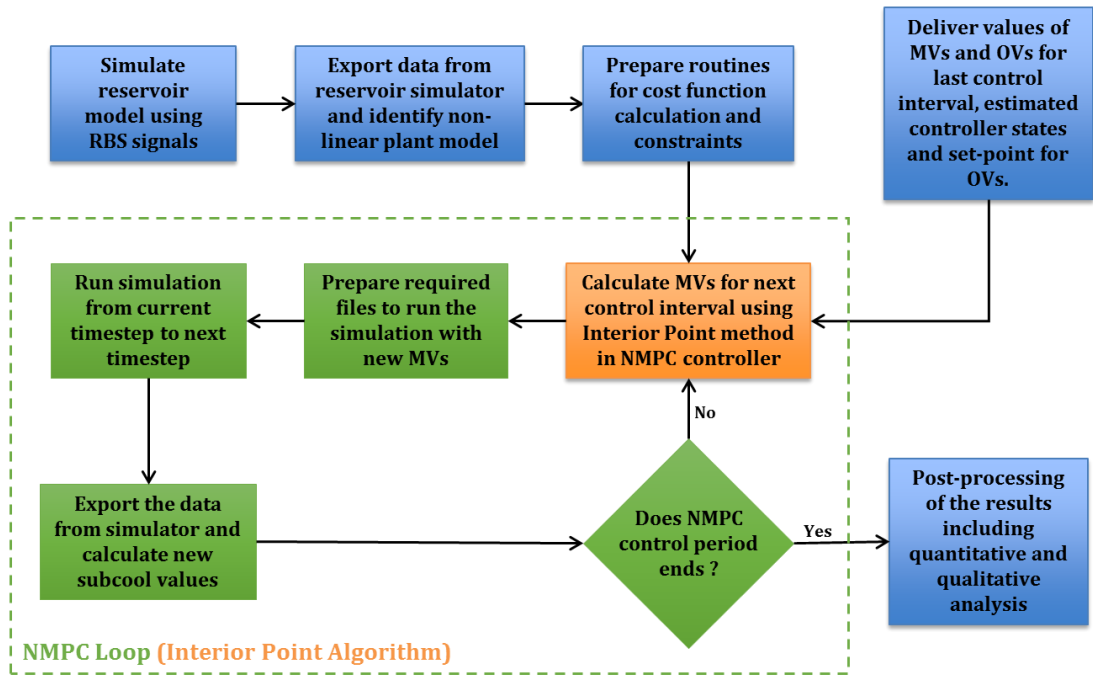
In the algorithm, e is the vector containing all ones, I is the identity matrix while J_g in Eq. (6.23) is the Jacobian of the constraints $g(x)$. In the barrier term, μ is a penalty parameter, which controls the strength of the barrier function in the reformulated objective function $f_\mu(x)$. Higher values of μ restricts the objective function away from the boundary, which is not desirable when optimal solution lies on the boundary. Therefore, μ is decreased gradually such that $\mu > 0$ to ensure the smooth convergence towards the optimal solution.

6.3.3 Advanced Control Workflows for SAGD Well Operations Using NMPC

To implement linearization and interior point method in NMPC, control workflows designed are shown in *Figure 6.3*. Like linear MPC workflows in *Chapter 5*, history-matched reservoir model is considered as a virtual plant model in this study. To obtain the training data for nonlinear model identification, initially, reservoir model is simulated considering RBS signals as input. Corresponding output data is exported to construct a training dataset in time domain using which appropriate input-output nonlinear black box models are identified. For these external dynamics model, linearization using a given/random input signal is implemented in NMPC as shown in *Figure 6.3(a)*. When NMPC phase is scheduled to commence, linear approximations along with past IVs/OVs, set-points, and estimated controller states are used to calculate optimum MVs for the next control interval. Required input files are prepared for the reservoir simulator and model is simulated for the next control interval. Necessary data is stored to calculate latest OVs (i.e. subcools) and the NMPC loop is repeated till the end of the control period after which results are analyzed qualitatively and quantitatively.



(a)



(b)

Figure 6.3 – Control framework for real-time SAGD well operations using NMPC with (a) Linearization and (b) Interior Point algorithm.

The only difference in NMPC with nonlinear optimization (see *Figure 6.3(b)*) is the preparation of additional subroutines for cost function and nonlinear constraints and use of interior point algorithm in NMPC controller. Significant changes as compared to linear MPC are highlighted with orange blocks in both workflows.

6.4 SAGD Field Application

Performance of proposed NMPC workflows is tested using the history-matched reservoir model explained in section 5.4.1 and therefore, details are not repeated here. Like linear MPC workflows in *Chapter 5*, routines and subroutines were developed to establish the communication link between NMPC controller coded in MATLAB® (MathWorks 2014), the thermal reservoir simulator CMG STARS™ (CMG 2013a) which acts as a virtual process plant, and Results Report™ (CMG 2013b) that facilitates the data acquisition/transfer. Also, the results of NMPC are analyzed and compared with linear MPC explained in section 5.4.3. In this section, details regarding the application of nonlinear model identification and both NMPC workflows in the case study are given.

6.4.1 Identification of Nonlinear Dynamic Model

As mentioned by Henson (1998), five tasks involved in the identification of nonlinear models are 1) selection of the structure, 2) design of the input sequence, 3) identification of noise model, 4) model parameter estimation, and 5) model validation. In this work, they were performed using System Identification Toolbox™ (Ljung 2016) in MATLAB. As explained in section 5.4.2, the well pair in reservoir model was segmented into five divisions and subcool of each division was considered as an output variable while steam injection rate for short tubing as well as long tubing and liquid production rate were specified as input variables of the nonlinear model. To decouple the complex reservoir process, individual MISO system was identified for each subcool considering all three input variables mentioned before.

Initially, an attempt was made to identify the nonlinear models using field data; however, it was concluded that the data is not persistently excited. In other words, the data might be missing some important operating points and hence not representing the nonlinear dynamics of the process effectively, ultimately leading to substandard nonlinear models. Also, more data samples are required for identification

of black-box nonlinear models as compared to linear models (Ljung 2016). Therefore, it was decided to design an input sequence and obtain the corresponding output using history-matched reservoir model considered in the case study.

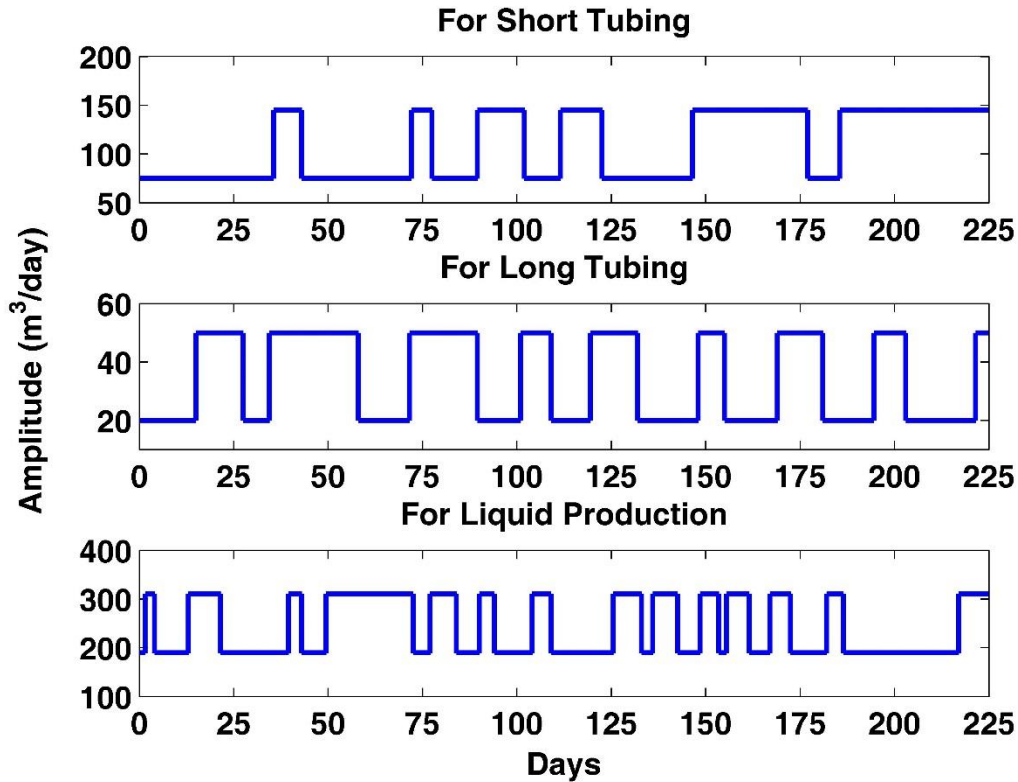


Figure 6.4 – RBS signals generated for nonlinear system identification in NMPC.

Random Binary Signal (RBS), a widely used input sequence in process control is implemented in this study. As the name suggests, the input randomly varies between the binary ranges. To determine the design parameters for an RBS sequence, separate step tests were performed and first order plus dead time (FOPDT) models were generated for each subcool and input variable. The minimum time constant (τ) of all SISO systems was chosen as the time constant for the MIMO system since it allows to capture the change in output variables accurately. Guidelines provided by Huang et al. (2013) and Vembadi (2014) were followed to compute sampling time (T_s), bandwidth, and range which are reported in *Table 6.1* and corresponding RBS input sequences are shown in *Figure 6.4*. RBS signals were further implemented in history-matched reservoir model and associated output variables were obtained to build the input-

output dataset containing 450 samples for nonlinear system identification. Note that bandwidth reported in *Table 6.1* is essentially a fraction of the highest required frequency (k/τ) to the Nyquist frequency (π/T_s).

Table 6.1 – Design parameters for input signals used in nonlinear system identification

Input Variables	Sampling Time (Days)	No. of Samples	Signal Type	Bandwidth	Range (m ³ /day)
Short Tub Inj Rate	0.5	450	RBS	0.06	-35 to +35
Long Tub Inj Rate	0.5	450	RBS	0.05	-15 to +15
Liquid Prod Rate	0.5	450	RBS	0.11	-60 to +60

From the input-output dataset, 350 samples (approximately 3/4th of the data) are utilized for the identification of nonlinear models while the other 100 samples are used for the model validation. Time delays considered here are same as those of linear models identified in section 5.4.2 since the system (reservoir model in our case) is identical in both cases. More than 100 combinations were tested with different nonlinear model structures (NARX and Hammerstein-Wiener models), input/output nonlinearities (piecewise linear, sigmoid, wavelet, and polynomial) and orders of process/noise models for each MISO system. Based on the performance in residual tests and cross-validation, Hammerstein-Wiener models with linear dynamics represented by OE model are chosen for all subcools. Details of these models including input/output nonlinearity, delay, model fit, model order, and AIC is given in *Table 6.2*.

Table 6.2 – Specifics of Hammerstein-Wiener models identified for each subcool

Output Variables	Nonlinear System Identification Models						AIC
	Input Nonlin.	Output Nonlin.	Delay	Order		Fit (%)	
				nB	nF		
Subcool 1	Polynomial	Polynomial	[1 2 1]	[3 3 3]	[3 3 3]	91.04	0.90
Subcool 2	PW Linear	PW Linear	[1 1 1]	[2 2 2]	[2 2 2]	91.75	-0.19
Subcool 3	Polynomial	Polynomial	[1 2 1]	[3 3 3]	[3 3 3]	92.35	1.97
Subcool 4	PW Linear	Polynomial	[1 1 1]	[3 3 3]	[3 3 3]	80.67	2.62
Subcool 5	PW Linear	Polynomial	[1 1 1]	[4 4 4]	[4 4 4]	81.97	2.16

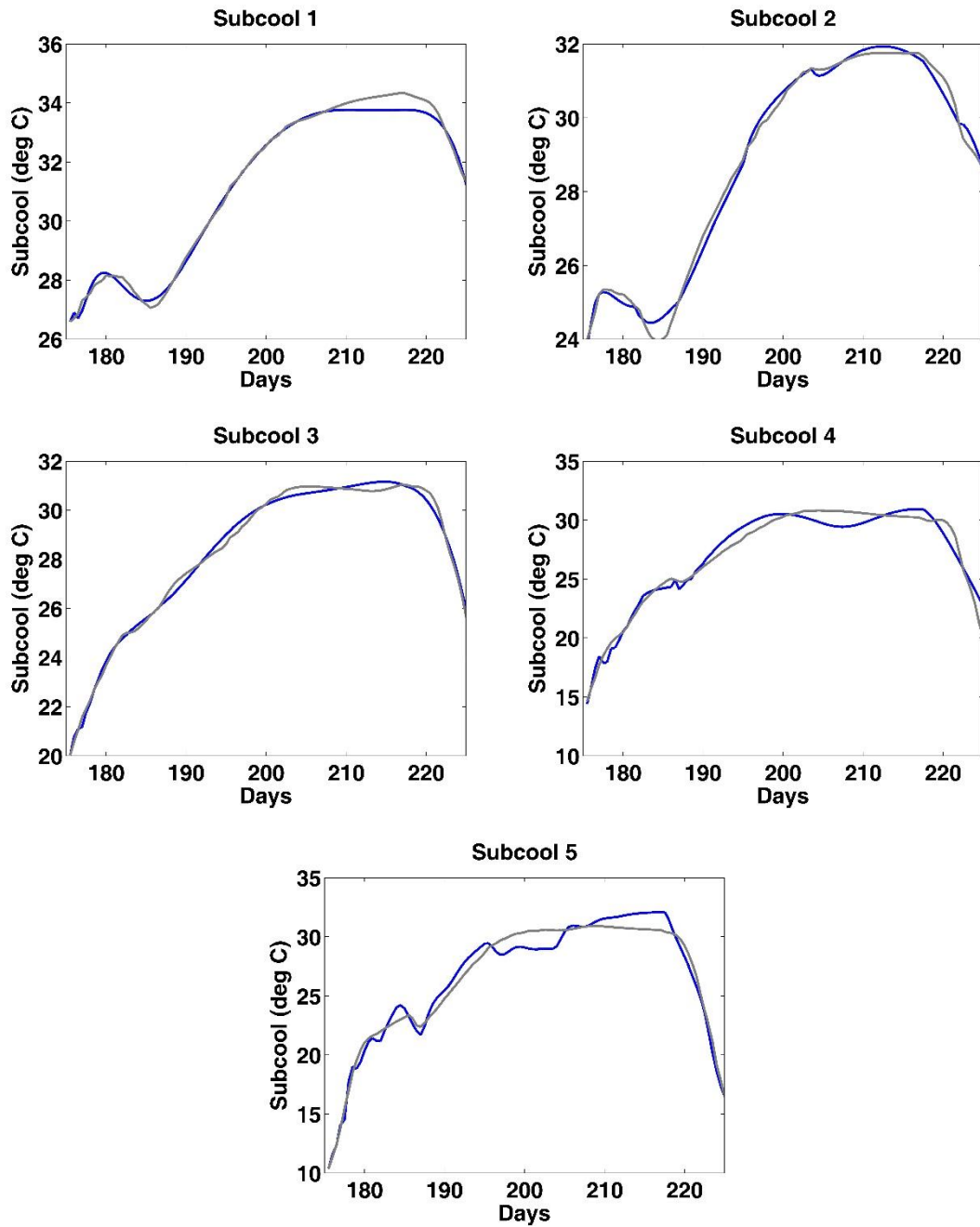


Figure 6.5 – Results of cross-validation for Hammerstein-Wiener models identified in nonlinear system identification. Blue line represents predicted output from the model while grey line depicts validation data.

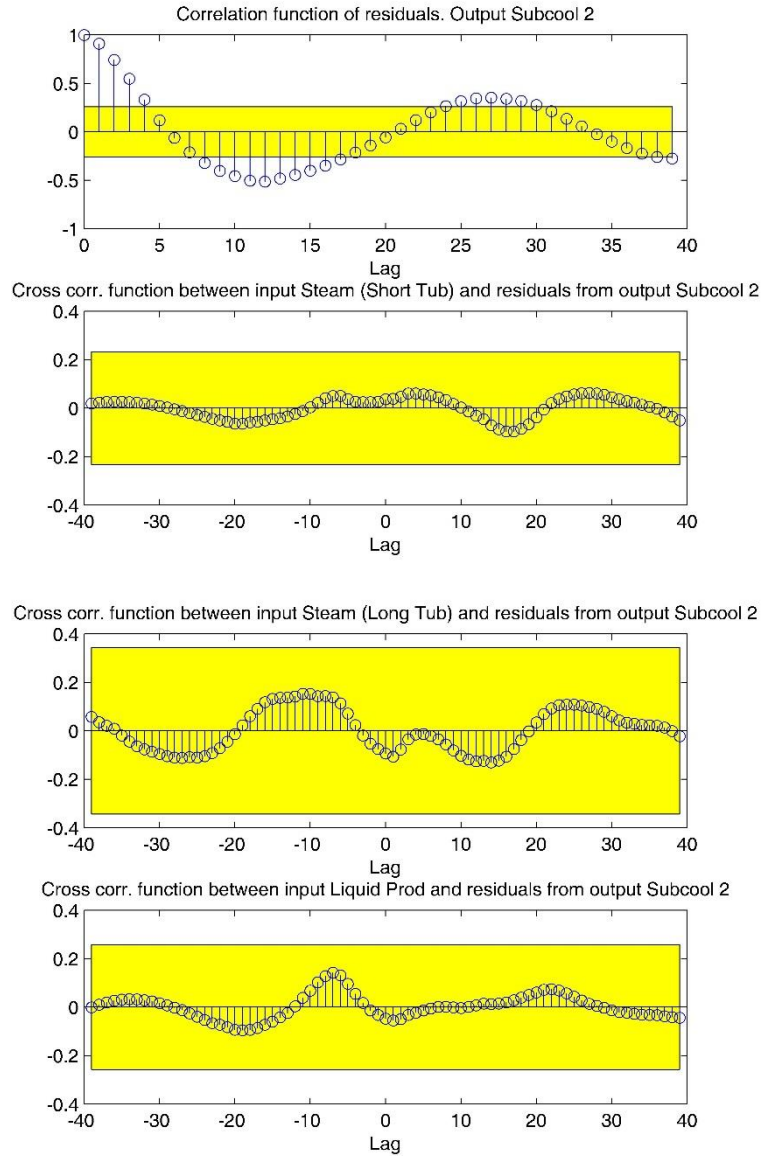


Figure 6.6 – Results of residual tests for Hammerstein-Wiener model of Subcool 2. Yellow rectangle box shows 99% confidence interval.

Results of the cross-validation tests for chosen nonlinear models displays satisfactory fit with validation data (not used before in model identification) in *Figure 6.5*. As shown in *Figure 6.6*, residuals are well within the 99% confidence interval in all cross-correlation tests. Also, no significant trend is displayed in case of the Hammerstein-Wiener model of Subcool 2, which endorses the legitimacy of the model. Similar results were obtained for the other nonlinear models presented in *Table 6.2*. Note that

autocorrelation test is not applicable to identified Hammerstein-Wiener models since linear dynamics (G_p) is represented using OE model in which noise model is unity (see section 5.2). Orders of the polynomials $B(z^{-1})$ and $F(z^{-1})$ (see Eq. (5.3)) of this OE model are denoted as nB and nF respectively in *Table 6.2*. Finally, identified nonlinear models are implemented in NMPC workflows explained in *Figure 6.3*.

6.4.2 Application of NMPC Using Linearization

After the identification of nonlinear dynamic models, they were linearly approximated by employing one of the linearization techniques discussed in section 6.3.1. As mentioned in *Figure 6.3(a)*, it was performed using a given input signal since Hammerstein-Wiener models identified in this study are input-output black box models. A linear model with similar structure and order as G_p of Hammerstein-Wiener model (i.e. OE model with orders nB and nF shown in *Table 6.2*) was approximated for each subcool such that, considering an RBS input sequence (with 350 samples) used to identify nonlinear models as input, difference between output predicted using linearized model and simulated output of nonlinear model is minimum in mean-square-error sense. Linearized MISO systems were then combined to create a MIMO system that was converted to state space formulations subsequently. Since NMPC problem was reduced to linear MPC problem, Model Predictive Control Toolbox™ (Bemporad et al. 2016) was implemented for NMPC using linearization. Constraints and design parameters of NMPC controller were considered same as those for linear MPC (see *Table 5.3*). Sampling time for the controller was 1 day while for nonlinear dynamic models, it was 0.5 days. To avoid this discrepancy, discrete-time dynamic model was resampled using controller's sampling time by implementing the zero-order-hold on the inputs. Steady state Kalman filter is applied as a state observer in the NMPC controller. Like linear MPC workflows, NMPC was applied from 800 days to 1355 days to maintain a common basis for comparison.

6.4.3 Application of NMPC Using Nonlinear Optimization

As noted before, prediction of output variables using nonlinear model in MPC can improve the control performance; however, it makes the optimization problem nonlinear and nonconvex. Using the workflow shown in *Figure 6.3(b)*, interior point

method (explained in section 6.3.2) was implemented to solve the nonlinear optimization of cost function in NMPC. Additional codes were written to define the cost function and linear/nonlinear constraints in the NMPC controller. The mismatch between sampling time of NMPC controller and Hammerstein-Wiener models identified in this study was managed by cloning the input signal for the consecutive control interval in the evaluation of the cost function. In other words, one control interval of NMPC controller was represented by two identical consecutive control intervals of the nonlinear model in the cost function. Optimization Toolbox™ (MathWorks 2014) was used to implement interior point method in NMPC workflow. It was observed that optimization problem was feasible and termination criteria were satisfied for almost all the control intervals. Instead of using state observer, controller states were updated using input-output data of the immediate past 50 days. The control period considered in this workflow was same as that of NMPC using linearization.

6.5 Results and Discussion

Primary aim of invoking NMPC in this case study is to maintain subcool near the set-point in real-time, which ensures the uniform steam chamber propagation along the wellbore, optimal automated operation of SAGD well pair, and maximum monetary benefits. In this section, the efficacy of NMPC in achieving these objectives is analyzed by presenting and discussing qualitative as well as quantitative results on performance in subcool control, adjustment in IVs, and change important production parameters. Also, results are compared with the base case where no control algorithm was used and linear MPC.

6.5.1 Subcool Control with NMPC

Ideally, control algorithms should maintain subcool in all the segments near the set-point in order to be considered successful; however, it is not possible in this case study due to the lack of degree of freedom in MPC controller. In *Figure 6.7*, all subcool values are presented for the base case, linear MPC, and proposed NMPC workflows. While steam breakthrough is evident in base case with zero subcools, linear MPC also displays inferior performance with all subcools away from the set-point for most of the control intervals. In contrast, both NMPC workflows show satisfactory performance

with all subcools near or above the set-point throughout the control period. Except in the beginning of the NMPC phase when OV's are converging towards the set-point, no significant variations can be observed. In addition, subcool 1 is maximum among all the OV's in the linear/nonlinear MPC workflows shown in *Figure 6.7*, indicating highest liquid level between injector and producer well. Therefore, probability of steam breaking through at heel end of the well pair seems to be minimum.

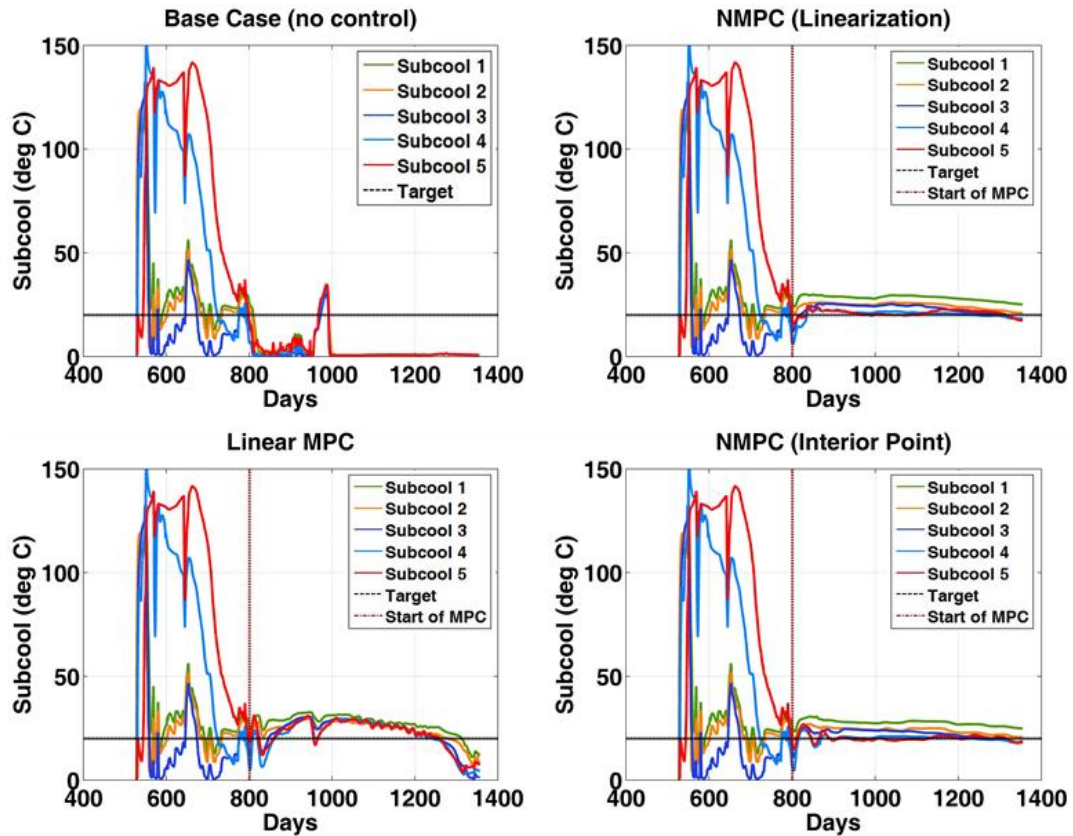


Figure 6.7 – Subcool of all segments of the well pair obtained using different linear/nonlinear control methods in real-time production optimization.

Among all the OV's, minimum subcool is important since its value lower or higher than the optimum indicates the deficient usage of steam or adverse effect on steam chamber propagation, respectively. *Figure 6.8* shows the minimum subcool throughout the control period in different control workflows. In case of linear MPC, significant fluctuations are apparent in the minimum subcool around 1100 days. At the end of the control period, its value is almost equal to zero which clearly suggests that linear models are not sufficient for the control of the nonlinear system in MPC. Swift increase

in minimum subcool of both NMPC frameworks is evident after the start of the control period. It follows the set-point after the convergence with the maximum offset from the set-point being less than 2 °C. Hence, satisfactory performance of both NMPC workflows can be concluded in real-time subcool control of SAGD reservoirs.

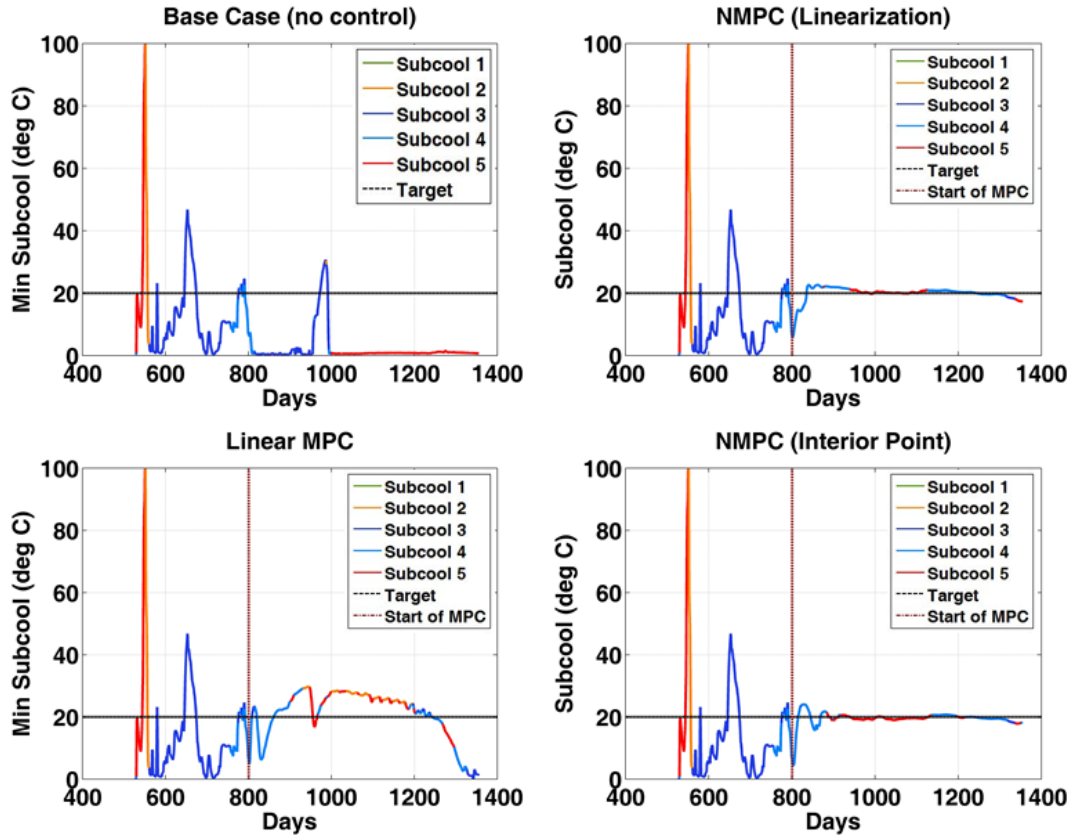


Figure 6.8 - Minimum subcool of the well pair obtained using different linear/nonlinear control methods in real-time production optimization.

6.5.2 Behavior of Manipulated Variables

It is important to assess the adjustment in MVs since they should be within the constraints provided by surface facilities to ensure smooth operation of the SAGD well pair. *Figure 6.9*, *Figure 6.10*, and *Figure 6.11* demonstrate the behavior of steam injection rate in short tubing, long tubing, and liquid production rate respectively in different control algorithms. Steam injection and liquid production rates are significantly high in the base case while in case of linear MPC, maximum fluctuations in all MVs are exhibited, which may lead to wear and tear of actuators. Also, it indicates

the unstable control operations as reference trajectory for no MVs are followed. In NMPC workflows, steam injection rates of both long and short tubing fluctuate slightly in the beginning until it converges to the optimum inputs. However, the duration of convergence is much smaller as compared to the overall control period. Linearization shows slightly deteriorated performance in NMPC with higher variations in MVs. It might be due to the linear state observer (Kalman filter) that could not update the controller states accurately in case of the nonlinear systems like SAGD reservoirs.

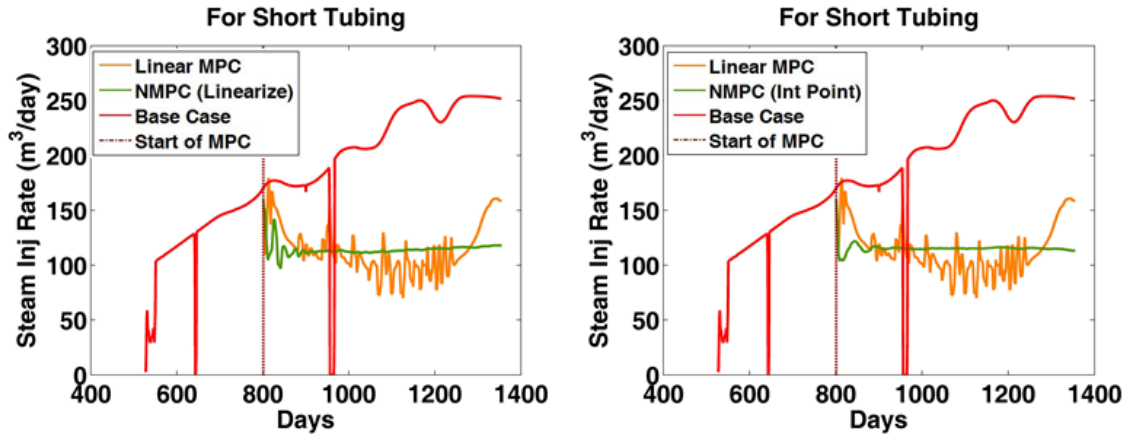


Figure 6.9 – Performance of steam injection rate (short tubing) in NMPC using linearization (left) and interior point algorithm (right) when compared with base case and linear MPC.

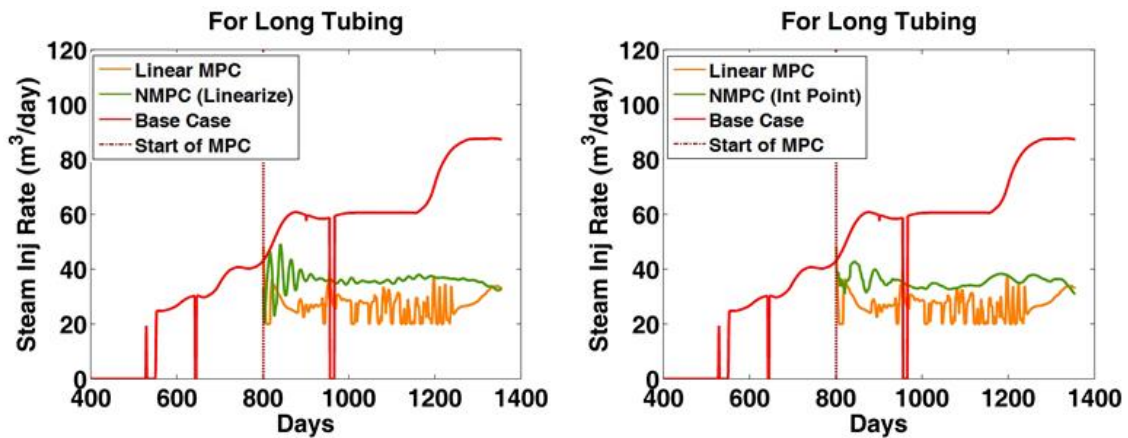


Figure 6.10 – Performance of steam injection rate (long tubing) in NMPC using linearization (left) and interior point algorithm (right) when compared with base case and linear MPC.

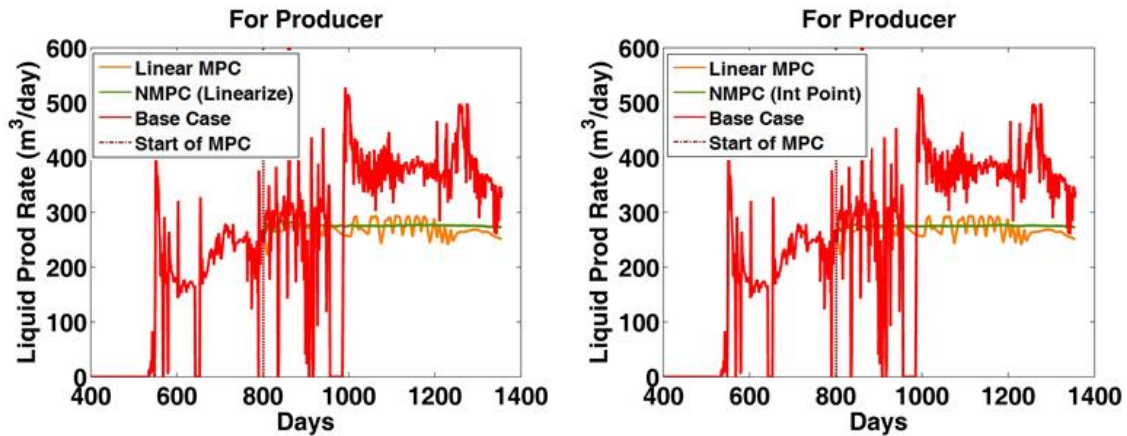


Figure 6.11 – Performance of liquid production rate in NMPC using linearization (left) and interior point algorithm (right) when compared with base case and linear MPC.

When compared to linearization, NMPC using interior point algorithm exhibits marginal deviations (see *Figure 6.9* and *Figure 6.10*) in terms of amplitude as well as frequency since the controller states are updated using immediate past data that represents the current reservoir conditions. Once the MVs converge towards the respective optimum values, no significant deviations can be observed. It indicates the overall stable control performance of proposed NMPC workflows, especially in case of liquid production rate (see *Figure 6.11*).

6.5.3 Impact on Production Performance

Subsequent effects of manipulating MVs using NMPC on daily oil rate, cumulative oil production, and cSOR are evaluated in *Figure 6.12*, *Figure 6.13*, and *Figure 6.14* respectively. As compared to linear MPC, for almost 80% of the total control period, higher oil rate in both proposed NMPC approaches can be observed from *Figure 6.12*. In the last few control intervals, oil rate in linear MPC increased suddenly. It is due to the control failure which drove subcools much below the set-point (see *Figure 6.7*), indicating the inadequacy of linear control workflows in nonlinear reservoir systems. Further, a much lower plateau in oil rate of proposed NMPC workflows as compared to the base case is due to the subcool set-point of the controller. Lower subcool set-point would have allowed higher steam injection/oil production. Hence, optimum subcool set-point should be defined by considering it as one of the variables to be optimized in mid-term field development planning.

Cumulative oil production in *Figure 6.13* is almost equal for both proposed NMPC workflows and marginally higher as compared to linear MPC. Similarly, cSOR at the end of the control period is slightly lower in linear MPC (2.422) as compared to NMPC using linearization (2.468) and interior point method (2.482). However, when compared to the base case that represents the current scenario of the SAGD field operations, reduction in cSOR is evident after implementing the NMPC workflows (see *Figure 6.14*). Despite higher oil production in the base case, it signifies the necessity of real-time production optimization in SAGD operations for efficient steam usage and better financial consequences.

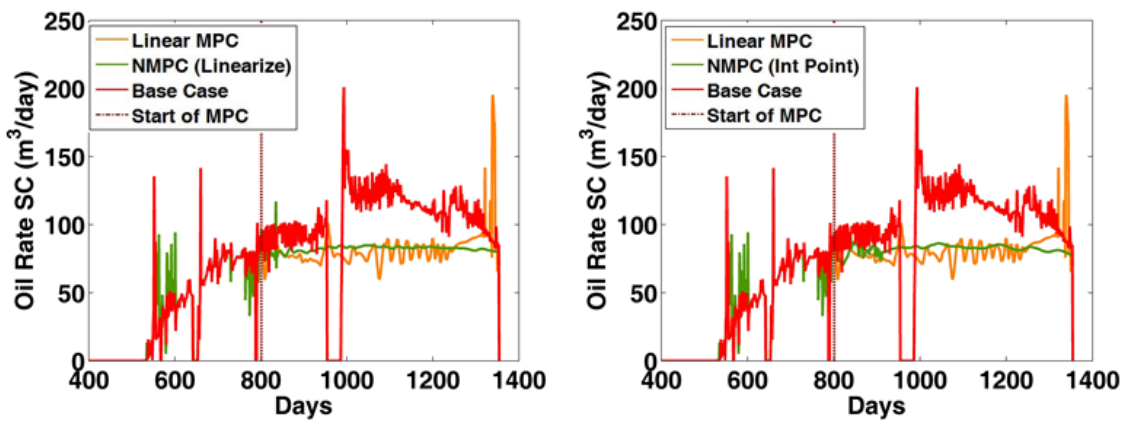


Figure 6.12 – Effect of NMPC using linearization (left) and interior point algorithm (right) on oil production rate. SC = surface conditions.

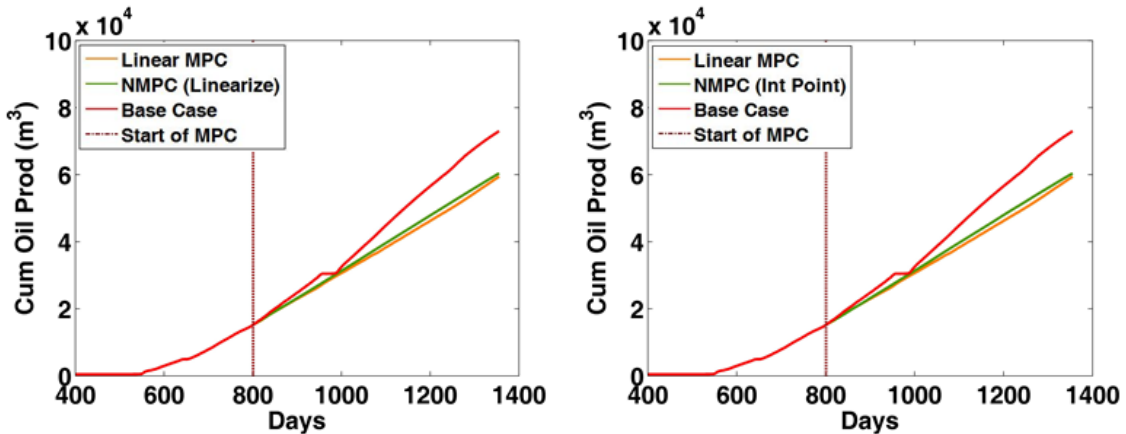


Figure 6.13 – Effect of NMPC using linearization (left) and interior point algorithm (right) on cumulative oil production.

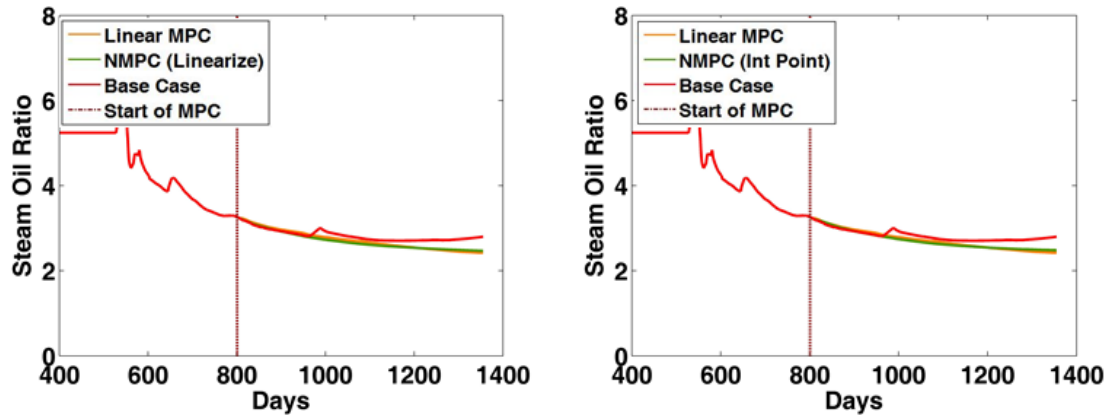


Figure 6.14 – Effect of NMPC using linearization (left) and interior point algorithm (right) on cumulative steam oil ratio.

6.5.4 Statistical Analysis of NMPC Performance

To analyze the performance of NMPC workflows statistically, NPV and RMSE are computed using Eq. (5.18) and Eq. (5.19) respectively. NPV demonstrates the economic feasibility of the NMPC while RMSE depicts its capability to reduce the error in subcools with respect to set-point. Parameters such as oil price, cost of steam generation, discount rate, reference time for discounting cash flow etc. used to calculate the quantitative measures are same as those explained in section 5.5.4. In addition, RMSE is reported in Table 6.3 for both minimum as well as all subcools.

Table 6.3 – Statistical analysis of nonlinear control algorithms used for real-time production optimization

Case	Performance Statistics		
	Net Present Value	RMSE	RMSE
	(in million \$)	(Min Subcool)	(All Subcool)
Base Case (no control)	5.623	18.035	32.367
Linear MPC	7.239	11.652	28.963
NMPC (Linearization)	7.002	9.677	28.528
NMPC (Interior Point)	6.973	9.765	28.461

In the base case, higher cumulative oil production (see *Figure 6.13*) is achieved at the cost of significantly greater RMSE in subcools; however, it does not turn out to be the best strategy as NPV is lowest among all the cases considered in this study (refer *Table 6.3*). Although linear MPC exhibits maximum NPV, it is mainly due to unsuccessful subcool control mentioned before, which is also reflected by increased RMSE for minimum subcool. In contrast, NMPC workflows studied here display better control performance with minimum RMSE and significantly higher NPV as compared to the base case. Minor difference in RMSE (for all subcools) between linear and nonlinear control workflows is most probably due to lack of degree of freedom in MPC controller. Intelligent well completions using inflow/outflow control devices (ICDs/OCDs) may have established the superiority of NMPC thoroughly since it allows the steam injection/oil production from a particular segment of the well pair unlike dual tubing string configuration considered in this study.

Finally, it is important to discuss regarding the field application of the NMPC framework. Most of the current SAGD fields (also known as i-fields/e-fields/smart fields) are equipped with permanent downhole sensors and fiber optic arrays or distributed temperature sensors (DTS) mounted on the tubings that can be utilized to determine the subcools. To implement the MVs in the next control interval, pressure/flow controller (PC/FC) or pressure/flow indicator and controller (PIC/FIC) along with actuators such as automatic control valves can be employed. Note that the only cost an operator company has to incur is for actuators, which is a fraction of a total gain in NPV (refer *Table 6.3*) over a lifecycle of the SAGD reservoir. Also, NMPC automates the well pair operations, further reducing the operational costs. Next, the computational cost of NMPC using linearization is equivalent to the linear MPC as the optimization problem to be solved is a standard QP problem. However, in case of interior point algorithm, computing cost increases by almost 2.5 times since a nonlinear optimization problem is solved at every control interval. Depending on the complexity of the control problem that relies upon the reservoir parameters such as heterogeneity in flow properties, fluid saturations as well as wellbore geometry and completions, either of the proposed NMPC approaches can be chosen. If appropriate, adaptive or gain-scheduled MPC (explained in *Chapter 5*) can be implemented to handle the nonlinearity of the system, which provides the best trade-off between accuracy (NMPC) and computational efficiency (linear MPC).

6.6 Summary

In this research, an efficacy of SAGD well operations using NMPC in real-time production optimization is investigated. Two NMPC workflows, one using linearization and the other one using nonlinear optimization are proposed. Linearization basically reduces an NMPC problem to linear MPC by estimating an equivalent linear model of a nonlinear black box model for a given input signal in a mean-square-error sense. The second approach employs interior point method to solve the nonlinear optimization problem in NMPC. Both approaches are tested using a field-scale SAGD reservoir model and conclusions derived from the qualitative and quantitative analysis of the results are listed below:

1. With accurate estimations of subcools, Hammerstein-Wiener models can effectively capture the nonlinearity of the SAGD operations.
2. Both NMPC frameworks are successful in maintaining the minimum subcool above the predefined set-point while ensuring the stability of well operations.
3. More than 24% increment in NPV is achieved in NMPC as compared to the base case where no control strategy is used.
4. Computational cost of NMPC using interior point method is almost 2.5 times higher than other linear/nonlinear control methods due to the solution of nonlinear optimization problem at each control interval.

Overall, NMPC can be successfully employed in CLRM of SAGD reservoirs for improved real-time subcool control, energy efficiency, and CO₂ emissions while satisfying the constraints offered by the surface facilities.

Chapter 7

Concluding Remarks and Recommendations

7.1 Concluding Remarks

Application of CLRM in SAGD fields can potentially improve the reservoir performance in terms of oil recovery and monetary benefits. Therefore, two principal challenges in CLRM – the high computational cost of data assimilation and incorporating nonlinearity of the SAGD process in short-term production optimization – are addressed in this research. Numerous approaches developed to alleviate these issues are verified using a field-scale model of SAGD reservoir. Through analysis of various results, important outcomes are listed in this section for each of the proposed workflow/framework.

Initial sampling involves the selection of few realizations from original ensemble to reduce the computing cost of data assimilation. Difference between the selected subset and original ensemble represented by Kantorovich distance is minimized using constrained MILP model. From the results, it can be said that statistical characteristics of the subset selected using proposed "scenario reduction" method are similar to those of original ensemble. Also, equivalent history matching results as an original ensemble are obtained, unlike other sampling methods. As compared to full physics reservoir simulation, the computational cost of static measures is negligible in proposed approach, hence, improving overall computing efficiency of data assimilation. However, selection of appropriate static measures is crucial as they provide a unique identity to each realization in an original ensemble. Flow based static measures or dynamic measures using streamline simulation can be considered for complex reservoirs displaying non-Gaussian features.

Another approach employs KL-PCE based forecast model in data assimilation. KL parameterization is used to reduce the dimensions of model parameters and PCE to predict production parameters using random variables and corresponding orthogonal polynomials. From the results of the blind test, accuracy of PCE in production forecast is evident as it can capture the nonlinearity of the SAGD process. Despite uncertainty introduced by proposed metamodel, a reasonable estimation of posterior pdf and production parameters is obtained in history matching using EnKF. Also, sequential nature of EnKF assisted in diminishing the effect of forecast model uncertainty on the estimation of model parameters. Further, MCMC showed robust performance with proposed KL-PCE metamodel as uncertainty in model parameters is minimum among all three cases considered. The computational cost of proposed workflow is minimal as

compared to conventional iterative EnKF since full physics simulations are required only at collocation nodes. If the spatial variance of the model parameters is very high, the number of terms and hence, required simulation runs will increase exponentially.

To incorporate nonlinearity of SAGD process in real-time production optimization, variants of MPC i.e. adaptive MPC, gain-scheduled MPC, NMPC using linearization and interior point method are proposed. Both adaptive and gain-scheduled MPC utilize linear models; however, in adaptive MPC, model coefficients are estimated at each control interval using the latest available real-time data while gain-scheduled MPC uses multiple controllers and switching is performed based on minimum subcool. In contrast, both NMPC approaches employ nonlinear black box models. When linearization is implemented, an equivalent linear model in a mean-square-error sense is identified for a given input signal, thus, reducing NMPC problem to linear MPC. Otherwise, interior point method is used to solve the nonlinear optimization problem in NMPC. Primarily, it can be concluded that Hammerstein-Wiener models provide the better estimation of OVs as compared to linear (BJ, OE) models in the case study. All four variants performed well in subcool control while displaying stable adjustment in MVs. However, more fluctuations can be observed in the liquid production rate of gain-scheduled MPC due to frequent switching between controllers. Also, due to the same reason, only 10.36% increment in NPV is achieved as compared to 23.69%, 24.52%, and 24% in adaptive MPC, NMPC using linearization, and NMPC using interior point method respectively. The computational cost of NMPC using interior point method is approximately 2.5 folds higher than other workflows since nonlinear optimization problem is solved at each control interval. Hence, based on the desired accuracy, anticipated control environment, and complexity of the reservoir, appropriate control workflow can be chosen. In addition, results in the case study indicate that the subcool set-point should be selected carefully as higher value restricts the steam injection/liquid production and therefore, the oil rate in SAGD.

Finally, the major contributions of this research in improving CLRM of SAGD reservoirs can be summarized as follows:

1. An effective optimization based sampling algorithm that can maintain diversity in the ensemble and applicable to any assisted history matching/uncertainty quantification method.

2. An encyclopedic KL-PCE based metamodel which can handle large number of unknown parameters and be easily integrated in different assisted history matching and uncertainty assessment workflows while expediting the overall process.
3. An advanced control workflow using adaptive MPC for real-time production optimization in which coefficients of linear plant model are updated at each control interval to maintain the subcool effectively.
4. An efficient application of gain scheduling by creating a controller bank and switching based on output feedback, enabling automatic well operations as well as precise subcool control in adverse control situations.
5. A state-of-the-art control framework that implements nonlinear MPC for efficacious subcool control, which ultimately leads to better cumulative steam oil ratio and hence monetary benefits while minimizing the environmental and carbon footprints.

7.2 Recommendations for Future Research

In this thesis, attempts have been made to provide the solutions for some of the research questions pertaining to CLRM. However, as you gain more insights during this quest of in-depth knowledge, a larger scope of enhancement and possible course of future actions arises as an outgrowth. Below here, some of the important research objectives to be pursued in near future and influenced by the work in this dissertation are listed:

1. Static measures in "Scenario Reduction" method provides a unique identity to various realizations in the initial ensemble. Inclusion of connectivity based measures can improve the identity of the realization and hence ensure the better performance of initial sampling method, especially in case of SAGD reservoirs with excessive uncertainty in location and volume of the impermeable zones.
2. Identical static measures as proposed for the case study considered in this research will not be useful for different types of reservoirs. Therefore, novel

static measures should be developed based on the non-Gaussian features and other characteristics of the reservoir. For example, in case of fractured plays, global and local fracture intensity, fracture orientation parameters such as trend and plunge, number of fractures, matrix-fracture interaction parameters etc. can be used. For shale plays with multiple facies, CHV and harmonic average of permeability within a search window can be considered.

3. PCE metamodel or other machine learning techniques can be implemented in discrete fracture network (DFN) model based assisted history matching workflows for fractured reservoirs to avoid the high computational cost of construction and simulation of DFN models.
4. Successful application of NMPC for real-time subcool/production control is demonstrated in this work. However, an extensive study of robustness and stability of NMPC is required – especially for oil sands reservoirs with significant shale barriers and inclined heterolithic strata (IHS) zones – before the method/workflow is ready to cater the industry.
5. Receding horizon concept of MPC can be extended for the steam allocation to different well-pads in heavy oil thermal recovery processes. A proactive steam allocation workflow using real-time data acquisition, adaptive parametric system identification models that represent the relationship between input variables and key performance indicators (KPI), and appropriate optimization algorithm that considers the constraints offered by surface facilities can be designed for efficient usage of steam as compared to conventional reservoir model based open-loop optimization.
6. Several endogenous and exogenous uncertainties can be considered in real-time optimization of SAGD well pair operations along with appropriate parameterization techniques and linear/nonlinear programming algorithms for improved yet computationally efficient CLRM.

Bibliography

- Aanonsen, S.I., Naevdal, G., Oliver, D.S., Reynolds, A.C., Valles, B., 2009. The ensemble Kalman filter in reservoir engineering – a review. *SPE Journal* **14**(3): 393-412. SPE-117274-PA.
- Agarwal, B., Hermansen, H., Sylte, J.E., Thomas, L.K., 2000. Reservoir characterization of Ekofisk field: a giant, fractured chalk reservoir in the Norwegian North Sea – history match. *SPE Reservoir Evaluation & Engineering* **3**(6): 534-543. SPE-68096-PA.
- Akram, F., 2011. Multimillion-cell SAGD models – opportunity for detailed field analysis. Presented at *World Heavy Oil Congress*, Edmonton, Alberta, Canada, 14-17 March. WHOC11-534.
- Alexopoulos, C., Drakopoulos, V., 2012. On the computation of the Kantorovich distance for images. *Chaotic Modelling and Simulation* **2**: 345-354.
- Anderson, J.L., 2001. An ensemble adjustment Kalman filter for data assimilation. *Monthly Weather Review* **129**(12): 2884–2903.
- Anderson, J.L., 2010. A non-Gaussian ensemble filter update for data assimilation. *Monthly Weather Review* **138**(11): 4186-4198.
- Armstrong, M., Ndiaye, A., Razanatsimba, R., Galli, A., 2013. Scenario reduction applied to geostatistical simulations. *Mathematical Geosciences* **45**(2): 165-182.

- Ates, H., Bahar, A., El-Abd, S., Charfeddine, M., Kelkar, M., Datta-Gupta, A., 2003. Ranking and upscaling of geostatistical reservoir models using streamline simulation: a field case study. Presented at the *Middle East Oil Show*, Bahrain, 9-12 June. SPE-81497-MS.
- Augustin, F., Gilg, A., Paffrath, M., Rentrop, P., Wever, U., 2008. Polynomial chaos for the approximation of uncertainties: chances and limits. *European Journal of Applied Mathematics* **19**(2): 149-190.
- Azad, A., Chalaturnyk, R.J., 2013. Application of analytical proxy models in reservoir estimation for SAGD process: UTF-Project case study. *Journal of Canadian Petroleum Technology* **52**(3): 219-232. SPE-165576-PA.
- Aziz, K., Settari, A., 1979. *Petroleum Reservoir Simulation*. London: Applied Science Publishers.
- Babaei, M., Alkhatib, A., Pan, I., 2015. Robust optimization of subsurface flow using polynomial chaos and response surface surrogates. *Computational Geosciences* **19**(5): 979-998.
- Ballin, P.R., Journel, A.G., Aziz, K., 1992. Prediction of uncertainty in reservoir performance forecast. *Journal of Canadian Petroleum Technology* **31**(4): 52-62. PETSOC-92-04-05.
- Banerjee, S., Abdelfattah, T.A., Nguyen, H.T., 2013b. Benefits of passive inflow control devices in a SAGD completion. Presented at the *SPE Heavy Oil Conference*, Calgary, Alberta, Canada, 11-13 June. SPE-165478-MS.
- Banerjee, S., Jobling, R., Abdelfattah, T.A., Nguyen, H.T., 2013a. The role of autonomous flow control in SAGD well design. Presented at the *SPE Annual Technical Conference and Exhibition*, New Orleans, Louisiana, USA, 30 September-2 October. SPE 166266-MS.
- Bao, X., Chen, Z., Wei, Y., Dong, C.C., Sun, J., Deng, H., Yu, S., 2010a. Numerical simulation and optimization of the SAGD process in Surmont oil sands lease. Presented at the *Abu Dhabi International Petroleum Exhibition & Conference*, Abu Dhabi, UAE, 1-4 November. SPE-137579-MS.

- Bao, X., Chen, Z., Wei, Y., Dong, C.C., Sun, J., Deng, H., Yu, S., 2010b. Geostatistical modeling and numerical simulation of the SAGD process: case study of an Athabasca reservoir with top water and gas thief zones. Presented at the *Canadian Unconventional Resources & International Petroleum Conference*, Calgary, Alberta, Canada, 19-21 October. SPE-137435-MS.
- Barker, J.W., Cuypers, M., Holden, L., 2001. Quantifying uncertainty in production forecasts: another look at the PUNQ-S3 problem. *SPE Journal* **6**(4): 433-441. SPE-74707-PA.
- Bazargan, H., 2014. *An Efficient Polynomial Chaos-based Proxy Model for History Matching and Uncertainty Quantification of Complex Geological Structures*. Ph.D. Thesis, Heriot-Watt University, Edinburgh, UK.
- Bazargan, H., Christie, M., Elsheikh, A.H., Ahmadi, M., 2015. Surrogate accelerated sampling of reservoir models with complex structures using sparse polynomial chaos expansion. *Advanced Water Resources* **86**(B): 385-399.
- Bemporad, A., Morari, M., Ricker, N.L., 2016. *Model Predictive Control Toolbox™ User's Guide R2015a*. Natick, Massachusetts: The MathWorks Inc.
- Bhagade, S.S., Nageshwar, G.D., 2011. *Process Dynamics and Control*. New Delhi: PHI Learning Private Limited.
- Bixby, R.E., 2012. A brief history of linear and mixed-integer programming computation. *Documenta Mathematica – Extra Volume ISMP*: 107-121.
- Bruyelle, J., Guerillot, D., 2014. Neural networks and their derivatives for history matching and reservoir optimization problems. *Computational Geosciences* **18**(3): 549-561.
- Burgers, G., Leeuwen, P.J., Evensen, G., 1998. Analysis scheme in the ensemble Kalman filter. *Monthly Weather Review* **126**(6): 1719-1724.
- Camacho, E.F. and Bordons, C. 2007. *Model Predictive Control*. London: Springer-Verlag.

- Cancelliere, M., Verga, F., Viberti, D., 2011. Benefits and limitations of assisted history matching. Presented at the *SPE Offshore Europe Oil and Gas Conference and Exhibition*, Aberdeen, UK, 6-8 September. SPE-146278-MS.
- Chen, Y., Oliver, D.S., 2010. Cross-covariances and localization for EnKF in multiphase flow data assimilation. *Computational Geosciences* **14**(4): 579-601.
- Chen, Y., Zhang, D., 2006. Data assimilation for transient flow in geologic formations via ensemble Kalman filter. *Advanced Water Resources* **29**(8): 1107-1122.
- Chitralkhha, S.B., Trivedi, J.J., Shah, S.L., 2010. Application of the ensemble Kalman filter for characterization and history matching of unconventional oil reservoirs. Presented at the *Canadian Unconventional Resources and International Petroleum Conference*, Calgary, Alberta, Canada, 19-21 October. SPE-137480-MS.
- Clark, H.P., Ascanio, F.A., Van Kruijsdijk, C.P.J.W., Chavarria, J.L., Zatzka, M.J., Williams, W., Yahyai, A.H., Shaw, J.D., Bedry, M., 2010. Method to improve thermal EOR performance using intelligent well technology: Orion SAGD field trial. Presented at the *Canadian Unconventional Resources and International Petroleum Conference*, Calgary, Alberta, Canada, 19-21 October. SPE-137133-MS.
- Clarke, D.W., Mohtadi, C., Tuffs, P.S., 1987. Generalized predictive control – part I. the basic algorithm. *Automatica* **23**(2): 137-148.
- Computer Modelling Group (CMG). 2013a. *STARS User's Guide, Version 2013*. Calgary, Alberta, Canada: Computer Modelling Group Ltd.
- Computer Modelling Group (CMG). 2013b. *Results Report User's Guide, Version 2013*. Calgary, Canada: Computer Modelling Group Ltd.
- Costa, L.A.N., Maschio, C., Schiozer, D.J., 2014. Application of artificial neural networks in a history matching process. *Journal of Petroleum Science and Engineering* **124**(C): 30-45.

- Cotter, S.L., Roberts, G.O., Stuart, A.M., White, D., 2013. MCMC methods for functions: modifying old algorithms to make them faster. *Statistical Science* **28**(3): 424-446.
- Cullick, A.S., Johnson, D., Shi, G., 2006. Improved and more-rapid history matching with a nonlinear proxy and global optimization. Presented at the *SPE Annual Technical Conference and Exhibition*, San Antonio, Texas, USA, 24-27 September. SPE-101933-MS.
- Cutler, C.R., Ramaker, B.L., 1979. Dynamic matrix control – a computer control algorithm. Presented at *AIChE National Meeting*, Houston, Texas, USA, April.
- Das, S., 2005. Improving the performance of SAGD. Presented at the *SPE International Thermal Operations and Heavy Oil Symposium*, Calgary, Alberta, Canada, 1-3 November. SPE-97921-MS.
- de Oliveira, N.M.C., Biegler, L.T., 1994. Constraint handling and stability properties of model-predictive control. *AIChE Journal* **40**(7): 1138-1155.
- Debusschere, B.J., Najm, H.N., Pebay, P.P., Knio, O.M., Ghanem, R.G., Le Maitre, O.P., 2004. Numerical challenges in the use of polynomial chaos representations for stochastic processes. *SIAM Journal on Scientific Computing* **26**(2): 698-719.
- Deutsch, C.V., 1999. Reservoir modeling with publicly available software. *Computers and Geosciences* **25**(4): 355-363.
- Deutsch, C.V., 2002. *Geostatistical Reservoir Modeling*. New York: Oxford University Press.
- Deutsch, C.V., Srinivasan, S., 1996. Improved reservoir management through ranking stochastic reservoir models. Presented at the *SPE/DOE Improved Oil Recovery Symposium*, Tulsa, Oklahoma, USA, 21-24 April. SPE-35411-MS.
- Devegowda, D., Arroyo, E., Datta-Gupta, A., Douma, S.G., 2007. Efficient and robust reservoir model updating using ensemble Kalman filter with sensitivity-based covariance localization. Presented at the *SPE Reservoir Simulation Symposium*, Houston, Texas, USA, 26-28 February. SPE-106144-MS.

- Dupacova, J., Growe-Kuska, N., Romisch, W., 2003. Scenario reduction in stochastic programming. *Mathematical Programming* **95**(3): 493-511.
- Edmunds, N. 2000. Investigation of SAGD steam trap control in two and three dimensions. *Journal of Canadian Petroleum Technology* **39**(1): 30-40. PETSOC-00-01-02.
- Edmunds, N.R., Gittins, S.D., 1993. Effective application of steam assisted gravity drainage of bitumen to long horizontal well pairs. *Journal of Canadian Petroleum Technology* **32**(6): 49-55. PETSOC-93-06-05.
- Efendiev, Y., Datta-Gupta, A., Ma, X., Mallick, B., 2009. Efficient sampling techniques for uncertainty quantification in history matching using nonlinear error models and ensemble level upscaling techniques. *Water Resources Research* **45**(11): 1-11.
- Emerick, A.A., Reynolds, A.C., 2010. EnKF-MCMC. Presented at the *SPE EUROPEC/EAGE Annual Conference and Exhibition*, Barcelona, Spain, 14-17 June. SPE-131375-MS.
- Emerick, A.A., Reynolds, A.C., 2012. Combining the ensemble Kalman Filter with Markov chain Monte Carlo for improved history matching and uncertainty characterization. *SPE Journal* **17**(2): 418-440.
- Emerick, A.A., Reynolds, A.C., 2013. Investigation of the sampling performance of ensemble-based methods with a simple reservoir model. *Computational Geosciences* **17**(2): 325-350.
- Evensen, G., 1994. Sequential data assimilation with a nonlinear quasi-geostrophic model using Monte Carlo methods to forecast error statistics. *Journal of Geophysical Research: Oceans* **99**(C5): 10143-10162.
- Evensen, G., 2004. Sampling strategies and square root analysis schemes for the EnKF. *Ocean Dynamics* **54**(6): 539-560.
- Evensen, G., 2009. The ensemble Kalman filter for combined state and parameter estimation. *IEEE Control Systems* **29**(3): 83-104.

- Evensen, G., van Leeuwen, P.J., 1996. Assimilation of Geosat altimeter data for the Agulhas current using the ensemble Kalman filter with a quasi-geostrophic model. *Monthly Weather Review* **124**(1): 85–96.
- Fedutenko, E., Yang, C.C., Nghiem, L., 2012. Forecasting SAGD process under geological uncertainties using data-driven proxy model. Presented at the *SPE Heavy Oil Conference*, Calgary, Alberta, Canada, 12-14 June. SPE-157942-MS.
- Fenik, D.R., Nouri, A., Deutsch, C.V., 2009. Criteria for ranking realizations in the investigation of SAGD reservoir performance. Presented at the *Canadian International Petroleum Conference*, Calgary, Alberta, Canada, 16-18 June. PETSOC-2009-191.
- Foss, B., Jensen, J.P., 2011. Performance analysis for closed-loop reservoir management. *SPE Journal* **16**(1): 183-190. SPE-138891-PA.
- Foss, B.A., Lohmann, B., Marquardt, W., 1998. A field study of the industrial modeling process. *Journal of Process Control* **8**(5-6): 325-338.
- Fukushima, H., Kim, T.H., Sugie, T., 2007. Adaptive model predictive control for a class of constrained linear systems based on the comparison model. *Automatica* **43**(2): 301-308.
- Gamerman, D., Lopes, H., 2006. *Markov Chain Monte Carlo: Stochastic Simulation for Bayesian Inference*. Boca Raton: Chapman & Hall/CRC.
- Gao, G., Zafari, M., Reynolds, A., 2006. Quantifying uncertainty for the PUNQ-S3 problem in a Bayesian setting with RML and EnKF. *SPE Journal* **11**(4): 506–515. SPE-93324-PA.
- Gates, I.D., Leskiw, C., 2010. Impact of steam trap control on performance of steam-assisted gravity drainage. *Journal of Petroleum Science and Engineering* **75**(1-2): 215-222.
- Gelman, A., Roberts, G.O., Gilks, W.R., 1996. Efficient Metropolis jumping rules. *Bayesian Statistics* **5**(5): 599–607.
- Genceli, H., Nikolaou, M., 1996. New approach to constrained predictive control with simultaneous model identification. *AIChE Journal* **42**(10): 2857-2868.

- Ghanem, R.G., Spanos, P.D., 1991. *Stochastic Finite Elements: A Spectral Approach*. New York: Springer.
- Gilman, J.R., Meng, H., Uland, M., Dzurman, P.J., Cosic, S., 2002. Statistical ranking of stochastic geomodels using streamline simulation: a field application. Presented at the *SPE Annual Technical Conference and Exhibition*, San Antonio, Texas, USA, 29 September-2 October. SPE- 77374-MS.
- Goodwin, N., 2015. Bridging the gap between deterministic and probabilistic uncertainty quantification using advanced proxy based methods. Presented at the *SPE Reservoir Simulation Symposium*, Houston, Texas, USA, 23-25 February. SPE-173301-MS.
- Gotawala, D.R., Gates, I.D., 2009. SAGD subcool control with smart injection wells. Presented at the *SPE EUROPEC/EAGE Annual Conference and Exhibition*, Amsterdam, The Netherlands, 8-11 June. SPE-122014-MS.
- Gotawala, D.R., Gates, I.D., 2012. A basis for automated control of steam trap subcool in SAGD. *SPE Journal* **17**(3): 680–686. SPE-159170-PA.
- Gu, Y., Oliver, D.S., 2006. The ensemble Kalman filter for continuous updating of reservoir simulation models. *Journal of Energy Resources Technology* **128**(1): 79-87.
- Guangyue, L., Shangqi, L., Pingping, S., Liu, Y., Luo, Y., 2016. A new optimization method for steam-liquid level intelligent control model in oil-sands steam-assisted gravity drainage (SAGD) process. *Petroleum Exploration and Development* **43**(2): 301-307.
- Guevara, J.L., Ortega, A., Canelon, J.I., Nava, E., Queipo, N.V., 2015. Model-Based adaptive-predictive control and optimization of SAGD under uncertainty. Presented at the *SPE Latin American and Caribbean Petroleum Engineering Conference*, Quito, Ecuador, 18-20 November. SPE-177270-MS.
- Guyaguler, B., Papadopoulos, A.T., Philpot, J.A., 2010. Feedback controllers for the simulation of field processes. *SPE Reservoir Evaluation & Engineering* **13**(1): 10-23. SPE-118969-PA.

- He, J., Sarma, P., Durlofsky, L.J., 2011. Use of reduced-order models for improved data assimilation within an EnKF context. Presented at the *SPE Reservoir Simulation Symposium*, The Woodlands, Texas, USA, 21-23 February. SPE-141967-MS.
- He, Q., 2016. *Investigating Continuously Updated History Matching Using Smart Proxy (Surrogate Reservoir Model)*. Ph.D. Thesis, West Virginia University, West Virginia, USA.
- Henson, M.A., 1998. Nonlinear model predictive control: current status and future directions. *Computers & Chemical Engineering* **23**(2): 187-202.
- Hird, K.B., Dubrule, O., 1998. Quantification of reservoir connectivity for reservoir description applications. *SPE Reservoir Evaluation & Engineering* **1**(1): 12-15. SPE-30571-PA.
- Houtekamer, P.L., Mitchell H.L., 1998. Data assimilation using an ensemble Kalman filter technique. *Monthly Weather Review* **126**(3): 796-811.
- Hovadik, J.M., Larue, D.K., 2007. Static characterizations of reservoirs: refining the concepts of connectivity and continuity. *Petroleum Geoscience* **13**(3): 195-211.
- Huang, B., Qi, Y. and Murshed, A.K.M.M. 2013. *Dynamic Modeling and Predictive Control in Solid Oxide Fuel Cells: First Principle and Data-Based Approaches*. West Sussex: John Wiley & Sons.
- Huang, S.P., Quek, S.T., Phoon, K.K., 2001. Convergence study of the truncated Karhunen-Loeve expansion for simulation of stochastic processes. *International Journal for Numerical Methods in Engineering* **52**(9): 1029-1043.
- IBM, 2010. *User's Manual for CPLEX V12.1*. New York: IBM.
- Idrobo, E.A., Choudhary, M.K., Datta-Gupta, A., 2000. Swept volume calculations and ranking of geostatistical reservoir models using streamline simulation. Presented at the *SPE/AAPG Western Regional Meeting*, Long Beach, California, USA, 19-22 June. SPE-62557-MS.

- Iglesias, M.A., Law, K.J.H., Stuart, A.M., 2013. Evaluation of Gaussian approximations for data assimilation in reservoir models. *Computational Geosciences* **17**(5): 851-885.
- Ilka, A., 2015. *Gain-Scheduled Controller Design*. Ph.D. Thesis, Slovak University of Technology in Bratislava, Bratislava, Slovakia.
- Ito, Y., Suzuki, S., 1999. Numerical simulation of the SAGD process in the Hangingstone oil sands reservoir. *Journal of Canadian Petroleum Technology* **38**(9): 27-35. PETSOC-99-09-02.
- Jafarpour, B., McLaughlin, D.B., 2008. History matching with an ensemble Kalman filter and discrete cosine parameterization. *Computational Geosciences* **12**(2): 227-244.
- Jafarpour, B., Tarrahi, M., 2011. Assessing the performance of the ensemble Kalman filter for subsurface flow data integration under variogram uncertainty. *Water Resources Research* **47**(5): 1-26.
- Jain, T., Patel, R.G., Trivedi, J., 2016. Application of ANN based proxy models for efficient and fast track assisted history matching of SAGD reservoirs. Presented at the *World Heavy Oil Congress*, Calgary, Alberta, Canada, 6-9 September. WHOC16-164.
- Jain, T., Patel, R.G., Trivedi, J., 2017. Application of polynomial chaos theory as an accurate and computationally efficient proxy model for heterogeneous steam-assisted gravity drainage reservoirs. *Energy Science & Engineering* **5**(5): 270-289.
- Jansen, J.D., Douma, S.D., Brouwer, D.R., Van den Hof, P.M.J., Bosgra, O.H., Heemink, A.W., 2009. Closed-Loop reservoir management. Presented at the *SPE Reservoir Simulation Symposium*, The Woodlands, Texas, USA, 2-4 February. SPE-119098-MS.
- Jensen, J.P., 2007. *Ensemble Kalman Filtering for State and Parameter Estimation on a Reservoir Model*. Master's Thesis, Norwegian University of Science and Technology, Trondheim, Norway.

- Jeong, D., Jeong, K., Baik, H., Jonggeun, C., 2013. Uncertainty analyses of basement fracture reservoir performances using proxy models with high-quality history matching. *Energy Exploration & Exploitation* **31**(3): 395-410.
- Jurecka, F., 2007. *Robust Design Optimization Based on Metamodeling Techniques*. Ph.D. Thesis, Technical University of Munich, Munich, Germany.
- Kaipio, J.P., Somersalo E., 2005. *Statistical and Computational Inverse Problems*. New York: Springer.
- Karra, S., Shaw, R., Patwardhan, S.C., Noronha, S., 2008. Adaptive Model Predictive Control of Multivariable Time-Varying Systems. *Industrial & Engineering Chemistry Research* **47**(8): 2708-2720.
- Khaledi, R.R., Beckman, M.S., Pustanyk, K., Mohan, A., Wattenbarger, C.C., Dickson, J.L., Boone, T.T., 2012. Physical modelling of solvent-assisted SAGD. Presented at the *SPE Heavy Oil Conference Canada*, Calgary, Alberta, Canada, 12-14 June. SPE-150676-MS.
- Kisman, K.E., 2003. Artificial lift – a major unresolved issue for SAGD. *Journal of Canadian Petroleum Technology* **42**(8): 39-45. PETSOC-03-08-02.
- Kostuik, K., Valdez, A.A., Bordovsky, J., Mu, Y., Faig, C., 2013. Evaluation of multi-objective methods for portfolio tradeoff analysis. Presented at the *SPE Annual Technical Conference and Exhibition*, New Orleans, Louisiana, USA, 30 September-2 October. SPE-166372-MS.
- Kozak, S., 2014. State-of-the-art in control engineering. *Journal of Electrical Systems and Information Technology* **1**(1): 1-9.
- Kurtz, M.J., Henson, M.A., 1997. Input-output linearizing control of constrained nonlinear processes. *Journal of Process Control* **7**(1): 3-17.
- Le Ravalec, M., Morlot, C., Marmier, R., Foulon, D., 2009. Heterogeneity impact on SAGD process performance in mobile heavy oil reservoirs. *Oil & Gas Science and Technology – Rev. IFP* **64**(4): 469-476.
- Lee, E.B., Markus, L., 1967. *Foundations of Optimal Control Theory*. New York: John Wiley & Sons.

- Li, B., Friedmann, F., 2007. Semiautomatic multiple resolution design for history matching. *SPE Journal* **12**(4): 408-419. SPE-102277-PA.
- Li, H., Sarma, P., Zhang, D., 2011. A comparative study of the probabilistic-collocation and experimental-design methods for petroleum-reservoir uncertainty quantification. *SPE Journal* **16**(2): 429-439. SPE-140738-PA.
- Li, H., Zhang, D., 2007. Probabilistic collocation method for flow in porous media: comparisons with other stochastic methods. *Water Resources Research* **43**(9): 1-13.
- Li, S., Deutsch, C.V., Si, J., 2012. Ranking geostatistical reservoir models with modified connected hydrocarbon volume. Presented at the *Ninth International Geostatistics Congress, Oslo, Norway, 11-15 June*.
- Li, Z., Floudas, C.A., 2014. Optimal scenario reduction framework based on distance of uncertainty distribution and output performance: I. Single reduction via mixed integer linear optimization. *Computers and Chemical Engineering* **70**(C): 50-66.
- Lin, G., Tartakovsky, A.M., 2008. An efficient, high-order probabilistic collocation method on sparse grids for three-dimensional flow and solute transport in randomly heterogeneous porous media. *Advanced Water Resources* **32**(5): 712-722.
- Liu, N., Oliver, D.S., 2003. Evaluation of Monte Carlo methods for assessing uncertainty. *SPE Journal* **8**(2): 188-195. SPE-84936-PA.
- Ljung, L., 1999. *System Identification*. New Jersey: Prentice-Hall.
- Ljung, L., 2002. Prediction Error Estimation Methods. *Circuits, Systems and Signal Processing* **21**(1): 11-21.
- Ljung, L., 2016. *System Identification Toolbox™ User's Guide R2016b*. Natick, Massachusetts: The MathWorks Inc.
- Lorentzen, R.J., Fjelde, K.K., Froyen, J., Lage, A.C., Nævdal, G., Vefring, E.H., 2001. Underbalanced and lowhead drilling operations: real time interpretation of measured data and operational support. Presented at the *SPE Annual Technical*

Conference and Exhibition, New Orleans, Louisiana, USA, 30 September-3 October. SPE-71384-MS.

- Lu, D., Yao, K., 1988. Improved importance sampling technique for efficient simulation of digital communication systems. *IEEE Journal on Selected Areas in Communications* **6**(1): 67-75.
- Ma, X., Al-Harbi, M., Datta-Gupta, A., Efendiev, Y., 2008. An efficient two-stage sampling method for uncertainty quantification in history matching geological models. *SPE Journal* **13**(1): 77-87.
- Marianayagam, K.R., 2012. *Numerical simulation study on parameters related to Athabasca bitumen recovery with SAGD*. Master's Thesis, Norwegian University of Science and Technology, Trondheim, Norway.
- MathWorks, 2014. *MATLAB® Release R2014a*. The MathWorks Inc., Natick, Massachusetts.
- McLennan, J.A., Deutsch, C.V., 2005. Ranking geostatistical realizations by measures of connectivity. Presented at the *SPE International Thermal Operations and Heavy Oil Symposium*, Calgary, Alberta, Canada, 1-3 November. SPE-98168-MS.
- Metropolis, N., Rosenbluth, A.W., Rosenbluth, M.N., Teller, A.H., Teller, E., 1953. Equation of state calculations by fast computing machines, *The Journal of Chemical Physics* **21**(6): 1081-1092.
- Monfared, A.D., Helalizadeh, A., Parvizi, H., 2012. Automatic history matching using the integration of response surface modeling with a genetic algorithm. *Petroleum Science and Technology* **30**(4): 360-374.
- Myrseth, I., Saetrom, J., Omre, H., 2013. Resampling the ensemble Kalman filter. *Computers & Geosciences* **55**(C): 44-53.
- Naevdal, G., Johnsen, L.M., Aanonsen, S.I., Vefring, E.H., 2003. Reservoir monitoring and continuous model updating using ensemble Kalman filter. Presented at the *SPE Annual Technical Conference and Exhibition*, Denver, Colorado, USA, 5-8 October. SPE-84372-MS.

- Nejadi, S., Trivedi, J., Leung, J.Y., 2014. Estimation of facies boundaries using categorical indicators with P-field simulation and ensemble Kalman filter (EnKF). *Natural Resources Research* **24**(2): 121–138.
- Nelles, O. 2001. *Nonlinear System Identification*. Berlin Heidelberg: Springer.
- Nevistic, V., Morari, M., 1995. Constrained control of feedback-linearizable systems. Presented at the *3rd European Control Conference*, Rome, Italy, 5-8 September.
- Nikolaou, M., Cullick, A.S., Saputelli, L.A., Mijares, G., Sankaran, S., Reis, L.C., 2006. A consistent approach toward reservoir simulation at different time scales. Presented at the *SPE Intelligent Energy Conference and Exhibition*, Amsterdam, The Netherlands, 11-13 April. SPE-99451-MS.
- Oladyshkin, S., Nowak, W., 2012. Data-Driven uncertainty quantification using the arbitrary polynomial chaos expansion. *Reliability Engineering and System Safety* **106**(C): 179-190.
- Oliver, D.S., Chen, Y., 2009. Improved initial sampling for the ensemble Kalman filter. *Computational Geosciences* **13**(1): 13-27.
- Oliver, D.S., Chen, Y., 2011. Recent progress on reservoir history matching: a review, *Computational Geosciences* **15**(1): 185-221.
- Oliver, D.S., Cunha, L.B., Reynolds, A.C. 1997. Markov chain Monte Carlo methods for conditioning a permeability field to pressure data. *Mathematical Geology* **29**(1): 61–91.
- Patel, K., Aske, E.M., Fredriksen. M., 2014. Use of model-predictive control for automating SAGD well-pair operations: a simulation study. *SPE Production & operations* **29**(2): 105-133. SPE-165535-PA.
- Patel, R.G., Jain, T., Trivedi, J.J., 2017. Polynomial-Chaos-Expansion based integrated dynamic modelling workflow for computationally efficient reservoir characterization: a field case study. Presented at the *SPE Europec featured at 79th EAGE Conference and Exhibition*, Paris, France, 12-15 June. SPE-185847-MS.

- Patel, R.G., Trivedi, J., Rahim, S., Li, Z., 2015. Initial sampling of ensemble for steam-assisted-gravity-drainage-reservoir history matching. *Journal of Canadian Petroleum Technology* **54**(6): 424-441. SPE-178927-PA.
- Potra, F.A., Wright, S.J., 2000. Interior-point methods. *Journal of Computational and Applied Mathematics* **124**(1-2): 281-302.
- Purkayastha, S.N., Gates, I.D., Trifkovic, M., 2015. Model-Predictive-Control (MPC) of steam trap subcool in steam-assisted gravity drainage (SAGD). *IFAC-Papers Online* **48**(8): 539-544.
- Qin, S.J., Badgwell, T.A., 2003. A survey of industrial model predictive control technology. *Control Engineering Practice* **11**(7): 733-764.
- Queipo, N.V., Pintos, S., Rincon, N., Contreras, N., Colmenares, J., 2000. Surrogate modeling-based optimization for the integration of static and dynamic data into a reservoir description. Presented at the *SPE Annual Technical Conference and Exhibition*, Dallas, Texas, 1-4 October. SPE-63065-MS.
- Rahim, S., Li, Z., Trivedi, J., 2015. Reservoir geological uncertainty reduction: an optimization-based method using multiple static measures. *Mathematical Geosciences* **47**(4): 373-396.
- Richalet, J., 1993. Industrial applications of model based predictive control. *Automatica* **29**(5): 1251-1274.
- Richalet, J., Rault, A., Testud, J.L., Papon, J., 1978. Model predictive heuristic control: applications to industrial processes. *Automatica* **14**(5): 413-428.
- Robert, C.P., Casella, G., 2004. *Monte Carlo Statistical Methods*. New York: Springer.
- Roberts, G.O., Gelman, A., Gilks, W.R., 1997. Weak convergence and optimal scaling of random walk Metropolis algorithm. *The Annals of Applied Probability* **7**(1): 110-120.
- Roberts, G.O., Rosenthal, J.S., 2001. Optimal scaling of various Metropolis-Hastings algorithms. *Statistical Science* **16**(4): 351-367.
- Rugh, W.J., Shamma, J.S., 2000. Research on gain scheduling. *Automatica* **36**(10): 1401-1425.

- Saad, G., 2007. *Stochastic Data Assimilation with Application to Multi-Phase Flow and Health Monitoring Problems*. Ph.D. Thesis, University of Southern California, California, USA.
- Saad, N., Maroongroge, V., Kalkomey, C.T., 1996. Ranking geostatistical models using tracer production data. Presented at the *European 3-D Reservoir Modeling Conference*, Stavanger, Norway, 16-17 April. SPE-35494-MS.
- Sakov, P., Bertino, L., 2011. Relation between two common localisation methods for the EnKF. *Computational Geosciences* **15**(2): 225– 237.
- Saputelli, L., Nikolaou, M., Economides, M.J., 2005. Self-Learning reservoir management. *SPE Reservoir Evaluation & Engineering* **8**(6): 534-547. SPE-84064-PA.
- Saputelli, L.A., Mochizuki, S., Hutchins, L., Cramer, R., Anderson, M.B., Mueller, J.B., Escorcia, A., Harms, A.L., Sisk, C.D., Pennebaker, S., Han, J.T., Brown, A., Kabir, C.S., Reese, R.D., Nunez, G.J., Landgren K.M., McKie, C.J., Airlie, C., 2003. Promoting real-time optimization of hydrocarbon producing systems. Presented at *Offshore Europe*, Aberdeen, UK, 2-5 September. SPE-83978-MS.
- Sarma, P., Chen W.H., 2013. Preventing ensemble collapse and honoring multipoint geostatistics with the subspace EnKF/EnS and Kernel PCA parameterization. Presented at the *SPE Reservoir Simulation Symposium*, The Woodlands, Texas, USA, 18-20 February. SPE-163604-MS.
- Sarma, P., Xie, J., 2011. Efficient and robust uncertainty quantification in reservoir simulation with polynomial chaos expansion and non-intrusive spectral projection. Presented at the *SPE Reservoir Simulation Symposium*, The Woodlands, Texas, USA, 21-23 February. SPE-141963-MS.
- Sayarpour, M., Kabir, C.S., Sepehrnoori, K., Lake, L.W., 2011. Probabilistic history matching with the capacitance-resistance model in waterfloods: a precursor to numerical modelling. *Journal of Petroleum Science and Engineering* **78**(1): 96-108.
- Scheidt, C., Caers, J., 2009. Representing spatial uncertainty using distances and kernels. *Mathematical Geosciences* **41**(4): 397-419.

- Seborg, D.E., Edgar, T.F., Mellichamp, D.A., Doyle, F.J., 2011. *Process Dynamics and Control*. New Jersey: John Wiley & Sons.
- Shad, S., Yazdi, M.M., 2014. Wellbore modeling and design of nozzle-based inflow control device (ICD) for SAGD wells. Presented at the *SPE Heavy Oil Conference*, Alberta, Canada, 10-12 June. SPE-170145-MS.
- Shi, J., Leung, J.Y., 2013. Physics-Based proxy for vapex process modelling in heterogeneous reservoirs. Presented at the *SPE Heavy Oil Conference*, Calgary, Alberta, Canada, 11-13 June. SPE-165558-MS.
- Shin, H., Hwang, T., Chon, B., 2012. Optimal grid system for SAGD simulation. Presented at the *SPE Heavy Oil Conference Canada*, Calgary, Canada, 12-14 June. SPE-157900-MS.
- Siripatana, A., Mayo, T., Sraj, I., Knio, O., Dawson, C., Le Maitre, O., Hoteit, I., 2017. Assessing an ensemble Kalman filter inference of Manning's n coefficient of an idealized tidal inlet against a polynomial chaos-based MCMC. *Ocean Dynamics* **67**(8): 1067–1094.
- Slotte, P.A., Smorgrav, E., 2008. Response surface methodology approach for history matching and uncertainty assessment of reservoir simulation models. Presented at the *SPE Europe/EAGE Annual Conference and Exhibition*, Rome, Italy, 9-12 June. SPE-113390-MS.
- Soderstrom, T., Stoica, P., 1989. *System Identification*. Hertfordshire: Prentice Hall International (UK) Ltd.
- Stalder, J.L., 2013. Test of SAGD flow-distribution-control liner system in the Surmont field, Alberta, Canada. *Journal of Canadian Petroleum Technology* **52**(2): 95-100. SPE-153706-PA.
- Stone, T.W., Bailey, W.J., 2014b. Optimization of subcool in SAGD bitumen processes. Presented at *World Heavy Oil Congress*, New Orleans, Louisiana, USA, 5-7 March. WHOC14-271.

- Stone, T.W., Brown, G., Guyaguler, B., Bailey, W.J., Law, D.H.S., 2014a. Practical control of SAGD wells with dual-tubing strings. *Journal of Canadian Petroleum Technology* **53**(1): 32–47. SPE-149352-PA.
- Stone, T.W., Law, D. H.S., Bailey, W.J., 2013. Control of reservoir heterogeneity in SAGD bitumen processes. Presented at the *SPE Heavy Oil Conference Canada*, Calgary, Alberta, Canada, 11-13 June. SPE-165388-MS.
- Strand, S., Sagli, J.R., 2004. MPC in STATOIL – advantages with in-house technology. *IFAC Proceedings Volumes* **37**(1): 97-103.
- Tarantola, A., 2005. *Inverse Problem Theory and Methods for Model Parameter Estimation*. Philadelphia: Society for Industrial and Applied Mathematics.
- Tatang, M.A., Pan, W., Prinn, R.G., McRae, G.J., 1997. An efficient method for parametric uncertainty analysis of numerical geophysical models. *Journal of Geophysical Research* **102**(D18): 21925-21932.
- Taubner, S.P., Subramanian, V., Kaiser, M.V., 2015. Assessing subcool control issues in SAGD producers and methods for mitigation. Presented at the *SPE Thermal Well Integrity and Design Symposium*, Banff, Alberta, Canada, 23-25 November. SPE-178453-MS.
- Tavakoli, R., Reynolds, A., 2011. Monte Carlo simulation of permeability fields and reservoir performance predictions with SVD parameterization in RML compared with EnKF. *Computational Geosciences* **15**(1): 99–116.
- van Essen, G.M., Van den Hof, P.M.J., Jansen, J.D., 2013. A two-level strategy to realize life-cycle production optimization in an operational setting. *SPE Journal* **18**(6): 1057-1066. SPE-149736-PA.
- Vander Valk, P.A., Yang, P., 2007. Investigation of key parameters in SAGD wellbore design and operation. *Journal of Canadian Petroleum Technology* **46**(6): 49-56. PETSOC-07-06-02.
- Vanegas P, J.W., Deutsch, C.V., Cunha, L.B., 2008. Uncertainty assessment of SAGD performance using a proxy model based on Butler’s theory. Presented at the *SPE*

Annual Technical Conference and Exhibition, Denver, Colorado, USA, 21-24 September. SPE-115662-MS.

- Vembadi, S.S., 2014. *Real-Time Feedback Control of the SAGD Process using Model Predictive Control to Improve Recovery: A Simulation Study*. Master's Thesis, University of Alberta, Edmonton, Canada.
- Vembadi, S.S., Trivedi, J.J., Prasad, V., 2015. Real-Time feedback control of SAGD wells using model predictive control to optimize steam chamber development under uncertainty. Presented at *World Heavy Oil Congress*, Edmonton, Alberta, Canada, 24-26 March. WHOC15-242.
- Wang, Y., Li, M., 2011. Reservoir history matching and inversion using an iterative ensemble Kalman filter with covariance localization. *Petroleum Science* **8**(3): 316-327.
- Webster, M., Tatang, M.A., McRae, G.J., 1996. *Application of the probabilistic collocation method for an uncertainty analysis of a simple ocean model*. Report. Massachusetts: MIT Joint Program on the Science and Policy of Global Change.
- Wen, X., Chen, W., 2007. Some practical issues on real-time reservoir model updating using ensemble Kalman filter. *SPE Journal* **12**(2): 156-166.
- Wiener, N., 1938. The Homogeneous Chaos. *American Journal of Mathematics* **60**(4): 897-936.
- Yao, S., Trivedi, J.J., Prasad, V., 2015. Proxy modeling of the production profiles of SAGD reservoirs based on system identification. *Industrial Engineering & Chemistry Research* **54**(33): 8356-8367.
- Yazdi, M.M., Jensen, J., 2014. Fast screening of geostatistical realizations for SAGD reservoir simulation. *Journal of Petroleum Science and Engineering* **124**(C): 264-274.
- Yu, T., Wilkinson, D., Castellini, A., 2008. Constructing reservoir flow simulator proxies using genetic programming for history matching and production forecast analysis. *Journal of Artificial Evolution and Applications* **2008**: 1-13.

Zubarev, D.I., 2009. Pros and cons of applying proxy-models as a substitute for full reservoir simulations. Presented at the *SPE Annual Technical Conference and Exhibition*, New Orleans, Louisiana, USA, 4-7 October. SPE-124815-MS.